5-2015

Calibration and Rescaling Principles for Nonlinear Inverse Heat Conduction and Parameter Estimation Problems

Yinyuan Chen
University of Tennessee - Knoxville, cyinyuan@vols.utk.edu

To the Graduate Council:

I am submitting herewith a dissertation written by Yinyuan Chen entitled "Calibration and Rescaling Principles for Nonlinear Inverse Heat Conduction and Parameter Estimation Problems." I have examined the final electronic copy of this dissertation for form and content and recommend that it be accepted in partial fulfillment of the requirements for the degree of Doctor of Philosophy, with a major in Mechanical Engineering.

Jay Frankel, Major Professor

We have read this dissertation and recommend its acceptance:

Majid Keyhani, Rao Arimilli, Jayne Wu

Accepted for the Council:
Dixie L. Thompson

Vice Provost and Dean of the Graduate School

(Original signatures are on file with official student records.)

Calibration and Rescaling Principles for Nonlinear Inverse Heat Conduction and Parameter Estimation Problems

A Dissertation Presented for the

Doctor of Philosophy

Degree

The University of Tennessee, Knoxville

Yinyuan Chen

May 2015

Acknowledgements

I would like to acknowledge the many people who have facilitated the completion of this dissertation. I am grateful to my research advisor, Dr. Jay Frankel, for his advice, guidance and support. His encouragement provided significant assistance into my graduate career and the completion of this dissertation. I am also grateful to Dr. Majid Keyhani for his assistance and insight. I would also like to express my sincere gratitude to the other committee members, Dr. Rao Arimilli and Dr. Jayne Wu, for their suggestions and participation on this committee.

I would like to thank Dr. Tsiwei Wang for her suggestion that I contact Drs. Frankel and Keyhani. I would also like to express my gratitude to my fellow graduate students, Mr. Jake Plewa, Mr. Hongchu Chen, Mr. Abhay Pande, and Mr. Justin Myrick for their assistance, continual friendship and moral support.

Financial support throughout my graduate career was provided through several avenues. I would like to thank the Mechanical, Aerospace, and Biomedical Engineering Department for supporting me through Graduate Research/Teaching Assistantships for two semesters. I am also grateful to the National Science Foundation (CBET-1234419) for these years of financial support for my doctoral work.

Abstract

This dissertation provides a systematic method for resolving nonlinear inverse heat conduction problems based on a calibration formulation and its accompanying principles. It is well-known that inverse heat conduction problems are ill-posed and hence subject to stability and uniqueness issues. Regularization methods are required to extract the best prediction based on a family of solutions. To date, most studies require sophisticated and combined numerical methods and regularization schemes for producing predictions. All thermophysical and geometrical properties must be provided in the simulations. The successful application of the numerical methods relies on the accuracy of the related system parameters as previously described. Due to the existence of uncertainties in the system parameters, these numerical methods possess bias of varying magnitudes. The calibration based approaches are proposed to minimize the systematic errors since system parameters are implicitly included in the mathematical formulation based on several calibration tests. To date, most calibration inverse studies have been based on the assumption of constant thermophysical properties. In contrast, this dissertation focuses on accounting for temperature-dependent thermophysical properties that produces a nonlinear heat equation. A novel rescaling principle is introduced for linearzing the system. This concept generates a mathematical framework similar to that of the linear formulation. Unlike the linear formulation, the present approach does require knowledge of thermophysical properties. However, all geometrical properties and sensor characterization are completely removed from the system.

In this dissertation, a linear one-probe calibration method is first introduced as background. After that, the calibration method is generalized to the one-probe and two-probe, one-dimensional thermal system based on the assumption of temperature-dependent thermophysical properties. All previously proposed calibration equations are expressed in terms of a Volterra integral equation of the first kind for the unknown surface (net) heat flux and hence requires regularization owning to the ill-posed nature of first kind equations. A new strategy is proposed for determining the optimal regularization parameter that is independent of the applied regularization approach. As a final application, the described calibration principle is used for estimating unknown thermophysical properties above room temperature.

Table of Contents

List of Tables

List of Figure

List of Symbols

Symbols

A = Unknown Coefficient in Laplace Transform Solution corresponding to $cosh$

b = Depth of the Sensor, m

B = Unknown Coefficient in Laplace Transform Solution corresponding to $sinh$

c_p = Specific Heat Capacity, $Jkg^{-1}K^{-1}$

$D_{q\theta}$ = Impulsive Heat Flux Solution for Kirchhoff Transform Variable $\theta(x,t)$, Km^2J^{-1}

D_q= Impulsive Heat Flux Solution for Temperature $T(x,t)$, Km^2J^{-1}

D_T= Impulsive Temperature Solution for Temperature $T(x,t)$, s^{-1}

E_r = Ratio between Predicted Total Energy and Exact Total Energy

f_c = Cutoff Frequency, Hz

F = Known Right Hand Side of the Calibration Equation

F_θ = Known Right Hand Side of the Calibration Equation for Kirchhoff Transform Variable, $\theta(x,t)$

F_M= Localized Right Hand Side of the Calibration Equation for $t \in [t_M, t_{M+S}]$

$\boldsymbol{F}$ = Vector with $\boldsymbol{F}(i) = F^*(t_i^*)$

$\boldsymbol{F_\theta}$ = Vector with $\boldsymbol{F_\theta}(i) = F_\theta^*(t_i^*)$

$\boldsymbol{F_M}$ = Vector with $\boldsymbol{F_M}(i) = F_M^*(t_i^*)$

G = Left Hand Side of the Calibration Equation involving $q"_r$

G_θ = Left Hand Side of the Calibration Equation for Kirchhoff Transform Variable $\theta(x,t)$ involving $q"_r$

h_L = Heat Transfer Coefficient at the Back Boundary, W/mK

i = Index

I = Index as Regularization Parameter for SVD based Regularization

j = Index

J = Function to be Minimized

J_θ = Function to be Minimized for Kirchhoff Transform Variable $\theta(x,t)$

k = Thermal Conductivity, $Wm^{-1}K^{-1}$

K = Kernel for the Calibration Equation

k_0 = Thermal Conductivity at Initial Temperature, $Wm^{-1}K^{-1}$

$\boldsymbol{K}$ = Square Matrix with $\boldsymbol{K}(i,j) = \Delta t^* \times K^*\left(b, t^*_{i-j+1}\right)$, for $i \geq j$ and $\mathbf{K}(i,j) = 0$ for $i < j$, ^oC

L = Thickness of the Sample, m

LF = L-curve function

LF_θ = L-curve function for Kirchhoff Transform Variable $\theta(x,t)$

m = Weight Coefficient between $P1$ and $P2$

m_i = Thermal Conductivity Rescaling Coefficient for $t \in [i\Delta t, (i+1)\Delta t]$

M = Index for Discrete Time Points, $M \in [0, N]$

M_r = Maximum Value Ratio

n_i = Thermal Diffusivity Rescaling Coefficient for $t \in [i\Delta t, (i+1)\Delta t]$

$N+1$ = Number of Uniformly Distributed Time Interval

P = Two-Component Exponential Function to be Minimized for Optimal Regularization

$P1$ = Relative Function Smoothness based Exponential Function

$P2$ = Relative Residual based Exponential Function

q'' = Heat Flux, W/m^2

q''_i = Heat Flux for $t \in [i\Delta t, (i+1)\Delta t]$, W/m^2

$\boldsymbol{q}$ = Vector with $\boldsymbol{q}(i) = q''^{*}(0, t^{*}_{i-1})$, W/m^2

$\boldsymbol{q_M}$ = Vector with $\boldsymbol{q_M}(i) = q''^{*}(0, t^{*}_{i+M-1})$, W/m^2

R = Residual, the Norm of the Difference between G^* and F^*

R_N = Relative Residual based on the Norm of F^*

S = Index for Discrete Future Time Points

s = Laplace Transform Variable in Frequency Domain

T = Temperature, ^{o}C

T_b= Temperature Measurement at $x = b$, ^{o}C

T_w= Temperature Measurement at $x = w$, ^{o}C

T_i = Temperature for $t \in [i\Delta t, (i+1)\Delta t]$, ^{o}C

$\mathbf{T}$ = Square Matrix with $\mathbf{T}(i,j) = \Delta t^* \times T^*\left(b, t^{*}_{i-j+1}\right)$, for $i \geq j$ and $\mathbf{T}(i,j) = 0$ for $i < j$, ^{o}C

t = Time, s

$t_i = i\Delta t$, s

t_{max} = Maximum Heating Time, s

u = Dummy Variable

v = Dummy Variable

$\mathbf{v_i}$ = ith Column of $\mathbf{V}$

$\mathbf{V}$ = Right Orthogonal Matrix after Singular-Value Decomposition

w = Depth of the Sensor (w $> b$), m

w_c = Circular Frequency $2\pi f_c$, Hz

$\mathbf{w_i}$ = ith Column of $\mathbf{W}$

$\mathbf{W}$ = Left Orthogonal Matrix after Singular-Value Decomposition

x = Spatial Variable in the x-Direction, m

Greek

α = Thermal Diffusivity, m^2/s

β = Noise Factor

ρ = Density, kg/m^3

λ_0 = Tikhonov Regularization Parameter, Ks

σ = Standard Deviation of Error, W/m^2

σ_i = ith Singular Value of the Diagonal Matrix $\sum$

ε_i = Added Noise at Time $i\Delta t$, ^oC

γ = Local Future Time, s

θ = Kirchhoff Transform Temperature, ^oC

θ_i = Kirchhoff Transform Temperature for $t \in [i\Delta t, (i+1)\Delta t]$, ^oC

$\boldsymbol{\Theta}$ = Square Matrix with $\boldsymbol{\Theta}(i,j) = \Delta t^* \times \theta^*\left(b, t^*_{i-j+1}\right)$, for $i \geq j$ and $\boldsymbol{\Theta}(i,j) = 0$

$\sum$ = Diagnoal Matrix after Singular-Value Decomposition

Δt = Time Step, s

Δx = Distance of Spatial Nodes, m

Accents

$\left(\widehat{\ }\right)$ = Variable in Laplace Transform Frequency Domain

$\left(\overline{\ }\right)$ = Absolute Variable

Superscripts

$*$ = Rescaled Variable

Subscripts

c = Calibration Test

ci = ith Calibration Test

Exact = Exact Result

f = Gauss Filter

$initial$ = Initial State

$Preq$ = Predicted Result

q = One Probe System based on Surface Heat Flux

$q2$ = Two Probe System based on Surface Heat Flux

r = Reconstruction Test

s = Surface

T = One Probe System based on Surface Temperature

tM = Pasted Variable for $t \in [0, (M+1)\Delta t]$

Chapter 1: Literature Review

Classic inverse heat conduction problems (IHCPs) involve estimating the surface thermal condition using in-depth sensors in lieu of boundary conditions. All inverse heat conduction problems are mathematically ill-posed and require additional mathematical devices for producing well-conditioned prediction. Hadamard's [1] definition of well-posed is given through the postulates: (1) existence of a solution, (2) uniqueness of the solution (3) behavior of the solution changes continuously with the data. For inverse heat conduction problems, violation of these criteria is apparent as the data are discrete and hence stability is not assured in the prediction process. Measurement noise is magnified during this prediction process, thereby destabilizing the outcome. Conventional doctrine for both linear and nonlinear inverse heat conduction problems rely on numerical methods or iterative strategies for forming the approximate surface reconstructions. In this view, all parameters characterizing the system are required for insertion into the mathematical model. The system parameters include thermophysical properties, geometrical properties, and sensor characteristics. A recently proposed alternative that removes this specification is based on calibration principles. Systematical errors will be substantially reduced as the system parameters are implicitly incorporated through the calibration tests. This literature review (Section 1.1-1.6) provides sufficient background identifying a gap and justifying the development of a nonlinear calibration inverse heat conduction method. Section 1.7 provides the scope for the research investigation.

1.1 Introduction of Inverse Heat Conduction Problems

Physical theories that can be mathematically formulated in term of functional equations permit outcomes to be predicted based on the provided inputs. This defines the conventional forward direct problem normally proposed in physical studies. In contrast, the inverse problem consists of using measurements from a sensor to infer the values of the parameters that characterize the system [1]. Inverse problems lie at the heart of scientific inquiry and technological development. Applications include: diagnostic-based medical and imaging techniques [2], locating oil and mineral deposits in the earth substructure [3], creating astrophysical images from telescope data [4], finding cracks and interfaces within materials [5], developing shape optimizations [6] and more recently, modeling of biological systems in the life sciences [7]. Since there are a substantial number of books and papers on this subject, an exhaustive review of all available works on inverse problems is formidable. This literature review focuses on several general and classical techniques associated with the inverse heat conduction problems and provides context to the present state of their development.

Inverse heat conduction problems (IHCPs) are one of the most important applications associated with inverse analysis. In heat transfer processes, severe working conditions are often encountered that make direct boundary condition measurement difficult. Hence, the IHCP was originally considered as an approach to estimate the surface heat flux through the use of in-depth temperature measurements during the course of an experiment [8]. This problem originated in 1950s' as a response to the needs of the space program and aerospace industries. The Russian paper by Shumakov [9] in 1957 is the earliest research publication in the IHCP field. This

experimental study focused on the heating process associated with nose cones of missile, rocket nozzle and other devices. Another early IHCP paper was published in 1960 by Stolz [10]. This paper provides a numerical solution for resolving the surface heat flux in a quenching process. Although the IHCP was initially introduced by an aerospace engineering application, their relevance have broadened to include: nuclear reactor components [11], solidification of glass [12], and periodic heating in internal combustion engines [13].

Based on the type of causal characteristics to be estimated, IHCPs can be classified as: (1) boundary-value problem determination inverse problems, (2) initial-value determination inverse problems, (3) material property determination inverse problems, (4) source determination inverse problems and (5) shape determination inverse problems [14]. Boundary-value determination inverse problems involve resolving an unknown boundary condition based on in-depth temperature measurements or mixed in-depth temperature and other prescribed boundary conditions. The measured values are called internal responses. These responses are distributed and interpret as a discrete set of points. However, the selection of internal responses is not arbitrary as they should possess all system physics. For instance, characterizing a one-dimensional problem requires information from at least two distinct positions or overspecified at the back surface as required by the heat equation. References 15-18 contain several examples describing the applications for this category subset. For initial-value determination problems, a spatially distributed initial condition is not known. To estimate the initial temperature distribution, either the spatial temperature profile at a given time [19] or the temperature measurements on a part of boundary [20] are required to be specified. This class of problems is also referred to as the backward heat conduction problem. Material property determination

inverse problems focus on estimating system thermophysical properties, such as the thermal conductivity, specific heat capacity and/or thermal diffusivity, from temperature measurements taken from interior points [21, 22]. In general, these specifications may be functions of temperature or spatial coordinates. In the case of the source determination inverse problems, a successful reconstruction of the volumetric source requires identification in terms of magnitude, spatial distribution and temporal behavior. For this purpose, the temperature sensors are distributed over the spatial domain to collect the necessary data. The complexity of these problems depends on the functional form of the source. The prediction of a stationary source is relatively easy to obtain. However, predicting a moving source with varying intensity is difficult. Physical examples of such cases can be found in Refs. 23-25. The shape determination inverse problem can be additionally subdivided into two classes. The first class of problem is considered as a design problem. The boundary location and shape requires to be reconstructed such that either a specified temperature or heat flux can be recovered at some intended locations [26]. It is extremely difficult to recover the boundary shape if the sample is multiply connected. The other class of problem is termed as the Stefan problem. This class involves determining temperature distribution within a domain and the position of the moving interface between two phases in a body when all the other parameters characterizing the system are known [27].

1.2 Analytic Method for Inverse Heat Conduction

Generally speaking, a successful quasi-solution for an inverse heat conduction problem depends on its reformulation as a forward problem, which either has an exact analytical solution or can be resolved through an accurate numerical method. An objective function can then be

proposed to minimize the residual, which is normally referred as the difference between the discrete measurement set at fixed position and the computed result based on the forward problem at the identical position. The residue is expected to be small and uncorrelated if the analytical or numerical solution of the forward problem is close to the physical system under the estimated parameters [28]. Next, a proposed least-square method can be applied to retrieve these parameters of interest. A formulation of this descriptive procedure is normally instituted for resolving inverse heat conduction problems.

To find an analytical solution for the forward problem, commonly used methodologies include separation of variables [29], Laplace transformation [30-32], Green's function [33], and Duhamel's theorem [29, 33]. Separation of variables is one of the most common methods available and normally applied to linear partial differential equations [29]. This method is simple and easy to apply. It reduces the partial differential equation into a set of ordinary differential equations. However, application of this method possesses several restrictions. First, the partial differential equation describing the problem must be linear and homogeneous. If the field equation is satisfied by a specific function, then it must additionally be satisfied by the product of the specific function and an arbitrary constant. The boundary conditions must also be linear and homogeneous. If the system is a two-dimensional rectangle with four specified boundary conditions, at least three of them must be homogeneous. Otherwise, the superposition rule must be applied where repeated use of separation of variables is required. The last condition requires the domain to be a simple geometric shape in an orthogonal coordinate system.

The Laplace transformation technique has been widely used in the solution of time-dependent heat-conduction problems [30-33]. This transformation is defined in the semi-infinite domain and transforms time into the frequency domain. As a result, the partial derivative with respect to time can be removed from the field equation. The Laplace transformation technique has several merits. For the one-dimensional heat equation, the partial differential equation can be reduced to an ordinary differential equation by directly applying the Laplace transformation technique. For multi-dimensional heat equations, this technique can also be combined with other transformation techniques, such as the Fourier transform method, to obtain exact solutions. Feng et al. [30] have employed the Laplace transform technique to form a real-time prediction that relates the measured conditions at one end of a domain to the unknown conditions at the remote surface. Monde and Mitsutake [31], and Monde et al. [32] developed an analytical method available for both one-dimensional and two-dimensional inverse heat conduction problems based on the Laplace transformation. However, the application of Laplace transformation technique has some constraints. The inversion of the transformed quasi-solution is not straightforward if the inversion does not exist in the standard transformation table. Contour integration must be used in these cases.

The Green's function is the impulse response of an inhomogeneous differential equation defined on a domain, with specified initial conditions or boundary conditions [33]. If the superposition rule is available then the convolution of the Green's function with an arbitrary function on that domain can be considered as the solution to the inhomogeneous differential equation for the same function. This method is quite general in that all inhomogeneous problems are handled in the same way and the solutions for one-, two-, and three-dimensional problems

can be formally presented in a compact form. The principle difficulty in using the Green's function approach appears to be in deriving the appropriate Green's function for a given problem, as it depends on the coordinate system, boundary conditions and the extent of the region.

The extension of the Green's function method leads to the generation of Duhamel's theorem [29, 33] which provides a method for solving problems with time-dependent inhomogeneous terms. The function specification method proposed by Beck [34], Beck et al. [35] and Beck [36] is constructed from Duhamel's theorem. In this method, the exact temperature distribution can be expressed as a convolution of the surface heat flux with its corresponding thermal response from an impulsive heat flux. Afterwards, the functional form of surface heat flux in a small time step is approximated through a Taylor series expansion. A conventional least-square approach can then be used to minimize the residue in order to recover the local heat flux. This procedure can be repeated sequentially for the ensuing time step accuracy with high computational efficiency since it operates in a causal way. However, defining the length of the time step requires care in order for the method to remain stable. This stabilizing process, which is called "regularization", is actually required by all inverse problems due to being inherently unstable. Discussion on this aspect is postponed until later. Similar to the Green's function method, Duhamel's theorem requires knowledge of fundamental solutions.

A substantial effort has been placed on acquiring analytical solutions for inverse heat conduction problems. In 1964, Burggraf [37] formed an exact solution to a one-dimensional transient boundary-value inverse problem in a slab when the time-dependent temperature response was known at one internal point. Continuity was assumed in the derivation prior to

viewing data as discrete. The temperature function of the entire slab can be reconstructed from the local temperature and heat flux measurements with the aid of two accessory functions. Both the surface heat flux and temperature can then be directly reconstructed. It is interesting that no initial condition is needed for this solution. This follows from the assumption that both heat flux and temperature measurements are continuous and have been known for the complete time domain. This initial condition does not need to be uniform.

Although numerous analytical solution methods have been proposed for solving heat conduction problems, the number of analytical solutions is limited and only available for special cases. As an analytical compromise, approximate analytical solutions have been proposed as a substitution to the exact solutions. The Trefftz method, first presented in 1926, is an excellent example [38]. Trefftz's method forms an approximate solution through a linear combination of characteristic functions that satisfy the governing partial differential equation. The characteristic functions are termed as T-functions whose corresponding coefficients can be determined through some least-square approach satisfying the boundary and initial conditions. However, this methodology does not permit the existence of any volumetric source term. Another example is the integral transform technique [33], which provides a systematic, efficient, and straightforward approach for solving homogeneous and inhomogeneous, steady and time-dependent boundary-value problems of heat conduction. To manipulate this technique, it is necessary to make the integration through the spatial domain in order to reduce the partial derivatives with respective to the space variables in the field equation. A polynomial form can be chosen to represent the temperature distribution. The coefficient functions expressed in terms of time can easily be obtained from the resulting first-order, ordinary differential equation subject to the transformed

initial condition. One disadvantage of the integral technique is that the accuracy of the solution cannot be ensured all the times.

The Function Decomposition Method is a robust means of resolving ill-posed problems through approximate solutions, and proposed by Osborne, et al. [39]. This method is predicated by a functional representation for either the unknown surface temperature or surface heat flux, and, if necessary, followed by the application of Bellman's quasi-linearization technique. The dependent variable is then decomposed into a finite sum of functions defined in terms of a baseline function and a finite set of sensitivity functions. The decomposition results in a series of well-posed partial differential equations which can be resolved by the weighted-residual method using a spectral basis set for both space and time. Once the baseline function and sensitivity functions have been determined, a least-square method can be applied to obtain the sensitivity coefficients such that the unknown boundary condition can be reconstructed.

An alternative approach for resolving inverse heat conduction problems involves system calibration [40-45]. System calibration relies on analytical reasoning to form an apparent calibration or measurement equation. One major advantage of this approach is that the systematic errors can be substantially reduced since the probe position and thermophysical properties and sensor characteristics are implicitly included in the calibration tests. However, during the calibration process, the imposed net surface heat flux must be quantitatively known in advance if it is the goal to reconstruct the net surface heat flux for reconstructive test runs. Loehle et al. [40], Loehle et al. [41] and Gardarein et al. [42] have demonstrated the application of a calibration method that is based on system identification for estimating the surface heat flux using a single

in-depth sensor. The Non-Integer System Identification (NISI) method involves developing an impulse response function from a calibration test. A finite series expansion is formed in terms fractional derivatives of the measured calibration temperature and calibration surface heat flux. The unknown expansion coefficients are determined during the calibration stage. Next, the unknown surface heat flux can be recovered based on the impulsive response. In contrast, Frankel and Keyhani [43], Frankel et al. [44] and Elkins et al. [45] have proposed an alternative calibration methodology that eliminates the use of fractional derivatives and the resolution of expansion coefficients described by the NISI method. This method relates the net unknown surface heat flux to the calibration surface heat flux and the corresponding in-depth temperature measurements during the calibration test and reconstruction test runs. The resulting inverse statement is then expressed in terms of a Volterra integral equation of the first kind for the unknown surface heat flux.

Both proposed calibration methods are based on the constant property (linear) heat equation. Their application has been limited at small temperature differences from the initial state. However, for many practical applications, the assumption of constant thermophysical properties does not hold true due to a large temperature variation from its initial state. For example, in hypersonic flight, a large temperature variation is expected due to aerothermodynamic heating effects. Under this scenario, the variable thermophysical property effects can be significant depending on the material and temperature range. As a result, it is best that a new calibration method can be designed such that it can be applied in both a linear and nonlinear framework.

1.3 Numerical Methods for Inverse Heat Conduction

The forward solution or inverse prediction to heat conduction can also be generated by a purely numerical method. The most common method available is the finite difference method (FDM) [46]. In this technique, the heat conducting material is divided into discrete finite control volumes, upon which the energy balance is performed to determine the proper temperature relationship at each node. By marching forward in time, the spatial temperature distribution at every time step can be obtained. The finite difference method has explicit or implicit forms for marching time. The explicit form is direct and sequential. However, the length of its time step needs to be modulated in order to insure both convergence and stability. In contrast, the fully implicit form is not constrained by the time step for stability though its accuracy must be considered. The manipulation of the implicit form can be achieved by either matrix inversion or Gauss-Seidel iteration at each time step [46]. For example, Pourgholi et al. [47] resolved a two-dimensional inverse heat conduction problem through the finite difference method and used a least-square scheme to modulate and suppress the noisy data.

For inverse heat conduction problems, the finite difference method can also be reformulated into a space-marching form [48-50]. Similar to the conventional finite difference method, space marching finite difference methods discretize both the spatial and temporal domains. The only difference is that the calculation always starts from the sensor position, where both temperature and heat flux are assumed to be known, while the normal finite difference method needs both surface and initial conditions. In 1992, Carasso [48, 49] considered the space marching finite difference method for numerically resolving a nonlinear inverse heat conduction

problem. Carasso [49] presented a survey comparing different discretizations. Murio and Hinestroza [50] made use of this approach to identify the initial temperature distribution for the backward heat equation. Al-Khalidy [51] combined the space-marching finite difference method with a Savitzky-Gollay digital filter to predict the boundary condition. The filtering technique was used to suppress the high frequency noise contributions in the measurement.

The global-time treatment of the inverse heat conduction problem by Elkins et al. [52] is motivated by the space marching finite difference method. However, this method does not require the numerical computation of the temperature at spatial nodes. Instead of finite differencing each time derivative in spatial domain, the global time method presents the numerical solution in a functional form such that the thermal conditions between the probe site and surface can directly communicate. This approach works well for linear problems.

Another group of important numerical methods useful for solving direct and resolving inverse heat conduction problems includes the finite element method (FEM) and the boundary element method (BEM). The finite element method is based on the idea of dividing the complicated object into small and manageable pieces. On each element, the function is approximated by a characteristic form. This form is always represented by a linear combination of some shape functions, such as T-function [38]. The coefficients of these shape functions can be computed through (1) mean-square fitting of the approximated temperature field to the initial and boundary conditions, (2) least squaring the difference between the measurements and temperature approximation at probe sites, or (3) requiring temperature continuity from element to element though a heat flux jump is permitted. Boundary element methods are based on

Green's function approach. For this method, and in the context of linear analysis, discretization is only performed on boundary surface rather than the entire volume. As a result, the number of elements can be significantly reduced. Since the construction of basic solution includes the convolution between the boundary conditions and the fundamental solutions, the least-square process is only required for minimizing the difference between measurement and temperature approximation at the probe sites. These two numerical approaches have been successfully applied and demonstrated for resolving inverse heat conduction problems [53-56].

1.4 Iterative Methods for Inverse Heat Conduction

A well-presented group of the analytical and numerical solutions for the forward heat conduction problems have been introduced in the previous sections. However, their application in inverse heat conduction problems may be limited without the assistance of an optimization technique [28]. Optimization techniques are often referred as the parameter estimation approaches if the mathematical or numerical formulation of the physical process is known. Under this construct, it is best that the functional form of the unknown quantity for the IHCP be known a priori in order to minimize the number of unknown parameters. If not then the mathematical setting of the inverse problem requires an infinite dimensional space of functions. To make use of optimization techniques, an objective function should first be proposed. Minimization can be achieved by taking the first derivative of the objective function with respective to the parameters of interest and setting the results to zero. Moreover, a sensitivity matrix, whose components are always considered as the first derivative of measurement with respect to the unknown parameter, can be built for reformulating the minimization problem in a

closed matrix form. For linear problems, the sensitivity matrix is invariant and the parameter estimation can be achieved through simple matrix inversion in just one step. However, for complex nonlinear inverse heat conduction problems, an iterative procedure is necessary.

A Gauss method [57] is one of the simplest iterative procedures for resolving a nonlinear inverse heat conduction problem. This method represents the next estimation by a first order Taylor series expansion about the current estimation. The sensitivity matrix is also required to be evaluated at the current estimation and assumed invariant until next iterative step. This linearization allows for updating the parameter of interest. The iterative procedure of this method can be repeated until a stopping criterion is satisfied. Khajehpour et al. [58] combined the domain decomposition approach with the Gauss method for resolving nonlinear inverse heat conduction problems. In this process, both the time and spatial domains are divided into several sub-domains to overcome the nonlinearity. The Gauss method is then used at each sub-domain to predict the heat flux at the interface. However, the Gauss method is not able to ensure the existence of a unique solution if the columns of its corresponding sensitivity matrix are not linearly independent. This method is actually an approximation for the well-known Newton-Raphson method [28].

The conjugate gradient method [59] is another powerful iterative technique used for resolving both linear and nonlinear inverse problems. In the iterative procedure, at each step a suitable step size is chosen along a direction of descent in order to minimize the objective function. The direction of descent is represented by a linear combination of the negative gradient direction at the current step and the direction of descent from the previous iteration step. The

resulting angle between the direction of descent and the negative gradient direction should be smaller than ninety degrees. Zhou et al. [60] and Huang and Chen [61] used the conjugate gradient method for estimating the surface heating condition in a three-dimensional object. Hasanov and Pektas [62] identified an unknown time-dependent volumetric source term using the conjugate gradient method.

The Levenberg-Marquardt method [63] was first presented by Levenberg in 1944. This approach modifies the ordinary least-square norm with a penalty term that limits the variation in the parameter set at each step. Later, in 1963, Marquardt [64] derived basically the same technique but through a different approach. His intention was to arrive at an iteration method that will tend to the Gauss method in the neighborhood of the exact solution and tend to the steepest descent method if the estimation is far away from the exact solution. Compared to Gauss method, the Levenberg-Marquardt method possesses a major advantage as it can alleviate the effects of an ill-conditioned sensitivity matrix [59]. The Levenberg-Marquardt method was originally designed for nonlinear parameter estimation problems. More recently, it has been successfully demonstrated and applied to both linear and nonlinear inverse heat conduction problems. For example, Rouquette et al. [65] applied this technique to an electron beam welding study for estimating the parameters of the Gaussian heat source.

Iterative methods can be classified as gradient or deterministic. Gradient means that the computation is along a feasible search direction related to the local gradient direction. All of the iterative methods described above are considered as gradient type. However, some stochastic minimization techniques [66] also work well for inverse heat conduction problems. One good

example is the genetic algorithm [67]. This optimization technique starts with a randomly generated population of individuals. After entering a loop over the generations, one needs to evaluate the objective function with respect to each individual, and attributes a fitness ranking that will drive the selection process. Once this time consuming step is done, proper selection, crossover and mutation operators can be used in a sequential way to update the initial population. This iterative process can be repeated until the stopping criterion has been met. The application of this method is broad. Jones et al. [68] used genetic algorithms to locate inhomogeneities in a material by localizing variation in its thermal conductivity. In this process, an inverse heat conduction problem based on reconstruction of the thermal conductivity map was resolved through the temperature measurement in a two-dimensional surface. A standard genetic algorithm minimizes the error between measured and estimated temperature. Successive zooming was applied around the identified inhomogeneities to finesse the conductivity map. Verma and Balaji [69] studied the combined inverse heat conduction and inverse radiative heat transfer problem with genetic algorithms. Three properties, including surface emissivity, optical thickness and radiation parameter were estimated based on in-depth temperature measurements using a one-dimensional model. Raudensky et al. [70] determined a transient heat transfer coefficient in a one-dimensional inverse heat conduction problem. The objective function chosen minimized the error between estimated and measured temperature profiles with the aid of a genetic algorithm. A penalty term was added for the regularization when the heat transfer coefficient varied too abruptly. In this case, regularization is used to control stability.

In addition, the rapid development of artificial neural network technology [71] has lead to an entirely new approach for resolving IHCPs. Neural networks are artificial intelligence systems

that mimic the biological processes of a human brain by using non-linear processing units to simulate the functions of the biological neurons. The processing units are fully interconnected by joints of invariable strength that mimic the synaptic behavior of the human brain. As a result, neural networks have a self-learning function, which can be achieved through training. The process is similar to how the human brain comprehends new things. Neither the analytical solution nor the numerical process needs to be understood in advanced for the inverse process. However, it is still necessary to know the causality of the system. Otherwise, the training will not be successful. For example, Deng and Hwang [72] presented a real-time method for processing temperature data to resolve an inverse heat conduction problem by training through a neural network set. In this process, the local temperature measurement is considered as input and the real-time heat flux is considered as output. After sufficient training, an accurate approximate relationship between the input and output can be built. Filtering techniques [73] are also preferred to aid stabilizing the result.

1.5 Regularization for Stability Augmentation

All inverse problems are difficult to resolve since they are mathematically ill-posed [8]. Unlike forward mathematical problems that possess unique and stable solutions with respect to the input data, inverse problems display significant error magnification when small errors are present in the input. This magnification quickly destabilizes the prediction. To deal with this situation, special techniques are required for introducing regularization [74-90]. Here regularization refers to stabilization.

Filtering has been demonstrated as an effective regularization approach. A Gauss low-pass digital filter [74] devised from Fourier convolution principles removes high frequency noise in a manner that retains smoothness in the first time derivative of the filtered data. The regularization parameter for this filter is the cutoff frequency, which corresponds to the region near the elbow of a power spectrum formed by the discrete Fourier transformation. Wiener's filtering principle can be used to estimate this parameter. Elkins et al. [52] showed that this filtering technique provides excellent results for inverse heat conduction problems when combined with the global-time method. Generalizing Gauss digital filter leads to the concept of mollification [75]. Here, the basic idea is to convolute noisy data with a smooth function possessing a tunable parameter that filters the high frequency component of the noisy data, such that the problem reappears as well-posed. For Gauss digital filtering, the smooth functions are the Gaussian functions which possess a key property when commuting between frequency and time domain, i.e., self reciprocation.

The Kalman filter method uses a set of mathematical equations that provides an efficient computational solution of the least-square method [76]. It estimates a process using a form of feedback control. To be precise, it estimates the process state at some time and then obtains feedback in the form of the noisy measurement. Hence, the Kalman filter can be classified as a time update and measurement update scheme. The time update projects the current state forward to obtain a priori estimate while the measurement update incorporates a new measurement into the a priori estimate to obtain an improved a posteriori estimate. For example, when the Kalman filter is applied to remove high frequency noise in temperature measurements, the predicted temperature in future time steps can be obtained through a Taylor series expansion about the past

filtered temperature data which are assumed to be known. The noisy temperature measurements can then be used to update these predictions. In this process, an optimal scaling parameter is required to minimize the difference between the updated prediction and exact temperature data according to probability theory. This technique is both simple and straightforward, takes explicit measurement uncertainty incrementally, and explains the a priori information. Ijaz et al. [77] employed a Kalman filter to resolve a two-dimensional transient inverse heat conduction problem. LeBreux et al. [78] combined a Kalman filter for improved state estimation with a recursive least-squares estimator to predict the dynamic wall thickness of a furnace.

Additionally, some other regularization approaches have been designed to control system instability thereby transforming an ill-posed problem into a well-posed one. The Lamm's local future-time method [86] is based on conventional theory that a Volterra equation of first kind, which is ill-posed, can be approximately transformed into a Volterra equation of second kind, which is well-posed. The name "future time" is actually the regularization parameter to be specified. Frankel et al. [43-45] have showed that if the heat flux is held constant in some amount of future time, then an accurate surface heat flux prediction can be resolved through the calibration integral equation method without filtering the temperature data.

Singular-value decomposition (SVD) is a well understood and easily implemented method that has been widely accepted for resolving inverse problems. It is well-known that the sensitivity matrices for inverse problems are ill-conditioned. Direct inversion leads to unstable results. SVD works through decomposing the sensitivity matrix into two new orthogonal matrices and one diagonal matrix whose diagonal elements (singular values) are arranged in a

descending sequence. The ill-conditiong of the sensitivity matrix comes from small singular values since they contribute little to the recovery of physics but their reciprocals significantly amplify the measurement noise. Therefore, for this technique, a condition number of reduced dimension is defined as the regularization parameter. Once the ratio between the first diagonal element and any other element is beyond a defined conditional number, this element must be truncated from the diagonal matrix. After that, the pseudo inversion process can alleviate the instability from ill-posed problems while retaining sufficient physics. The SVD can be operated in either global or sequential way. Shenefelt et al. [80] applied a global singular-value decomposition method to the matrix form of Duhamel's principle in order to resolve a linear inverse heat conduction problem possessing temperature data containing significant noise. Garcia et al. [81] analyzed a nonlinear two-dimensional inverse heat conduction problem by sequential singular value decomposition.

Tikhonov regularization method [82], named after Andrey Tikhonov, is perhaps the most commonly used regularization method for ill-posed problems. Similar to the Levenberg-Marquardt method, this regularization method constructs a modified objective function seeking to minimize the sum of the L_2 norm of the residue and the L_2 norm of the penalty norm. The penalty norm is designed for controlling system instability and can be expressed in terms of the predictive function or its derivative. To balance the bias and variance, the penalty norm needs to be weighted by a regularization parameter to ensure that both two terms involved in the objective function are comparable. However, searching an optimal regularization parameter remains nontrivial. Several approaches have been proposed for this purpose, including L-curve analysis [83], Morozov's discrepancy principle [84] and maximum likelihood methods [85]. Similar to

the singular-value decomposition method, the Tikhonov regularization method can be formulated in a sequential way. Both Lamm [86] and Berntsson [87] have demonstrated this formulation. In their approaches, a limited number of past predictions are retained. A new smaller problem is then formulated by incorporating the prior known information and a small set of available data in the future time. After removing the internal responses of the past predictions from the measurements, new predictions for the future time can be obtained through the Tikhonov regularization method. To ensure the accuracy at each step, only the first value of the prediction is retained such that these formulations operate in a sequential way.

Alifanov's iterative regularization [89] is another approach available as a regularization scheme. In this approach, the number of iterations is chosen so that reasonably stable solutions are obtained. Therefore, as opposed to Tikhonov regularization method, there is no need to modify the original objective function with a penalty term though it is still based on the L_2 norm of the residue. The unknown function is not required to be discretized a priori since all the required mathematical derivations with Alifanov's iterative regularization approach are made in the space of functions. The discretization of the function, resulting from the fact that measurements are taken at discrete times and positions, is then only made a posteriori. This iterative regularization approach is quite general and can be applied to both linear and nonlinear inverse problems. Jarny et al. [88] used the Alifanov's iterative regularization to resolve a multidimensional inverse heat conduction problem. Alifanov [89] applied his method for designing and testing heat-loaded engineering objects.

Bayesian regularization is a statistical inference using a posteriori probability density function. This function is the model for evaluating the conditional probability density for the unknown parameters given the measurements [90]. It relies fundamentally on the principles of the Bayesian statistics for stabilizing the prediction of the inverse problem. Compared with the common Tikhonov regularization methods, the penalty term in Bayesian regularization is designed to yield error estimates that would have a reasonable statistical interpretation rather than just focusing on a stabilized form of the original objective function. This objective function is denoted as the maximum a posteriori (MAP) objective function, meaning that its minimization corresponds to the maximization of the a posteriori error distribution. Deng and Hwang [73] have shown that the Bayesian regularization method can be combined with neural networks for resolving inverse heat conduction problems.

As noted in this literature survey, numerous techniques have been proposed for resolving inverse heat conduction problems over the past 50 years by the international community. A glaring commonality exists among all methods. That is, the identification of the optimal regularization parameter is critical to the success of any method.

1.6 Thermophysical Properties Identification

Quantitative understanding of heat transfer in industrial applications requires accurate knowledge of thermophysical properties, such as the thermal diffusivity and thermal conductivity. The magnitude of these properties significantly impacts the temperature distribution and heat transfer in a material during heating and cooling studies associated with direct analysis.

Additionally, thermophysical properties strongly affect the stability of the inverse heat conduction problem. For example, in inverse problems, the optimal selection of thermal protection systems depends on the ability to accurately predict the surface thermal condition based on in-depth temperature measurements. Also, the system reliability strongly depends on the accuracy and understanding of the thermophysical properties during the preparation and fabrication of the TPS. Accurate estimation of temperature-dependent thermophysical properties is a non-trivial task. Difficulties include: (1) thermophysical properties are a function of temperature; hence the resulting heat equation used to retrieve these unknown properties become nonlinear; (2) the identification of thermophysical properties is sensitive to measurement uncertainty; and, (3) the accuracy of the estimation is related the quality and accuracy of the defined boundary conditions and sensor locations. Fortunately, many theoretical and experimental methods have been proposed for this purpose, including steady-state methods, probe methods, periodic heating methods, pulse heating methods and least-square methods.

The steady-state method [91] is a relatively simple method for deducing thermal conductivity. Beck et al. [92] applied this method for estimating the thermal conductivity of rocks. In this process, a rock disk is prepared and introduced between two well characterized cylindrical metal bars. Heat is then supplied to the remote end of one bar while the remote end of the other is cooled with thermostatically controlled water. Temperature measurements are made along the bars after steady state is reached. The thermal conductivity is determined in terms of the conductivity of the bars which are assumed to be well characterized and known. The probe method [93] is a transient method for both thermal conductivity and thermal diffusivity. It estimates the thermophysical properties using the following steps. A body (the “probe”

containing heat-source and thermometer) of known dimensions and thermophysical properties is immersed into a medium whose thermophysical properties are unknown. With the aid of suitable theoretical relations, these properties are then calculated from a record of the "probe" temperature versus elapsed time. Herzen [94] successfully applied this probe method for estimating the thermal conductivity of deep-sea sediments while Lobo and Cohen [95] made use of it for measuring the thermal conductivity of polymer melts. The periodic heating method [96-98] uses a well-defined periodic heat source to excite a time-dependent temperature distribution in a sample. The temperature difference between two locations along a one-dimensional sample or the apparent phase lag can be used to extract the thermal diffusivity of the material. Additionally, the temperature at different modulation frequencies instead of different locations is also available to obtain the same property estimation. This periodic heating method is particularly suitable for thin films. For example, Coufal and Hefferle [96], Kato et al. [97] applied this method to measure the thermal diffusivity of thin films using various calorimeters.

A representative and classical pulse heating approach for estimating thermal diffusivity is the Flash method [98]. This method utilizes the exact temperature solution of the linear heat equation for a thermally insulated solid exposed to a pulse of radiant energy impacting the front surface. Parker et al. [98] proposed this means of estimating thermal diffusivity based on a single graphical representation involving a dimensionless backside temperature versus dimensionless time plot. This method is appealing as knowledge of the amount of energy absorbed at the front surface is not required for estimating the thermal diffusivity. However, the energy input must be specified when estimating the thermal conductivity. The Flash method is popular and has received s significant amount of attention over the past 50 years. Clark and Taylor [99]

investigated radiation heat loss associated with Flash method in a high temperature range and provided an experimental basis for evaluating radiation heat losses and forming a correction procedure. James [100] extended the Flash method to other one-dimensional heat conduction problems for measuring thermal diffusivity. James [100] considered one-dimensional heat conduction through slabs of two materials in direct thermal contact. In his process, the Laplace transformation technique is used to obtain the temperature in the frequency domain. However, instead of inverting the transform through integration in the complex plane, a convenient expansion of the transform is presented that permits term-by term inversion using a standard Laplace transform table. Baba and Ono [101] improved the Flash method to reduce uncertainty in thermal diffusivity measurements of solid materials above room temperature. This revised laser Flash method is constructed based on following technical improvements: (1) introducing laser source that achieves near uniform pulse heating (decreasing the error due to non-uniform heating); (2) including a fast infrared radiation thermometer (decreasing the error due to nonlinear temperature detection); and, (3) introducing a curve-fitting method for data analysis using the temperature history (decreasing the heat loss error). Gaal et al. [102] utilized the original Flash method for estimating the thermal conductivity measurement. In their interpretation, the heat capacity is obtained through calibration. In principle, this process involves testing a sample with known heat capacity and then replacing it with the sample with unknown capacity in the same apparatus. The magnitudes of both resulting temperature curves are then compared for estimating the unknown heat capacity. Sato and Taira [103] measured the thermal conductivity of $GdVO_4$, YVO_4, and $Y_3Al_5O_{12}$ by a quasi-one-dimensional Flash method. The quasi-one-dimensional concept is introduced for simplifying three-dimensional thermal diffusion effects.

The least-square method is the most common approach for parameter estimation [104-110]. A significant amount of attention has been directed toward this approach since it is suitable to any experimental situation that can utilize either analytical or numerical solutions. After the initial guess is provided, optimization methods are introduced for updating the parameter space that minimizes the difference between the experimental results and the model solution. The thermal diffusivity and thermal conductivity can simultaneously be determined by successive iteration. Monde and Mitsutake [104] solved for the unknown thermal diffusivity based an inverse reconstruction prediction. The inverse prediction resolves the surface temperature based on in-depth temperature measurements. After the initial guess is supplied, an update for the next iteration is calculated through the comparison between two surface temperature predictions corresponding to two different probe sites. Sawaf and Ozisik [21] estimated the linearly temperature-dependent thermal conductivity components and heat capacity of an orthotropic medium through the combination of numerical solution and the Levenberg-Marquardt iterative procedure. Huang and Yan [105] utilized the conjugate gradient method of minimization and the adjoint equation in the optimization process such that the temperature-dependent thermal conductivity and heat capacity can be simultaneously estimated. Battaglia et al. [106] indentified thermophysical properties from a metallic thin layer deposited on a silicon substrate through the combination of a Bayesian technique based on Monte Carlo Markov Chain and the Levenberg-Marquardt technique. In this process, the thermal conductivity of the layer; the thermal resistance at the interface between the layer and substrate; and, the extension of the heat source at the initial temperature can simultaneously be identified. Chen and Lin [107] applied a hybrid numerical algorithm combining the Laplace transform technique and the control-volume method for simultaneously estimating the temperature-dependent thermal conductivity and heat capacity

from in-depth temperature measurements. Finally, Darcia and Scott [108, 109] applied genetic algorithms for simultaneously estimating thermophysical properties. This brief literature review illustrates the vast choices of methods developed for estimating the thermophysical properties based on inverse methods.

1.7 The Scope of Research

The previous sections presented a literature review describing the state of the recent approaches for resolving inverse heat conduction for variety of physical applications. Additionally, several noticeable gaps were identified involving fully nonlinear systems. This dissertation describes a systematic investigation to fill these gaps by expanding the calibration methodology initially proposed in Ref [43-45] to both nonlinear inverse heat conduction problems and thermophysical property estimation based on rescaling principles.

Chapter 2 introduces the linear one-probe calibration method [43-45] relating the unknown surface (net) heat flux/temperature to a single in-depth temperature measurement for the one-dimensional heat equation. This formulation is applicable to constant backside thermophysical properties with a passive side boundary condition that maintains a constant heat transfer coefficient between the calibration and reconstruction tests. The final mathematical expression for the inverse statement appears as a Volterra integral equation of the first kind for the unknown surface (net) heat flux or temperature in the reconstruction test. Regularization is required for extracting an optimal prediction. The chapter is the basis of the dissertation. The calibration approach is used in all future chapters.

Chapter 3 generalizes the one-probe linear calibration method to a nonlinear framework. A time domain rescaling principle is combined with the Kirchhoff transform to form a quasi-linearization of the mathematical system. In this process, the Kirchhoff transformation is exploited for linearizing temperature in the thermal conductivity. Time domain rescaling is incorporated for linearizing the temperature-dependent thermal diffusivity. The reliability of this quasi-linearization lies in the piecewise time-step linearization assumption. That is, at each time step, the thermophysical properties are held constant throughout the spatial domain though they are allowed to vary with advancing time. The rescaled forms are then resolved through the calibration framework. The modified calibration method will be shown to work well for a variety of practical isotropic materials.

Chapter 4 introduces the two-probe calibration method for nonlinear one-dimensional inverse heat conduction. This method combines the attributes of the linear two-probe calibration formulation [111] with the nonlinear one-probe calibration equation [112]. Unlike the one-probe calibration method, two distinct calibration tests are required in the test campaign. In this way, the back boundary condition does not need to be passive and can varying among all tests (calibration and reconstruction). The final calibration equation is also expressed in terms of a Volterra integral equation of the first kind. However, additional attention is required as the kernel is more sensitive to noise than the one-probe system. A reduction of the ill-conditioning effects imposed by the kernel requires a careful design of the back boundary condition for the calibration tests. Results verify that a combination of cooling (first calibration test) and heating (second calibration test) back boundary conditions form an improved kernel for resolving the surface (net) heat flux.

Chapter 5 introduces another version of nonlinear one-probe calibration method and a new strategy for estimating the optimal regularization parameter. This new calibration method linearizes the thermal conductivity through heat flux rescaling rather than the Kirchhoff transformation. The optimal regularization parameter search strategy is implemented independent of the applied regularization approach. This new search strategy is shown to be applicable regularization methods. This new strategy uses a Gaussian filtering of the probe temperature data sets for estimating the variance in the group of predictions. The best regularization parameters are obtained by balancing the weighted bias and variance. The effectiveness of this method is examined through three common regularization approaches. Encouraging results are consistently observed in presence of a significant noise. The over-smoothness involved in the final prediction is avoided while the stability is still maintained.

Chapter 6 applies the described calibration principle for estimating unknown thermophysical properties above room temperature. The estimation of thermophysical properties is also an inverse problem in the classical sense though it is less sensitive to noise than inverse heat conduction problems. This approach utilizes a single in-depth temperature measurement and a known set of boundary conditions. To acquire both the thermal diffusivity and thermal conductivity, two distinct stages are proposed for extracting these temperature-dependent properties. The first stage uses a temperature calibration equation for estimating the unknown thermal diffusivity. This process determines the thermal diffusivity by minimizing the residual of the temperature calibration equation with respect to the thermal diffusivity. The second stage uses the estimated thermal diffusivity and a heat flux calibration equation for estimating the unknown thermal conductivity. This stage produces the desired thermal conductivity by

minimizing the residual of the heat flux calibration equation with respect to the thermal conductivity. Results verify that the proposed estimation process works well in presence of significant noise for two test representative materials.

Chapter 7 provides general conclusions and recommendations for future research that is suggested by the merits of this investigation.

Chapter 2: Introduction to a Surface Heat Flux and Temperature Calibration Formulation

This chapter revisits previously published works [43-45] for introducing the concept of inverse heat conduction. The derivations for both the one-probe surface heat flux and temperature calibration equations are presented based on exact analytical solutions.

2.1 Definition of Inverse Heat Conduction in a One-Dimensional Slab

Physical theories that can be mathematically formulated in term of functional equations permit outcomes to be predicted based on the provided inputs. This defines the conventional forward direct problem normally proposed in physical studies. In contrast, the inverse problem consists of using the actual measurements from a sensor to infer the values of the inputs that characterize the system [1]. The difference between the forward direct problem and the inverse problem is presented in Fig. 2.1.1. Inverse problems lie at the heart of scientific inquiry and technological development. Inverse heat conduction problems (IHCP's) are one of the most important applications associated with inverse studies. In heat transfer processes, severe working conditions are often encountered that make direct boundary condition measurement be difficult. The IHCP was originally considered as an approach for estimating the surface heat flux through the use of in-depth temperature measurements during the course of an experiment [8]. This problem originated in 1950's as a response to the needs of the space program and aerospace industries. In 1957, the Russian scientist Shumakov [9] published the earliest research paper in

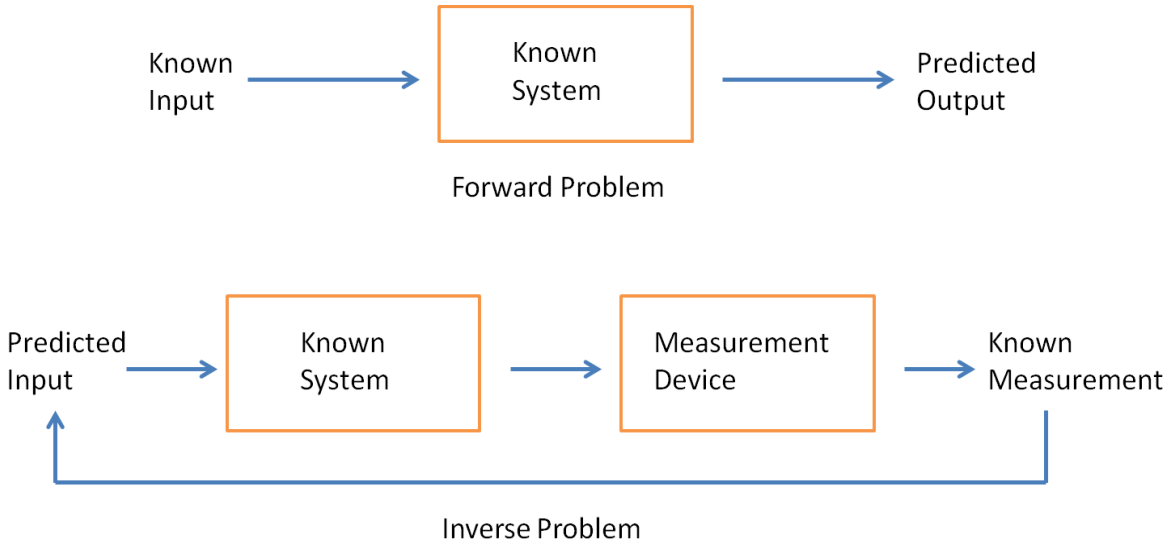

Figure 2.1.1: The difference between the forward and the inverse problems.

the field of IHCP's. Stolz [10] published another early IHCP paper in 1960 that provides a numerical solution for resolving the surface heat flux in a quenching process. Presently, the application of IHCP's has broadened to various fields, including: nuclear reactor components [11], solidification of glass [12], and periodic heating in internal combustion engines [13].

In this chapter, we consider a one-dimensional heat conduction problem in the Cartesian coordinates having a front surface heat flux source at $x = 0$ and an adiabatic back surface at $x = L$. The geometric configuration is displayed in Fig. 2.1.2. This basic geometry and back boundary condition specification are often used in aerothermal applications [115]. The inverse problem under consideration involves resolving the net surface heat flux, $q"(0,t)$ based on a thermocouple located at $x = b$ with adiabatic condition at $x = L$.

If the density ρ; specific heat c_p; and, thermal conductivity k are assumed constant then the heat equation is [33]

$$\frac{1}{\alpha}\frac{\partial T}{\partial t}(x,t) = \frac{\partial^2 T}{\partial x^2}(x,t), \qquad x \in (0,L), \quad t \geq 0, \qquad (2.1.1a)$$

where T is the temperature; x is the spatial variable; t is the time variable; α represents the thermal diffusivity, $\alpha \triangleq k/(\rho c_p)$; and, L is the slab thickness. The Type equation here.boundary conditions are given as

$$-k\frac{\partial T}{\partial x}(0,t) \triangleq q"(0,t) = q"_s(t), \qquad (2.1.1b)$$

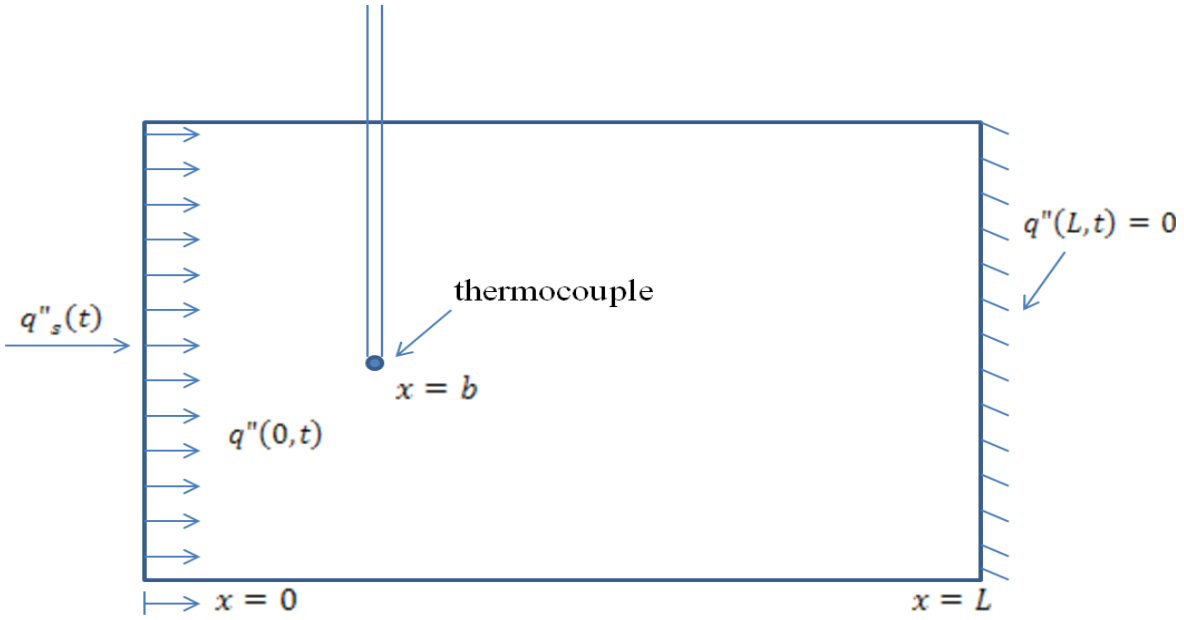

Figure 2.1.2: System setup for the one-dimensional heat conduction problem showing adiabatic back boundary and the thermocouple position.

$$k\frac{\partial T}{\partial x}(L,t)=0, \qquad t\geq 0, \tag{2.1.1c}$$

where $q"(0,t)$ is the net surface heat flux entering the body per Fig 2.1.2 while $q"_s(t)$ describes the total surface heat flux externally contacting at $x=0$. The initial condition is given as

$$T(x,0)=0, \qquad x\in[0,L]. \tag{2.1.1d}$$

The direct solution for the temperature distribution, $T(x,t)$ and heat flux distribution, $q"(x,t)$ can be obtained by a classic integral transform technique [33].

2.2 One-Probe Calibration Equation for Surface Heat Flux in a Linear Framework

The derivation of the linear temperature calibration equation follows the approach of Frankel and Keyhani [43-45]. The Laplace transform is introduced to Eq. (2.1.1a) as

$$\frac{1}{\alpha}\mathcal{L}\left\{\frac{\partial T}{\partial t}(x,t)\right\}=\mathcal{L}\left\{\frac{\partial^2 T}{\partial x^2}(x,t)\right\}, \quad x\in(0,L), \quad t\geq 0, \tag{2.2.1a}$$

based on its definition [31]

$$\mathcal{L}\{f(t)\}=\hat{f}(s)\triangleq\int_{t=0}^{\infty}f(t)e^{-st}dt, \qquad Re(s)\geq 0, \tag{2.2.1b}$$

where "s" is a complex variable having units, 1/s and $\hat{f}(s)$ is the image of $f(t)$ in the frequency domain [31]. This procedure transforms the original partial differential equation given by Eq. (2.1.1a) into the linear ordinary differential equation

$$\frac{d^2\hat{T}}{dx^2}(x,s) - \frac{s}{\alpha}\hat{T}(x,s) = 0, \quad x \in (0,L), \quad Re(s) \geq 0, \tag{2.2.2}$$

where $\hat{T}(x,s)$ is the Laplace transformed function of $T(x,t)$.

The general solution of Eq. (2.2.2) is

$$\hat{T}(x,s) = A_q(s)cosh\sqrt{\frac{s}{\alpha}}x + B_q(s)sinh\sqrt{\frac{s}{\alpha}}x, \quad x \in (0,L), \ Re(s) \geq 0, \tag{2.2.3}$$

where $A_q(s)$ and $B_q(s)$ are unknown coefficients. Their evaluation requires taking the Laplace transformation of both auxiliary conditions given by Eq. (2.1.1b) and Eq. (2.1.1c). Doing so produces

$$\mathcal{L}\left\{k\frac{\partial T}{\partial x}(0,t)\right\} = k\sqrt{\frac{s}{\alpha}}B_q(s) = -\hat{q}"(0,s), \quad Re(s) \geq 0, \tag{2.2.4a}$$

$$\mathcal{L}\left\{k\frac{\partial T}{\partial x}(L,t)\right\} = k\sqrt{\frac{s}{\alpha}}\left[A_q(s)sinh\sqrt{\frac{s}{\alpha}}L + B_q(s)cosh\sqrt{\frac{s}{\alpha}}L\right] = 0, \quad Re(s) \geq 0, \tag{2.2.4b}$$

respectively.

The unknown coefficients $A_p(s)$ and $B_p(s)$ can be expressed in terms of these two boundary conditions as

$$A_q(s) = \frac{1}{k}\sqrt{\frac{\alpha}{s}}coth\left(\sqrt{\frac{s}{\alpha}}L\right)\hat{q}"(0,s), \tag{2.2.5a}$$

$$B_q(s) = -\frac{1}{k}\sqrt{\frac{\alpha}{s}}\hat{q}"(0,s). \tag{2.2.5b}$$

Upon substituting Eqs. (2.2.5a, b) into Eq. (2.2.3), we obtain

$$\hat{T}(x,s) = \hat{D}_{q,q}(x,\alpha,k,s,L)\hat{q}"(0,s), \quad x \in (0,L), \quad Re(s) \geq 0, \tag{2.2.6a}$$

where

$$\hat{D}_{q,q}(x,\alpha,k,s,L) = \frac{1}{k}\sqrt{\frac{\alpha}{s}}\left(coth\left(\sqrt{\frac{s}{\alpha}}L\right)cosh\left(\sqrt{\frac{s}{\alpha}}x\right) - sinh\left(\sqrt{\frac{s}{\alpha}}x\right)\right),$$

$$x \in (0,L), \quad Re(s) \geq 0. \tag{2.2.6b}$$

Equation (2.2.6b) represents the exact "forward" or "direct" transformation solution for an impulsive surface heat flux. Implementing the inverse Laplace transformation would produce the exact solution in the time domain. The heat flux distribution, $q"(x,t)$ could be recovered through Fourier's law.

It is necessary to note that the impulsive function $\widehat{D}_{q,q}(x,\alpha,k,s,L)$ in the frequency domain is solely function of the thermophysical properties and system configuration. As a result, if these parameters are assumed fixed throughout a test campaign then it is possible to eliminate $\widehat{D}_{q,q}(x,\alpha,k,s,L)$ through a calibration test whose surface condition is known. For this purpose, the subscripts "c" and "r" are defined and introduced to represent the calibration and reconstruction tests, respectively. The term $\widehat{D}_{q,q}(x,\alpha,k,s,L)$ can be isolated in terms of an input-output relationship and thus represented by the transfer function

$$\widehat{D}_{q,q}(x,\alpha,k,s,L)=\frac{\hat{T}(x,s)}{\hat{q}"(0,s)}. \tag{2.2.7a}$$

Due to the assumption of consistent system parameters, it is possible to eliminate this function based on experimental data in the calibration test. Next, we evaluate Eq. (2.2.7a) at the inserted probe position $x=b$ to get

$$\widehat{D}_{q,q}(b,\alpha,k,s,L)=\frac{\hat{T}_c(b,s)}{\hat{q}"_c(0,s)}. \tag{2.2.7b}$$

Upon substituting Eq. (2.2.7b) into Eq. (2.2.6a) after evaluation at $x=b$ and taking its inverse Laplace transform, we formally obtain

$$\mathcal{L}^{-1}\left(\hat{q}"_r(0,s)\hat{T}_c(b,s)\right)=\mathcal{L}^{-1}\left(\hat{q}"_c(0,s)\hat{T}_r(b,s)\right), \tag{2.2.8}$$

where the inverse Laplace transform operator $\mathcal{L}^{-1}$ is defined with the aid of the convolution theorem [31] through

$$\mathcal{L}^{-1}\left(\hat{f}_1(s)\hat{f}_2(s)\right) = \int_{u=0}^{t} f_1(u) f_2(t-u)\, du, \qquad t \geq 0. \tag{2.2.9}$$

Finally, Eq. (2.2.8) is explicitly expressible in time domain [43-45] as

$$\int_{u=0}^{t} q"_r(0,u) T_c\,(b, t-u) du = \int_{u=0}^{t} q"_c(0,u) T_r\,(b, t-u) du, \quad b \in [0, L], \quad t \geq 0. \tag{2.2.10}$$

This one probe linear calibration equation relates the net unknown surface heat flux to the calibration surface heat flux and the corresponding in-depth temperature measurements during the calibration and reconstruction tests. The resulting inverse statement is expressed in terms of a Volterra integral equation of the first kind for the unknown surface heat flux and hence is ill-posed and will require regularization. This calibration method in linear framework has been experimentally verified with excellent accuracy at low temperatures [45]. In addition, though this derivation is based on an adiabatic back boundary condition, it is also suitable for either a semi-infinite geometry or a slab with a fixed heat transfer coefficient at the back-face under the uniform initial condition assumption.

2.3 One-Probe Calibration Equation for Surface Temperature

To derive the one-probe calibration equation for the surface temperature, the surface heat flux boundary condition at $x = 0$ given by Eq. (2.1.1b) is replaced by the temperature boundary condition

$$T(0,t) \triangleq T_s(t), \qquad t \geq 0, \tag{2.3.1}$$

where $T_s(t)$ describes the surface temperature at $x = 0$. The Laplace transform can then be applied to Eq. (2.1.1a) to produce the general solution

$$\hat{T}(x,s) = A_T(s)cosh\sqrt{\frac{s}{\alpha}}x + B_T(s)sinh\sqrt{\frac{s}{\alpha}}x, \quad x \in (0,L), \ Re(s) \geq 0. \tag{2.3.2}$$

where $A_T(s)$ and $B_T(s)$ are undetermined coefficients to be obtained through the transformed boundary conditions Eq. (2.3.1) and Eq. (2.1.1c). Utilizing these boundary conditions produce

$$\hat{T}(0,s) = \hat{T}_s(s) = A_T(s), \qquad Re(s) \geq 0, \tag{2.3.3a}$$

$$\mathcal{L}\left\{k\frac{\partial T}{\partial x}(L,t)\right\} = k\sqrt{\frac{s}{\alpha}}\left[A_T(s)sinh\sqrt{\frac{s}{\alpha}}L + B_T(s)cosh\sqrt{\frac{s}{\alpha}}L\right] = 0, \quad Re(s) \geq 0, \tag{2.3.3b}$$

respectively.

The unknown coefficients $A_T(s)$ and $B_T(s)$ can then be expressed in terms of these two boundary conditions as

$$A_T(s) = \hat{T}(0,s), \tag{2.3.4a}$$

$$B_T(s) = -\hat{T}(0,s)tanh\sqrt{\frac{s}{\alpha}}L. \tag{2.3.4b}$$

Upon substituting Eqs. (2.3.4a, b) into Eq. (2.3.2), we obtain

$$\hat{T}(x,s) = \hat{D}_{T,T}(x,\alpha,s,L)\hat{T}(0,s), \quad x \in (0,L), \quad Re(s) \geq 0, \tag{2.3.5a}$$

where

$$\hat{D}_{T,T}(x,\alpha,s,L) = cosh\left(\sqrt{\frac{s}{\alpha}}x\right) - tanh\left(\sqrt{\frac{s}{\alpha}}L\right) sinh\left(\sqrt{\frac{s}{\alpha}}x\right),$$
$$x \in (0,L), \quad Re(s) \geq 0. \tag{2.3.5b}$$

The impulsive transfer function $\hat{D}_{T,T}(x,\alpha,s)$ in the frequency domain can also be incorporated in a calibration test when the in-depth probe is located at $x = b$. Doing so produces

$$\hat{D}_{T,T}(b,\alpha,s,L) = \frac{\hat{T}(b,s)}{\hat{T}(0,s)}, \tag{2.3.6}$$

where all four system parameters (b, α, s, L) are explicitly contained in the transfer function. As before, the impulsive transfer function can be removed in terms of calibration data assuming that these parameters remain unchanged among all tests. Therefore, Eq. (2.3.6) can equivalently expressed as

$$\frac{\hat{T}_c(b,s)}{\hat{T}_c(0,s)} = \frac{\hat{T}_r(b,s)}{\hat{T}_r(0,s)}, \qquad Re(s) \geq 0, \tag{2.3.7}$$

where $\hat{T}_r(0,s)$ represents the unknown surface temperature to be resolved and expressed in the frequency domain. To obtain a time-varying functional equation, we introduce the convolution theorem to invert Eq. (2.3.7). Doing so produces

$$\int_{u=0}^{t} T_r(0,u) T_c(b,t-u) du = \int_{u=0}^{t} T_c(0,u) T_r(b,t-u) du, \quad b \in [0,L], \quad t \geq 0. \tag{2.3.8}$$

Similar to the one-probe linear calibration equation for surface heat flux presented in Section 2.2, the linear calibration equation for temperature has a broader geometrical application. It is suitable for either a semi-infinite geometry or a slab with a fixed heat transfer coefficient at the back surface under the uniform initial condition assumption.

Chapter 3: A Nonlinear Surface Heat Flux Calibration Method based on Kirchhoff Transformation and Rescaling Principles

This chapter is a revised version of the paper published by Yinyuan Chen, Jay I. Frankel and Majid Keyhani:

Chen, Y.Y., Frankel, J.I., and Keyhani, M., 2014, "A New Nonlinear Surface Heat Flux Calibration Method based on Kirchhoff Transformation and Rescaling Principles," Inverse Problems in Science and Engineering, Vol. 22, No.8, pp. 1394-1421.

My primary contributions to this paper include (1) conceptualization of the new model, (2) development of numerical and regularization methods (3) writing and implementing of the computer code (4) and served as lead writer of the manuscript.

3.1 Introduction

Accurately quantifying surface thermal conditions based on in-depth temperature measurements represents one commonly defined inverse heat conduction problem (IHCP) scenario. In aerospace engineering, it is a critical topic and applicable to a variety of short- and long-duration, ground- and flight-based experiments. For example, hypersonic flight requires reliable and predictable **T**hermal **P**rotection **S**ystems (TPS's) in order to maintain the structural integrity of a flight vehicle. Optimal selection of a TPS depends on the ability to accurately predict the surface heat flux and temperature based on in-depth temperature measurements. Hostile thermal conditions at the surface often preclude the use of surface mounted thermal sensors. A variety of methods have been employed to resolve inverse problems, including "exact

solutions" [37], function specification [34-36], space marching and finite difference [49,110,114] and other well-studied technique.

An alternative to purely numerically-based inverse heat conduction involves system calibration. Presently, two approaches have been proposed. There are several advantages to this view as systemic errors are substantially reduced. However, during the calibration test, the imposed net surface heat flux must be accurately measured. Loehle et al. [40], Loehle et al. [41] and Gardarein et al. [42] have demonstrated the application of a calibration method based on system identification for estimating the surface heat flux using measured in-depth temperature data. This Non-Integer System Identification (NISI) method involves developing an impulse response function from a calibration test. The NISI method [40-42] is presently derived based on the constant property (linear) heat equation. A finite series expansion is formed in terms fractional derivatives of the measured calibration temperature and calibration surface heat flux. The unknown expansion coefficients are determined during the calibration stage. In contrast, an alternative calibration methodology has been proposed [43-45] that eliminates the use of fractional derivatives and the resolution of expansion coefficients in the linear framework. This method relates the net unknown surface heat flux to the calibration surface heat flux and the corresponding in-depth temperature measurements during the calibration and reconstruction tests. The resulting inverse statement is then expressed in terms of a Volterra integral equation of the first kind for the unknown surface heat flux.

The linear one-probe calibration method [43,44] has been experimentally verified [45] with excellent accuracy in a low temperature range. However, in hypersonic flight, a large

temperature variation is expected due to aerothermodynamic heating effects [115]. Under this scenario, the variable thermophysical property effects can be significant depending on the material and temperature range. To account for the temperature varying property effects that lead to a fully nonlinear description, a piecewise time-step linearization assumption is introduced and used in conjunction with the Kirchhoff transformation. The Kirchhoff transform is a basic transformation often used in nonlinear diffusion problem. It essentially converts the nonlinear operator equation into a linear operator equation if the thermal diffusivity is held constant [116]. However, over the temperature range of interest, the change in the thermal diffusivity of most materials with temperature is not negligible. This situation often restricts the use of the Kirchhoff transformation. To overcome this obstacle, a piecewise time-step linearization assumption is now introduced. It involves a whole time domain discretization involving a successive series of small time steps in increments of Δt. At each time interval, all thermal properties are assumed constant and evaluated at the probe ($x = b,$ as shown in Fig 2.1.2) temperature. However, at each advancing time step the thermal diffusivity may vary. Through this simplification, the nonlinear one-dimensional heat conduction problem can be equivalently expressed as a series of linear ones whose thermal diffusivity has been evaluated at their respective small time step Δt using the local temperature measurement. It is then possible to map the piecewise thermal diffusivities at various times back to the one evaluated at the initial temperature through rescaling the time domain based on the sensor temperature history. This rescaling principle and its analysis are the major contribution of this chapter.

The main numerical difficulty associated with the above calibration formulation is that it has the form of Volterra integral equation of the first kind which is ill-posed. An arbitrarily small

uncertainty, emanating from either or both computing errors from the numerical process or experimental noise, destabilizes the predicted result. Hence, stabilizing the process through regularization becomes necessary. Fortunately, many regularization schemes have been proposed for this purpose. These include Tikhonov regularization [82], iterative regularization [16], local future-time method [8] and Singular- Value Decomposition (SVD) [80-81].

In this chapter, Section 3.2 presents the derivation of the new surface heat flux calibration formulation based on the Kirchhoff transformation and the proposed rescaling principle. Section 3.3 presents the Tikhonov regularization approach for generating a family of predictions based on the Tikhonov parameter. The L-curve strategy is then used for selecting a proper regularization parameter. Section 3.4 presents numerical results verifying both accuracy and robustness of this new calibration formulation in presence of significant experiment noise. Finally, Section 3.5 provides some concluding remarks on the rescaling concept.

3.2 Formulation

Consider a nonlinear one-dimensional heat conduction problem in Cartesian coordinates having a front surface heat flux source at $x = 0,$ and an adiabatic back surface at $x = L.$ This basic geometry and back boundary condition specification is often used in aerothermal applications [115]. The heat equation can be written as [33]

$$\frac{\partial}{\partial x}\left[k\big(T(x,t)\big)\frac{\partial T}{\partial x}(x,t)\right] = \rho c_p\big(T(x,t)\big)\frac{\partial T}{\partial t}(x,t), \qquad x \in (0,L), \;\; t \geq 0, \qquad (3.2.1a)$$

where T is the temperature, k represents the thermal conductivity, and ρc_p represents the heat capacity. The boundary conditions are given as

$$-k\big(T(0,t)\big)\frac{\partial T}{\partial x}(0,t) \triangleq q"(0,t) = q"_s(t),$$

$$\frac{\partial T}{\partial x}(L,t) = 0, \qquad t \geq 0, \tag{3.2.1b-c}$$

where $q"_s(t)$ describes the total surface heat flux externally contacting at $x = 0$ while $q"(0,t)$ is the net surface heat flux entering the body. The initial condition is given as

$$T(x,0) = 0, \qquad x \in [0,L]. \tag{3.2.1d}$$

Notice that for simplicity but without loss of generality, all the temperatures used in this chapter can be interpreted as the relative temperature from the physically imposed constant initial condition.

The inverse problem under consideration involves resolving the net surface heat flux based on a thermocouple located at $x = b$ with adiabatic condition at $x = L$ which is displayed in Figure 3.2.1. For this situation, Frankel and Keyhani [43] developed the linear calibration equation as

$$\int_{u=0}^{t} q"_r(0,u)T_c\,(b,t-u)du = \int_{u=0}^{t} q"_c(0,u)T_r\,(b,t-u)du, \qquad t \geq 0, \tag{3.2.1e}$$

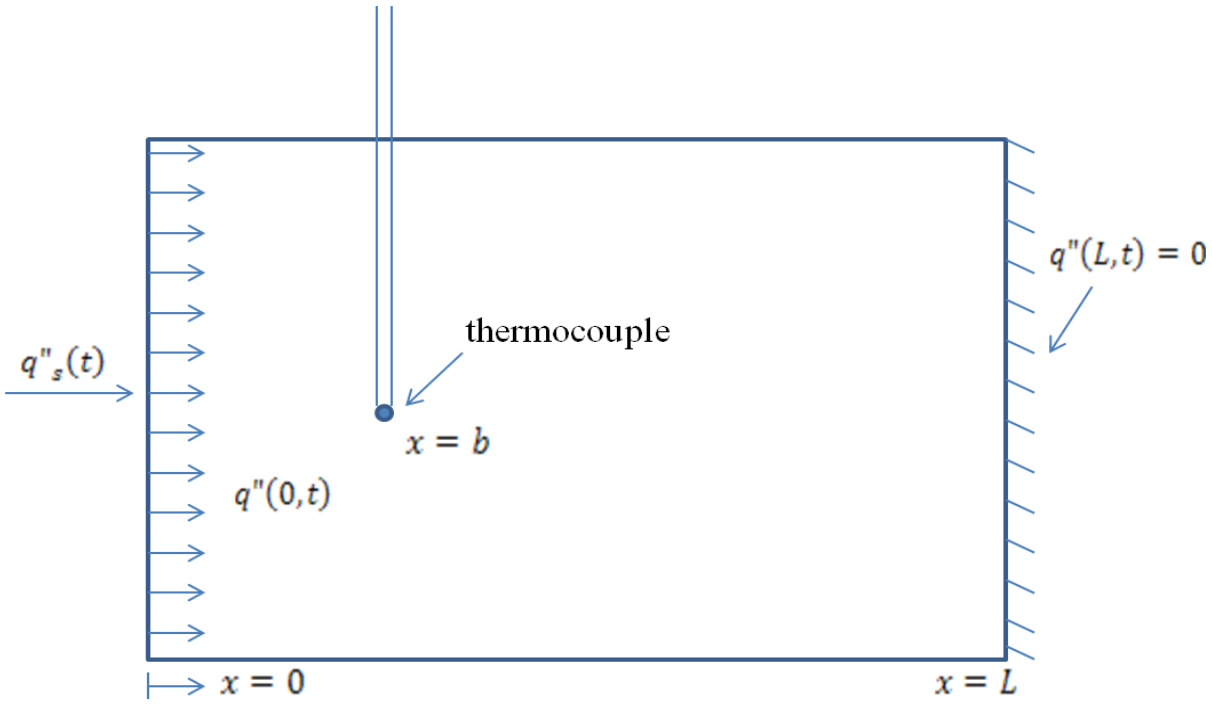

Figure 3.2.1: System setup for the one-dimensional heat conduction problem showing adiabatic back boundary and the thermocouple position.

where $T_c(b,t)$ is the measured calibration temperature at some depth $x = b, b \in [0, L]$; $q"_c(0,t)$ is the net surface heat flux imposed during the calibration test; $T_r(b,t)$ is the measured temperature of the same thermocouple in response to the unknown heat flux; and $q"_r(0,t)$ is the unknown surface heat flux to be predicted in the reconstruction test. This calibration integral equation has broad appeal as it is also valid for the semi-infinite geometry as well as a finite slab whose back surface is subjected to the same constant heat transfer coefficient between the two tests.

The Kirchhoff transformation introduces a new dependent variable possessing the form [116]

$$\theta \triangleq \frac{1}{k_0}\int_{u=0}^{T} k(u)du, \tag{3.2.2}$$

where u is the dummy variable used for the integration of $k(T)$ and k_0 represents the thermal conductivity precisely defined according to the initial temperature. T is relative remperature. The constant k_0 can also be written as $k\big(T(b,0)\big)$ since the initial temperature is uniform in space at time $t = 0$. Using this definition, Eqs. (3.2.1a-d) can be recast in terms of the Kirchhoff transformation variable as

$$\alpha\big(T(x,t)\big)\,\frac{\partial^2\theta}{\partial x^2}(x,t) = \frac{\partial\theta}{\partial t}(x,t), \qquad x \in (0,L),\ \ t \geq 0, \tag{3.2.3a}$$

subject to the boundary conditions

$$-k\big(T(b,0)\big)\frac{\partial\theta}{\partial x}(0,t) \triangleq q"(0,t) = q"_s(t),$$

$$\frac{\partial\theta}{\partial x}(L,t) = 0, \qquad t \geq 0, \tag{3.2.3b-c}$$

and initial condition

$$\theta(x,0) = 0, \qquad x \in [0,L], \tag{3.2.3d}$$

where $\alpha\big(T(x,t)\big) = k\big(T(x,t)\big)/\rho c_p\big(T(x,t)\big)$ represents the thermal diffusivity evaluated at temperature $T(x,t)$. If the thermal diffusivity is insensitive to temperature, (i.e., $\alpha(T)$ is a constant) then according to Duhamel's principle, the final analytical solution becomes

$$\theta(x,t) = \int_{u=0}^{t} q"(0,u)D_{q\theta}(x,t-u)du, \qquad x \in [0,L], \;\; t \geq 0, \tag{3.2.4a}$$

where $D_{q\theta}(x,t)$ is the solution for $\theta(x,t)$ when the front surface $q"(0,t)$ is exposed to impulsive heat flux. First, suppose that both calibration and reconstruction test data have been collected. A new linear calibration formulation in term of Kirchhoff transformed variable can be derived through the exchange of integral sequences using

$$\theta_c(b,t) = \int_{u=0}^{t} q"_c(0,u) D_{q\theta}(b,t-u)du, \quad t \geq 0, \tag{3.2.4b}$$

such that

$$\int_{u=0}^{t} q"_r(0,u)\theta_c\,(b,t-u)du$$

$$= \int_{u=0}^{t} q"_r(0,u) \int_{v=0}^{t-u} q"_c(0,v) D_{q\theta}(b,t-u-v)dv\ du$$

$$= \int_{v=0}^{t} q"_c(0,v) \int_{u=0}^{t-v} q"_r(0,u) D_{q\theta}(b,t-v-u)du\ dv$$

$$= \int_{v=0}^{t} q"_c(0,v)\theta_r\,(b,t-v)dv$$

$$= \int_{u=0}^{t} q"_c(0,u)\theta_r\,(b,t-u)du. \tag{3.2.4c}$$

Comparing Eq. (3.2.4c) to the linear calibration equation in Eq. (3.2.1e), the Kirchhoff transformed based calibration equation shown in Eq. (3.2.4c) can still be applied to problems with a semi-infinite geometry but will not hold true when the back surface is subjected to a heat transfer coefficient $h(T)$=constant since the Kirchhoff's transformation of a Robin's condition retains the nonlinearity. The new equation shown in Eq. (3.2.4c) works well when the thermal diffusivity is approximately constant. However, for some materials the thermal diffusivity can significantly vary over the temperature range of interest and it must be accounted for. For this purpose, a piecewise time-step linearization assumption is now proposed to form the quasi-linearization. That is, the thermal diffusivity distribution is viewed as uniform in the spatial

domain but permitted to vary in the time domain. In this way, the thermal diffusivity at each time step can be evaluated and approximated from its corresponding probe temperature at $x = b$ which is located near the desired surface being resolved.

To display the time stepping process and rescaling concept, several time steps involving this concept are now presented. If we apply the piecewise, time-step linearization assumption to Eqs. (3.2.3a-d) between time $t = 0$ and $t = \Delta t$ then the heat equation becomes

$$\alpha\big(T(b,0)\big)\,\frac{\partial^2\theta_0}{\partial x^2}(x,t) = \frac{\partial\theta_0}{\partial t}(x,t), \qquad x \in (0,L),\ \ t \in [0,\Delta t], \tag{3.2.5a}$$

subject to the boundary conditions

$$-k\big(T(b,0)\big)\frac{\partial\theta_0}{\partial x}(0,t) = q"(0,t),$$

$$\frac{\partial\theta_0}{\partial x}(L,t) = 0, \qquad t \in [0,\Delta t], \tag{3.2.5b-c}$$

and initial condition

$$\theta_0(x,0) = 0, \qquad x \in [0,L]. \tag{3.2.5d}$$

During the first time step, the thermal diffusivity is evaluated at the initial temperature and it is assumed spatially invariant over the entire slab. The heat conduction problem now

becomes “linearized” in the time interval, $t \in [0, \Delta t]$. Thus, Eq. (3.2.4c) can be applied to obtain the unknown surface heat flux prediction in the interval, $t \in [0, \Delta t]$.

For notational convenience and consistency, we define

$$\theta^*_{t0}(x,t) = \theta_0(x,t), \qquad t \in [0, \Delta t], \tag{3.2.5e}$$

$$q"^*_{t0}(0,t) = q"(0,t), \qquad t \in [0, \Delta t]. \tag{3.2.5f}$$

The superscript “star” notation is introduced to relate the rescaling concept. The subscript "ti" is introduced to explicitly relate that the rescaling has been made in the time interval, $t \in [0, (i+1)\Delta t]$ based on temperature data collected from the experiment. Hence, in the first time step, $t \in [0, \Delta t]$, the Kirchhoff transformed based one-probe calibration equation from Eq. (3.2.4c) is

$$\int_{u=0}^{t} q"^*_{t0,r}(0,u)\theta^*_{t0,c}(b, t-u)du = \int_{u=0}^{t} q"^*_{t0,c}(0,u)\theta^*_{t0,r}(b, t-u)du, \quad t \in [0, \Delta t]. \tag{3.2.5g}$$

Similarly, for the second time step, $t \in [\Delta t, 2\Delta t]$, the heat equation expressed in Eq. (3.2.3a) becomes

$$\alpha\big(T(b,\Delta t)\big)\,\frac{\partial^2\theta_1}{\partial x^2}(x,t)=\frac{\partial\theta_1}{\partial t}(x,t),\qquad x\in(0,L),\ \ t\in[\Delta t,2\Delta t],\qquad (3.2.6a)$$

subject to the boundary conditions

$$-k\big(T(b,0)\big)\frac{\partial\theta_1}{\partial x}(0,t)=q"(0,t),$$

$$\frac{\partial\theta_1}{\partial x}(L,t)=0,\qquad t\in[\Delta t,2\Delta t],\qquad (3.2.6b-c)$$

and initial condition

$$\theta_1(x,\Delta t)=\theta(x,\Delta t),\qquad x\in[0,L].\qquad (3.2.6d)$$

A substantial variability in thermal diffusivity can result from a large temperature variation due to the imposed heating process. In such cases, a nonlinear analysis must be sought. To avoid this difficulty, one possible method involves rescaling the time domain based on the thermal diffusivity function. After introducing the rescaling, all piecewise governing equations and boundary conditions can be transformed into the same functional form for each new rescaled time step. For instance, if we can let $(t-\Delta t)=n_1 v$ then the original system can then be recast into

$$\alpha\big(T(b,\Delta t)\big)\,\frac{\partial^2\theta_1}{\partial x^2}(x,n_1v+\Delta t)=\frac{\partial\theta_1}{\partial(n_1v)}(x,n_1v+\Delta t),\ \ x\in(0,L),\ n_1v\in[0,\Delta t],\ \ (3.2.7a)$$

subject to the boundary conditions

$$-k\big(T(b,0)\big)\frac{\partial\theta_1}{\partial x}(0,n_1v+\Delta t)=q"(0,n_1v+\Delta t),$$

$$\frac{\partial\theta_1}{\partial x}(L,n_1v+\Delta t)=0,\quad v\in\left[0,\frac{\Delta t}{n_1}\right], \qquad (3.2.7b-c)$$

and initial condition

$$\theta_1(x,n_1v+\Delta t=\Delta t)=\theta(x,t=\Delta t),\qquad x\in[0,L]. \qquad (3.2.7d)$$

To map the local thermal diffusivity $\alpha\big(T(b,\Delta t)\big)$ shown in Eq. (3.2.7a) back to the $\alpha\big(T(b,0)\big)$ given in Eq. (3.2.5a), we define

$$\theta_1^*(x,v)=\theta_1(x,n_1v+\Delta t),\qquad v\in\left[0,\frac{\Delta t}{n_1}\right],$$

$$q"_1^*(0,v)=q"(0,n_1v+\Delta t),\qquad v\in\left[0,\frac{\Delta t}{n_1}\right], \qquad (3.2.7e-f)$$

where

$$n_1=\frac{\alpha\big(T(b,0)\big)}{\alpha\big(T(b,\Delta t)\big)}. \qquad (3.2.7g)$$

Based on these definitions, Eqs. (3.2.7a-d) can be simplified to

$$\alpha\big(T(b,0)\big)\,\frac{\partial^2\theta_1^*}{\partial x^2}(x,v)=\frac{\partial\theta_1^*}{\partial v}(x,v),\qquad x\in(0,L),\;\; v\in\left[0,\frac{\Delta t}{n_1}\right], \tag{3.2.8a}$$

subject to the boundary conditions

$$q''^*_1(0,v)=-k\big(T(b,0)\big)\frac{\partial\theta_1^*}{\partial x}(0,v),$$

$$\frac{\partial\theta_1^*}{\partial x}(L,v)=0,\quad v\in\left[0,\frac{\Delta t}{n_1}\right], \tag{3.2.8b-c}$$

and initial condition

$$\theta_1^*(x,v=0)=\theta(x,t=\Delta t),\qquad x\in[0,L]. \tag{3.2.8d}$$

A scaling coefficient n_1 is introduced into the second-time step. The resulting rescaling Kirchhoff transformed variable θ_1^* can be considered as the "linearized" solution using q''^*_1 and having a thermal diffusivity evaluated at its relevant initial temperature. The initial condition in this second step is merely the final state of the first time step $\theta(x,t=\Delta t)$. Next, we define

$$\theta_0^*(x,v)=\theta_0(x,n_0v),\qquad v\in\left[0,\frac{\Delta t}{n_0}\right],$$

$$q''^{*}_{0}(0,v) = q''(0,n_0 v), \qquad v \in \left[0, \frac{\Delta t}{n_0}\right], \tag{3.2.9a-c}$$

$$n_0 \triangleq 1.$$

The rescaling coefficient n_0 is set to one in order to illustrate that the heat flux q'' and the Kirchhoff transformed variable θ_0 for the first-time step can also be rescaled into the new time domain.

Combining definitions from Eqs. (3.2.7e-g) with (3.2.9a-c), one can show that if θ_0^* and θ_1^* are collected in sequence; the final "linearized" solution obtained from the heat flux q''^{*}_{1} followed by q''^{*}_{2} will match the initial temperature at 0°C.

We define this collecting process through

$$q''^{*}_{t1}(0,t) = \begin{cases} q''^{*}_{0}(0,t) & t \in \left[0, \dfrac{\Delta t}{n_0}\right) \\ q''^{*}_{1}\left(0, t - \dfrac{\Delta t}{n_0}\right) & t \in \left[\dfrac{\Delta t}{n_0}, \displaystyle\sum_{i=0}^{1} \frac{\Delta t}{n_i}\right), \end{cases} \tag{3.2.10a}$$

$$\theta^{*}_{t1}(x,t) = \begin{cases} \theta^{*}_{0}(x,t) & t \in \left[0, \dfrac{\Delta t}{n_0}\right) \\ \theta^{*}_{1}\left(x, t - \dfrac{\Delta t}{n_0}\right) & t \in \left[\dfrac{\Delta t}{n_0}, \displaystyle\sum_{i=0}^{1} \frac{\Delta t}{n_i}\right). \end{cases} \tag{3.2.10b}$$

Implementing this process, the resulting one-probe integral calibration equation based on the Kirchhoff transform for the first two time steps becomes

$$\int_{u=0}^{t} q''^{*}_{t1,r}(0,u)\theta^{*}_{t1,c}(b,t-u)du = \int_{u=0}^{t} q''^{*}_{t1,c}(0,u)\theta^{*}_{t1,r}(b,t-u)du,$$

$$t \in \left[0, \sum_{i=0}^{1} \frac{\Delta t}{n_i}\right). \qquad (3.2.10c)$$

A calibration equation becomes available for arbitrary time length by repeating the previously outlined procedure for all future time steps. For a heating process with $t_{max} = (N+1)\Delta t$, with any small step $t \in [i\Delta t, (i+1)\Delta t]$ $(i = 0,1 \ldots N)$, the governing equation under piecewise time-step linearization assumption becomes

$$\alpha\big(T(b,i\Delta t)\big)\,\frac{\partial^2\theta_i}{\partial x^2}(x,t) = \frac{\partial\theta_i}{\partial t}(x,t), \quad x \in (0,L), \;\; t \in [i\Delta t, (i+1)\Delta t], \qquad (3.2.11a)$$

subject to the boundary conditions

$$-k\big(T(b,0)\big)\frac{\partial\theta_i}{\partial x}(0,t) = q''(0,t),$$

$$\frac{\partial\theta_i}{\partial x}(L,t) = 0, \;\; t \in [i\Delta t, (i+1)\Delta t], \qquad (3.2.11b-c)$$

and initial condition

$$\theta_i(x, i\Delta t) = \theta(x, i\Delta t), \quad x \in [0, L]. \tag{3.2.11d}$$

Time domain rescaling is accomplished through

$$\theta_i^*(x, v) = \theta_i(x, n_i v + i\Delta t), \qquad v \in \left[0, \frac{\Delta t}{n_i}\right],$$

$$q"_i^*(0, v) = q"(0, n_i v + i\Delta t), \qquad v \in \left[0, \frac{\Delta t}{n_i}\right], \tag{3.2.11e-f}$$

$$n_i = \frac{\alpha\big(T(b,0)\big)}{\alpha\big(T(b, i\Delta t)\big)}. \tag{3.2.11g}$$

Upon implementing the above definitions, it is possible to express Eqs. (3.2.11a-d) using the thermal diffusivity evaluated at the initial temperature as

$$\alpha\big(T(b,0)\big)\,\frac{\partial^2 \theta_i^*}{\partial x^2}(x, v) = \frac{\partial \theta_i^*}{\partial v}(x, v), \quad x \in (0, L), \quad v \in \left[0, \frac{\Delta t}{n_i}\right], \tag{3.2.12a}$$

subject to the boundary conditions

$$-k\big(T(b,0)\big)\frac{\partial \theta_i^*}{\partial x}(0, v) = q"_i^*(0, v),$$

$$\frac{\partial \theta_i^*}{\partial x}(L, v) = 0, \qquad v \in \left[0, \frac{\Delta t}{n_i}\right], \tag{3.2.12b-c}$$

and initial condition

$$\theta_i^*(x, v = 0) = \theta(x, t = i\Delta t), \quad x \in [0, L]. \tag{3.2.12d}$$

Notice that the local thermal diffusivity $\alpha\big(T(b, i\Delta t)\big)$ can always be transformed to the initial temperature condition through rescaling the respective time domains by n_i. Thus, if all Kirchhoff transformed variables θ_i^* from time zero $(i = 0)$ to final time $(i = N)$ are collected in sequence then it can be regarded as a linearized solution of the heat equation leading to the surface heat flux following the reconstitution of q''^*_i from $i = 0$ to $i = N$.

It is possible to define the total sequential system as the collection given by

$$q''^*_{tN}(0, t) = \begin{cases} q''^*_0(0, t) & t \in \left[0, \dfrac{\Delta t}{n_0}\right) \\ q''^*_1\left(0, t - \dfrac{\Delta t}{n_0}\right) & t \in \left[\dfrac{\Delta t}{n_0}, \displaystyle\sum_{i=0}^{1} \frac{\Delta t}{n_i}\right) \\ \cdots & \\ q''^*_N\left(0, t - \displaystyle\sum_{i=0}^{N-1} \frac{\Delta t}{n_i}\right) & t \in \left[\displaystyle\sum_{i=0}^{N-1} \frac{\Delta t}{n_i}, \sum_{i=0}^{N} \frac{\Delta t}{n_i}\right), \end{cases} \tag{3.2.13a}$$

$$\theta_{tN}^{*}(x,t)=\begin{cases}\theta_0^{*}(x,t) & t\in\left[0,\dfrac{\Delta t}{n_0}\right)\\ \theta_1^{*}\left(x,t-\dfrac{\Delta t}{n_0}\right) & t\in\left[\dfrac{\Delta t}{n_0},\sum\limits_{i=0}^{1}\dfrac{\Delta t}{n_i}\right)\\ \cdots & \\ \theta_N^{*}\left(x,t-\sum\limits_{i=0}^{N-1}\dfrac{\Delta t}{n_i}\right) & t\in\left[\sum\limits_{i=0}^{N-1}\dfrac{\Delta t}{n_i},\sum\limits_{i=0}^{N}\dfrac{\Delta t}{n_i}\right).\end{cases} \qquad (3.2.13b)$$

Finally, the rescaled calibration integral equation corresponding to the physical time domain $t\in[0,t_{max}]$ becomes

$$\int_{u=0}^{t} q''^{*}_{tN,r}(0,u)\theta^{*}_{tN,c}(b,t-u)du=\int_{u=0}^{t} q''^{*}_{tN,c}(0,u)\theta^{*}_{tN,r}(b,t-u)du,$$

$$t\in\left[0,\sum_{i=0}^{N}\frac{\Delta t}{n_i}\right). \qquad (3.2.13c)$$

If a more general solution form is required then we can increase N such that $\Delta t=\lim_{N\to\infty}\frac{t_{max}}{N+1}$. Thus, for any time $t_M\in[0,t_{max}]$, it is always possible to find a real index $M\in[0,N]$ to ensure $t_M\approx M\Delta t$. Moreover, the sequential collecting procedure for the rescaled time domain can be approximated as a compact integral equation. From Eqs. (3.2.11e-g) and Eqs. (3.2.13a-c), we have

$$\sum_{i=0}^{M}\frac{\Delta t}{n_i}\approx\int_{u=0}^{t_{M+1}}\frac{\alpha\big(T(b,u)\big)}{\alpha\big(T(b,0)\big)}du,$$

therefore

$$\theta(x, t_{M+1}) = \theta^*_{tM}\left(x, \int_{u=0}^{t_{M+1}} \frac{\alpha\big(T(b,u)\big)}{\alpha\big(T(b,0)\big)} du\right), \qquad (3.2.14a-c)$$

$$q"(0, t_{M+1}) = q"^*_{tM}\left(0, \int_{u=0}^{t_{M+1}} \frac{\alpha\big(T(b,u)\big)}{\alpha\big(T(b,0)\big)} du\right).$$

The next step is to define

$$t^* = \int_{u=0}^{t} \frac{\alpha\big(T(b,u)\big)}{\alpha\big(T(b,0)\big)} du,$$

with

$$q"^*(0, t^*) = q"(0, t), \qquad (3.2.15a-c)$$

$$\theta^*(x, t^*) = \theta(x, t),$$

such that the final form of the nonlinear, one-probe calibration integral equation for the entire time domain becomes

$$\int_{u=0}^{t^*} q"^*_r(0,u)\theta^*_c(b, t^* - u)du = \int_{u=0}^{t^*} q"^*_c(0,u)\theta^*_r(b, t^* - u)du, \qquad t^* \geq 0. \qquad (3.2.15d)$$

Once the unknown surface heat flux in the rescaled time domain has been predicted, the necessary return to the physical time domain can be accomplished with the aid of

$$t = \int_{u=0}^{t^*} \frac{\alpha\left(T^*(b,0)\right)}{\alpha\left(T^*(b,u)\right)} du, \tag{3.2.16a}$$

where

$$T^*(b,t^*) = T(b,t). \tag{3.2.16b}$$

3.3 Regularization by Tikhonov Regularization and L-Curve

The quasi-linearized Kirchhoff transformed methodology yields Eq. (3.2.15d) which is a Volterra integral equation of first kind [79]. As such, it is ill-posed and requires careful computational considerations in hope of retrieving an accurate prediction since arbitrary input noise and computational errors can destabilize the entire prediction. In the present formulation, the thermal diffusivity distribution at any instant of time is fixed or frozen at the probe temperature evaluated value. Therefore, some model introduced bias is expected. Regularization must be introduced to control prediction stability. The strategy adopted here involves the classical Tikhonov regularization approach. L-curve analysis is then introduced for estimating the "best" regularization parameter. If discrete experimental data collected from the physical time domain are mapped onto the rescaled discrete domain, $t^* \in [0, t^*_{max}]$ with $\Delta\, t^* = \frac{t^*_{max}}{N+1}$, then the objective function to be minimized is given as

$$J_{\theta,q}(q''^{*}_{r}(0,t_i^*)|_{i=0}^{N}) = \sum_{i=1}^{N+1}\left[G^*_{\theta,q}(t_i^*) - F^*_{\theta,q}(t_i^*)\right]^2 + \lambda_0^2\sum_{i=0}^{N}[q''^{*}_{r}(0,t_i^*)]^2\,, \qquad (3.3.1a)$$

where

$$G^*_{\theta,q}(t_i^*) = \int_{u=0}^{t_i^*} q''^{*}_{r}(0,u)\theta^*_c\,(b,t_i^*-u)du,$$

$$F^*_{\theta,q}(t_i^*) = \int_{u=0}^{t_i^*} q''^{*}_{c}(0,u)\theta^*_r\,(b,t_i^*-u)du. \qquad (3.3.1b-c)$$

Here, λ_0 denoted the regularization parameter and $t_i^* = i\Delta t^*$. The regularization parameter retains the physical units (^{o}Cs) associated with the balancing of Eq. (3.3.1a). For this investigation, if Eqs. (3.3.1b,c) are numerically processed using a convenient left-handed rectangle, product integration rule then Eq. (3.3.1a) can be represented in a compact matrix form

$$J_{\theta,q}(\boldsymbol{q_r}) = \left\|\boldsymbol{\Theta_c q_r} - \boldsymbol{F_{\theta,q}}\right\|^2 + \lambda_0^2\|\boldsymbol{q_r}\|^2, \qquad (3.3.2)$$

where $\boldsymbol{\Theta_c}$ is a $(N+1)\times(N+1)$ matrix with $\boldsymbol{\Theta_c}(i,j) = \Delta t^* \times \theta_c^*\left(b, t^*_{i-j+1}\right)$ for $i \geq j$ and $\boldsymbol{\Theta_c}(i,j) = 0$ for $i < j$, $\boldsymbol{F_{\theta,q}}$ is a $(N+1)\times 1$ vector with $\boldsymbol{F_{\theta,q}}(i) = F^*_{\theta,q}(t_i^*)$, and $\boldsymbol{q_r}$ is a $(N+1)\times 1$ matrix to be determined with $\boldsymbol{q_r}(i) = q''^{*}_{r}(t^*_{i-1})$.

To obtain the minimum value of Eq. (3.3.2), the first derivative of $J_{\theta,q}(\boldsymbol{q_r})$ with respective to $\boldsymbol{q_r}$ must be computed and then the result is set to 0. Performing this operation yields

$$\boldsymbol{\Theta_c^{\mathrm{T}}}\left(\boldsymbol{\Theta_c q_r} - \boldsymbol{F_{\theta,q}}\right) + \lambda_0^2 \boldsymbol{q_r} = 0. \tag{3.3.3a}$$

Thus, $\boldsymbol{q_r}$ can be calculated through matrix inversion producing

$$\boldsymbol{q_r} = (\boldsymbol{\Theta_c^{\mathrm{T}}\Theta_c} + \lambda_0^2 \boldsymbol{I})^{-\mathbf{1}} \boldsymbol{\Theta_c^{\mathrm{T}}}\, \boldsymbol{F_{\theta,q}} \tag{3.3.3b}$$

An alternative way to represent this result makes use of the Singular-Value Decomposition (SVD) of $\boldsymbol{\Theta_c}$ [113]. Let

$$\boldsymbol{\Theta_c} = \boldsymbol{W}\sum\boldsymbol{V^T} = \sum_{i=1}^{N+1} \boldsymbol{w}_i \sigma_i \boldsymbol{v}_i^T, \tag{3.3.4}$$

with $\boldsymbol{W} = (\boldsymbol{w}_1, \boldsymbol{w}_2, \boldsymbol{w}_3, \cdots, \boldsymbol{w}_{N+1})$ and $\boldsymbol{V} = (\boldsymbol{v}_1, \boldsymbol{v}_2, \boldsymbol{v}_3, \cdots, \boldsymbol{v}_{N+1})$ satisfying $\boldsymbol{W^T W} = \boldsymbol{V^T V} = \boldsymbol{I}$. Here, the term $\sum$ is a $(N+1) \times (N+1)$ diagonal matrix whose diagonal value σ_i arranges in a descending order as

$$\sigma_1 \geq \sigma_2 \geq \cdots \geq \sigma_{N+1} \geq 0. \tag{3.3.5}$$

A new form of $J_{\theta,q}(\boldsymbol{q_r})$ is developed once Eq. (3.3.4) is substituted into Eq. (3.3.2). Doing so yields

$$J_{\theta,q}(\boldsymbol{q_r}) = \left\|\boldsymbol{W}\sum\boldsymbol{V^T q_r} - \boldsymbol{W W^T F_{\theta,q}}\right\|^2 + \lambda_0^2\|\boldsymbol{V V^T q_r}\|^2 \ ,$$

$$= \left\|\sum(\boldsymbol{V^T q_r}) - \left(\boldsymbol{W^T F_{\theta,q}}\right)\right\|^2 + \lambda_0^2\|(\boldsymbol{V^T q_r})\|^2 \ . \tag{3.3.6}$$

Minimizing Eq. (3.3.6) leads to the SVD based Tikhonov regularized prediction

$$\boldsymbol{q_r} = \sum_{i=1}^{N+1} \frac{\sigma_i}{\sigma_i^2 + \lambda_0^2} \boldsymbol{w_i^T F_{\theta,q} \nu}_i \quad . \tag{3.3.7}$$

It is crucial to determine a suitable value of the regularization parameter λ_0 for stabilizing the final prediction from the ill-condition matrix $\boldsymbol{\Theta_c}$. The L-curve criterion proposed by Hansen and O' Leary [83] is called upon for this purpose. This method defines the L-curve through

$$LF_{\theta,q}(\lambda_0) = \left\{\log\left(\left\|\boldsymbol{\Theta_c q_r} - \boldsymbol{F_{\theta,q}}\right\|^2\right), \log(\|\boldsymbol{q_r}\|^2), \lambda_0 \geq 0\right\} . \tag{3.3.8}$$

The L-curve mathematically described by Eq. (3.3.8) requires the evaluation of both heat flux and residual over the λ_0-spectrum. A suitable regularization parameter must be identified from the formed elbow region of the L-curve. This region is assumed to produce the optimal regularization parameter by balancing bias $\left(\left\|\boldsymbol{\Theta_c q_r} - \boldsymbol{F_{\theta,q}}\right\|^2\right)$ and variance($\|\boldsymbol{q_r}\|^2$). Section 3.4

presents a numerical investigation applying the proposed rescaling principle and regularization method.

3.4 Results

This section presents computational results based on numerically simulated data. To numerically verify the new rescaling integral calibration formulation displayed in Eq. (3.2.15d), a 1cm-thick slab of stainless steel 304 is considered with an adiabatic back surface. The front surface can be exposed to a time-varying heat flux during both the calibration or reconstruction test stages. An idealized thermocouple is placed at $b = 2\text{mm}$ whose leads are placed parallel to the isotherms. The term "idealized" is used here to indicate that this thermocouple can accurately measure the positional temperature. The impact of signal decay and delay associated with realistic thermocouples is ignored. Figure 3.2.1 presents a schematic of this system. Simulated thermocouple data require the generation of temperature data at $x = b$ from the forward or direct solution of the nonlinear heat equation. The direct problem for creating thermocouple probe data is defined between $x = 0$ and $x = L$ with known the net surface heat flux condition at $x = 0$ and adiabatic back boundary condition at $x = L$. For simplicity, the initial condition for all tests is assumed to be $T(x, 0) = 0^{\text{o}}\text{C}$. Again, fully temperature dependent thermophysical properties are assumed. A finite difference method [33] is applied to obtain $T(x, t)$ for the domain $x \in [0, L]$, $t \geq 0$. Hence, simulated data now become available at $x = b$ for all tests.

For demonstration purpose, the thermal conductivity and specific heat capacity functions for stainless steel 304 have been approximated as

$$k(T) = (14.4 + 0.0167T - 1.6 \times 10^{-6}T^2)(\mathrm{Wm^{-1}K^{-1}}),$$

$$c_p(T) = (20.08 + 0.0491T + 80.74\ln(T + 273.15))(\mathrm{Jkg^{-1}K^{-1}}), \qquad (3.4.1a-b)$$

respectively, where the density is estimated as $\rho = 7920(\mathrm{kg/m^3})$. Notice that all temperatures T in Eqs. (3.4.1a,b) are the relative temperature based on unit ^{o}C rather than K. Figures 3.4.1 and 3.4.2 display the thermal conductivity and specific heat capacity functions using Eqs. (3.4.1a,b). The thermal diffusivity function $\alpha(T) = k(T)/\rho c_p(T)$ is also shown in Fig. 3.4.3. If the temperature in the slab rises to about 1000^{o}C then nonlinearity effects must be accounted.

For the present analysis, Δx and Δt have been set to 0.2mm and 50μs, respectively. The maximum heating time is fixed to 30s. To ensure the accuracy of the time stepping process with respect to the nonlinearity, both the spatial and temporal grid sets have been varied as (Δx =0.1mm and Δt =25μs), (Δx =0.2mm and Δt =100μs) for demonstrating stability and accuracy using both the calibration and reconstruction tests. Convergence to a relative accuracy of 0.01 has been verified. Next, the known time-rescaled calibration heat flux $q''^{*}_{c}(0, t^*)$, the time-rescaled Kirchhoff transformed variables of $\theta^*_c(b, t^*)$ and $\theta^*_r(b, t^*)$ from rescaled temperatures $T^*_c(b, t^*)$ and $T^*_r(b, t^*)$ can be considered as inputs to Eq. (3.2.15d) for predicting the time-rescaled unknown surface heat flux $q''^{*}_{r}(0, t^*)$.

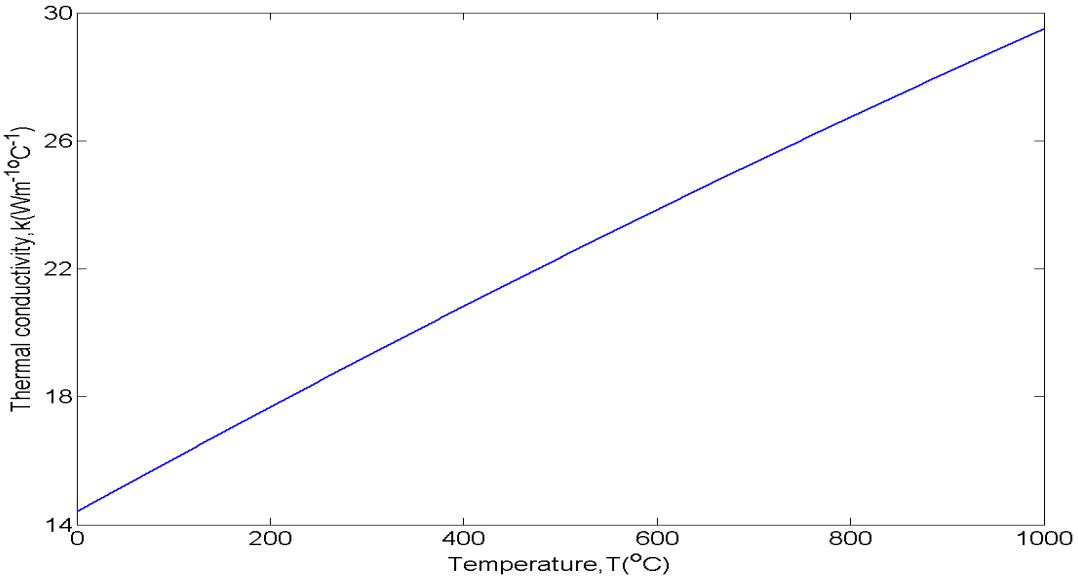

Figure 3.4.1: Approximate thermal conductivity for stainless steel 304, Eq. (3.4.1a), showing a nearly two-fold change in thermal conductivity over the prescribed temperature range.

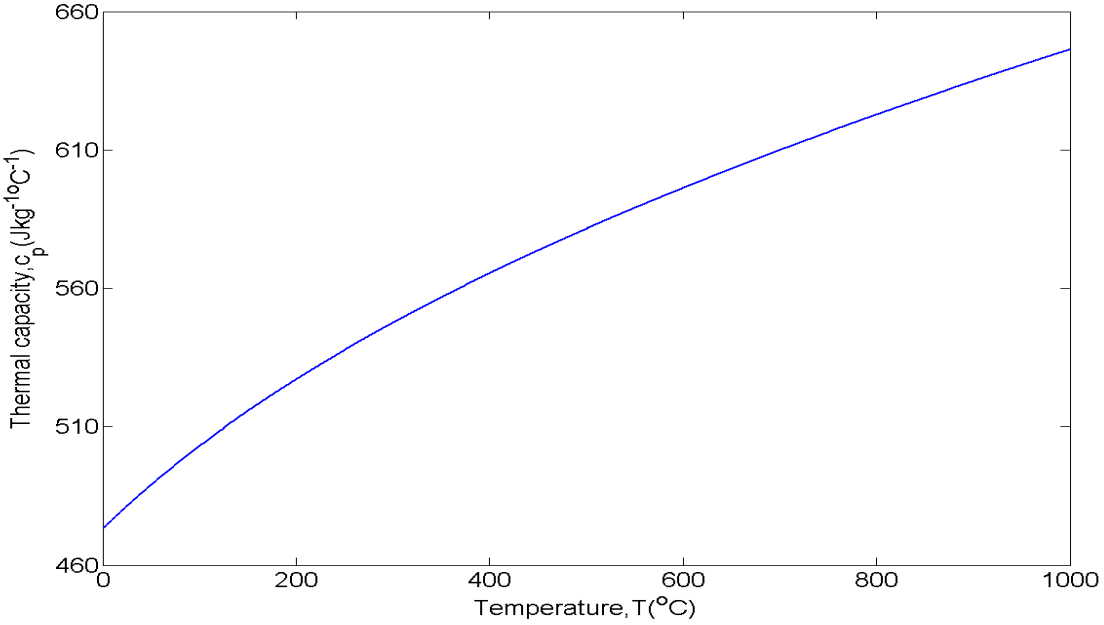

Figure 3.4.2: Approximate specific heat capacity for stainless steel 304, Eq. (3.4.1b).

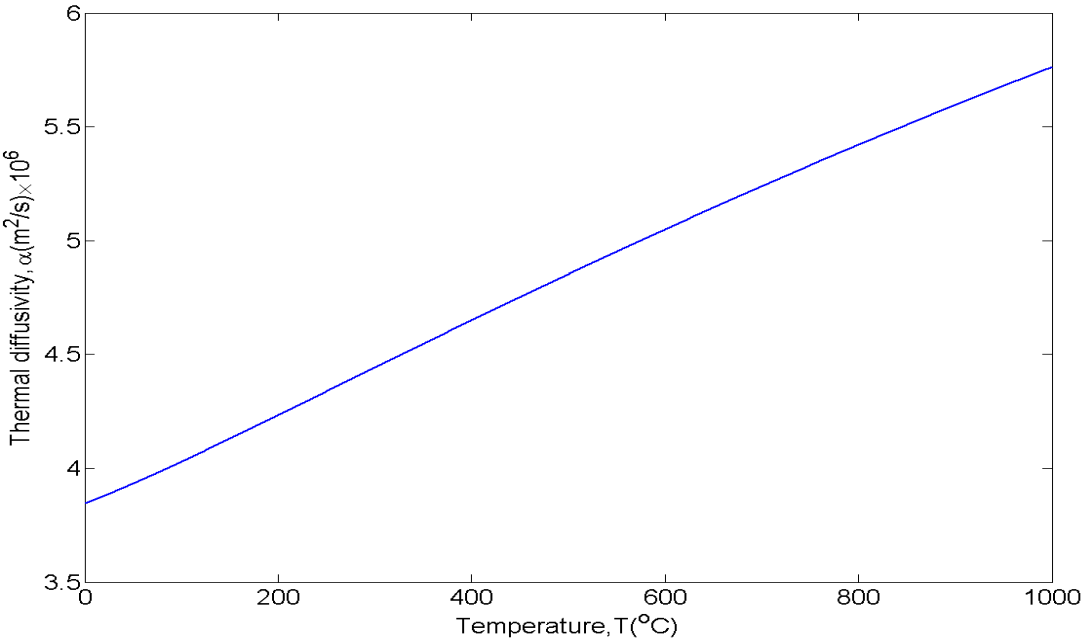

Figure 3.4.3: Approximate thermal diffusivity for stainless steel 304, $\alpha(T) = k(T)/\rho c_p(T)$.

A significant amount of nonlinearity is introduced into the system in order to understand the accuracy and limitations of the quasi-linearized calibration formulation displayed in Eq. (3.2.15d). In this regard, the calibration test is a constant heat flux ($q"_c = 120\text{W/cm}^2$) lasting 30s. An isosceles triangular net surface heat flux starting at 2.5s and ending at 22.5s is used for the reconstruction test possessing a peak of 400W/cm^2. The calibration and unknown heat fluxes are presented in Fig. 3.4.4 while their respective thermal responses at probe position $x = b$ as computed by the forward model are presented in Fig. 3.4.5. Figure 3.4.6 presents the temperature distribution at uniformly distributed spatial locations resulting from the forward solution for the triangular heat flux. Notice that the maximum surface temperature exceeds 1000^{o}C, hence, justifying the existence of a substantial nonlinearity. Between the surface and probe position, the observed temperature difference is approximately 200^{o}C. Figure 3.4.7 presents the dimensionless thermal diffusivity ratio distribution, $\alpha\big(T_r(x,t)\big)/\alpha\big(T_r(b,t)\big)$ in space at five specified time points indicating the variability of this function relative to probe position. This plot is useful for accessing the piecewise time-step linearization concept. From this figure, it is clear that the maximum thermal diffusivity ratio between the front and back surface is nearly 1.2 at about 10s. At first glance, this ratio appears excessive owing to the spatially invariant assumption at fixed time. However, it is noted that the calibration integral equation displayed in Eq. (3.2.15d) is only concerned with the temperature variation in $x \in [0, b]$. In that region the maximum thermal diffusivity ratio is about 1.06.

Two cases are now presented. The first case establishes the viability of this new calibration approach in the presence of noiseless data. As a result, the effect of bias associated

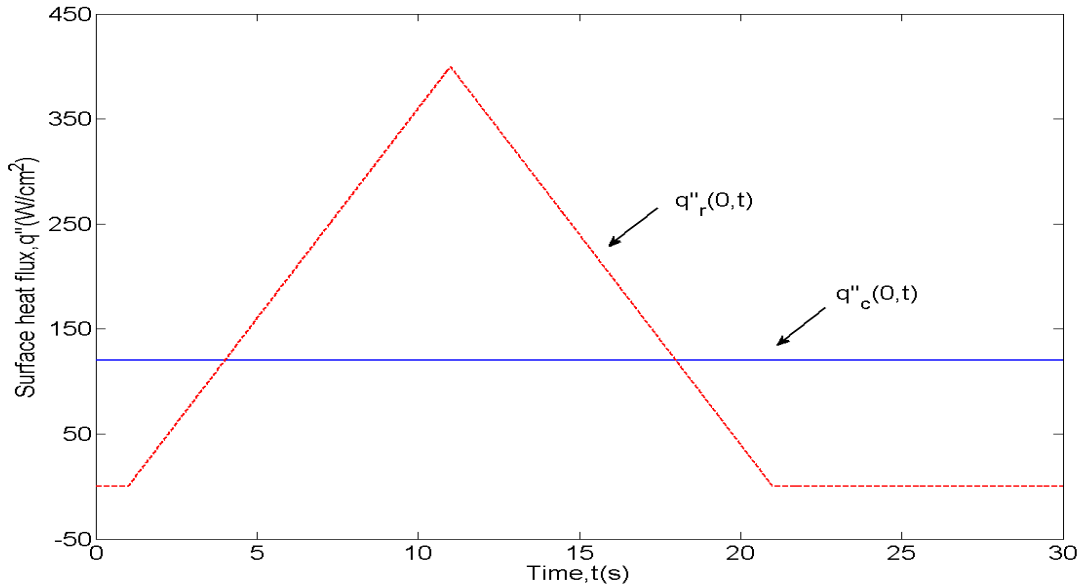

Figure 3.4.4: The known "calibration" surface heat flux $q"_c(0,t)$ and the "unknown" heat flux $q"_r(0,t)$ to be predicted.

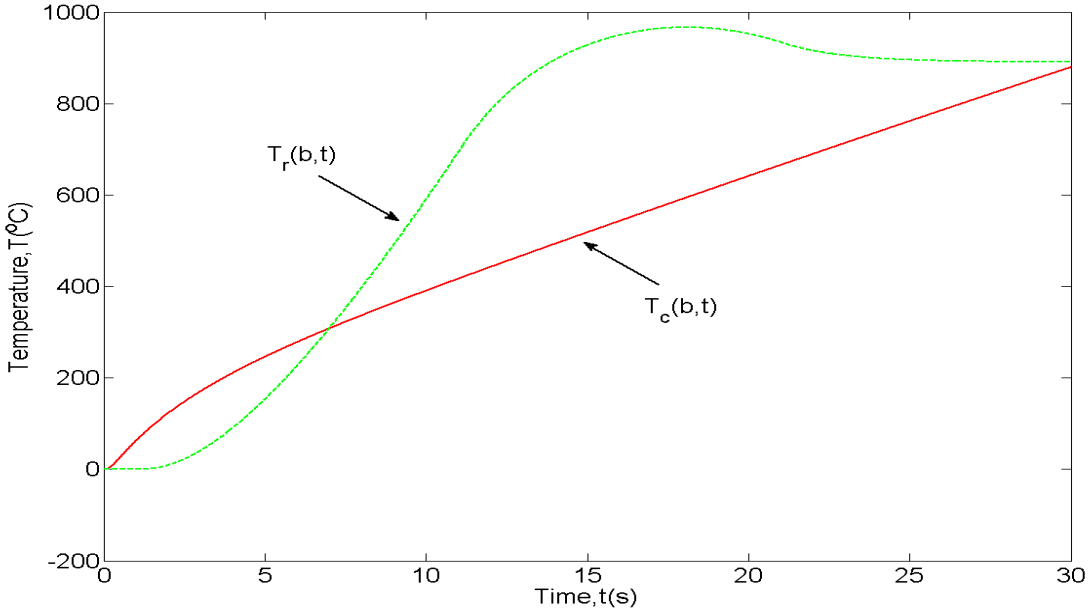

Figure 3.4.5: Noiseless temperature measurement $T_c(b,t)$ and $T_r(b,t)$ at the probe position ($b = 2\text{mm}$) for both the calibration and reconstruction tests, respectively.

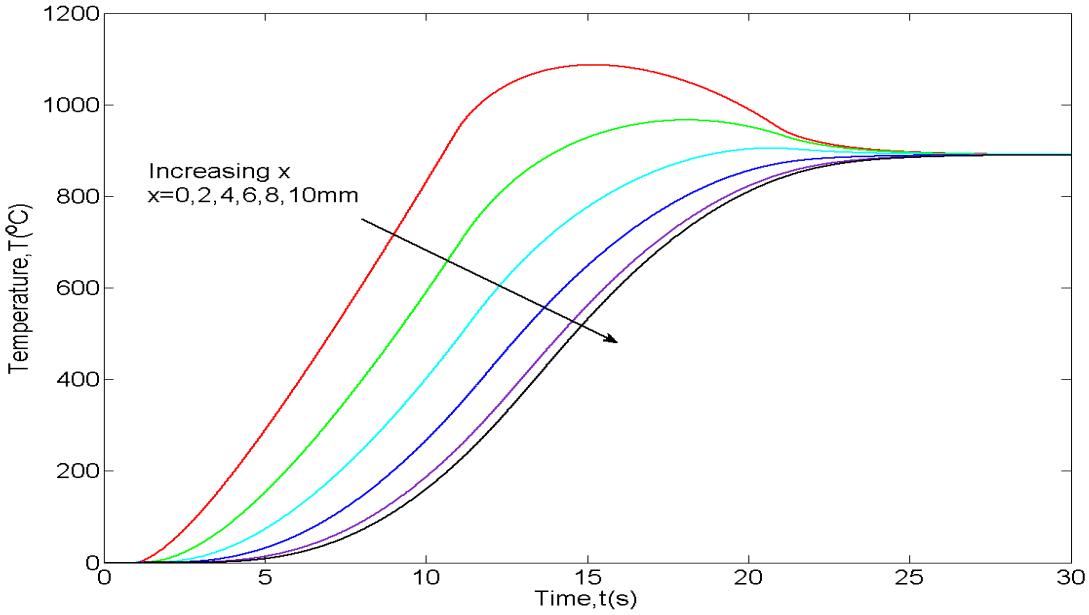

Figure 3.4.6: Temperature distribution resulting from the unknown imposed heat flux $q"_r(0,t)$. Note the probe is located at $x = b = 2\text{mm}$.

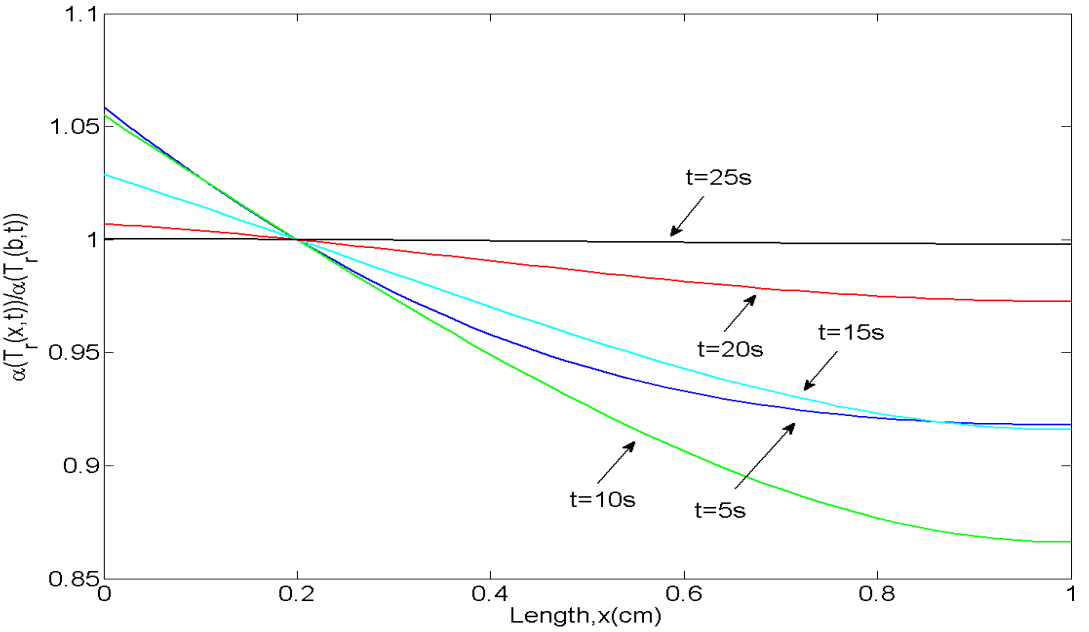

Figure 3.4.7: Dimensionless thermal diffusivity distribution over the spatial domain at five prescribed times.

with numerical implementation and model can be viewed and understood. The second case investigates the robustness and stability of the regularization methodology in the presence of noisy temperature data collected at $x = b$. Since the proposed rescaling calibration formulation displayed in Eq. (3.2.15d) is represented in terms of the rescaled Kirchhoff transformed variable θ^* rather than T, it is necessary to transform T to θ^* according to Eq. (3.2.2a) and Eq. (3.2.15c) before implementation. For the first case involving noiseless data, the resulting Kirchhoff transformed variables and their time-rescaled forms are displayed in Figs. 3.4.8 and 3.4.9, respectively. Notice that the rescaling is based on the noiseless probe temperature measurement at $b = 2mm$ in accordance to Eq. (3.2.15a). Similarly, the rescaled heat fluxes for both tests using Eq. (3.2.15b) are presented in Fig. 3.4.10. Figure 3.4.11 presents $G^*_{\theta,q}$ and $F^*_{\theta,q}$ over time in accordance to Eq. (3.3.1b,c) while their ratio is presented in Fig. 3.4.12. From this figure, it is evident that the maximum relative difference between $G^*_{\theta,q}$ and $F^*_{\theta,q}$ approaches to 2 percent which is lower than 8 percent if $q"(0,t)$ and $\theta(b,t)$ are directly substituted into Eq. (3.2.4c). Figure 3.4.13 presents the L-curve of Eq. (3.3.8) for the noiseless test case. Although this shape is not representative of an L-shaped, one must interpret that "best" regularization parameter λ_0 from the minimum of the residual $G^*_{\theta,q} - F^*_{\theta,q}$. Equation (3.3.7) can now be applied to predict the "best" rescaled surface heat flux, which has is shown in Fig. 3.4.14. This figure illustrates the model biasing as both shift and attenuation is observed. The predicted heat flux does not strictly fit the input due to the limitation of the piecewise time-step linearization assumption. However, the result is acceptable considering the magnitude of the nonlinearity imposed into the system.

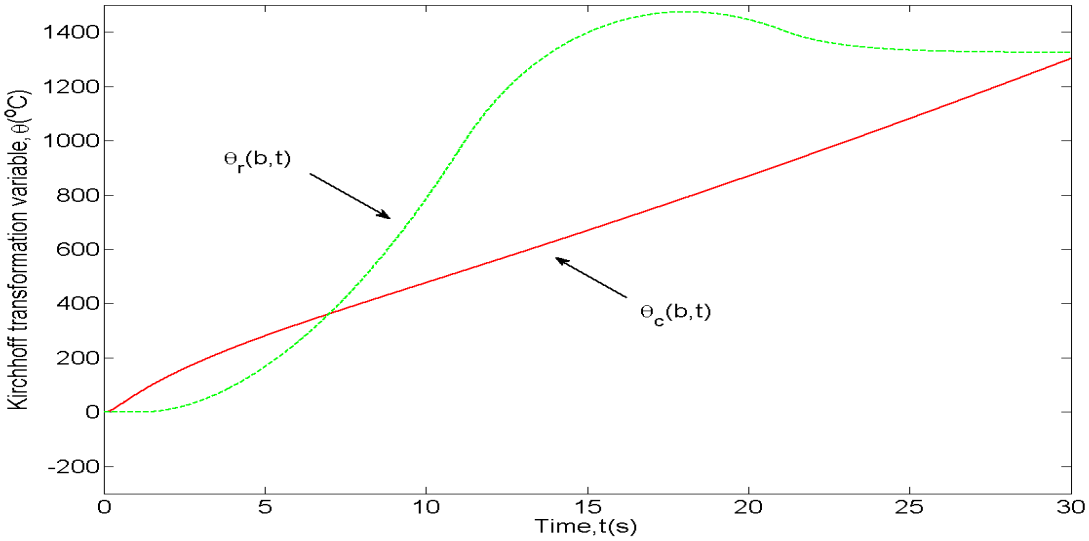

Figure 3.4.8: Noiseless Kirchhoff transformed variables $\theta_c(b,t)$ and $\theta_r(b,t)$ at the specified probe position for the calibration and reconstruction tests, respectively.

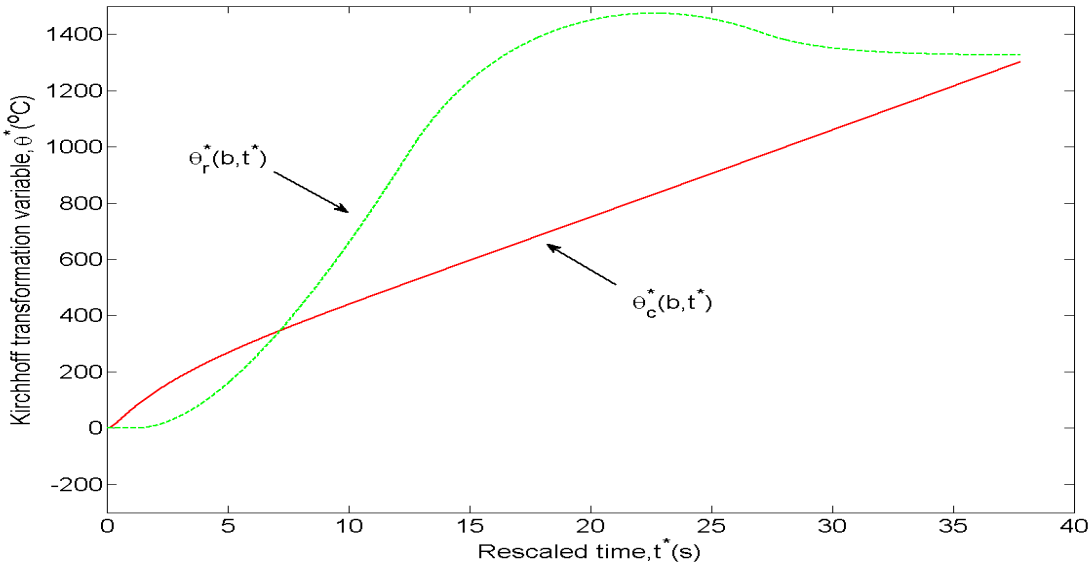

Figure 3.4.9: Noiseless time-rescaled Kirchhoff transformed variables $\theta_c^*(b,t^*)$ and $\theta_r^*(b,t^*)$ at the specified probe position for the calibration and reconstruction tests, respectively.

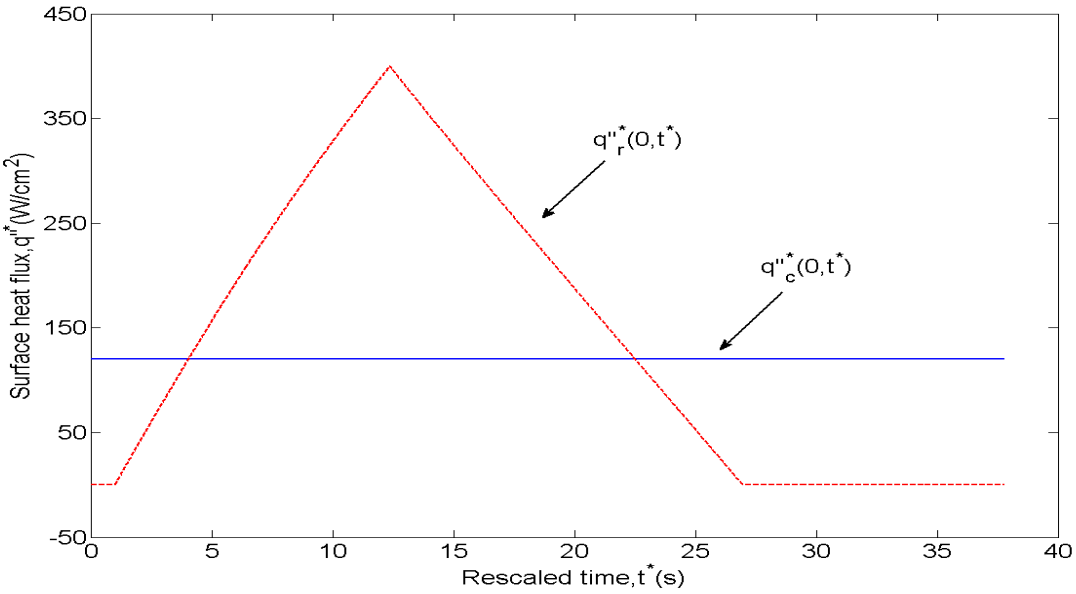

Figure 3.4.10: Time-rescaled known "calibration" surface heat flux $q"^{*}_{c}(0,t^{*})$ and the "unknown" heat flux $q"^{*}_{r}(0,t^{*})$ to be predicted based on noiseless temperature data at $x = b$.

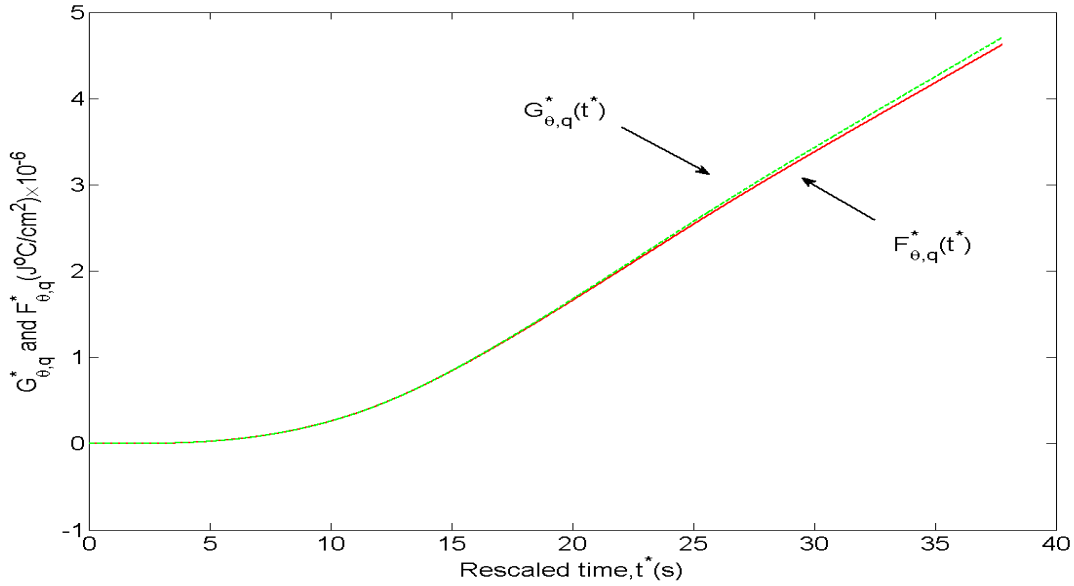

Figure 3.4.11: Comparison of $G^{*}_{\theta,q}$ and $F^{*}_{\theta,q}$ computed by Eqs. (3.3.1b-c) using noiseless temperature data collected at $x = b$.

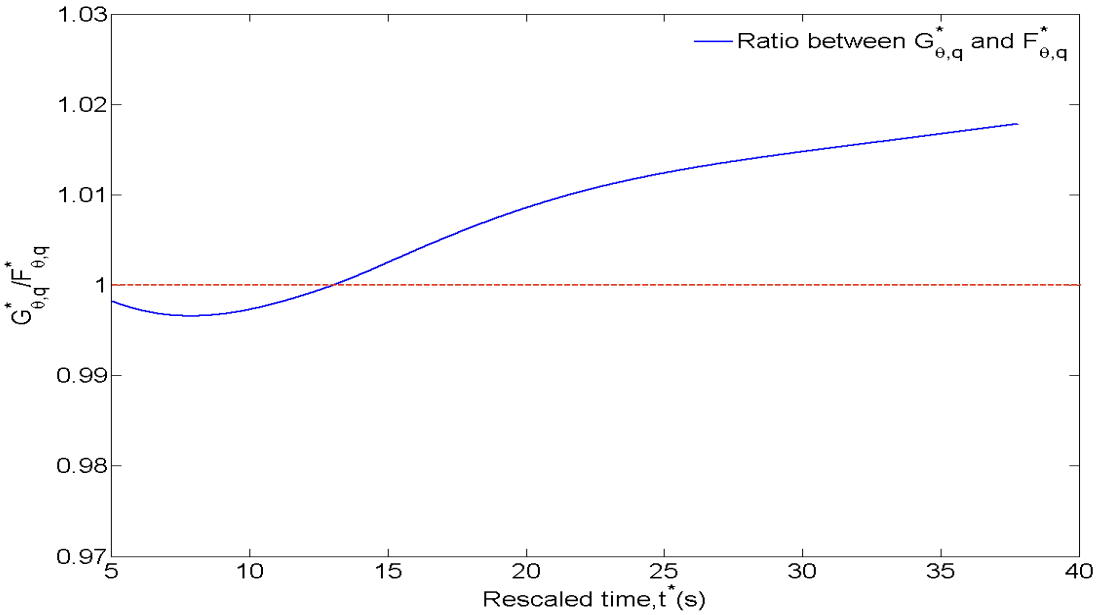

Figure 3.4.12: Ratio between $G^*_{\theta,q}$ and $F^*_{\theta,q}$ using noiseless temperature data collected at $x = b$.

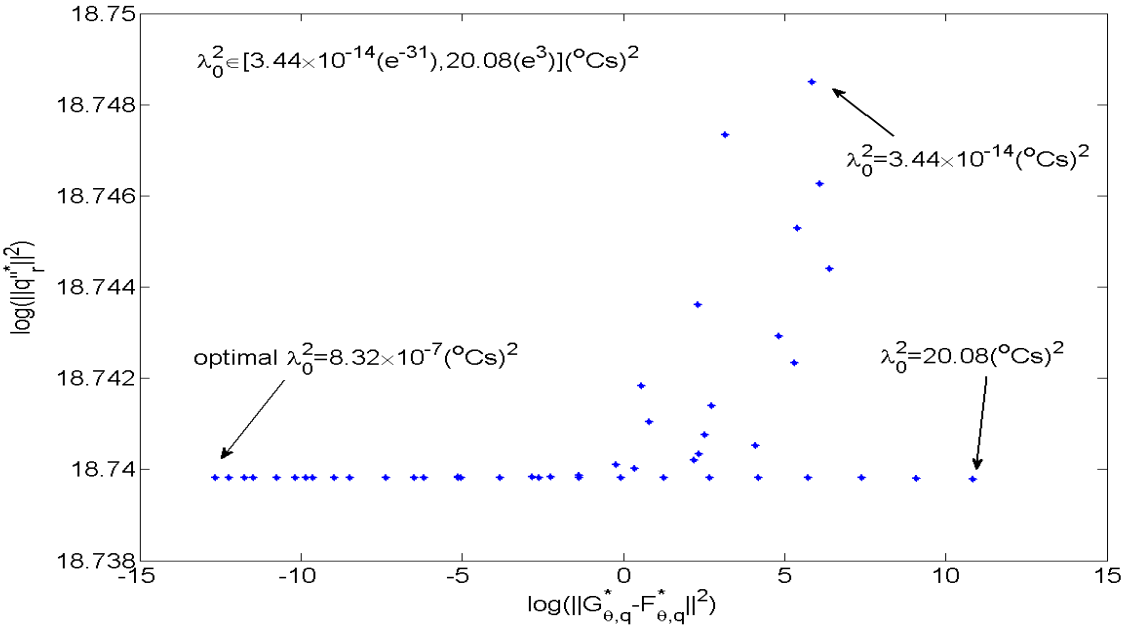

Figure 3.4.13: L-curve based on noiseless temperature data collected at $x = b$.

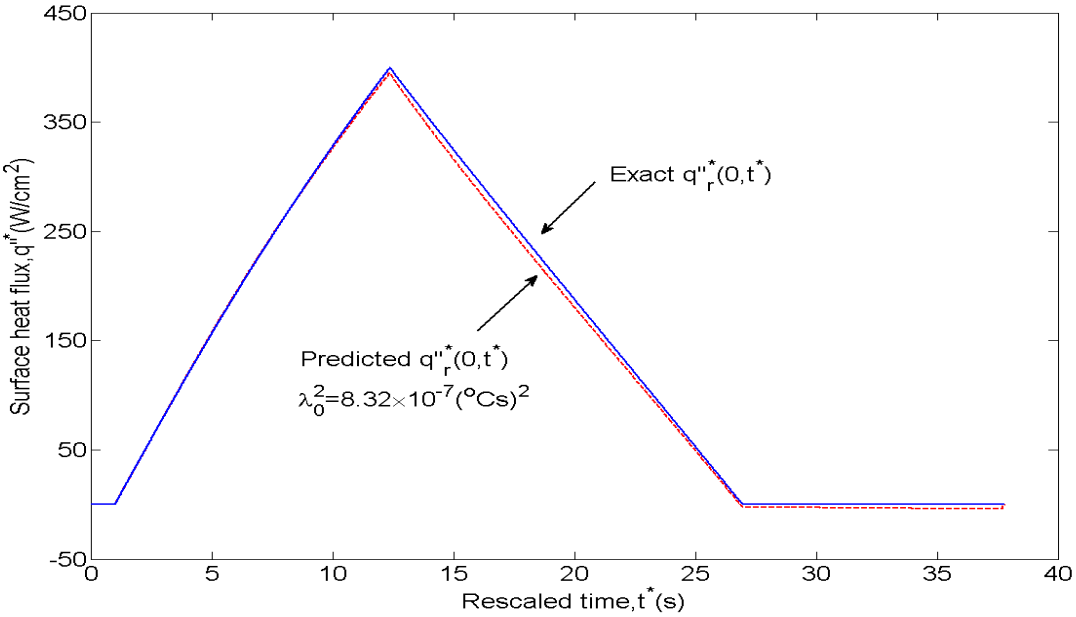

Figure 3.4.14: Predicted time-rescaled surface heat flux $q''^{*}_{r}(0,t^{*})$ based on noiseless temperature data at the regularization parameter, $\lambda_0^2 = 8.32 \times 10^{-7}(^{o}\mathrm{Cs})^2$.

Figure 3.4.15 presents the final prediction once the rescaled time domain is transformed or mapped back to the physical time domain in accordance to Eq. (3.2.16a).

For the second case, real experimental noise [117] has been added to the "noiseless" probe temperature data at $x = b$. For definiteness, the simulated noisy temperature data for the second case are generated through

$$T(b, t_i)|_2 = T(b, t_i)|_1 + \beta\varepsilon_i, \qquad i = 0,1,2 \cdots N + 1, \tag{3.4.2}$$

where $T(b, t_i)|_1$ represents the "noiseless temperature data" at time $t_i = i\Delta t$ at position $x = b$ for the first case; and, $T(b, t_i)|_2$ represents the corresponding noisy temperature data to be used for the second case. Here, β is a constant noise factor and ε_i is the discrete raw experimental noise ε_i collected at $t_i = i\Delta t$. These noise estimators have been generated from the inverse heat conduction experiment described in Ref. 117. Note that the number *N* of discrete data points is set to 6000 in the provided 30s time period. That is, the sampling rate is 200 Hz. Here, the noise factor is set to $\beta = 50$. This chosen value substantially amplifies the magnitude of the raw noise distribution. The added noise now has a standard deviation of error at about 1^{o}C. The scaling noise distribution $\beta\varepsilon_i$ and the noisy temperature $T(x,\ t_i)|_2$ at probe position $x = b$ applied for the second case are shown in Figs. 3.4.16 and 3.4.17, respectively. The identical numerical procedure previously described in the context of ideal data is implemented in the case of noisy data. Figure 3.4.18 presents the Kirchhoff transformed variable $\theta(x, t)$ for both calibration and reconstruction tests. Their corresponding rescaled forms of $\theta^*(x, t^*)$ and surface heat flux $q''^*(0, t^*)$ are displayed in Figs. 3.4.19 and 3.4.20, respectively. All transformations are based

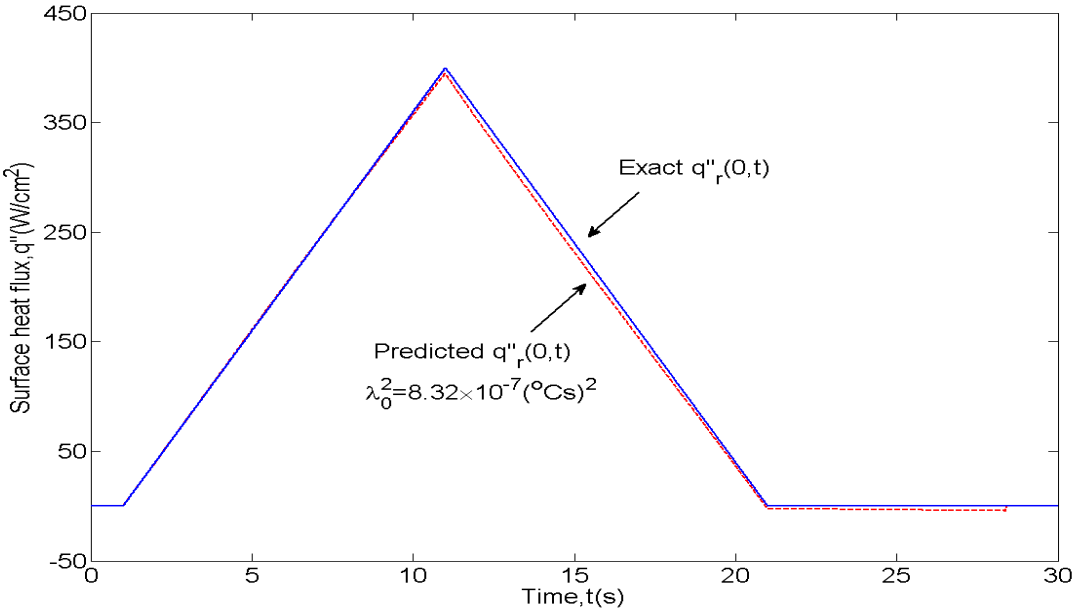

Figure 3.4.15: Predicted surface heat flux $q"_r(0,t)$ based on noiseless temperature data at the regularization parameter, $\lambda_0^2 = 8.32 \times 10^{-7}(^{o}\mathrm{Cs})^2$.

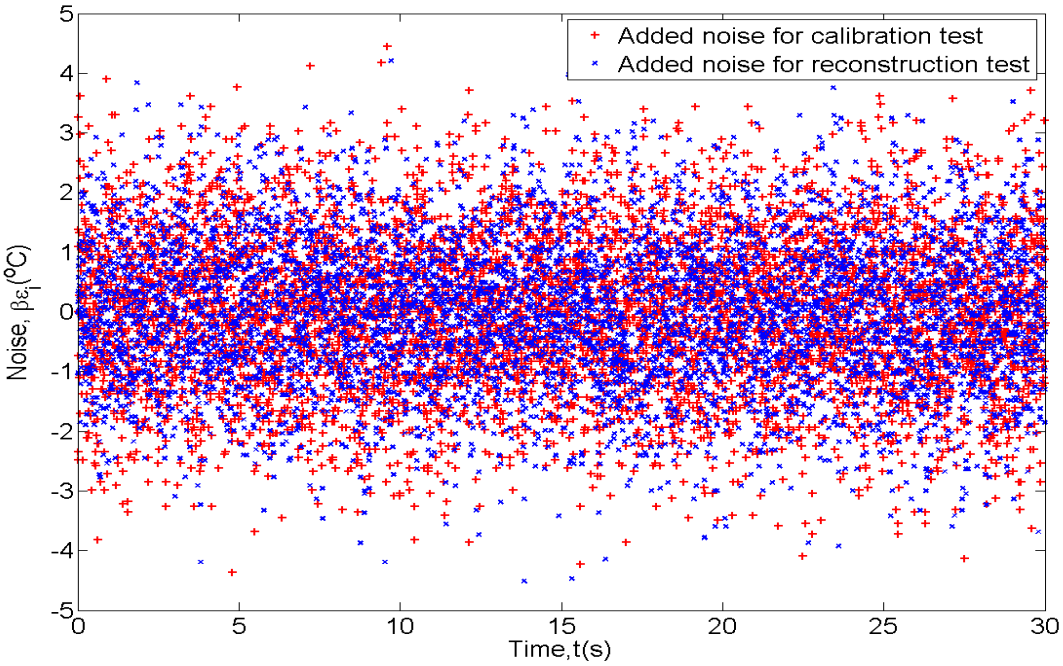

Figure 3.4.16: Added experimentally obtained noise per Eq. (3.4.2) using Ref.117 data.

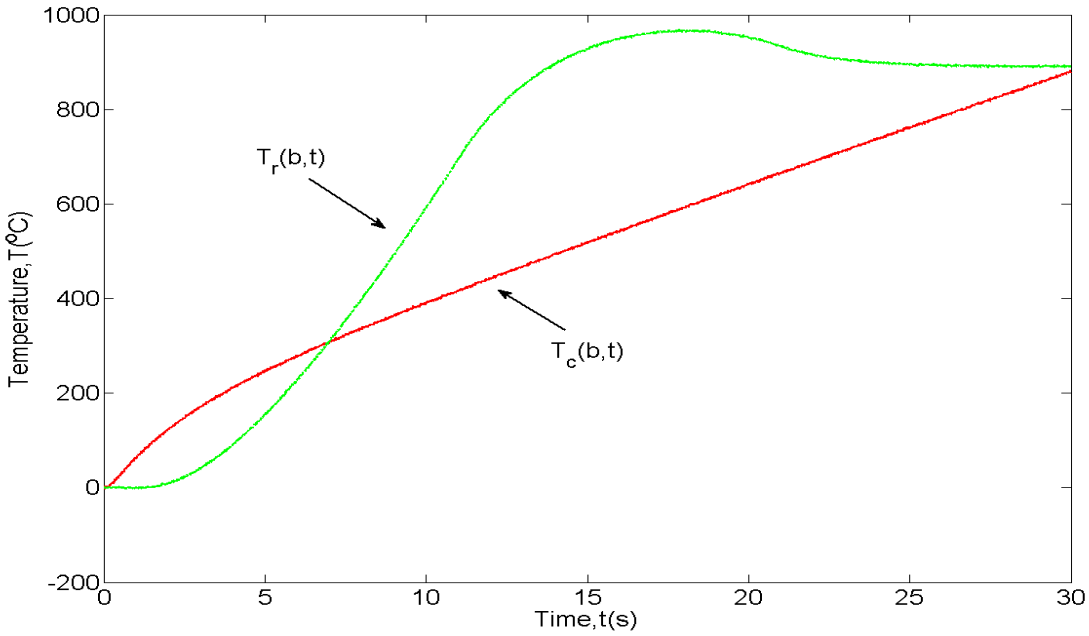

Figure 3.4.17: Noisy temperature data $T_c(b,t)$ and $T_r(b,t)$ at the specified probe position, $x = b$ for the calibration and reconstruction tests, respectively.

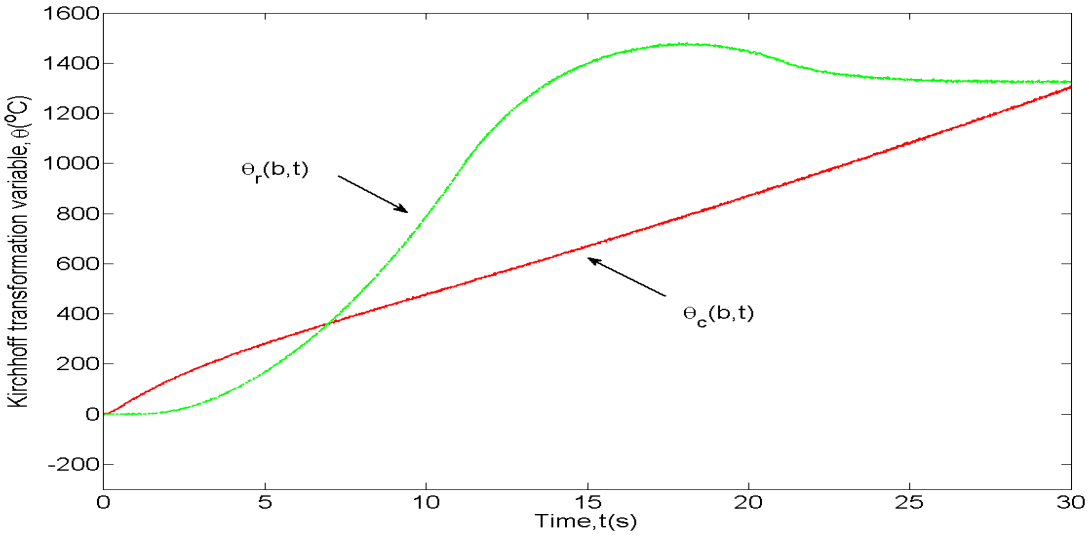

Figure 3.4.18: Kirchhoff transformed variable $s\ \theta_c(b,t)$ and $\theta_r(b,t)$ at the specified probe position $x = b$ for the calibration and reconstruction tests, respectively (noisy data).

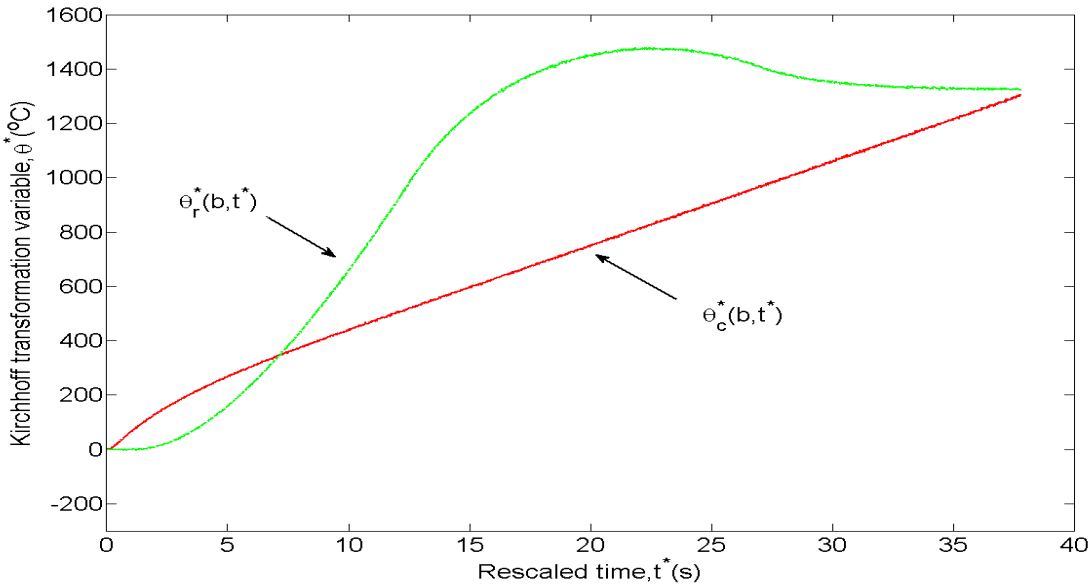

Figure 3.4.19: Time-rescaled Kirchhoff transformed variables $\theta_c^*(b,t^*)$ and $\theta_r^*(b,t^*)$ at the specified probe position for the calibration and reconstruction test, respectively (noisy data).

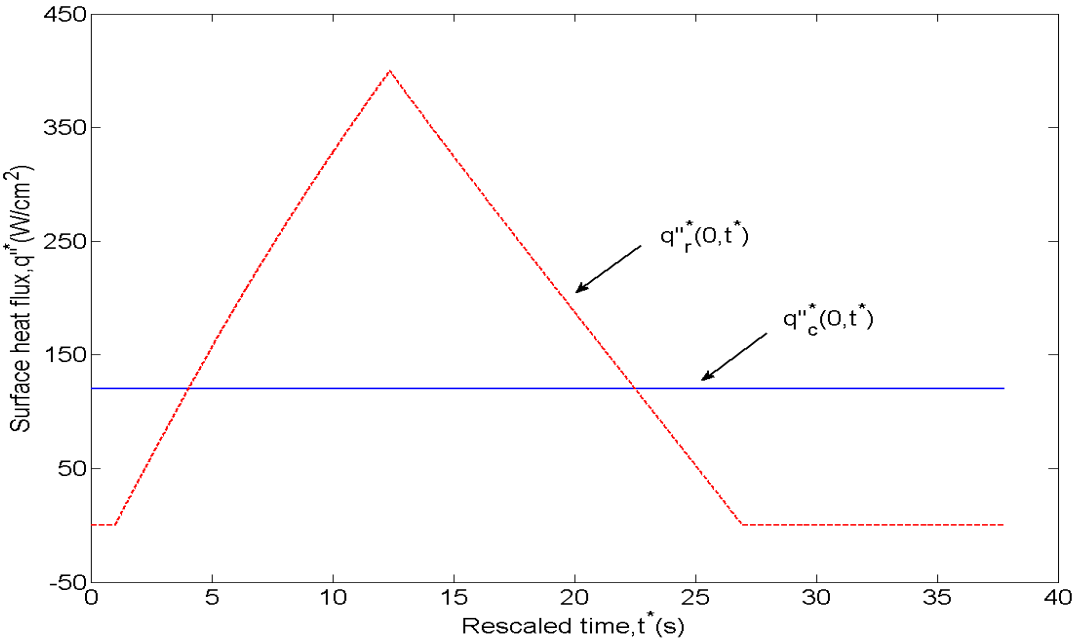

Figure 3.4.20: Time-rescaled known "calibration" surface heat flux $q''^*_c(0,t^*)$ and the "unknown" heat flux $q''^*_r(0,t^*)$ to be predicted based on noisy temperature data.

on the noisy probe temperature data displayed in Fig. 3.4.17. Figure 3.4.21 presents $G^*_{\theta,q}$ and $F^*_{\theta,q}$ over time while their ratio is presented in Fig. 3.4.22. Again, we find that the relative difference between $G^*_{\theta,q}$ and $F^*_{\theta,q}$ remains about 2 percent even after introduction of the magnified experimental noise shown in Fig. 3.4.16. This reflects the robustness of the proposed rescaling calibration formulation displayed in Eq. (3.2.15d).

Figure 3.4.23 presents the L-curve associated with this case where the L-shape emerges. A conventional L shape is now observed displaying a clear elbow. Two extreme values about the elbow, as indicated in Fig. 3.4.23, have been chosen to demonstrate robustness in the choice of the regularization parameter λ_0. Figures 3.4.24 and 3.4.25 present the rescaled surface heat flux prediction $q''^*_r(0,t^*)$ using the two highlighted regularization parameters from Fig. 3.4.23. Results show that $\lambda_0^2 = 5.20 \times 10^{-3}(℃s)^2$ produces excessive noise amplification while $\lambda_0^2 = 1.74 \times 10^{-1}(℃s)^2$ produces less error amplification. Higher frequencies are retained in the signal as the regularization parameter λ_0 decreases, as shown in Eq. (3.3.7). For this application, both of the predictions are stable. However, the optimal value chosen for this case is $\lambda_0^2 = 1.74 \times 10^{-1}(℃s)^2$. Figure 3.4.26 presents the physical time prediction of the surface (net) heat flux based on this choice of λ_0. The standard deviation of error between predicted surface heat flux and exact input value, energy balance and the recovery of maximum heat flux are also analyzed and shown in Table 3.4.1. Result shows that the prediction is accurate even in presence of a significant experiment noise, justifying the application of the rescaling principle in conjunction with Kirchhoff transformation for this nonlinear inverse heat conduction problem.

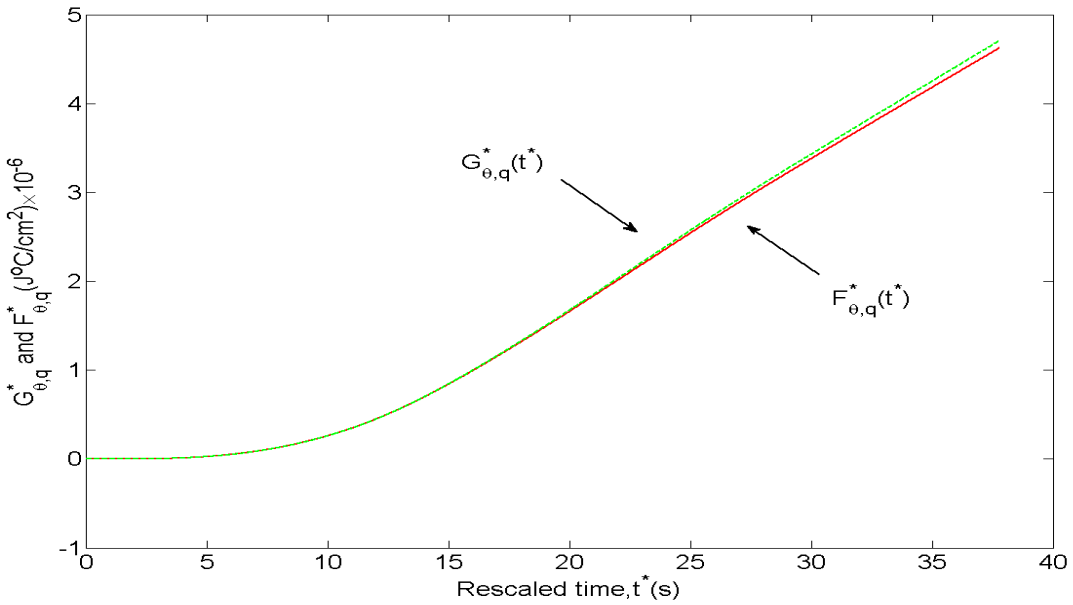

Figure 3.4.21: Comparison of $G^*_{\theta,q}$ and $F^*_{\theta,q}$ computed by Eqs. (3.3.1b-c) using noisy data.

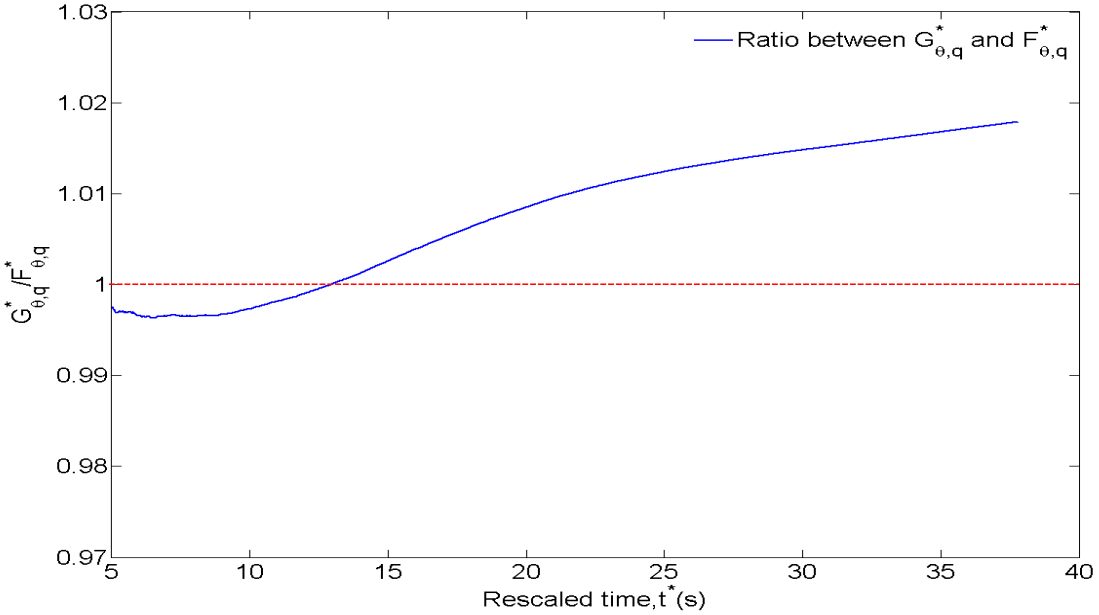

Figure 3.4.22: Ratio between $G^*_{\theta,q}$ and $F^*_{\theta,q}$ using noisy temperature data collected at $x = b$.

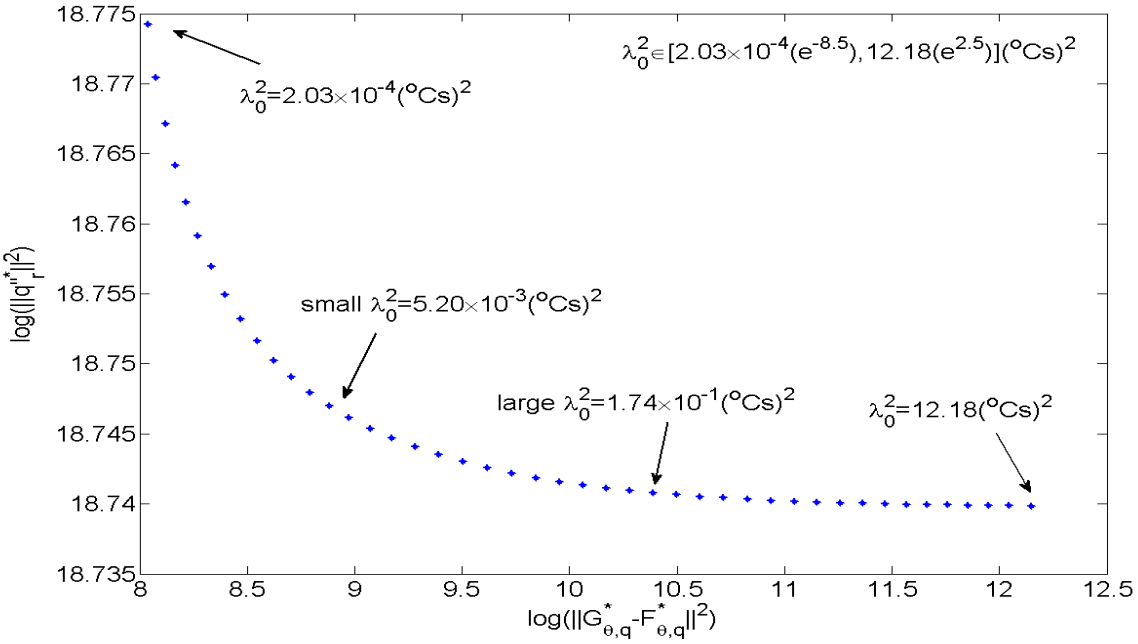

Figure 3.4.23: L-curve based on noisy temperature data collected at $x = b$.

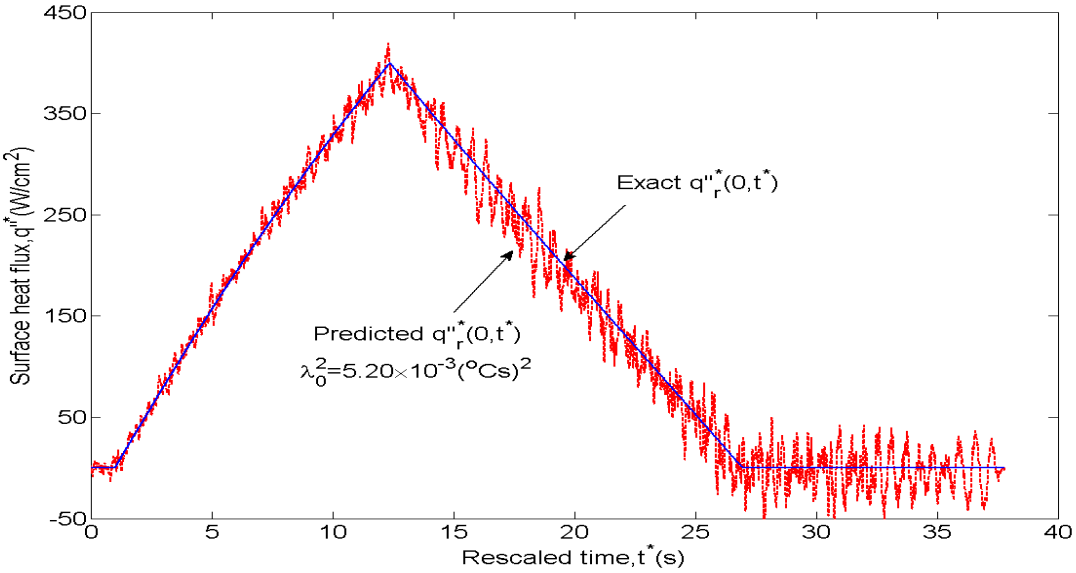

Figure 3.4.24: Predicted time-rescaled surface heat flux $q''^*_r(0,t^*)$ based on noisy temperature data using the lower choice of the regularization parameter from Fig. 3.4.23 ($\lambda_0^2 = 5.20 \times 10^{-3}(^oCs)^2$).

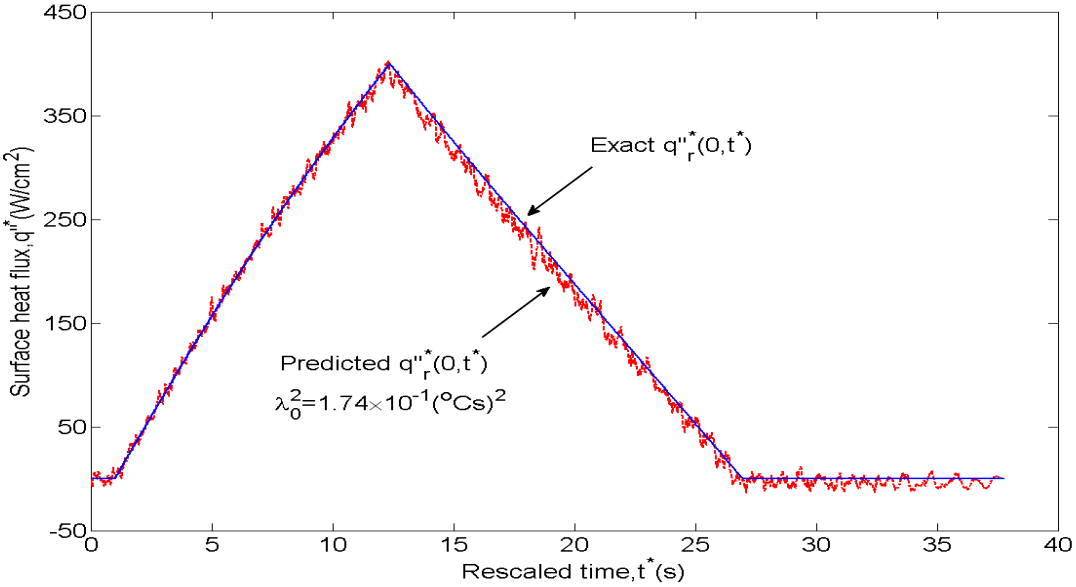

Figure 3.4.25: Predicted time-rescaled surface heat flux $q''^{*}_{r}(0,t^{*})$ based on noisy temperature data using the higher choice of the regularization parameter from Fig. 3.4.23 ($\lambda_0^2 = 1.74 \times 10^{-1}(^{o}\mathrm{Cs})^2$).

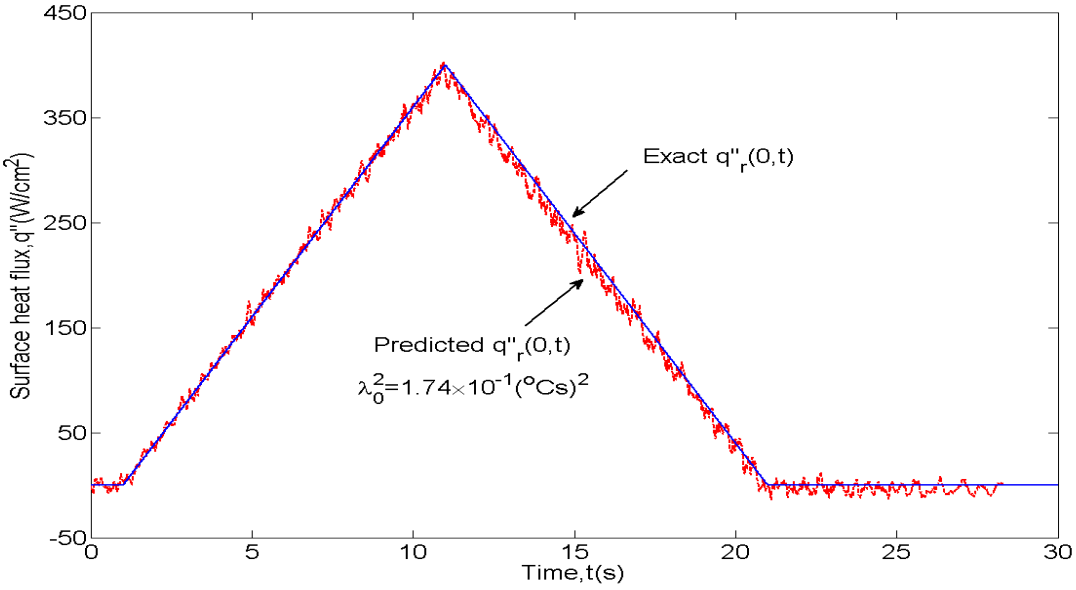

Figure 3.4.26: Predicted unknown surface heat flux $q''_{r}(0,t)$ based on noisy temperature data when $\lambda_0^2 = 1.74 \times 10^{-1}(^{o}\mathrm{Cs})^2$, $b = 2\mathrm{mm}$ for stainless steel 304.

Table 3.4.1: Quantitative comparison of standard deviation of error, total energy input and maximum value for the predicted surface heat flux, $q"_r(0,t)$ at the chosen optical regularization parameter, $\lambda_0^2 = 1.74 \times 10^{-1}(^{o}\mathrm{Cs})^2$, $b = 2\mathrm{mm}$ for stainless steel 304.

Metric	**Exact $q"_r(0,t)$**	**Prediction (noiseless data)**	**Prediction (noisy data)**
Standard deviation of error (W/cm^2)	0	2.97	7.15
Total energy input(J/ cm^2)	4000	3907	3906
Maximum value(W/cm^2)	400	393	402

3.5 Conclusions

This study demonstrates a novel idea integrating the Kirchhoff transformation and a time-domain rescaling principle about a local-temperature measurement. A nonlinear inverse heat conduction problem can be quasi-linearized using a piecewise time-step linearization assumption. The resulting linearized calibration integral equation then utilizes the Tikhonov framework for predicting the surface heat flux. Classical L-curve analysis assists in identifying a near optimal regularization parameter, λ_0 based on locating the elbow region of the resulting L-curve over the λ_0 spectrum. The "exact" optimal value for this parameter is not necessary for the present formulation as substantial robustness has been demonstrated. The accuracy of this new formulation depends on quasi-linearization principle associated with the thermal diffusivity. The prediction accuracy increases if the thermal diffusivity distribution along the spatial domain is nearly uniform. Several aerospace materials, including the stainless steel, copper and carbon-carbon are suitable for this analysis. In the present calibration framework, the precise sensor position does not require specification as it is implicitly included in the calibration test.

Chapter 4: A New Front Surface Heat Flux Calibration Method for 1-D Nonlinear Thermal System with a Time-Varying Back Boundary Condition

This chapter is based on a paper under review by Yinyuan Chen, Jay I. Frankel and Majid Keyhani:

Chen, Y.Y., Frankel, J.I., and Keyhani, M., in review, "A New Front Surface Heat Flux Calibration Method for 1-D Nonlinear Thermal System with a Time-Varying Back Boundary Condition", Mathematical Problems in Engineering.

My primary contributions to this paper include (1) conceptualization of the new model, (2) development of numerical and regularization methods (3) writing and implementing of the computer code (4) and served as lead writer of the manuscript.

4.1 Introduction

In many engineering environments, hostile thermal conditions preclude the use of surface mounted sensors. Hence, the surface thermal conditions can only be quantified through in-depth temperature measurements. This temperature projection from an in-depth sensor position to the surface is representative of the inverse heat conduction problem (IHCP). Many challenges are associated with resolving IHCPs, such as the well-known ill-posed mathematical nature that requires special regularization methods for extracting the best prediction [8, 59]. To deal with these issues, several specific techniques have been proposed, including "exact solutions" [37],

function specification [34-36], space marching and finite difference [49,110,114,118] and other well-studied techniques.

An alternative approach for resolving inverse heat conduction problems involves system calibration. System calibration relies on analytical processing to form a calibration or measurement equation. One major advantage of this approach lies in reducing the systematic errors introduced by uncertainties associated with probe positioning, probe signal delay and attenuation, and domain thermophysical properties. However, during the calibration process, the imposed net surface heat flux must be accurately measured. Loehle et al. [40], Loehle et al. [41] and Gardarein et al. [42] have demonstrated the application of a calibration based system identification method for estimating the surface heat flux using a single in-depth sensor. The Non-Integer System Identification (NISI) method involves developing an impulse response function from a calibration test. A finite series expansion is formed in terms of fractional derivatives of the measured calibration temperature and calibration net surface heat flux. The unknown expansion coefficients are determined during the calibration stage. The unknown surface heat flux can be recovered based on the impulsive response. In contrast, Frankel and Keyhani [43], Frankel et al. [44] and Elkins et al. [45] have proposed an alternative calibration methodology that eliminates the use of fractional derivatives and the resolution of expansion coefficients described by the NISI method. This method relates the net unknown surface heat flux to the net calibration surface heat flux and the corresponding in-depth temperature measurements during the calibration and reconstruction test runs. The resulting inverse statement is then expressed in terms of a Volterra integral equation of the first kind for the unknown surface heat flux.

The linear one-probe calibration integral equation method (CIEM) [43, 44] has been experimentally verified [45] with excellent accuracy in an appropriate temperature range. This method is derived assuming that an unchanging back boundary condition exists between the calibration and reconstruction tests. Hence, this formulation is applicable to the semi-infinite geometry or a slab with a fixed heat transfer coefficient at the back-face, and uniform initial condition. The initial condition can be dissimilar between the calibration and reconstruction tests, but the ambient temperature must be the same as the initial condition. However, in many practical situations, the calibration test environment is not the same as the reconstruction test environment. In addition, extending the applied temperature range normally requires the proper depiction of the thermophysical properties variation with temperature. That is, the properties need to be expressed in terms of temperature dependent functions. The inclusion of temperature dependency of the properties produces a fully nonlinear description of heat conduction. Therefore, expanding the linear one-probe calibration concept is germane such that variation of the back boundary condition and the system nonlinearity can be included. To account for a variation in the back boundary condition between calibration and reconstruction test, Frankel and Keyhani [111] designed a new calibration equation based on two in-depth probes. Inclusion of the second probe alleviates the need to quantify the back boundary conditions. As a result, an additional calibration test is also required. The final inverse statement can be expressed in terms of a Volterra integral equation of the first kind for the unknown front surface heat flux in the constant property framework. However, this calibration method is still derived in a linear framework. Recently, Chen et al. [112] proposed a novel one-probe calibration method achieving the quasi-linearization through the combination of Kirchhoff transformation and rescaling principles. In this process, the Kirchhoff transformation linearized the thermal conductivity while

time domain rescaling was used to handle the temperature-dependent thermal diffusivity. All predictions were performed in the rescaled variable and the final results were then obtained after mapping back to physical variables. However, this one-probe formulation maintained the previously noted back boundary condition restriction.

This chapter proposes a novel nonlinear two-probe calibration method absorbing all positive attributes of the two-probe linear calibration method [111] and the recently proposed nonlinear one-probe calibration method [112]. With regard to the system nonlinearity, a quasi-linearization approach is applied based on a rescaling principle that implements a piecewise time-step linearization assumption. This assumption involves a whole time domain discretization using a successive series of small time steps in increments of Δt. At any time interval, all the thermal properties are assumed fixed and evaluated at the closest probe to active boundary of interest. To allow for variability in the back boundary condition among tests, a second probe and additional calibration tests are introduced. This formulation produces a complicated but available discrete kernel that requires careful understanding as it possesses strong ill-posed effects. However, a proper calibration strategy can be implemented to overcome these difficulties based on physical understanding of diffusion.

It is well-known that all inverse problems are ill-posed. Arbitrary noise introduced into the measurements magnify as the information is projected toward the boundary. Therefore destabilization is always encountered that can produce useless predictions. Hence, it is necessary to stabilize the mathematical system through regularization. Common regularization approaches

include Tikhonov regularization [82], iterative regularization [16], local future-time method [8] and Singular-Value Decomposition (SVD) [80, 81].

Section 4.2 presents the detailed derivation of the new nonlinear two-probe calibration method based on rescaling principles. Section 4.3 presents the localized Tikhonov regularization approach used for generating a family of predictions based on the proper regularization parameters using an L-curve strategy. Section 4.4 presents numerical results using two common engineering materials, namely stainless steel 304 and a carbon composite. The back boundary condition strategy is also discussed and demonstrated for the calibration tests. Section 4.5 provides concluding remarks on this new calibration method.

4.2 Formulation of Nonlinear Two-Probe Calibration

The nonlinear two-probe calibration method is an extension of the linear two-probe calibration integral method [111]. Therefore, the derivation of the linear two-probe calibration method for estimating the front surface heat flux is presented first and then extended to the nonlinear problem. A schematic of the sample geometry is given in Fig. 4.2.1. This coupon geometry could also be representative of a plug sensor used in aerospace application. Here, the first temperature probe is located at $x = b$ while the second temperature probe is located at $x = w$. The addition of the second probe removes the need to specify the back boundary condition. The rescaling principle is then introduced to resolve the inverse problem in a nonlinear framework. This procedure leads to a new calibration equation that allows for system nonlinearities and alternative rear-side boundary conditions among test runs.

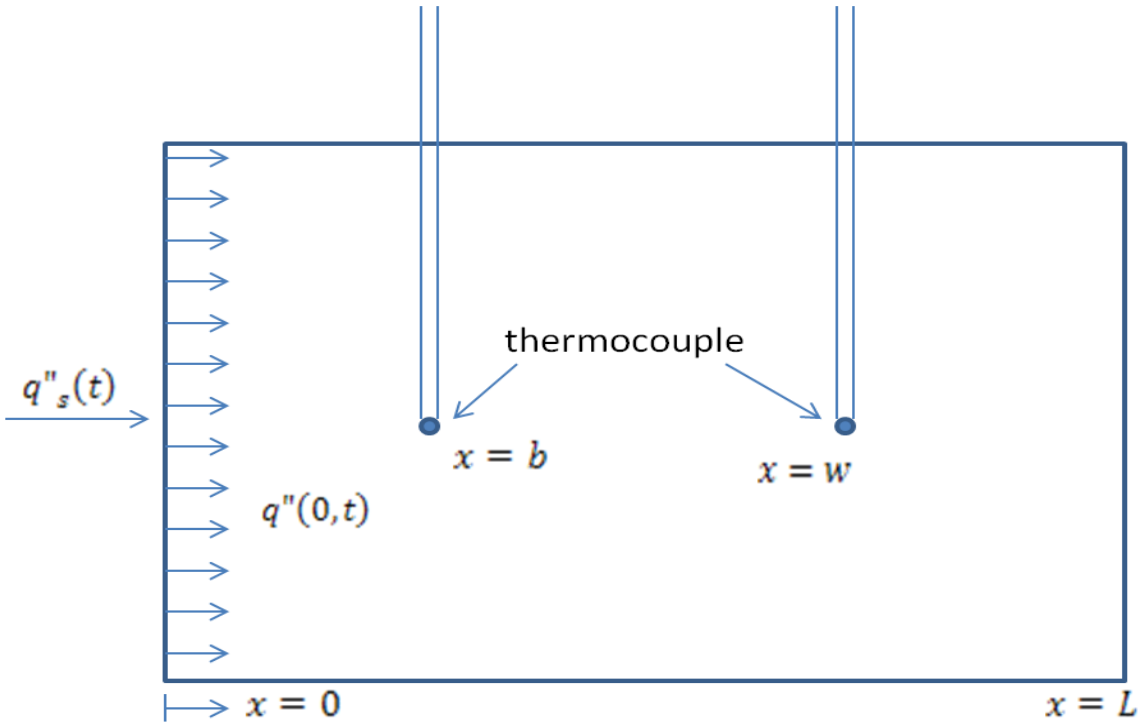

Figure 4.2.1: System set-up for one-dimensional heat conduction problem showing the positions of two in-depth temperature probes.

Consider a linear one-dimensional heat conduction problem in Cartesian coordinates having a front surface heat flux source at $x = 0$ and a time-varying back boundary condition at $x = L$ in terms of a Robin's condition [33] imposed either under laboratory conditions for coupon calibration or for practical implementation. For the moment, let us express the backside Robin's boundary condition possessing a heat transfer coefficient h_L and corresponding environment temperature T_∞. The heat equation can be written as [33]

$$\frac{1}{\alpha}\frac{\partial T}{\partial t}(x,t) = \frac{\partial^2 T}{\partial x^2}(x,t), \qquad x \in (0,L), \;\; t \geq 0, \tag{4.2.1a}$$

subject to the boundary conditions

$$-k\frac{\partial T}{\partial x}(0,t) \triangleq q"(0,t) = q"_s(t),$$

$$-k\frac{\partial T}{\partial x}(L,t) = h_L(T(L,t) - T_\infty), \;\; t \geq 0, \tag{4.2.1b-c}$$

Inclusion of the temperature measurement $T(w,t)$ at $x = w$ provides a means to eliminate the Robin's condition imposed at $x = L$ given by Eq. (4.2.1c), thereby bypassing the need to specify both h_L and T_∞. This reduces the analysis domain from $x \in [0,L]$ to $x \in [0,w]$ where $w < L$ for estimating $q"(0,t)$. The resulting thermal boundary condition at $x = w$ is defined as

$$T(w,t) = T_w(t), \qquad t \geq 0, \tag{4.2.1d}$$

where $T_w(t)$ represents the temperature measurement of the second probe at $x = w$. For presentation definition, the temperature data $T(b,t)$ at $x = b$ is denoted through

$$T(b,t) = T_b(t), \qquad t \geq 0, \tag{4.2.1e}$$

where $T_b(t)$ is the temperature measurement of the first probe at $x = b$. To reiterate, we use the second in-depth probe away from the active side of interest for defining the second boundary condition required by the boundary-value problem. In this way, we have no need to quantify or specify the state at $x = L$. The initial condition is

$$T(x,0) = 0, \qquad x \in [0, L]. \tag{4.2.1f}$$

Notice that for simplicity but without loss of generality, all the temperatures used in this chapter are interpreted as the relative temperature from the initial uniform temperature condition.

To obtain an exact solution for $T(x,t)$ using Eqs. (4.2.1a,b,d), one approach is to use the Laplace transform technique [31]. This technique is widely used for solving linear heat-conduction problems. This transformation is defined in the semi-infinite domain and transforms the time variable onto the frequency domain. Explicitly, the Laplace transformation operator $\mathcal{L}$ is defined as [33]

$$\mathcal{L}\{f(t)\} = \hat{f}(s) \triangleq \int_{t=0}^{\infty} f(t)e^{-st}dt, \qquad s \geq 0. \tag{4.2.2}$$

where s is a complex variable. For notation simplicity, we write $s \geq 0$ but formally it is interpreted as $Re(s) \geq 0$. To begin, we operate on the linear heat equation given by Eq. (4.2.1a) with the Laplace transformation operator $\mathcal{L}$ to get

$$\frac{1}{\alpha}\mathcal{L}\left\{\frac{\partial T}{\partial t}(x,t)\right\} = \mathcal{L}\left\{\frac{\partial^2 T}{\partial x^2}(x,t)\right\}, \quad x \in (0,w), \;\; s \geq 0. \tag{4.2.3}$$

This procedure transforms the original partial differential equation given by Eq. (4.2.1a) into the linear ordinary differential equation

$$\frac{d^2\hat{T}}{dx^2}(x,s) - \frac{s}{\alpha}\hat{T}(x,s) = 0, \quad x \in (0,w), \;\; s \geq 0. \tag{4.2.4}$$

The general solution of Eq. (4.2.4) is

$$\hat{T}(x,s) = A_{q2}(s)cosh\sqrt{\frac{s}{\alpha}}x + B_{q2}(s)sinh\sqrt{\frac{s}{\alpha}}x, \quad x \in (0,w), \;\; s \geq 0. \tag{4.2.5}$$

Here, the subscript "$q2$" indicates that we are dealing with the two-probe thermal system for resolving unknown surface heat flux. To determine the unknown coefficients $A_{q2}(s)$ and $B_{q2}(s)$, it is necessary to take the Laplace transform of both auxiliary conditions. These conditions are at $x = 0$ for the surface heat flux and $x = w$ for the in-depth temperature measurement. Doing so produces

$$\hat{q}"(0,s) = \mathcal{L}\left\{-k\frac{\partial T}{\partial x}(0,t)\right\} = -k\sqrt{\frac{s}{\alpha}}B_{q2}(s), \quad s \geq 0, \tag{4.2.6a}$$

$$\hat{T}(w,s) = \hat{T}_w(s) = A_{q2}(s)cosh\sqrt{\frac{s}{\alpha}}w + B_{q2}(s)sinh\sqrt{\frac{s}{\alpha}}w, \ \ s \geq 0, \tag{4.2.6b}$$

respectively.

Observe that the spatial domain of interest involves $x \in [0,w]$ rather than $x \in [0,L]$ since the temperature measurement at $x = w$ represents the required rear-side boundary condition. Next, we express unknown coefficients $A_{q2}(s)$ and $B_{q2}(s)$ in terms of these two boundary conditions to obtain

$$A_{q2}(s) = \frac{\hat{T}(w,s) + \hat{q}"(0,s)\left(\frac{1}{k}\sqrt{\frac{\alpha}{s}}\right)sinh\sqrt{\frac{s}{\alpha}}w}{cosh\sqrt{\frac{s}{\alpha}}w}, \tag{4.2.7a}$$

$$B_{q2}(s) = -\frac{1}{k}\sqrt{\frac{\alpha}{s}}\hat{q}"(0,s), \tag{4.2.7b}$$

respectively. Upon substituting Eqs. (4.2.7a, b) into Eq. (4.2.5) and evaluating the reconstruction solution $\hat{T}(x,s)$ at $x = b$, we obtain

$$\hat{T}(b,s) = \hat{D}_{T,q2}(b,w,\alpha,s)\hat{T}(w,s) + \hat{D}_{q,q2}(b,w,\alpha,k,s)\hat{q}"(0,s), \quad s \geq 0, \tag{4.2.8}$$

where

$$\widehat{D}_{T,q2}(b,w,\alpha,s)=\frac{cosh\sqrt{\frac{s}{\alpha}}b}{cosh\sqrt{\frac{s}{\alpha}}w}, \tag{4.2.9a}$$

$$\widehat{D}_{q,q2}(b,w,\alpha,k,s)=\left(\frac{1}{k}\sqrt{\frac{\alpha}{s}}\right)\frac{sinh\sqrt{\frac{s}{\alpha}}(w-b)}{cosh\sqrt{\frac{s}{\alpha}}w}. \tag{4.2.9b}$$

Here, the subscript "T" indicates that the thermal response function $\widehat{D}$ in frequency domain is based on an impulsive temperature at $x=w$ while the subscript "q" indicates that the corresponding thermal response function $\widehat{D}$ is based on an impulsive surface heat flux at $x=0$. It is necessary to note that both $\widehat{D}_{T,q2}(b,w,\alpha,s)$ and $\widehat{D}_{q,q2}(b,w,\alpha,k,s)$ are solely functions of the thermophysical properties and probe positions. Their forms are independent of the time-varying auxiliary conditions. As a result of this observation, it is possible to design a calibration strategy eliminating $\widehat{D}_{T,q2}(b,w,\alpha,s)$ and $\widehat{D}_{q,q2}(b,w,\alpha,k,s)$ in terms of two calibration tests using the known net heat flux input and measured temperature response [111]. These two calibration tests will be denoted with the aid of the additional "i" subscript notation as

$$\hat{T}_{ci}(b,s)=\widehat{D}_{T,q2}(b,w,\alpha,s)\hat{T}_{ci}(w,s)+\widehat{D}_{q,q2}(b,w,\alpha,k,s)\hat{q}"_{ci}(0,s),$$
$$s\geq 0,\ \ i=1,2. \tag{4.2.10}$$

Using Eq. (4.2.10), we can express the transfer functions as

$$\widehat{D}_{T,q2}(b,w,\alpha,s)=\frac{\hat{T}_{c1}(b,s)\hat{q}"_{c2}(0,s)-\hat{T}_{c2}(b,s)\hat{q}"_{c1}(0,s)}{\hat{T}_{c1}(w,s)\hat{q}"_{c2}(0,s)-\hat{T}_{c2}(w,s)\hat{q}"_{c1}(0,s)},\qquad(4.2.11a)$$

$$\widehat{D}_{q,q2}(b,w,\alpha,k,s)=\frac{\hat{T}_{c1}(b,s)\hat{T}_{c2}(w,s)-\hat{T}_{c2}(b,s)\hat{T}_{c1}(w,s)}{\hat{q}"_{c1}(0,s)\hat{T}_{c2}(w,s)-\hat{q}"_{c2}(0,s)\hat{T}_{c1}(w,s)}.\qquad(4.2.11b)$$

Replacing the transfer functions $\widehat{D}_{T,q2}(b,w,\alpha,s)$ and $\widehat{D}_{q,q2}(b,w,\alpha,k,s)$ in terms of calibration data through Eq. (4.2.8) produces

$$\hat{T}(b,s)=\frac{\hat{T}_{c1}(b,s)\hat{q}"_{c2}(0,s)-\hat{T}_{c2}(b,s)\hat{q}"_{c1}(0,s)}{\hat{T}_{c1}(w,s)\hat{q}"_{c2}(0,s)-\hat{T}_{c2}(w,s)\hat{q}"_{c1}(0,s)}\hat{T}(w,s)+$$

$$\frac{\hat{T}_{c1}(b,s)\hat{T}_{c2}(w,s)-\hat{T}_{c2}(b,s)\hat{T}_{c1}(w,s)}{\hat{q}"_{c1}(0,s)\hat{T}_{c2}(w,s)-\hat{q}"_{c2}(0,s)\hat{T}_{c1}(w,s)}\hat{q}"(0,s),\quad s\geq 0.\qquad(4.2.12)$$

It is now possible to represent the unknown front surface heat flux data $\hat{q}"_r(0,s)$ in terms of $\hat{T}_{ci}(b,s),\hat{T}_{ci}(w,s),\hat{q}"_{ci}(0,s)$ for $i=1,2$ and $\hat{T}_r(b,s)$, $\hat{T}_r(w,s)$. Here, the subscript "r" represents the reconstruction test from which the front surface heat flux needs to be resolved.

Expressing Eq. (4.2.12) in the framework of a reconstruction run produces

$$\left[\hat{T}_{c1}(b,s)\hat{T}_{c2}(w,s)-\hat{T}_{c2}(b,s)\hat{T}_{c1}(w,s)\right]\hat{q}"_r(0,s)=$$

$$\left[\hat{T}_{c2}(w,s)\hat{q}"_{c1}(0,s)-\hat{T}_{c1}(w,s)\hat{q}"_{c2}(0,s)\right]\hat{T}_r(b,s)+$$

$$\left[\hat{T}_{c1}(b,s)\hat{q}"_{c2}(0,s)-\hat{T}_{c2}(b,s)\hat{q}"_{c1}(0,s)\right]\hat{T}_r(w,s),\quad s\geq 0.\qquad(4.2.13)$$

The inverse Laplace transformation for a three-term product is [117]

$$\mathcal{L}^{-1}\left(\hat{f}_1(s)\hat{f}_2(s)\hat{f}_3(s)\right) = \int_{u=0}^{t} f_1(u) \int_{r=0}^{t-u} f_2(v)\, f_3(t-u-v)dvdu, \quad t \geq 0. \qquad (4.2.14)$$

With this inversion expression, we can apply the inverse Laplace transformation on Eq. (4.2.13) and use the Eq. (4.2.14) to obtain the two-probe linear calibration equation as

$$\int_{u=0}^{t} q_r"(0,u) \int_{v=0}^{t-u} [T_{c1}(b,v)T_{c2}(w,t-u-v) - T_{c2}(b,v)T_{c1}(w,t-u-v)]\, dvdu \; =$$

$$\int_{u=0}^{t} T_r(b,u) \int_{v=0}^{t-u} [q"_{c1}(0,v)T_{c2}(w,t-u-v) - q"_{c2}(0,v)T_{c1}(w,t-u-v)]\, dvdu +$$

$$\int_{u=0}^{t} T_r(w,u) \int_{v=0}^{t-u} [q"_{c2}(0,v)T_{c1}(b,t-u-v) - q"_{c1}(0,v)T_{c2}(b,t-u-v)]\, dvdu,$$

$$t \geq 0. \qquad (4.2.15)$$

Next, we consider the nonlinear situation. If the temperature range is large, then one should consider the effect of temperature dependent thermophysical properties. The nonlinear heat equation in the reduced spatial domain is [33]

$$\frac{\partial}{\partial x}\left[k(T)\frac{\partial T}{\partial x}(x,t)\right] = \rho c_p(T)\frac{\partial T}{\partial t}(x,t), \qquad x \in (0,w), \quad t \geq 0, \qquad (4.2.16a)$$

subject to reduced the boundary conditions

$$-k(T)\frac{\partial T}{\partial x}(0,t) \triangleq q"(0,t) = q"_s(t),$$

$$T(w,t) = T_w(t), \qquad t \geq 0, \qquad (4.2.16b-c)$$

which follows the logic previously described domain reduction and initial condition

$$T(x,0) = 0, \qquad x \in [0,w]. \qquad (4.2.16d)$$

Again, the resolution domain only involves $x \in [0,w]$ though physically $x \in [0,L]$ is affected during the calibration and reconstruction tests.

To account for the variable property effects involved in this fully nonlinear formulation, a piecewise time-step linearization assumption is proposed to form the quasi-linearization. This assumption implies that the thermal property is fixed in any small time step and evaluated at the forward probe position temperature $T(b,t)$.

For purpose of illustration, consider a heating process with $t_{max} = (N+1)\Delta t$, with any small interval $t \in [i\Delta t, (i+1)\Delta t]$ ($i = 0,1 \ldots N$), then the governing heat equation under piecewise time-step linearization assumption becomes

$$\alpha\big(T(b,i\Delta t)\big)\,\frac{\partial^2 T_i}{\partial x^2}(x,t) = \frac{\partial T_i}{\partial t}(x,t), \qquad x \in (0,w), \;\; t \in [i\Delta t, (i+1)\Delta t], \qquad (4.2.17a)$$

where $T_i(x,t) = T(x,t),\ t \in [i\Delta t, (i+1)\Delta t]$ and subject to the boundary conditions

$$-k\big(T(b, i\Delta t)\big)\frac{\partial T_i}{\partial x}(0,t) = q"(0,t),$$

$$T_i(w,t) = T_w(t), \qquad t \in [i\Delta t, (i+1)\Delta t], \qquad (4.2.17b-c)$$

and initial condition is given as

$$T_i(x, i\Delta t) = T(x, i\Delta t), \quad x \in [0, w]. \qquad (4.2.17d)$$

Again, observe that all thermal properties are momentarily frozen in time and evaluated at the probe temperature $T(b, i\Delta t)$ in the time interval $[i\Delta t, (i+1)\Delta t]$. This probe is nearest to the active side at $x = 0$;

Next, we define

$$T_i^*(x,v) = T_i(x, n_i v + i\Delta t), \qquad v \in \left[0, \frac{\Delta t}{n_i}\right],$$

$$q"_i^*(0,v) = m_i q"(0, n_i v + i\Delta t), \qquad v \in \left[0, \frac{\Delta t}{n_i}\right], \qquad (4.2.18a-c)$$

$$T_w^*(v) = T_w(n_i v + i\Delta t), \qquad v \in \left[0, \frac{\Delta t}{n_i}\right],$$

where

$$m_i = \frac{k\big(T(b,0)\big)}{k\big(T(b,i\Delta t)\big)},$$

$$n_i = \frac{\alpha\big(T(b,0)\big)}{\alpha\big(T(b,i\Delta t)\big)}. \qquad (4.2.18d-e)$$

Upon implementing the above definitions, it is possible to express Eqs. (4.2.17a-d) using the thermal properties evaluated at the initial temperature as

$$\alpha\big(T(b,0)\big)\,\frac{\partial^2 T_i^*}{\partial x^2}(x,v) = \frac{\partial T_i^*}{\partial v}(x,v), \quad x \in (0,w), \quad v \in \left[0, \frac{\Delta t}{n_i}\right], \qquad (4.2.19a)$$

subject to the boundary conditions

$$-k\big(T(b,0)\big)\frac{\partial T_i^*}{\partial x}(0,v) = q''^*_i(0,v),$$

$$T_i^*(w,v) = T_w^*(v), \quad v \in \left[0, \frac{\Delta t}{n_i}\right], \qquad (4.2.19b-c)$$

and initial condition

$$T_i^*(x, v=0) = T(x, t=i\Delta t), \quad x \in [0,w]. \qquad (4.2.19d)$$

The local thermal diffusivity $\alpha\big(T(b,i\Delta t)\big)$ and thermal conductivity $k\big(T(b,i\Delta t)\big)$ can be transformed to the values evaluated at the initial temperature through the two rescaling coefficients m_i and n_i. If all rescaled temperatures $T_i^*(b,v)$ from time zero $(i=0)$ to final time $(i=N)$ are collected in sequence then it can be regarded as the linear thermal response induced by both rescaled surface heat flux and rescaled furthest temperature boundary condition. Here, the rescaled heat flux is formed through the reconstitution of $q"_i^*(0,v)$ from $i=0$ to $i=N$ while the furthest rescaled temperature results from the reconstitution of $T_i^*(w,v)$ from $i=0$ to $i=N$.

Now, we define the total sequential system as the collection given by

$$q"_{tN}^*(0,t)=\begin{cases} m_0 q"_0^*(0,t) & t\in\left[0,\dfrac{\Delta t}{n_0}\right) \\ m_1 q"_1^*\left(0,t-\dfrac{\Delta t}{n_0}\right) & t\in\left[\dfrac{\Delta t}{n_0},\displaystyle\sum_{i=0}^{1}\dfrac{\Delta t}{n_i}\right) \\ \cdots & \\ m_N q"_N^*\left(0,t-\displaystyle\sum_{i=0}^{N-1}\dfrac{\Delta t}{n_i}\right) & t\in\left[\displaystyle\sum_{i=0}^{N-1}\dfrac{\Delta t}{n_i},\sum_{i=0}^{N}\dfrac{\Delta t}{n_i}\right), \end{cases} \tag{4.2.20a}$$

$$T_{tN}^*(x,t)=\begin{cases} T_0^*(x,t) & t\in\left[0,\dfrac{\Delta t}{n_0}\right) \\ T_1^*\left(x,t-\dfrac{\Delta t}{n_0}\right) & t\in\left[\dfrac{\Delta t}{n_0},\displaystyle\sum_{i=0}^{1}\dfrac{\Delta t}{n_i}\right) \\ \cdots & \\ T_N^*\left(x,t-\displaystyle\sum_{i=0}^{N-1}\dfrac{\Delta t}{n_i}\right) & t\in\left[\displaystyle\sum_{i=0}^{N-1}\dfrac{\Delta t}{n_i},\sum_{i=0}^{N}\dfrac{\Delta t}{n_i}\right). \end{cases} \tag{4.2.20b}$$

After the quasi-linearization has been performed, we can substitute Eqs. (4.2.20a-b) into the two-probe linear calibration equation given by Eq. (4.2.15) to obtain

$$\int_{u=0}^{t} q''^{*}_{tN,r}(0,u) \int_{v=0}^{t-u} \left[T^{*}_{tN,c1}(b,v)T^{*}_{tN,c2}(w,t-u-v) - T^{*}_{tN,c2}(b,v)T^{*}_{tN,c1}(w,t-u-v)\right] dvdu$$

$$= \int_{u=0}^{t} T^{*}_{tN,r}(b,u) \int_{v=0}^{t-u} \left[q''^{*}_{tN,c1}(0,v)T^{*}_{tN,c2}(w,t-u-v) - q''^{*}_{tN,c2}(0,v)T^{*}_{tN,c1}(w,t-u-v)\right] dvdu$$

$$+ \int_{u=0}^{t} T^{*}_{tN,r}(w,u) \int_{v=0}^{t-u} \left[q''^{*}_{tN,c2}(0,v)T^{*}_{tN,c1}(b,t-u-v) - q''^{*}_{tN,c1}(0,v)T^{*}_{tN,c2}(b,t-u-v)\right] dvdu,$$

$$t \in \left[0, \sum_{i=0}^{N} \frac{\Delta t}{n_i}\right). \qquad (4.2.21)$$

To generalize this solution procedure, let $\Delta t = \lim_{N\to\infty} \frac{t_{max}}{N+1}$ such that for any time $t_M \in (0, t_{max}]$, it is then possible to find an integer $M \in [0, N]$ to ensure $t_M \approx M\Delta t$. The collection procedure produces the compact integral relation

$$\sum_{i=0}^{M} \frac{\Delta t}{n_i} \approx \int_{u=0}^{t_{M+1}} \frac{\alpha\big(T(b,u)\big)}{\alpha\big(T(b,0)\big)} du,$$

where

$$T(x,t_{M+1}) = T^*_{tM}\left(x, \int_{u=0}^{t_{M+1}} \frac{\alpha\big(T(b,u)\big)}{\alpha\big(T(b,0)\big)}du\right), \qquad (4.2.22a-c)$$

$$q"(0,t_{M+1}) = \frac{k\big(T(b,t_M)\big)}{k\big(T(b,0)\big)} q"^*_{tM}\left(0, \int_{u=0}^{t_{M+1}} \frac{\alpha\big(T(b,u)\big)}{\alpha\big(T(b,0)\big)}du\right).$$

Next, we define the rescaled time domain as

$$t^* = \int_{u=0}^{t} \frac{\alpha\big(T(b,u)\big)}{\alpha\big(T(b,0)\big)}du,$$

$$q"^*(0,t^*) = \frac{k\big(T(b,0)\big)}{k\big(T(b,t)\big)} q"(0,t), \qquad (4.2.23a-c)$$

and

$$T^*(x,t^*) = T(x,t), \qquad x \in [0,w], \;\; t \in [0,t_{max}].$$

The final form of the nonlinear, two-probe calibration integral equation for the entire time domain becomes

$$\int_{u=0}^{t^*} q"^*_r(0,u) \int_{v=0}^{t^*-u} [T^*_{c1}(b,v)T^*_{c2}(w,t^*-u-v) - T^*_{c2}(b,r)T^*_{c1}(w,t^*-u-v)]\, dvdu =$$

$$\int_{u=0}^{t^*} T_r^*(b,u) \int_{v=0}^{t^*-u} [q''^*_{c1}(0,v) T_{c2}^*(w, t^*-u-v) - q''^*_{c2}(0,r) T_{c1}^*(w, t^*-u-v)]\, dvdu +$$

$$\int_{u=0}^{t^*} T_r^*(w,u) \int_{v=0}^{t^*-u} [q''^*_{c2}(0,v) T_{c1}^*(b, t^*-u-v) - q''^*_{c1}(0,r) T_{c2}^*(b, t^*-u-v)]\, dvdu,$$

$$t^* \geq 0. \qquad (4.2.24)$$

After the prediction in the rescaled time domain is complete, then it is still necessary to return the physical variables through the following transformation

$$t = \int_{u=0}^{t^*} \frac{\alpha\big(T^*(b,0)\big)}{\alpha\big(T^*(b,u)\big)}\, du,$$

$$q''_r(0,t) = \frac{k\big(T^*(b,t^*)\big)}{k\big(T^*(b,0)\big)} q''^*_r(0,t^*), \qquad t^* \geq 0. \qquad (4.2.25a-b)$$

4.3 Numerical Procedure and Regularization

The nonlinear two-probe calibration equation given by Eq. (4.2.24) is a Volterra integral equation of first kind for the unknown front surface heat flux, and hence it is ill-posed. Its computational procedure will require regularization for producing a stable and an accurate prediction. In this chapter, a localized Tikhonov method is adopted for this purpose [86]. The classic L-curve analysis [83] is then introduced for estimating the optimal regularization parameter. Before any numerical operation is made on Eq. (4.2.24), it is necessary to map the discrete experimental data from the physical time domain t onto the rescaled time domain t^* in

accordance to Eq. (4.2.23a). We let $t^* \in [0, t^*_{max}]$ with $t^*_{max} = (N+1)\Delta t^*$ and make the following definitions

$$G^*_{q2}(t^*_i) = \int_{u=0}^{t^*_i} q"^*_r(0,u) K^*_{q2}(b, t^*_i - u)du,$$

$$K^*_{q2}(t^*_i) = \int_{v=0}^{t^*_i} [T^*_{c1}(b,v)T^*_{c2}(w, t^*_i - v) - T^*_{c2}(b,v)T^*_{c1}(w, t^*_i - v)]\, dv, \quad (4.3.1a-c)$$

$$F^*_{q2}(t^*_i) =$$

$$\int_{u=0}^{t^*_i} T^*_r(b,u) \int_{v=0}^{t^*_i - u} [q"^*_{c1}(0,v)T^*_{c2}(w, t^*_i - u - v) - q"^*_{c2}(0,v)T^*_{c1}(w, t^*_i - u - v)]\, dvdu$$

$$+ \int_{u=0}^{t^*_i} T^*_r(w,u) \int_{v=0}^{t^*_i - u} [q"^*_{c2}(0,v)T^*_{c1}(b, t^*_i - u - v) - q"^*_{c1}(0,v)T^*_{c2}(b, t^*_i - u - v)]\, dvdu.$$

With these definitions for $G^*_{q2}(t^*_i)$ and $F^*_{q2}(t^*_i)$, the residual resulting from the approximation imposed in the calibration integral equation and its normalized form are given as

$$R_{q2}(q"^*_r(0,t^*_i)|^N_{i=0}) = \sum_{i=1}^{N+1} \left[G^*_{q2}(t^*_i) - F^*_{q2}(t^*_i)\right]^2,$$

$$R_{N,q2}(q"^*_r(0,t^*_i)|^N_{i=0}) = \frac{R(q"^*_r(0,t^*_i)|^N_{i=0})}{\sum_{i=1}^{N+1} F^{*2}_{q2}(t^*_i)}. \quad (4.3.2a-b)$$

In this chapter, all numerical examples possess long heating times (120s) with a sampling rate of 200Hz. The global Tikhonov method is not feasible in the present context owing to the extended time domain and sampling rate. As an alternative, a localized Tikhonov method is adopted here. Assuming the rescaled heat flux from 0 to $(M-1)\Delta t^*$ is known then we obtain the rescaled heat flux $q"_r^*(0, M\Delta t^*)$ through

$$\int_{u=t_M^*}^{t_{M+S}^*} q"_r^*(0,u)K_{q2}^*\,(t_{M+S}^* - u)du = F_{q2}^*(t_{M+S}^*) - \int_{u=0}^{t_M^*} q"_r^*(0,u)K_{q2}^*\,(t_{M+S}^* - u)du,$$

$$M \in [0, N+1-S]. \qquad (4.3.3)$$

Here, $S\Delta t^*$ represents the future time increment in which the regular Tikhonov method is used to resolve the localized front heat flux. This regularization parameter has no upper value. When one available S is defined, then larger S values work equally well for the identical test case. So it is conservative to use a larger value S. However, it is necessary to notice that as the future time increment $S\Delta t^*$ increases, a reduction in resolvable total time occurs. Therefore, it is prudent to retain temperature measurement data beyond the required analysis time span.

Now, we define

$$F_{M,q2}^*(t_i^*) = F_{q2}^*(t_{M+i}^*) - \int_{u=0}^{t_M^*} q"_r^*(0,u)K_{q2}^*\,(b, t_{M+i}^* - u)du, \qquad (4.3.4)$$

which allows Eq. (4.3.3) to be represented in a compact matrix form using a convenient left-handed rectangular integration rule as

$$\boldsymbol{K_{q2}q_{M,r}} = \boldsymbol{F_{M,q2}} \tag{4.3.5}$$

where $\boldsymbol{K_{q2}}$ is a $S \times S$ matrix with $\boldsymbol{K_{q2}}(i,j) = \Delta t^* \times K^*_{q2}\left(t^*_{i-j+1}\right)$ for $i \geq j$ and $\boldsymbol{K_{q2}}(i,j) = 0$ for $i < j$, $\boldsymbol{F_{M,q2}}$ is a $S \times 1$ vector with $\boldsymbol{F_{M,q2}}(i) = F^*_{M,q2}(t^*_i)$, and $\boldsymbol{q_{M,r}}$ is a $S \times 1$ vector to be determined with $\boldsymbol{q_{M,r}}(i) = q"^*_r(0, t^*_{i+M-1})$.

Since the present work involves an ill-posed problem, the direct inversion for $\mathbf{K_{q2}}$ produces an unacceptable result. To avoid this situation, a regularization parameter λ_0 with the physical units ($^oC^2s^2$) is introduced for regularization. The objective function now becomes

$$J_{q2}\left(\boldsymbol{q_{M,r}}\right) = \left\|\boldsymbol{K_{q2}q_{M,r}} - \boldsymbol{F_{M,q2}}\right\|^2 + \lambda_0^2\left\|\boldsymbol{q_{M,r}}\right\|^2. \tag{4.3.6}$$

Singular-value decomposition is imposed on $\boldsymbol{K_{q2}}$ to obtain

$$\boldsymbol{K_{q2}} = \boldsymbol{W}\sum\boldsymbol{V^T} = \sum_{i=1}^{S} \boldsymbol{w}_i \sigma_i \boldsymbol{v}_i^T, \tag{4.3.7}$$

where $\boldsymbol{W} = (\boldsymbol{w}_1, \boldsymbol{w}_2, \boldsymbol{w}_3, \cdots, \boldsymbol{w}_S)$ and $\boldsymbol{V} = (\boldsymbol{v}_1, \boldsymbol{v}_2, \boldsymbol{v}_3, \cdots, \boldsymbol{v}_S)$ satisfying $\boldsymbol{W^TW} = \boldsymbol{V^TV} = \boldsymbol{I}$. The symbol $\sum$ is a $S \times S$ diagonal matrix whose diagonal value σ_i arranges in a descending order as

$$\sigma_1 \geq \sigma_2 \geq \cdots \geq \sigma_S \geq 0. \tag{4.3.8}$$

Upon substituting Eq. (4.3.7) into Eq. (4.3.6), the first derivative of $J_{q2}(\boldsymbol{q_r})$ with respective to $\boldsymbol{q_r}$ is acquired and set equal to 0. After several steps of calculation, the final prediction for $\boldsymbol{q_{M,r}}$ is yielded, namely

$$\boldsymbol{q_{M,r}} = \sum_{i=1}^{S} \frac{\sigma_i}{\sigma_i^2 + \lambda_0^2} \boldsymbol{w_i^T F_{M,q2}} \boldsymbol{v}_i \,. \tag{4.3.9}$$

It is noted that when $\boldsymbol{q_{M,r}}$ is obtained, only its first term $q"_r^*(0, t_i^*)$ is retained [86]. The above procedure can be repeated for all unknown heat fluxes in next successive Tikhonov processing time intervals. In addition, the L-curve criterion proposed by Hansen and O' Leary [83] is called upon for determining optimal regularization parameter. This method defines the L-curve through

$$L_{q2}(\lambda_0) = \left\{ \log\left(\sum_{i=0}^{N-S+1} \left[G_{q2}^*(t_i^*) - F_{q2}^*(t_i^*) \right]^2 \right), \log\left(\sum_{i=0}^{N-S+1} [q"_r^*(0, t_i^*)]^2 \right), \lambda_0 \geq 0 \right\}. \tag{4.3.10}$$

Section 4.4 presents numerical results applying the proposed calibration equation given by Eq. (4.2.24) for two common engineering materials, stainless steel 304 and a representative carbon composite.

4.4 Results

In this section, the merit of the nonlinear two-probe calibration equation given by Eq. (4.2.24) is verified based on numerically simulated data from two in-depth temperature probes.

For demonstration purposes, the slab composition is (a) stainless steel 304 and (b) a carbon composite. The thermophysical property functions are approximated as

$$k(T) = (14.4 + 0.0167T - 1.6 \times 10^{-6}T^2)\ (\mathrm{Wm^{-1}K^{-1}}),$$

$$\rho c_p(T) = (1.59 \times 10^5 + 388.87T + 6.395 \times 10^5 \ln(T + 273.15))\ (\mathrm{Jm^{-3}K^{-1}}), \quad (4.4.1a - b)$$

for stainless steel 304 and

$$k(T) = (5.76 + 1.195 \times 10^{-3}T)\ (\mathrm{Wm^{-1}K^{-1}}),$$

$$\rho c_p(T) = (1.705 \times 10^6 + 3629T - 3.075T^2 + 9.334 \times 10^{-4}T^3)\ (\mathrm{Jm^{-3}K^{-1}}), \quad (4.4.2a - b)$$

for a representative carbon composite. Figures 4.4.1-4.4.3 and 4.4.4-4.4.6 display the thermal conductivity, heat capacity and thermal diffusivity $\alpha(T) = k(T)/\left(\rho c_p(T)\right)$ functions for stainless steel 304 and the carbon composite respectively, according to Eq. (4.4.1) and Eq. (4.4.2). From these figures, a pronounced temperature dependence can be observed for both cases as the temperature rises from 0 ^{o}C to 1000 ^{o}C. It is interesting to note that the thermal diffusivities for these two materials possess opposing slopes as the temperature rises (see Figs. 4.4.3 and 4.4.6). As a result, these material choices provide a good test for examining the nonlinear two-probe calibration equation.

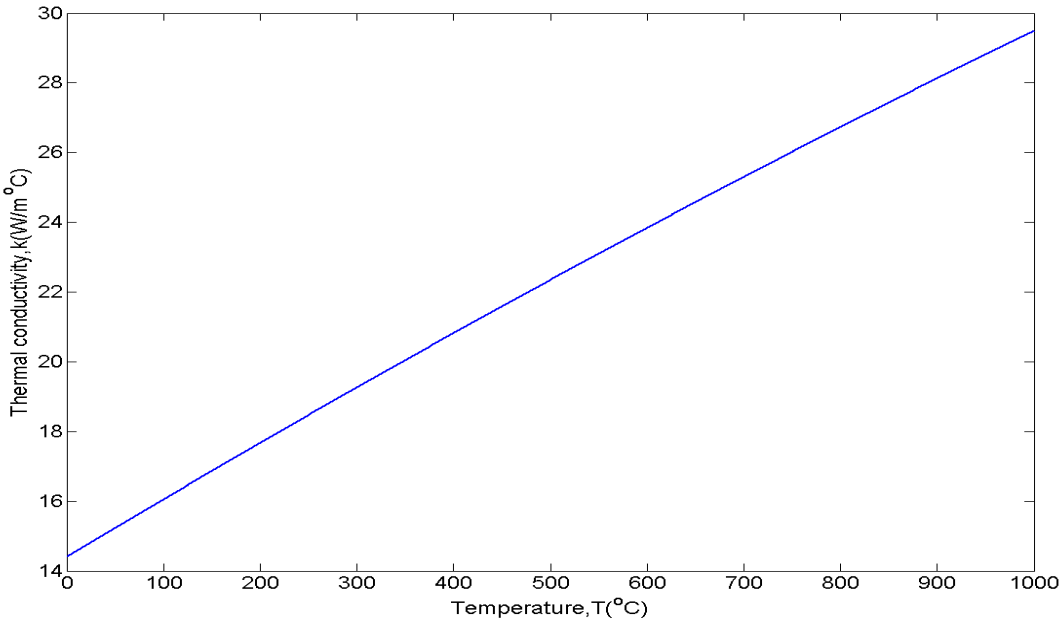

Figure 4.4.1: Approximate thermal conductivity for stainless steel 304, Eq. (4.4.1a).

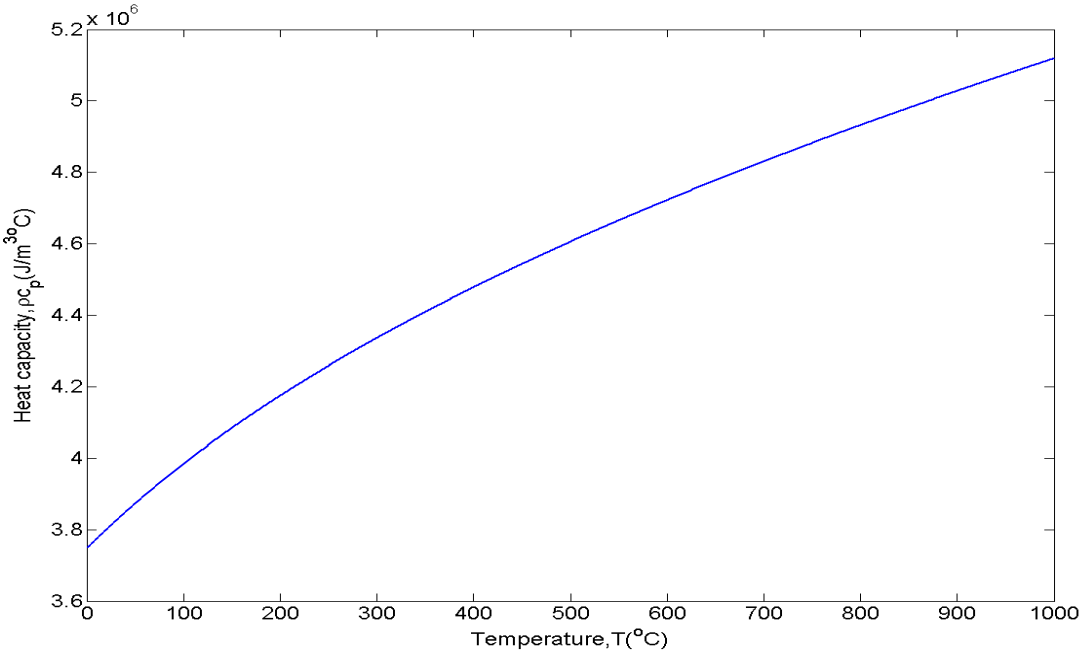

Figure 4.4.2: Approximate heat capacity for stainless steel 304, Eq. (4.4.1b).

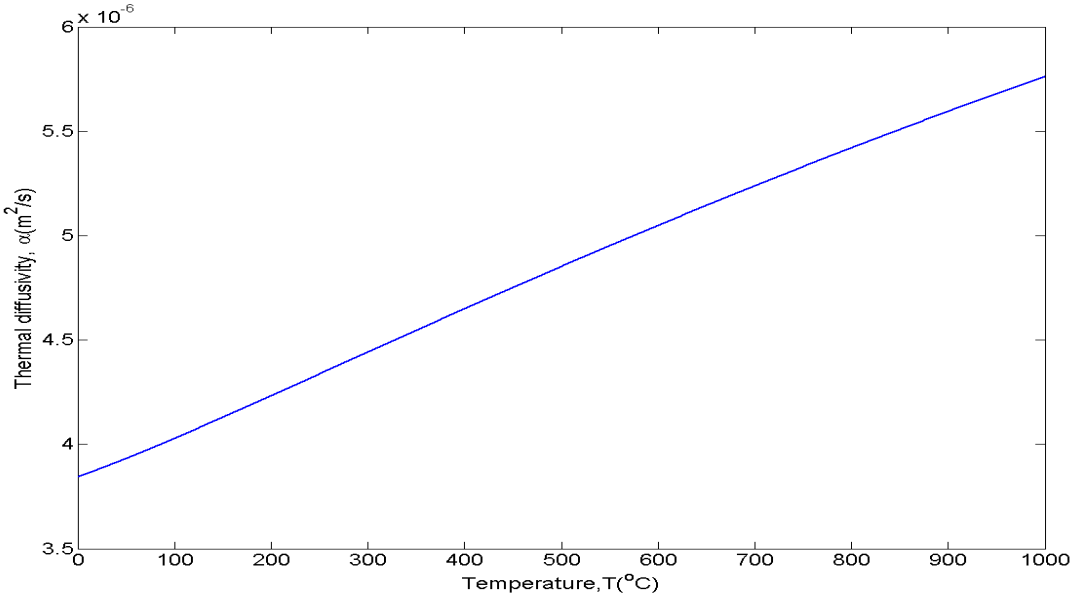

Figure 4.4.3: Approximated thermal diffusivity for stainless steel 304, $\alpha(T) = k(T)/\rho c_p(T)$.

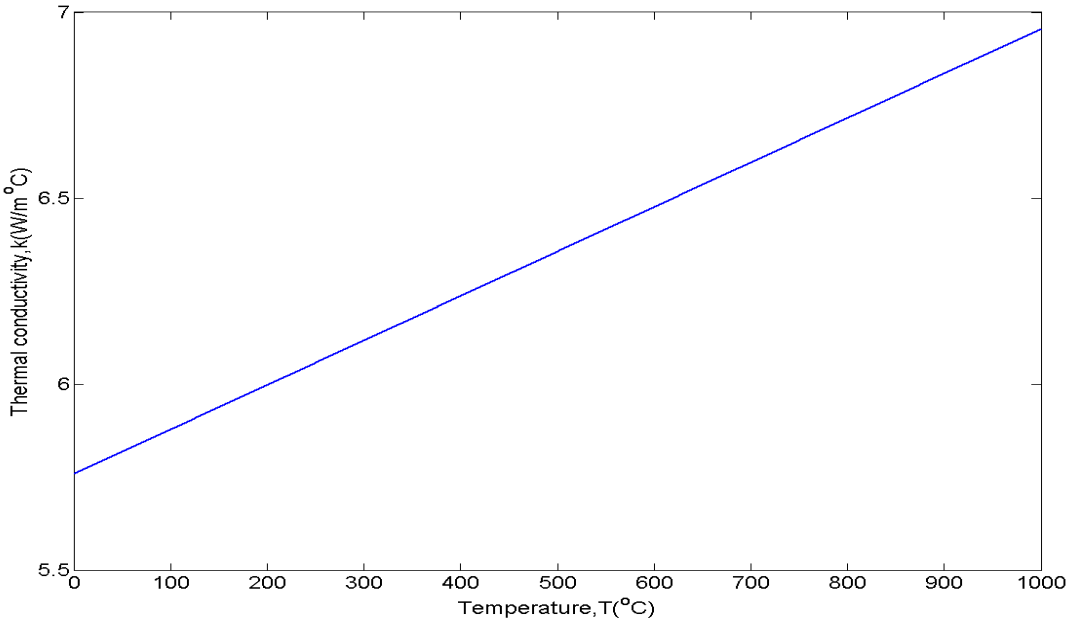

Figure 4.4.4: Approximate thermal conductivity for the carbon composite, Eq. (4.4.2a).

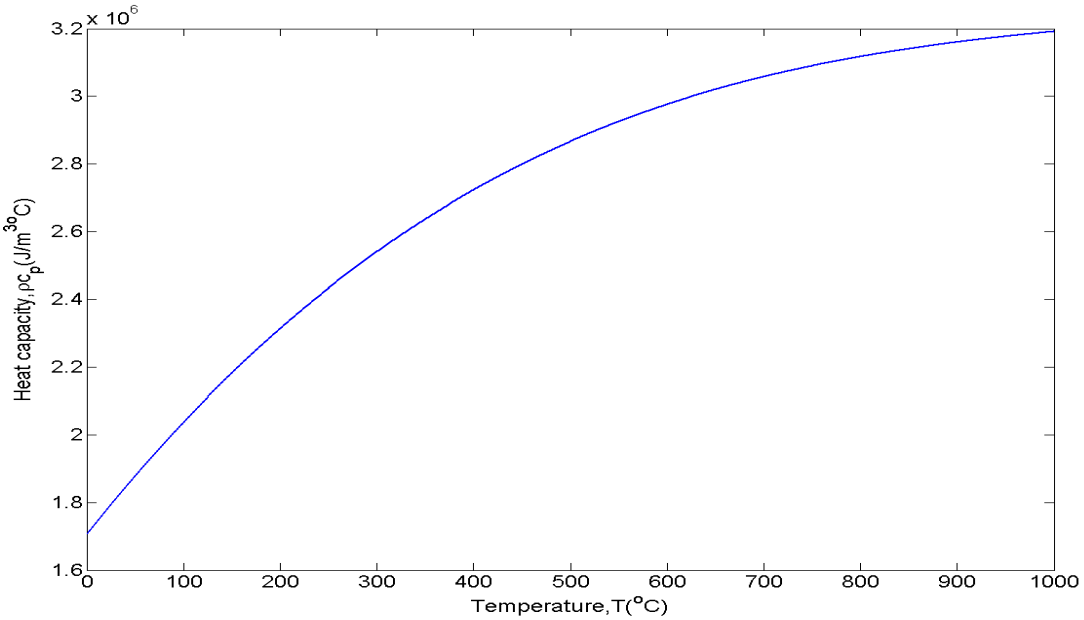

Figure 4.4.5: Approximate heat capacity for the carbon composite, Eq. (4.4.2b).

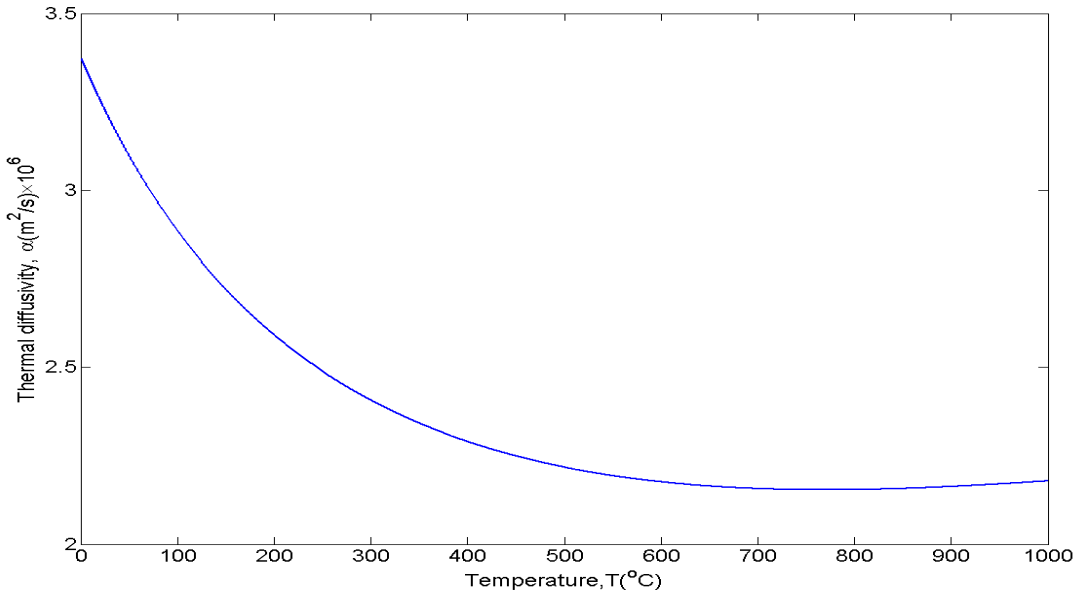

Figure 4.4.6: Approximate thermal diffusivity for the carbon composite, $\alpha(T) = k(T)/\rho c_p(T)$.

To numerically generate the simulated temperature data $T(x,t)$ for a slab of thickness L =10mm that is exposed to time-varying boundary conditions, a finite difference method (FDM) [33] is applied to the domain $x \in [0, L]$, $t \geq 0$ where fully temperature dependent thermophysical properties are included. To ensure the accuracy of the time stepping process with respect to the nonlinearity and time-varying rear-side boundary condition, both the spatial and temporal grid sets have been varied as (Δx=0.1mm and Δt =25μs), (Δx=0.2mm and Δt =50μs), and (Δx =0.2mm and Δt =100μs). Results verify grid convergence to a relative accuracy of 0.01. Therefore, for the present analysis, Δx and Δt are set to 0.2mm and 50μs, respectively. In addition, the impact of the probe position combination on the accuracy of the inverse predictions needs to be considered since the new calibration method given by Eq. (4.2.24) involves two probes rather than one. For this purpose, we used three combinations for the probe positions as (b=2mm and w =8mm), (b=2mm and w =6mm) and (b=3mm and w =7mm). It has been shown that the front heat flux prediction from all three probe position combinations have comparable accuracy for both stainless steel 304 and the carbon composite. In this section, results for probe positions b=2mm and w =8mm are provided as representative outcomes.

The kernel given by Eq. (4.3.1b) has the form of a residual. It possesses a strong self-canceling effect at early times if the back boundary condition is similar for the two calibration tests. Similar back boundary conditions reverts the two-probe system to the one-probe system, hence driving the kernel given by Eq. (4.3.1b) toward zero. This self-canceling effect further aggravates the ill-posed situation and thus increases the difficulty for resolving the front surface heat flux. To avoid this obstacle, strategies are required for designing the backside calibration tests boundary conditions for assuring a rapid departure from these cancelling effects. In this

chapter, five tests with different boundary condition combinations are constructed for demonstration and testing purposes. Figures 4.4.7 and 4.4.8 display three front surface heat flux histories to be applied for the five test suites of the stainless steel 304 and the carbon composite, respectively while the applied back boundary conditions are defined as: (1) adiabatic ($h_L = 0$); (2) back surface heating when $T(L,t) < T_\infty$, ($T_\infty = 200^{\circ}\text{C}$, $h_L = 500\text{W/m}^2{-}^{\circ}\text{C}$), and (3) back surface cooling when $T(L,t) > T_\infty$, ($T_\infty = 0^{\circ}\text{C}$, $h_L = 500\text{W/m}^2{-}^{\circ}\text{C}$). Table 4.4.1 summarizes the five constructed test suites (Run 1-5) through combination of the three front heat flux histories ($x = 0$) and three back boundary conditions ($x = L = 10\text{mm}$) referred above. Based on simulated temperature data from these five tests, four groups of experiments are proposed and defined as: (Group 1) Run 1 as calibration test 1, Run 3 as calibration test 2 and Run 4 as reconstruction test whose front surface heat flux is to be determined; (Group 2) Run 1 as calibration test 1, Run 3 as calibration test 2 and Run 5 as reconstruction test; (Group 3) Run 2 as calibration test 1, Run 3 as calibration test 2 and Run 4 as reconstruction test; and (Group 4) Run 2 as calibration test 1, Run 3 as calibration test 2 and Run 5 as reconstruction test. Since Run 1 and Run 2, Run 4 and Run 5 have identical front surface heat inputs, it is possible to observe the impact of varying the back boundary condition on the final prediction through comparison between Group 1 and Group 3, or Group 2 and Group 4. The reliability of the nonlinear two-probe calibration equation given by Eq. (4.2.24) can also be verified through comparison between Group 1 and Group 2, or Group 3 and Group 4.

Figures 4.4.9-4.4.13 and 4.4.14-4.4.18 present the noiseless temperature distributions at uniformly distributed spatial locations resulting from the forward solution for the five runs

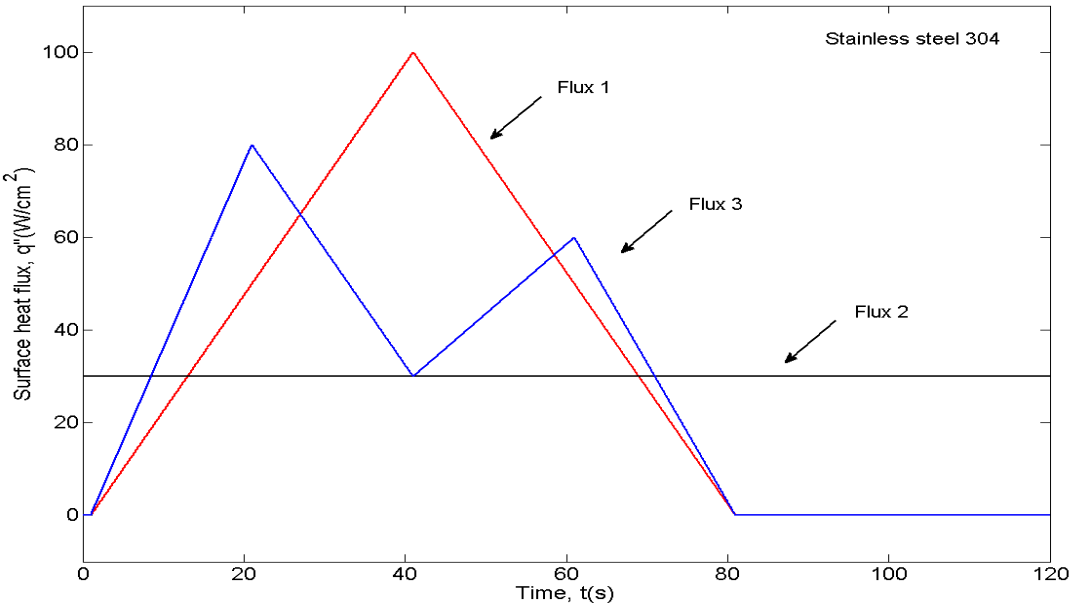

Figure 4.4.7: Surface heat fluxes 1, 2 and 3 designed for five tests of stainless steel 304.

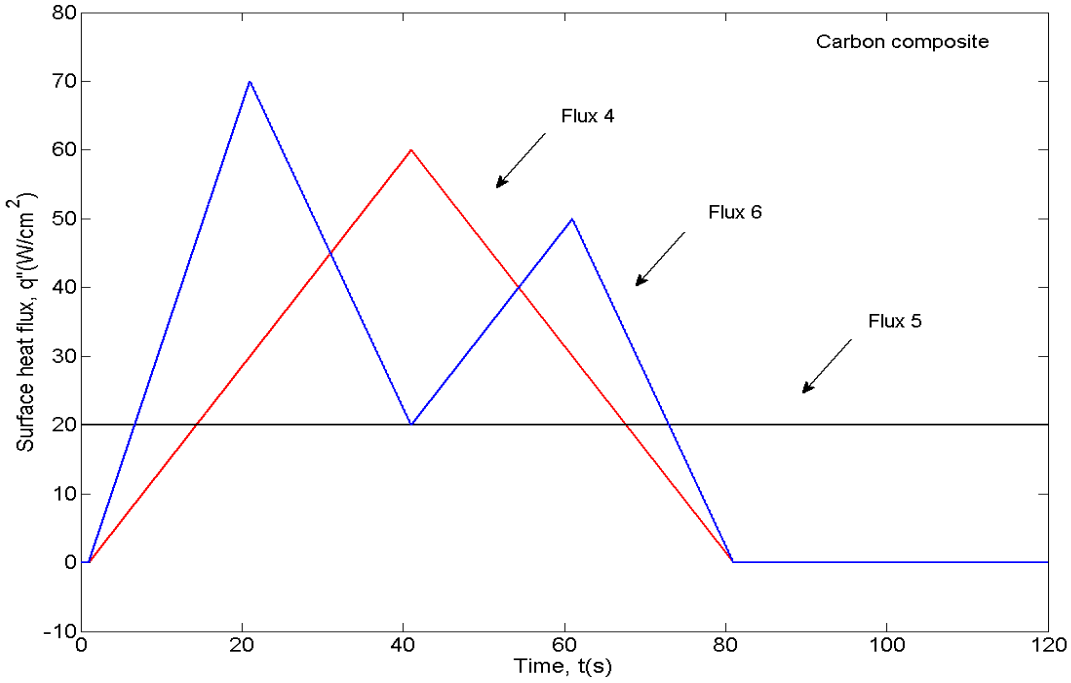

Figure 4.4.8: Surface heat fluxes 4, 5 and 6 designed for five tests of a carbon composite.

Table 4.4.1: Definition of test runs displaying different back boundary condition combinations for stainless steel 304 and the carbon composite.

Stainless steel 304	**Front boundary (Fig. 4.4.7)**	**Back boundary**
Run 1	Flux 1	(1) Adiabatic $(h_L = 0)$
Run 2	Flux 1	(2) Heating (when $T(L,t) > T_\infty$) $h_L = 500\text{W/m}^2\text{–°C},\ T_\infty = 200^\circ\text{C}$
Run 3	Flux 2	(3) Cooling (when $T(L,t) > T_\infty$) $h_L = 500\text{W/m}^2\text{–°C},\ T_\infty = 0^\circ\text{C}$
Run 4	Flux 3	(1) Adiabatic $(h_L = 0)$
Run 5	Flux 3	(3) Cooling (when $T(L,t) > T_\infty$) $h_L = 500\text{W/m}^2\text{–°C},\ T_\infty = 0^\circ\text{C}$
Carbon composite	**Front boundary (Fig. 4.4.8)**	**Back boundary**
Run 1	Flux 4	(1) Adiabatic $(h_L = 0)$
Run 2	Flux 4	(2) Heating (when $T(L,t) > T_\infty$) $h_L = 500\text{W/m}^2\text{–°C},\ T_\infty = 200^\circ\text{C}$
Run 3	Flux 5	(3) Cooling (when $T(L,t) > T_\infty$) $h_L = 500\text{W/m}^2\text{–°C},\ T_\infty = 0^\circ\text{C}$
Run 4	Flux 6	(1) Adiabatic $(h_L = 0)$
Run 5	Flux 6	(3) Cooling (when $T(L,t) > T_\infty$) $h_L = 500\text{W/m}^2\text{–°C},\ T_\infty = 0^\circ\text{C}$

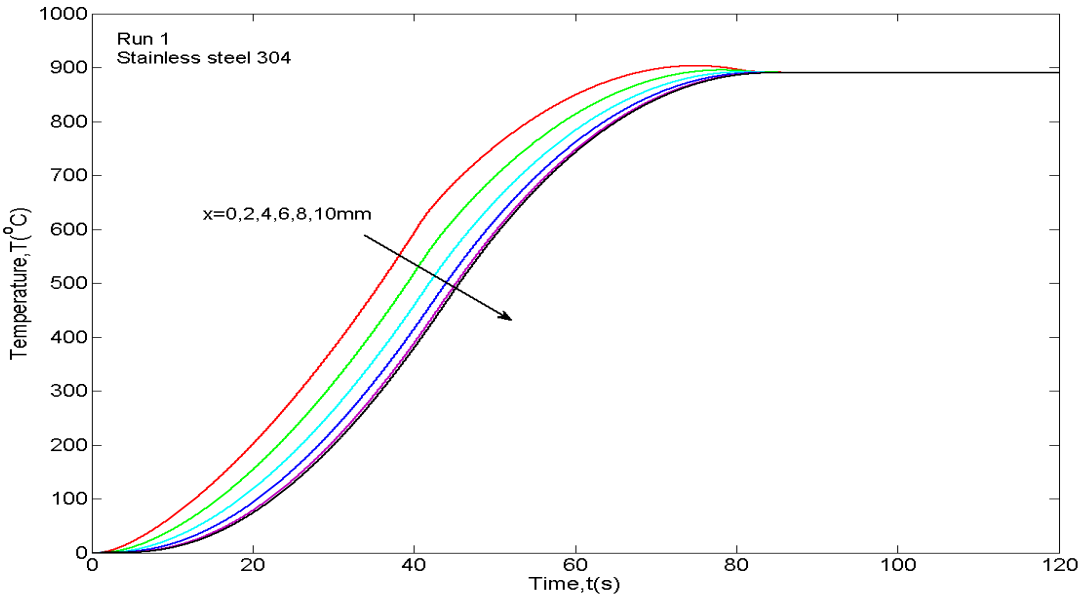

Figure 4.4.9: Stainless steel 304 temperature data at uniformly distributed spatial locations for Run 1 subjected to flux 1 and adiabatic back surface.

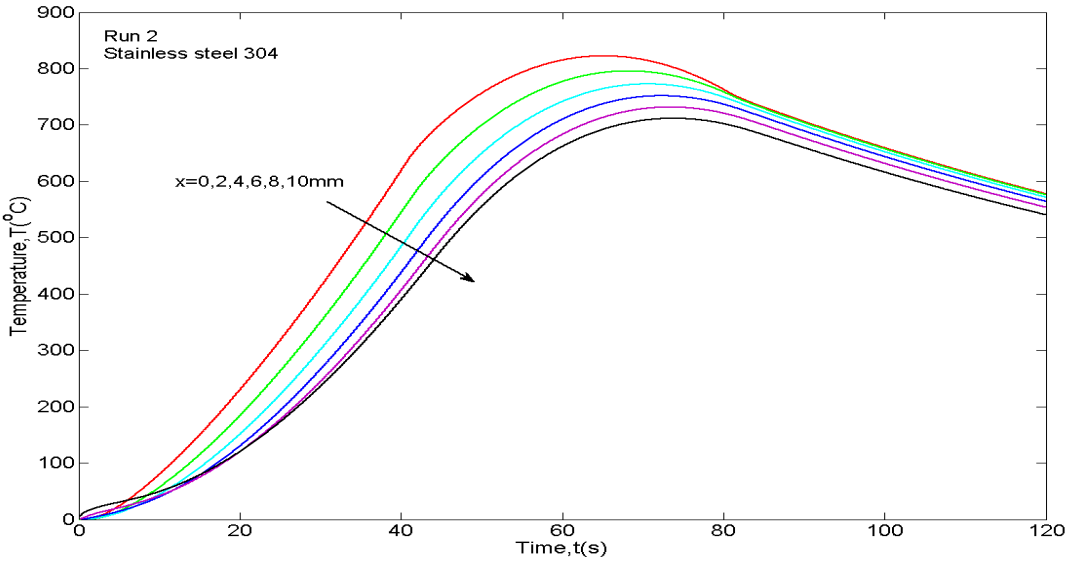

Figure 4.4.10: Stainless steel 304 temperature data at uniformly distributed spatial locations for Run 2 subjected to flux 1 and heating back surface ($T_\infty = 200^\circ\text{C}$, $h_L = 500\text{W/m}^2{-}^\circ\text{C}$).

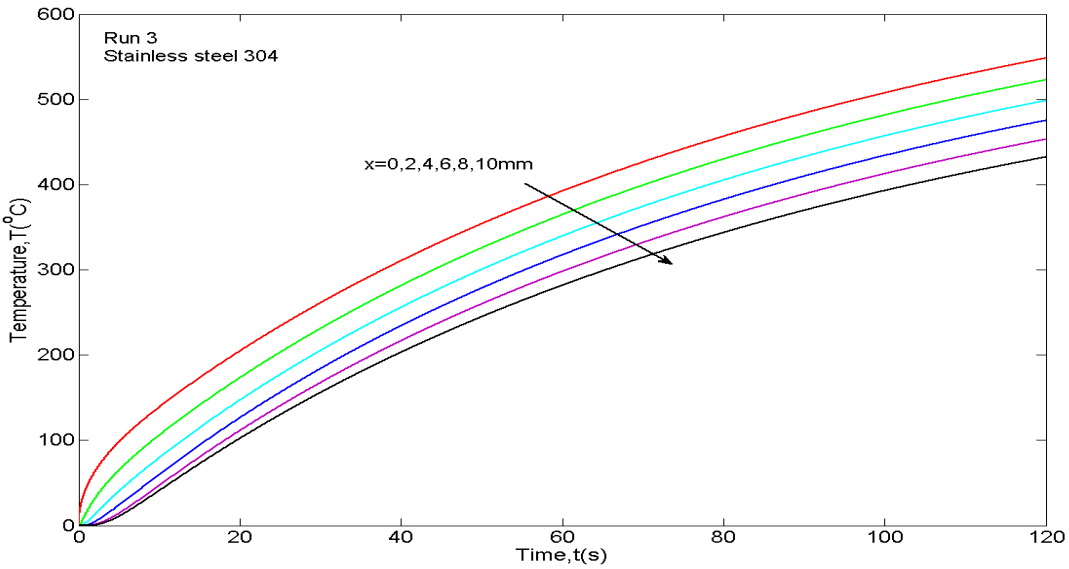

Figure 4.4.11: Stainless steel 304 temperature data at uniformly distributed spatial locations for Run 3 subjected to flux 2 and cooling back surface ($T_\infty = 0^\circ\text{C}$, $h_L = 500\text{W/m}^2{-}^\circ\text{C}$).

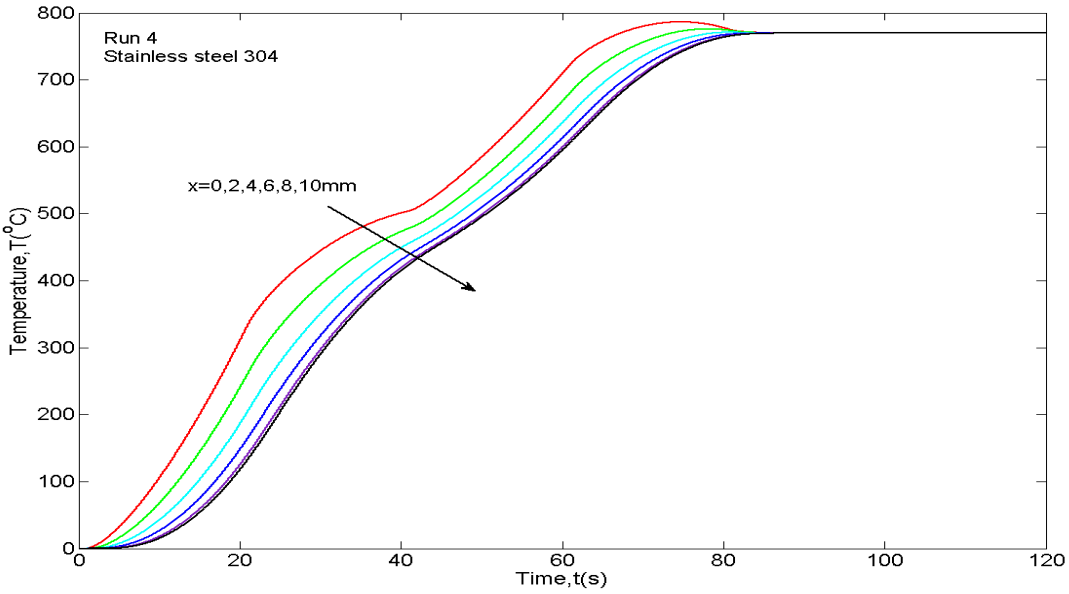

Figure 4.4.12: Stainless steel 304 temperature data at uniformly distributed spatial locations for Run 4 subjected to flux 3 and adiabatic back surface.

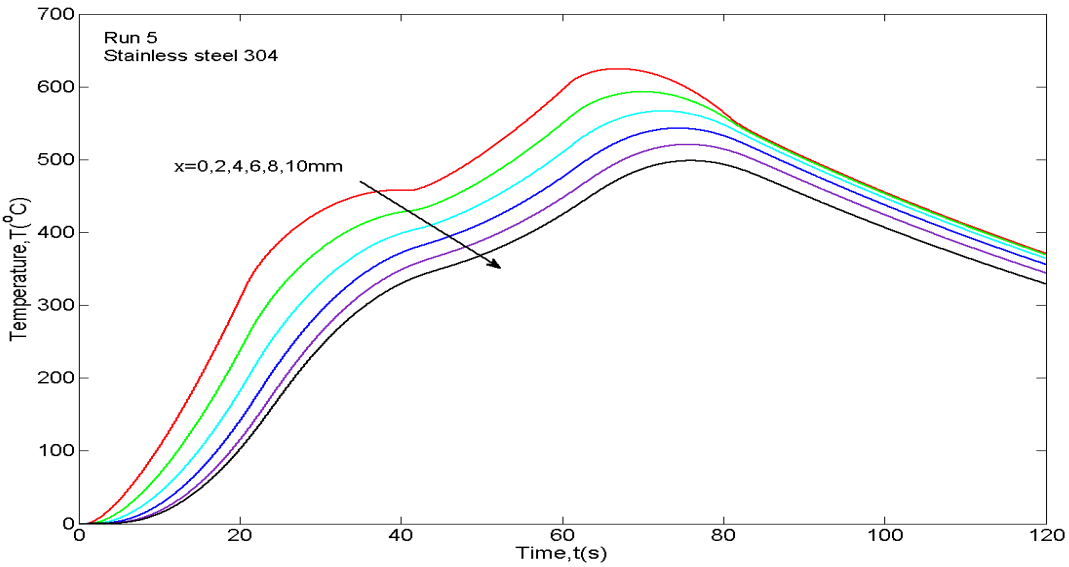

Figure 4.4.13: Stainless steel 304 temperature data at uniformly distributed spatial locations for Run 5 subjected to flux 3 and cooling back surface ($T_\infty = 0°\text{C}$, $h_L = 500\text{W/m}^2{-}°\text{C}$).

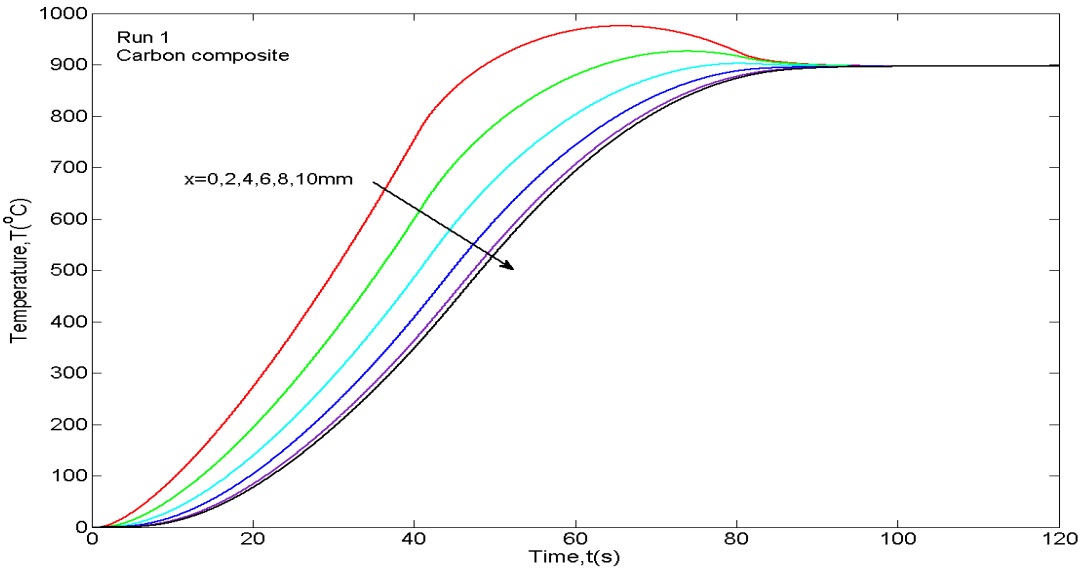

Figure 4.4.14: Carbon composite temperature data at uniformly distributed spatial locations for Run 1 subjected to flux 4 and adiabatic back surface.

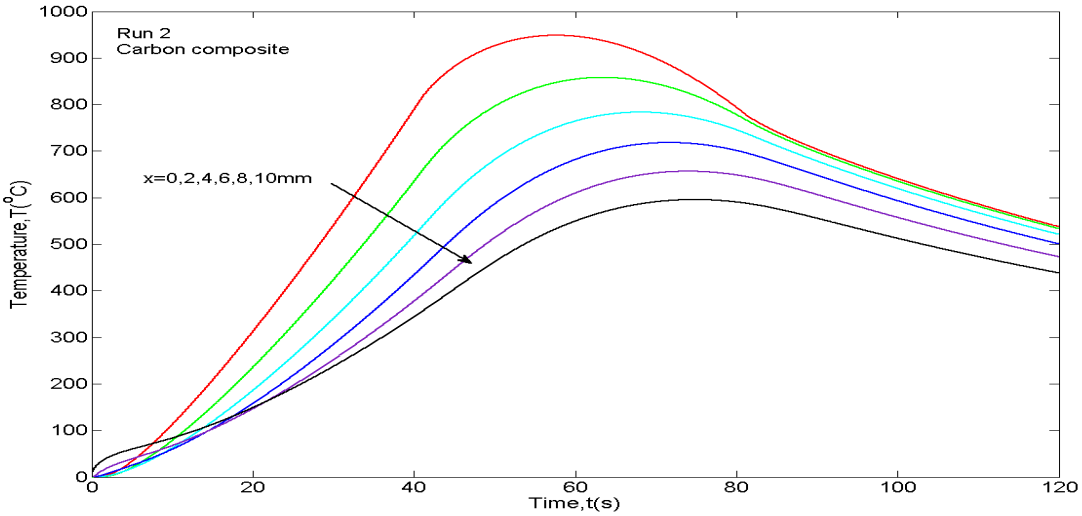

Figure 4.4.15: Carbon composite temperature data at uniformly distributed spatial locations for Run 2 subjected to flux 4 and heating back surface ($T_\infty = 200^\circ\text{C},\ h_L = 500\text{W/m}^2{-}^\circ\text{C}$).

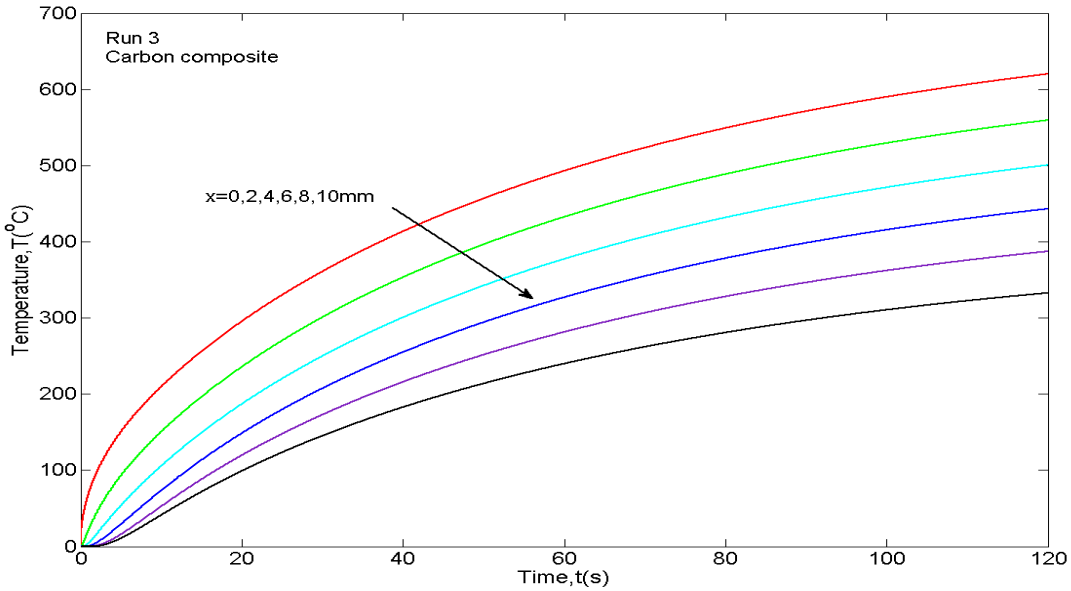

Figure 4.4.16: Carbon composite temperature data at uniformly distributed spatial locations for Run 3 subjected to flux 5 and cooling back surface ($T_\infty = 0^\circ\text{C},\ h_L = 500\text{W/m}^2{-}^\circ\text{C}$).

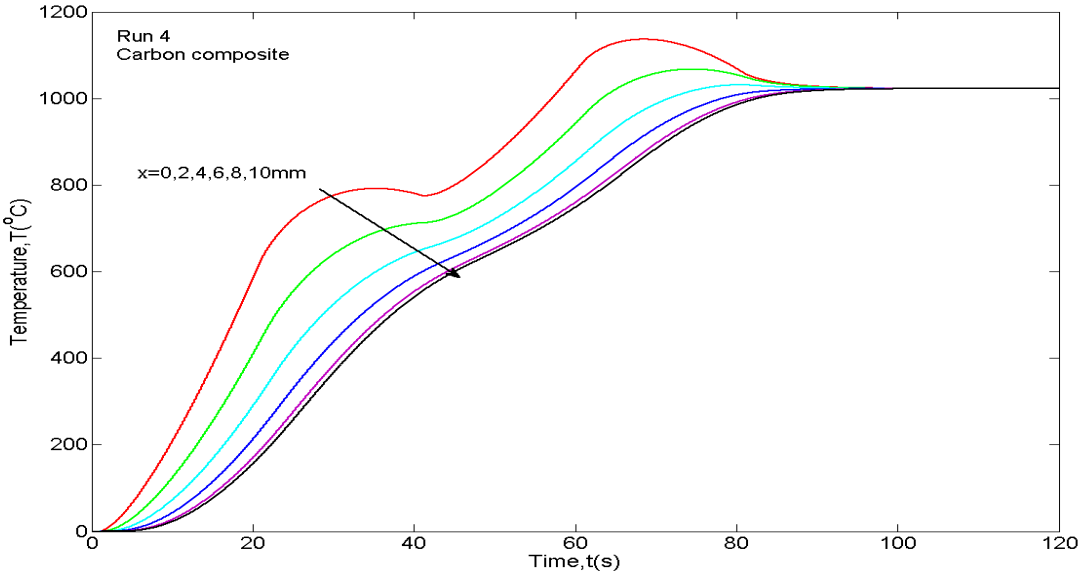

Figure 4.4.17: Carbon composite temperature data at uniformly distributed spatial locations for Run 4 subjected to flux 6 and adiabatic back surface.

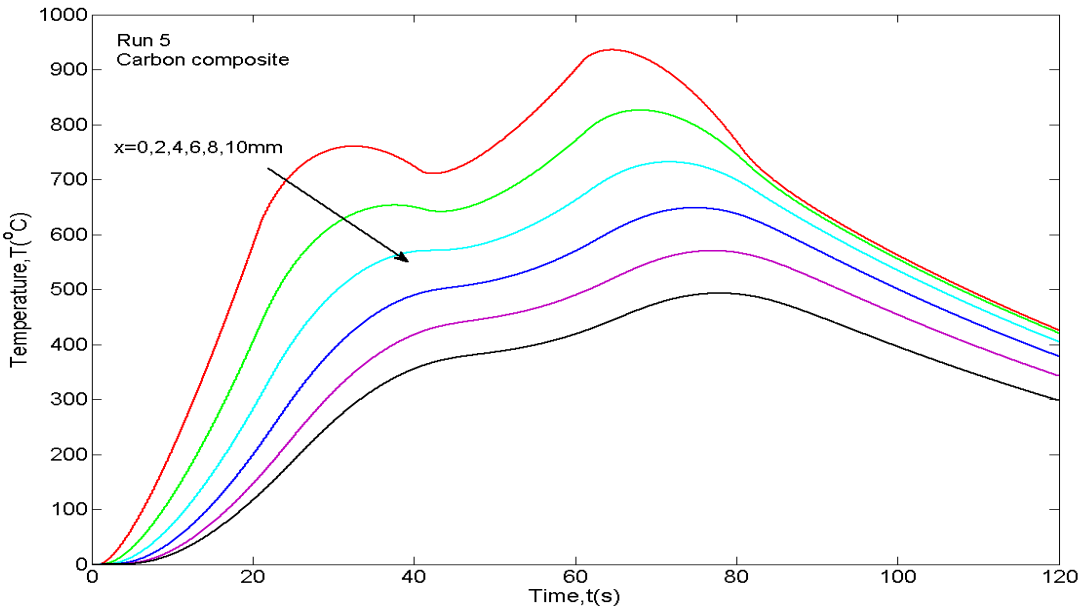

Figure 4.4.18: Carbon composite temperature data at uniformly distributed spatial locations for Run 5 subjected to flux 6 and cooling back surface ($T_\infty = 0^\circ\text{C}$, $h_L = 500\text{W/m}^2{-}^\circ\text{C}$).

involving both stainless steel 304 and the carbon composite, respectively as defined in Table 4.4.1. The noiseless temperature data at $x = b$ and $x = w$ are then used for resolving the front surface heat flux in the reconstruction phase. The purpose of applying the noiseless temperature data is to (1) confirm the suitability of the nonlinear two-probe calibration model, (2) verify the numerical method, and (3) check the system ill-conditioning situation due to the back boundary condition under ideal data.

For the same heat flux applied at the front surface of the stainless steel 304, variation of the back boundary condition results in significant temperature variations in the domain (shown by comparing Figs. 4.4.9 and 4.4.10 or Figs. 4.4.12 and 4.4.13). Also, comparison of Figs. 4.4.14 and 4.4.15 or Figs. 4.4.17 and 4.4.18 indicate significant variations in the temperature response of the carbon composite due to changes in the back surface boundary condition. The noted substantial temperature variation necessitates the use of the two-probe formulation. Additionally, the significant temperature range observed in the slab requires the proper accounting of the temperature-dependent thermophysical properties for all test groups. After rescaling the test data (heat flux, time and probe temperatures) during both calibration and reconstruction stages in accordance to Eq. (4.2.23a-c), the rescaled data are substituted into Eq. (4.3.2b) for computing the normalized residual.

Table 4.4.2 summarizes the normalized base residuals for all considered test groups if the exact rescaled unknown heat fluxes are applied. The small relative values observed from all test groups indicate that the calibration equation given by Eq. (4.2.24) is well suited for resolving a

Table 4.4.2: The normalized base residual $R_{N,q2}$, given by Eq. (4.3.2b) for all investigated groups of stainless steel 304 and the carbon composite using the exact rescaled heat flux and noiseless data.

Stainless steel 304	$\boldsymbol{R_{N,q2}\left(q''^{*}_{r}(0,t_i^*)\right)}$	**Carbon composite**	$\boldsymbol{R_{N,q2}\left(q''^{*}_{r}(0,t_i^*)\right)}$
Group 1	2.01×10^{-7}	**Group 1**	4.48×10^{-6}
Group 2	5.69×10^{-5}	**Group 2**	4.45×10^{-5}
Group 3	2.82×10^{-6}	**Group 3**	8.24×10^{-6}
Group 4	5.23×10^{-5}	**Group 4**	4.91×10^{-5}

1-D nonlinear problem with a time-varying back boundary condition. Also, it is noted that small magnitude of the base residual is expected for the two-probe nonlinear integral method since the piecewise time-step linearization assumption is a spatial approximation. The rescaled front surface heat flux $q"_r^*(0,t_i^*)$ is then resolved using Eq. (4.3.9). Since the predictions are presented in terms of the rescaled surface heat flux and time domain, they must be converted back to the physical variables in accordance to Eq. (4.2.25b) for final presentation. Figures 4.4.19-4.4.22 and 4.4.23-4.4.26 display the final predictions in physical time domain for all test groups of stainless steel 304 and the carbon composite, respectively while their accuracy is analyzed through

$$\sigma\left(q"_{r,pred}(0,t_i)\big|_{i=0}^{N}\right)=\left(\frac{1}{N}\sum_{i=1}^{N+1}\left(q"_{r,pred}(0,t_i)-q"_{r,exact}(0,t_i)\right)^2\right)^{1/2},$$

$$M_r\left(q"_{r,\mathrm{pred}}(0,t)\right)=\frac{\max\left(q"_{r,pred}(0,t)\right)}{\max\left(q"_{r,exact}(0,t)\right)}. \qquad (4.4.3a-b)$$

Here, σ represents the root-mean square of the heat flux error. Table 4.4.3 summarizes standard deviation of the prediction error σ, maximum value ratio M_r for all test groups associated with their chosen regularization parameter λ_0, and future time increment $S\Delta t^*$ based on noiseless data.

For this calibration approach, significant flexibility exists in choosing the proper regularization parameter since: (1) the kernel K_{q2}^* given by Eq. (4.3.1b) has a integration form that promotes damping temperature noise in this forward direction; and (2) the localized Tikhonov method is only utilized on the future time period $S\Delta t^*$ which only retains the first

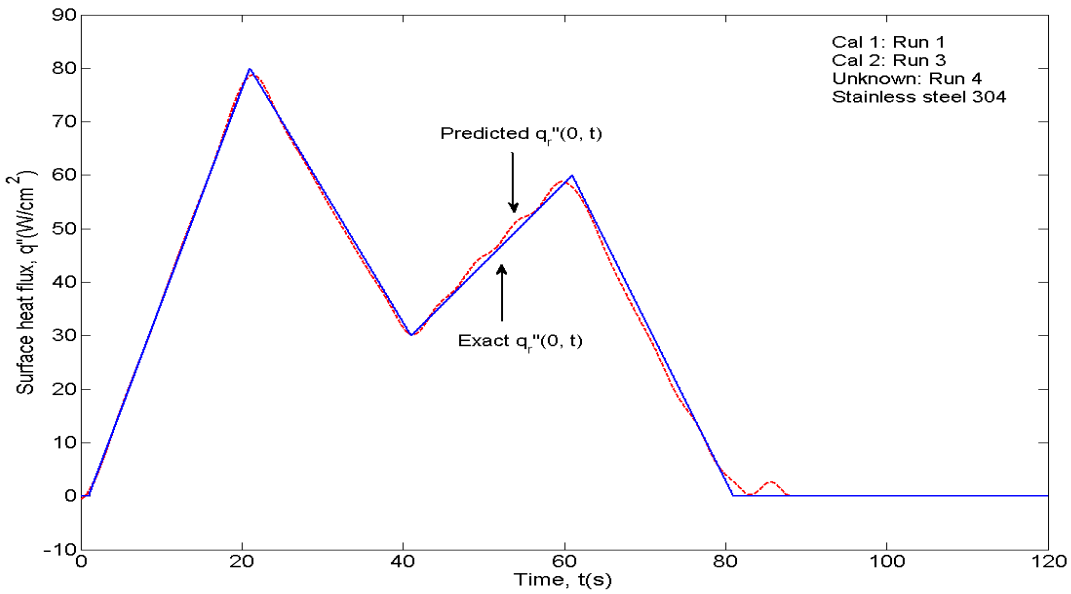

Figure 4.4.19: Predicted unknown surface heat flux $q_r"(0,t)$ for Group 1 of stainless steel 304 based on noiseless temperature data.

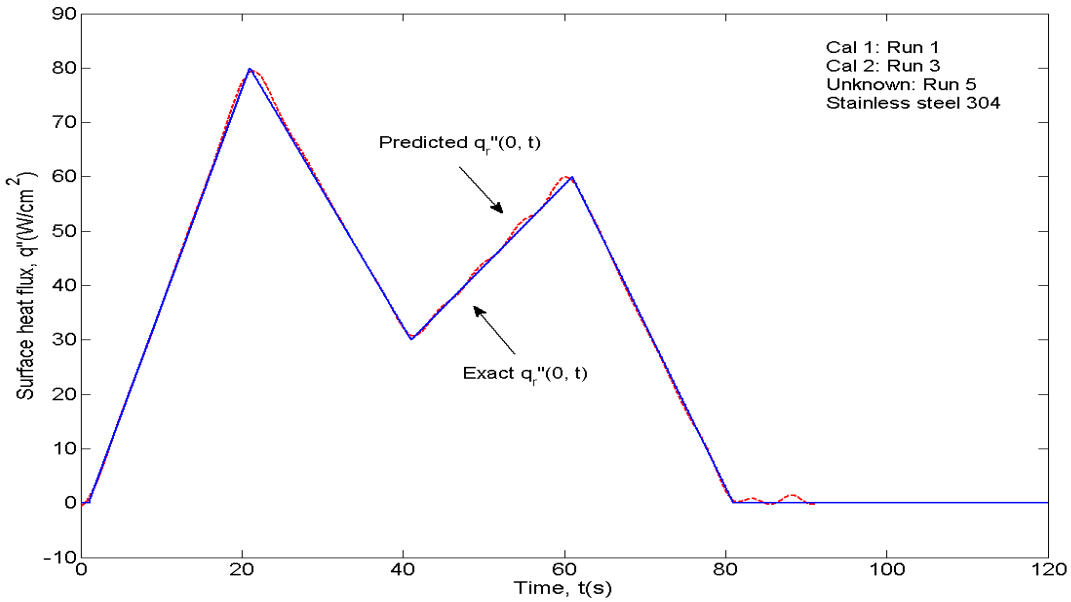

Figure 4.4.20: Predicted unknown surface heat flux $q_r"(0,t)$ for Group 2 of stainless steel 304 based on noiseless temperature data.

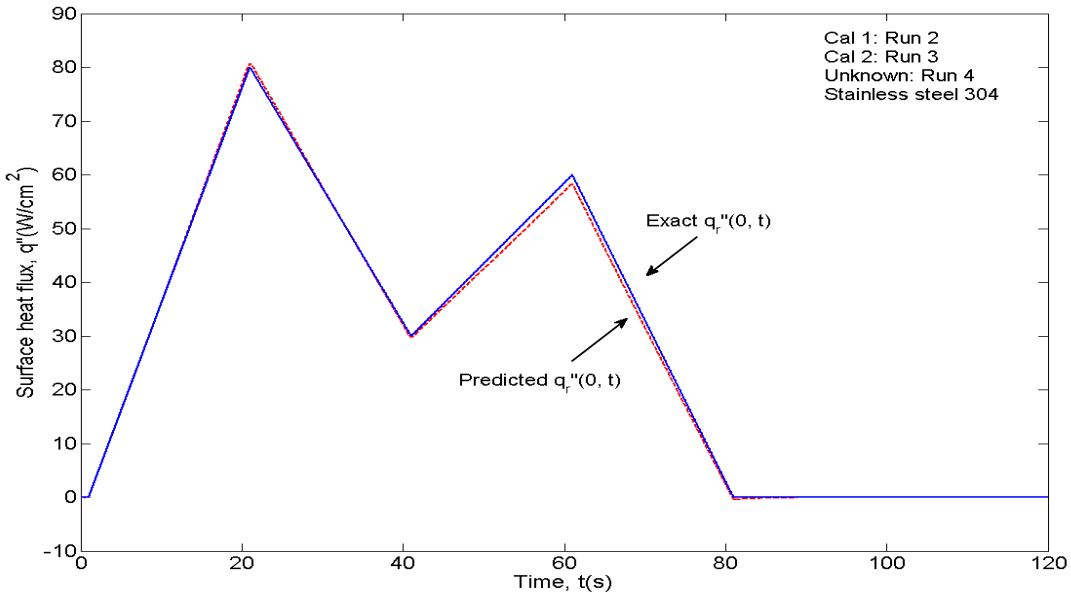

Figure 4.4.21: Predicted unknown surface heat flux $q_r"(0,t)$ for Group 3 of stainless steel 304 based on noiseless temperature data.

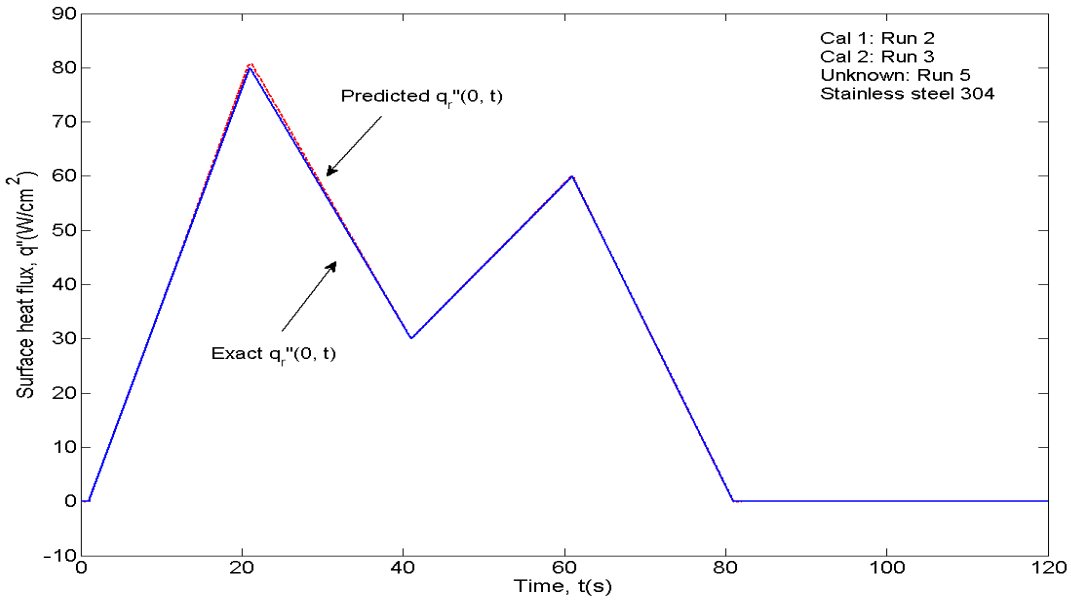

Figure 4.4.22: Predicted unknown surface heat flux $q_r"(0,t)$ for Group 4 of stainless steel 304 based on noiseless temperature data.

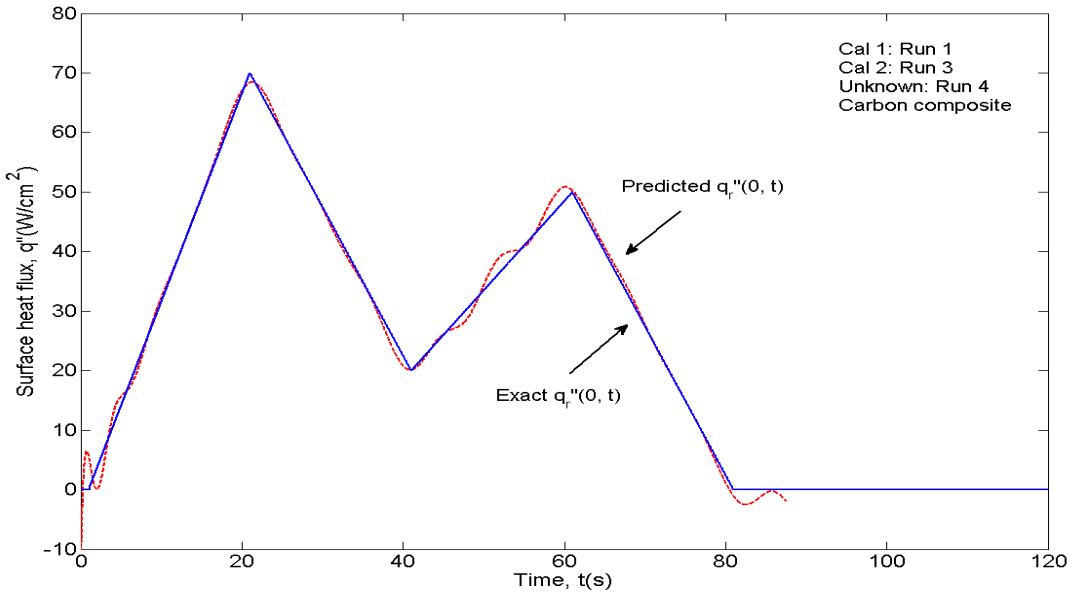

Figure 4.4.23: Predicted unknown surface heat flux $q_r"(0,t)$ for Group 1 of the carbon composite based on noiseless temperature data.

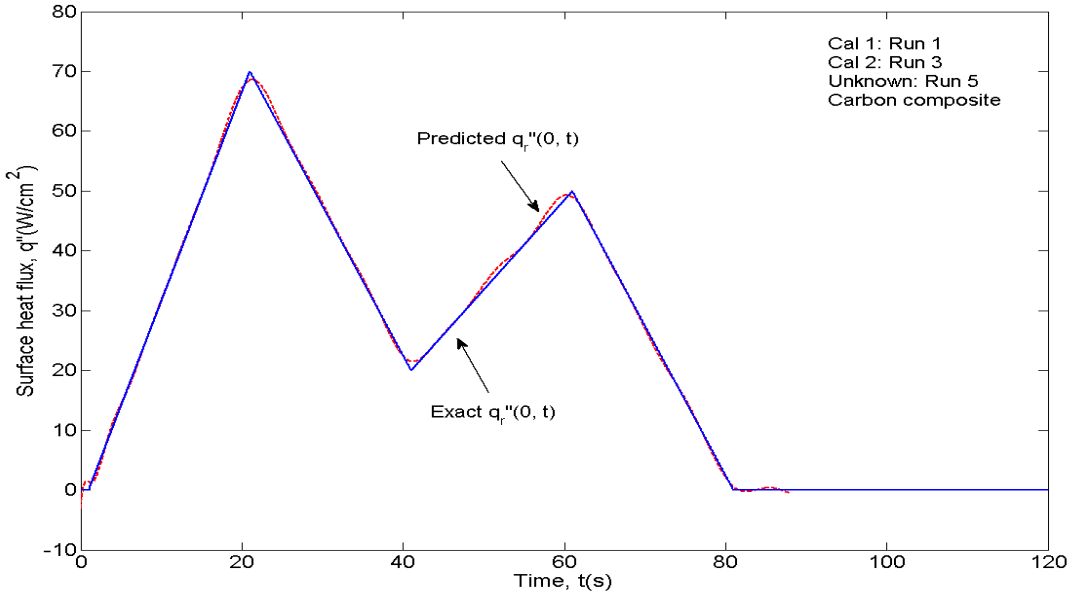

Figure 4.4.24: Predicted unknown surface heat flux $q_r"(0,t)$ for Group 2 of the carbon composite based on noiseless temperature data.

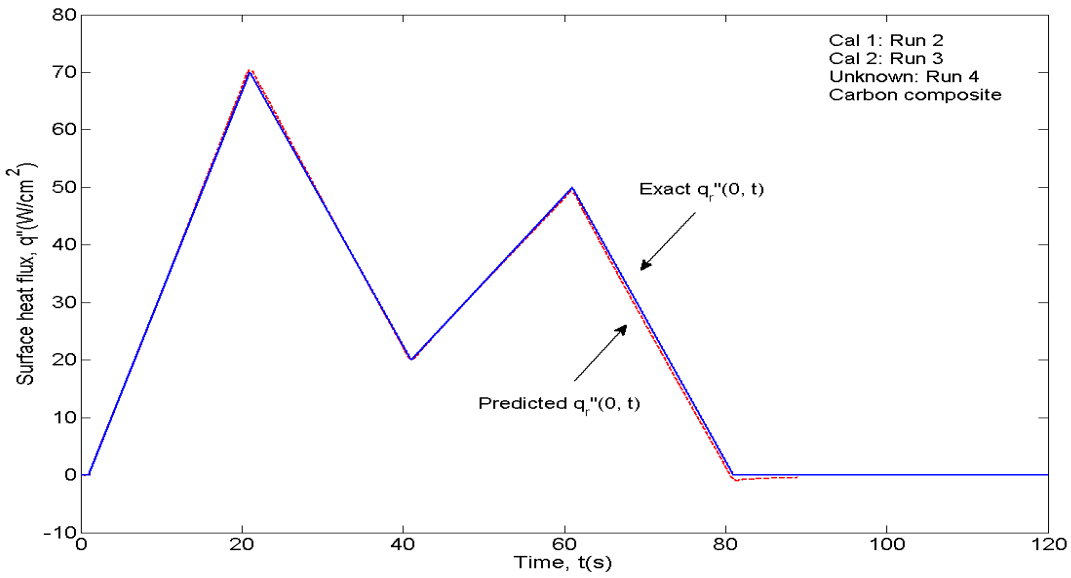

Figure 4.4.25: Predicted unknown surface heat flux $q_r"(0,t)$ for Group 3 of the carbon composite based on noiseless temperature data.

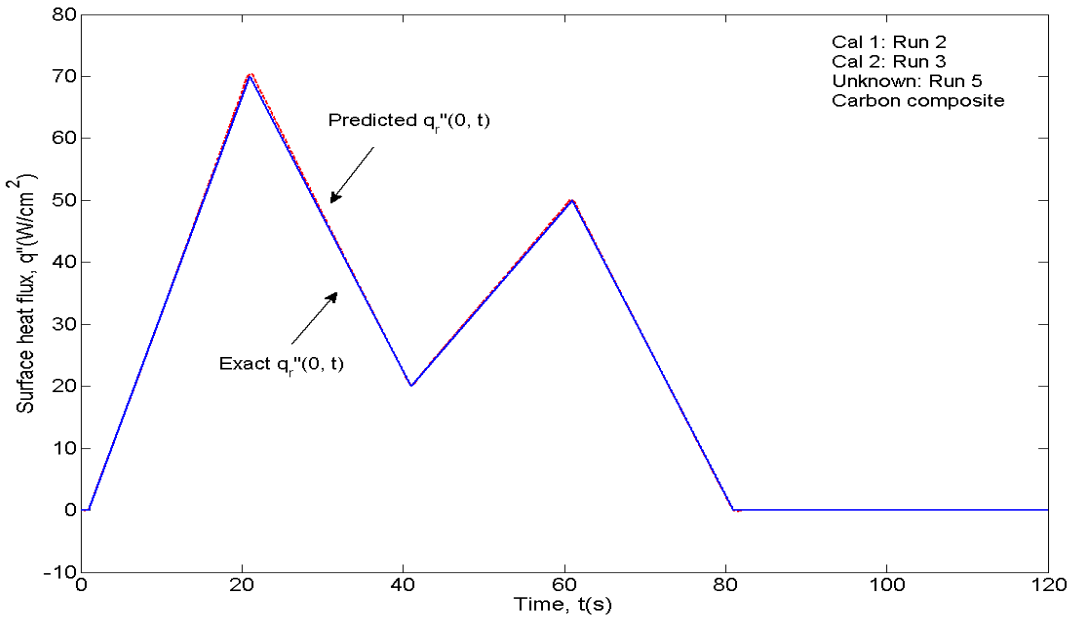

Figure 4.4.26: Predicted unknown surface heat flux $q_r"(0,t)$ for Group 4 of the carbon composite based on noiseless temperature data.

Table 4.4.3: Prediction accuracy metrics for the stainless steel 304 and the carbon composite results using the noiseless temperature data for all groups under the provided regularization parameters λ_0 and future time increment $S\Delta t^*$.

Stainless steel 304 (Table 1)	**Regularization Parameter λ_0 ($^oC^2s^2$)**	**Future Time Period $S\Delta t^*$ (s)**	**Standard deviation of Prediction Error σ(W/cm^2)**	**Peak ratio M_r**
Group 1	0.135	30	1.134	0.984
Group 2	0.135	30	0.564	0.993
Group 3	0.135	30	0.748	1.008
Group 4	0.135	30	0.336	1.010
Carbon composite (Table 1)	**Regularization Parameter λ_0($^oC^2s^2$)**	**Future Time Period $S\Delta t^*$ (s)**	**Standard deviation of Prediction Error σ(W/cm^2)**	**Peak ratio M_r**
Group 1	0.223	20	1.476	0.978
Group 2	0.223	20	0.534	0.981
Group 3	0.223	20	0.534	1.006
Group 4	0.223	20	0.277	1.007

prediction value hence promoting a good signal-to-noise ratio. For all the test groups based on noiseless data investigated, an optimal domain for λ_0 was determined lying in the range of (0.1-0.5$^oC^2s^2$) through the L-curve defined in Eq. (4.3.10). The prediction accuracy is satisfactory for all groups considering the magnitude of the nonlinearity and the varying extent of the back boundary conditions. In addition, the predictions from Group 3 and Group 4 are better than the predictions from Group 1 and Group 2 for both materials. This implies that the heating and cooling back boundary condition combination (Run 2 and Run 3) for calibration tests reduce the system ill-posed situation through the kernel K_{q2}^*, further improving the signal-to-noise ratio. The early time kernel formed by Run 1 and Run 3 stainless steel data is shown in Fig. 4.4.27(a) and the kernel formed by Run 2 and Run 3 data is displayed in Fig. 4.4.27 (b). The corresponding kernels for the carbon composite are presented in Figs. 4.4.28(a,b). It is clear that the kernel due to the combination of calibration tests involving early-time heating (Run 2) and cooling (Run 3) back boundary condition data produces a shorter signal delay (Figs. 4.4.27(b) for stainless steel 304 and Fig 4.4.28(b) for carbon composite).

It is also necessary to explore the robustness and stability of the localized Tikhonov regularization methodology in the presence of noisy data. For this purpose, normally distributed noise ε_i with a standard deviation 1 ^{o}C and mean 0 ^{o}C are added to "noiseless" probe temperature data $T(x, t_i)$ at $x = b$ and $x = w$. All simulated random noise is obtained through a Matlab random number generation function called "randn". Figure 4.4.29 displays a sample of the generated temperature noise. Since the combination of Run 2 and Run 3 (the heating and cooling back boundary condition) has been shown to be an appropriate calibration set, we apply Group 4 (Run 2 and Run 3 as calibration tests and Run 5 as reconstruction test whose front heat flux is to

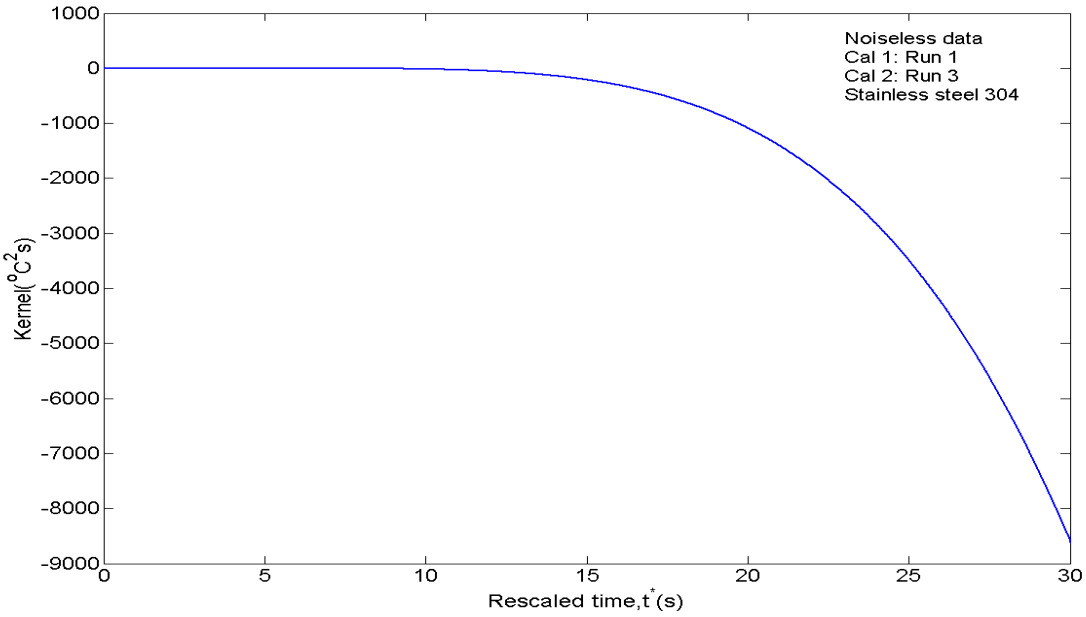

(a)

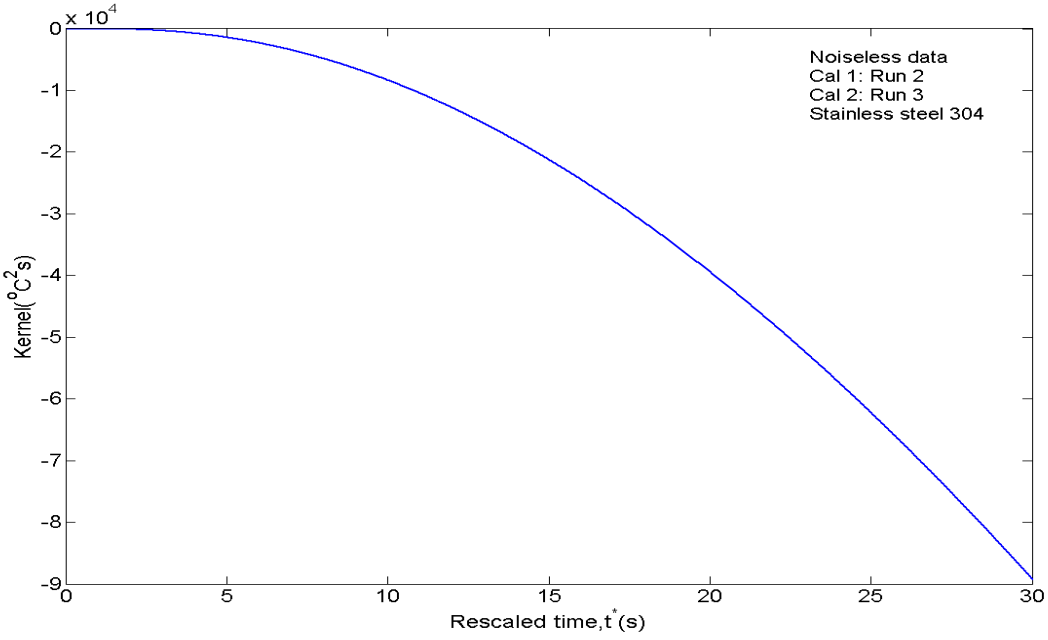

(b)

Figure 4.4.27: Kernel, Eq. (4.3.1b), based on noiseless calibration temperature data of stainless steel 304 formed by (a) Run 1 and Run 3 data, and (b) Run 2 and Run 3 data.

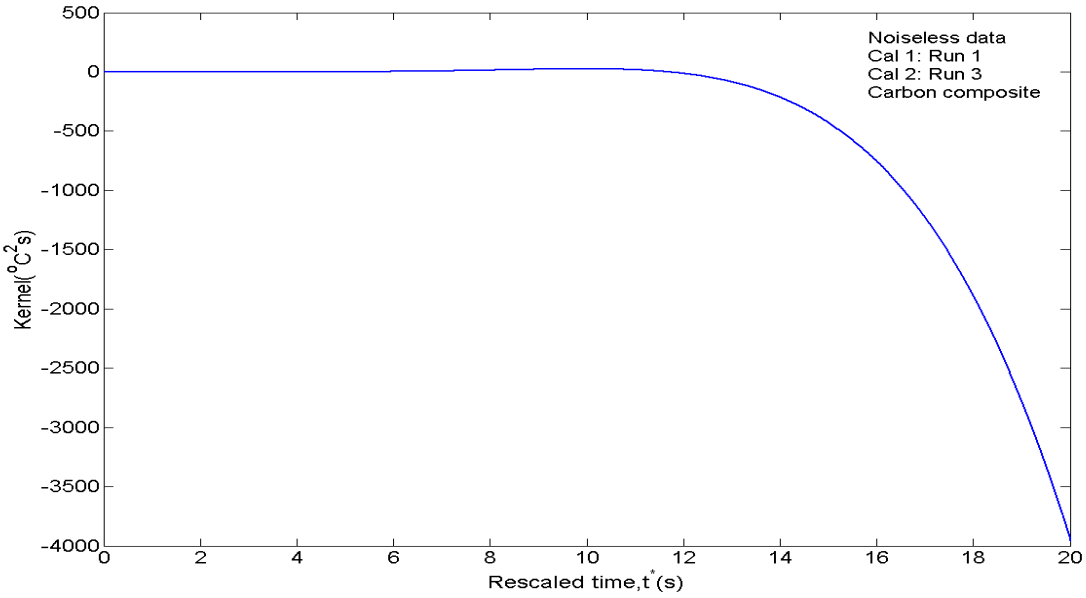

(a)

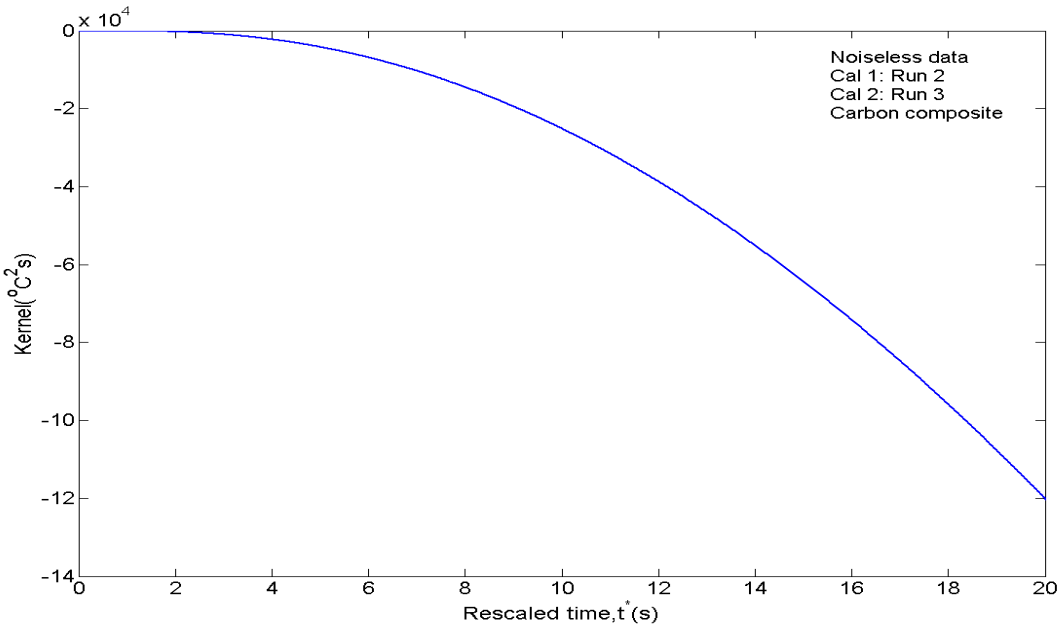

(b)

Figure 4.4.28: Kernel, Eq. (4.3.1b), based on noiseless calibration temperature data of carbon composite formed by (a) Run 1 and Run 3 data, and (b) Run 2 and Run 3 data.

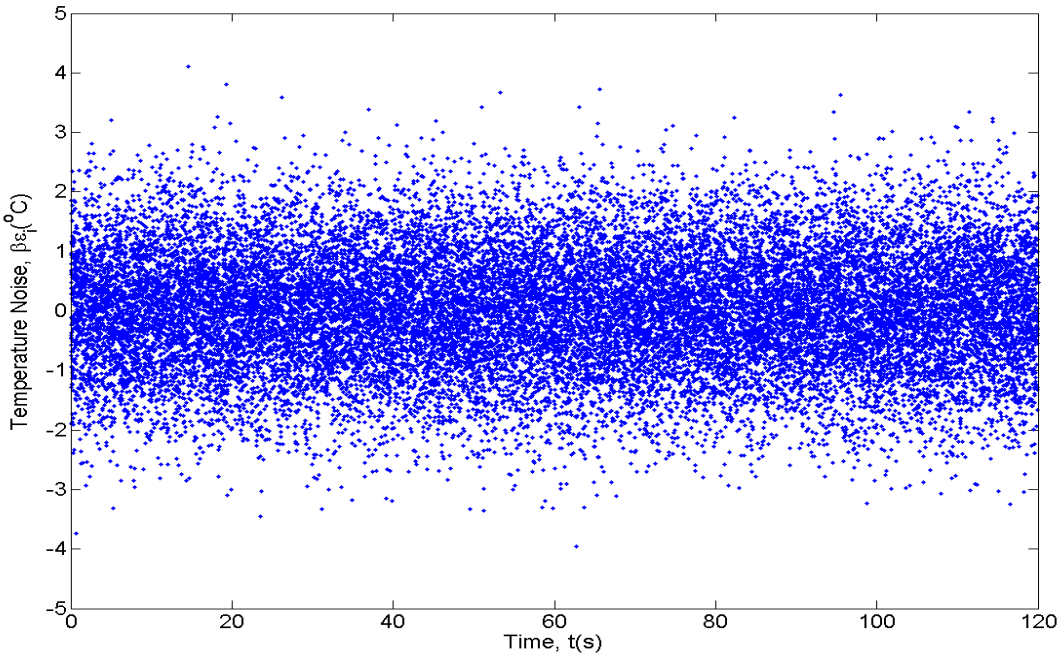

Figure 4.4.29: The simulated noise generated from the Matlab "randn" function with standard deviation 1°C and mean 0.

be reconstructed) for justifying the stabilization impact of the localized Tikhonov regularization methodology on the two-probe calibration model in the presence of noisy data. Figures 4.4.30(a,b) present the early-time kernel of Group 4 formed using noisy data for the stainless steel 304 and carbon composite samples, respectively. It is noted that both kernels retain a relative smooth character although noise has been added to the temperature data. This is because the kernel K_{q2}^{*} given by Eq. (4.3.1b) has the form of an integral that rapidly damps out temperature noise. Figures 4.4.31(a,b) present the L-curve analysis for extracting the optimal regularization parameter for the stainless steel 304 (λ_0 =0.368^{o}C^{2}s^{2}) and carbon composite (λ_0=0.135^{o}C^{2}s^{2}) samples, respectively. These parameters are chosen at the elbow of the shape L. Figures 4.4.32(a,b) present the final physical time domain net heat flux prediction $q"_r(0,t)$ based on above determined optimal regularization parameters in the presence of noise for the stainless steel 304 and the carbon composite samples, respectively. The regularization parameter, future time period, and prediction accuracy metrics for the stainless steel 304 and the carbon composite results using noisy temperature data are presented in Table 4.4.4. The standard deviation of prediction errors σ for stainless steel 304 and carbon compost are 1.357W/cm^{2} and 1.159W/cm^{2}, respectively. The ratios M_r of the predicted peak heat flux to the actual heat flux for stainless steel 304 and carbon compost are 1.032 and 1.017, respectively. Clearly stable and accurate results are obtained for both materials. This implies that an appropriate combination of the calibration test data with carefully designed back boundary conditions and the localized Tikhonov regularization methodology works well for resolving the front surface heat flux in the quasi-linearized two-probe system. It should also be noted that this approach works equally well for other high thermal diffusivity materials such as copper.

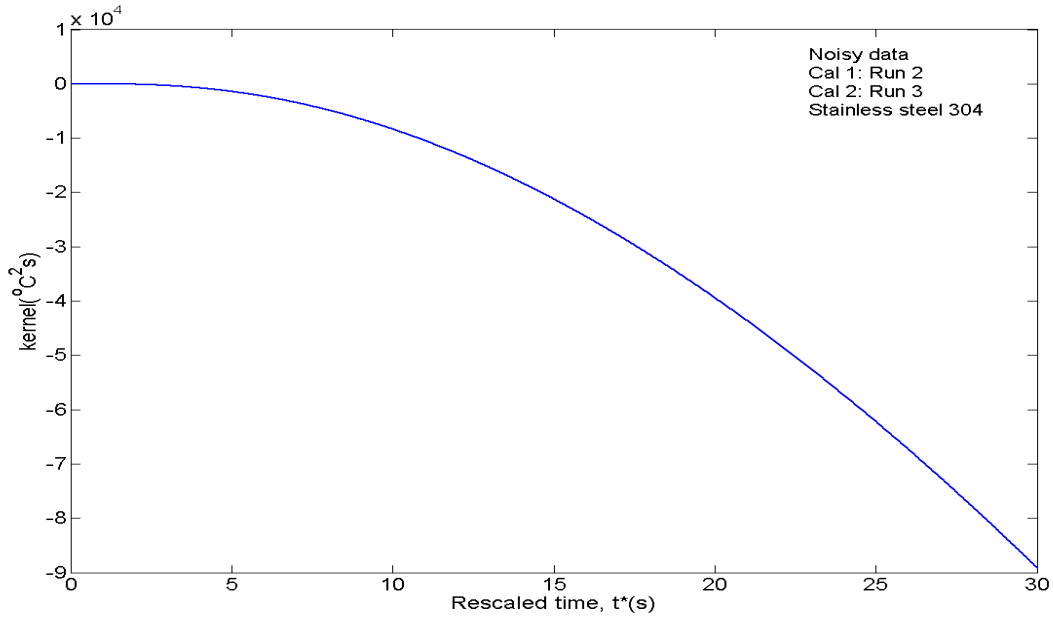

(a)

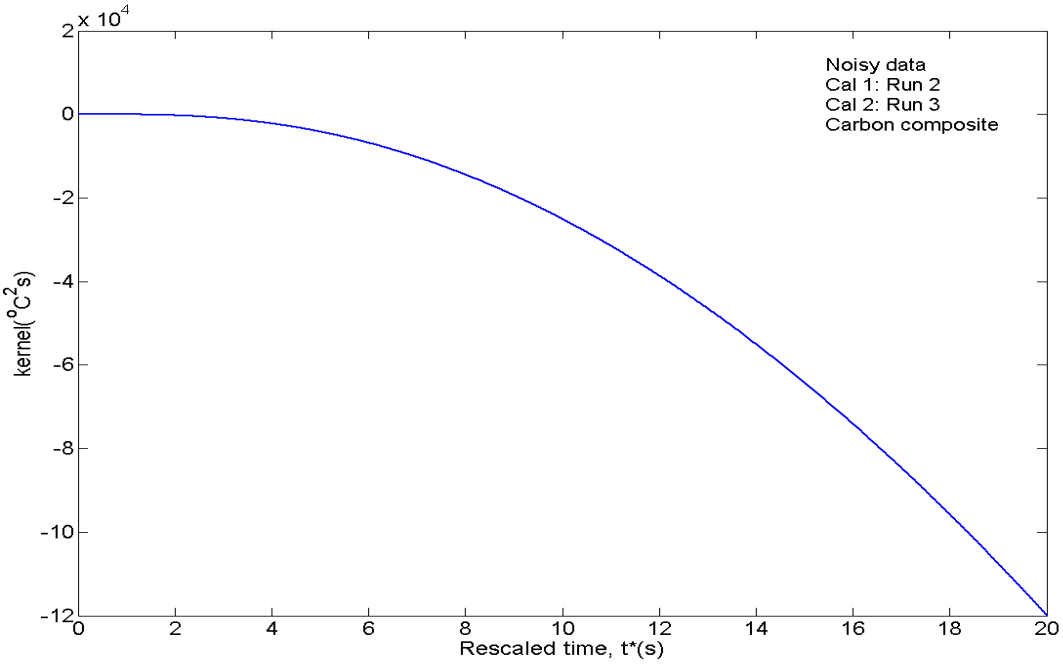

(b)

Figure 4.4.30: Kernel, Eq. (26b), formed by Run 2 and Run 3 noisy temperature data (a) stainless steel 304, and (b) the carbon composite.

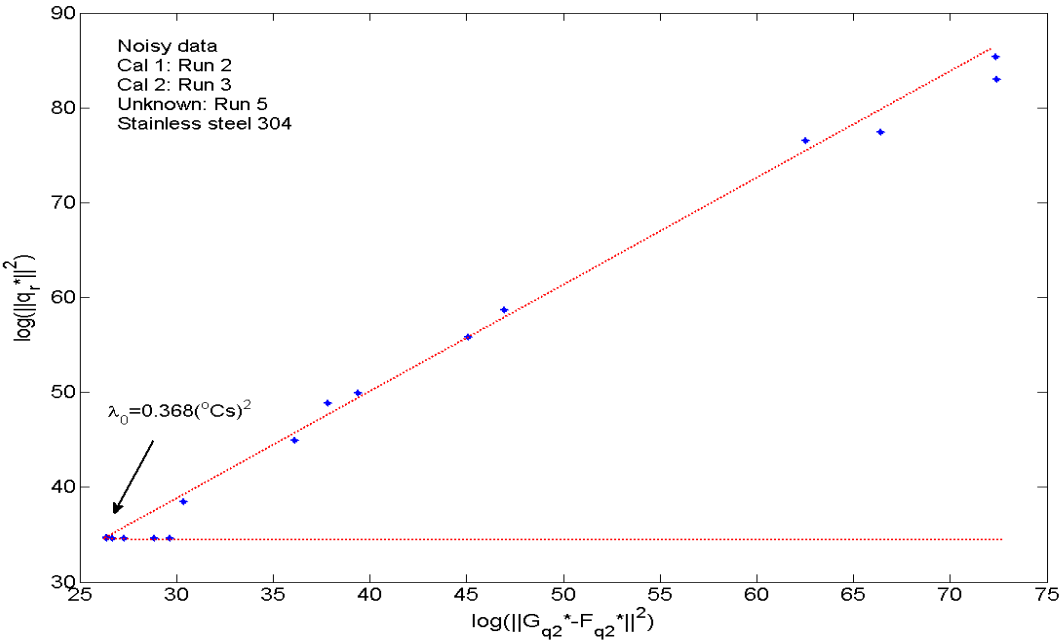

(a)

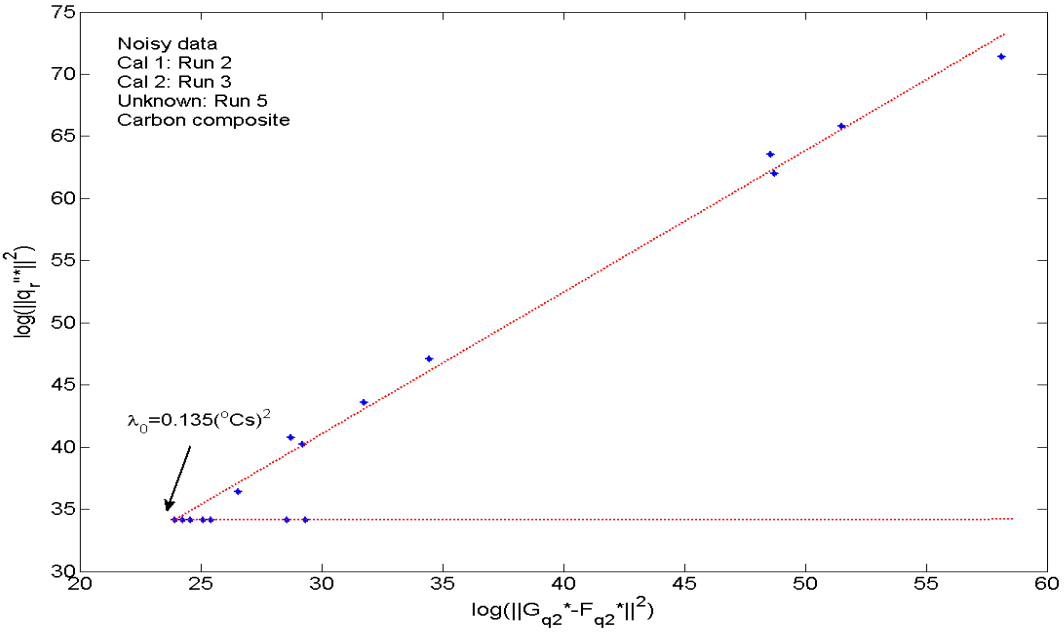

(b)

Figure 4.4.31: L-curve analysis for Group 4 based on noisy data (a) stainless steel 30, and (b) carbon composite.

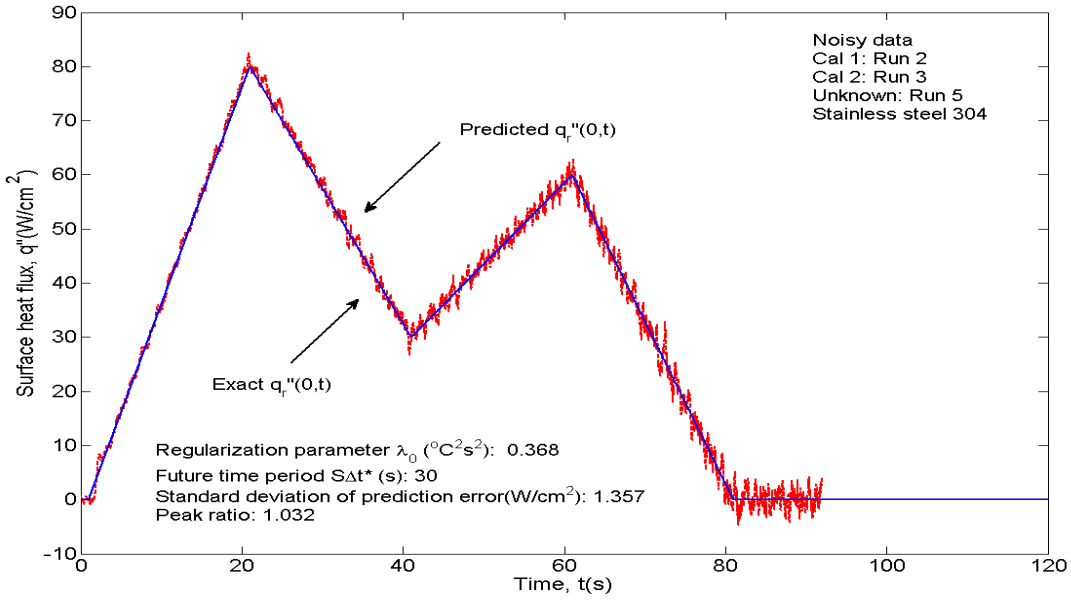

(a)

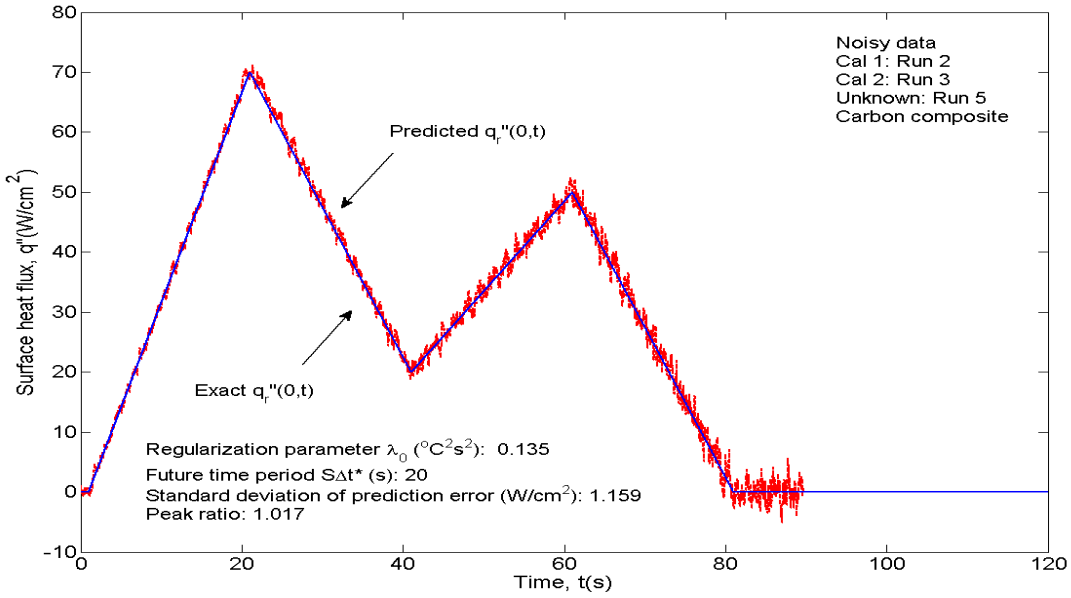

(b)

Figure 4.4.32: Predicted unknown surface heat flux $q_r"(0,t)$ for Group 4 based on noisy temperature data (a) stainless steel 304, and (b) carbon composite.

Table 4.4.4: Group 4 regularization parameter, future time period, and prediction accuracy metrics for the stainless steel 304 and the carbon composite results using noisy temperature data.

Parameter	Stainless steel 304	Carbon composite
Regularization Parameter λ_0 ($^oC^2s^2$)	0.368	0.135
Future Time Period $S\Delta t^*$ (s)	30	20
Standard deviation of Prediction Error σ (W/cm^2)	1.357	1.159
Peak ratio M_r	1.032	1.017

4.5 Conclusions

This chapter proposes a nonlinear two-probe calibration formulation that incorporates rescaling principles for resolving the front surface heat flux of a one-dimensional nonlinear heat conduction problem. Further, the back boundary condition variations among calibration and reconstruction tests were allowed to vary in order to demonstrate the importance of experimental design. Introduction of the second temperature probe removes the need to explicitly specifying the backside boundary condition as required by a boundary-value problem. However, careful selection of the calibration back boundary condition is required and demonstrated for reducing the ill-conditioning effects. To deal with the system nonlinearity, rescaling is introduced under a piecewise time-step linearization assumption. The ill-posed problem is resolved through the rescaled variables and then transformed back to the physical variables for presentation. A localized Tikhonov regularization scheme is introduced and shown to be effective and robust. L-curve analysis is applied for determining a proper regularization parameter. This new nonlinear two-probe calibration formulation has generality in application. It works well for both high thermal diffusivity materials, such as copper and low thermal diffusivity materials, such as stainless steel and the carbon composite.

Chapter 5: A Rescaling Based Inverse Heat Conduction Calibration Method and Optimal Regularization Parameter Strategy

This chapter is revised based on a paper to be published by Yinyuan Chen, Jay I. Frankel and Majid Keyhani:

Chen, Y.Y., Frankel, J.I., and Keyhani, M., accepted, "A Nonlinear, Rescaling Based Inverse Heat Conduction Calibration Method and Optimal Regularization Parameter Strategy", Journal of Thermophysics and Heat Transfer.

My primary contributions to this paper include (1) conceptualization of the new model, (2) development of numerical and regularization methods (3) writing and implementing of the computer code (4) and served as lead writer of the manuscript.

5.1 Introduction

Thermal protection systems require tools for accurately predicting the surface heat flux and temperature based on in-depth temperature measurements. Hostile thermal conditions at the surface preclude the use of surface mounted thermal sensors. Hence, sensors must be embedded below the surface and the resulting sensor temperature measurements must be projected to the surface for the surface prediction. This process is representative of the inverse heat conduction problem (IHCP), and is well-known to be ill-posed. There are many challenges associated with resolving inverse heat conduction problems [8, 59]. Fortunately, a variety of methods have been

proposed to deal with such issues. These includes: “exact solutions” [37], function specification [34-36], space marching and finite difference [49,110,114,118] and other well-studied techniques.

The accuracy of above classic inverse techniques relies on the accurate knowledge of the probe depth, thermophysical properties and probe response characteristics, i.e., signal delay and attenuation. To minimize the uncertainty associated with these physical parameters, system calibration is proposed as an alternative approach for resolving inverse heat conduction problems. This approach forms a calibration or measurement equation by analytical processing that eliminates the need to specify system parameters. The Non-Integer System Identification (NISI) method [40-42], involves developing an impulse response function from a calibration test. A finite series expansion is formed in terms of fractional derivatives of the measured calibration temperature and calibration surface heat flux. The unknown expansion coefficients are determined during the calibration stage. The unknown surface heat flux can be recovered based on the impulsive response. Frankel and Keyhani [43], Frankel et al. [44] and Elkins et al. [45] proposed an alternative calibration methodology that eliminates the use of fractional derivatives and the resolution of expansion coefficients described by the NISI method. This method relates the net unknown surface heat flux to the calibration surface heat flux and the corresponding in-depth temperature measurements during the calibration and reconstruction tests. The resulting inverse statement is then expressed in terms of a Volterra integral equation of the first kind for the unknown surface heat flux. In essence, the analytical transfer function is expressed in terms of experiment data.

The one-probe calibration method [43, 44] has been derived in a linear framework and has been experimentally verified [45] with excellent accuracy in an appropriate temperature range. However, in many practical situations, one should not assume that all the thermophysical properties can be considered constant as the temperature range is extended. As a result, the properties need to be considered as temperature dependent functions. This inclusion produces a fully nonlinear description of heat conduction. To account for the temperature varying property effects, a piecewise time-step linearization assumption is introduced to form the quasi-linearization. It involves a whole time domain discretization using a successive series of small time steps in increments of Δt. At each time interval, all thermophysical properties are assumed constant and evaluated at the forward probe temperature; i.e., probe closest to the active heating surface. Through this simplification, the nonlinear one-dimensional heat conduction problem can be equivalently expressed as a series of linear ones whose thermophysical properties are evaluated at their respective small time step Δt using the local temperature measurement as previously defined. Though all thermophysical properties vary at each time step, they can be transformed back to the values evaluated at the initial temperature through two rescaling coefficients. The inverse problem is then resolved in term of rescaled variables.

All inverse problems are ill-posed as previously noted. Arbitrary noise introduced into the measurements significantly magnifies the prediction uncertainty as the information is propagated toward the boundary of interest. Hence, it is necessary to stabilize the mathematical system through regularization. Common regularization approaches include: Tikhonov regularization [82], iterative regularization [16], local future-time method [8] and singular value decomposition (SVD) based regularization [80,81].

However, determining a suitable regularization parameter remains challenging as the bias and variance possess different magnitudes and sensitivities. In addition, no general method exists for obtaining the optimal regularization parameter for all cases independent of the applied regularization approach. Based on this consideration, a new optimal regularization parameter selection strategy is proposed in this chapter. This strategy exploits Gauss filter for evaluating or estimating the variance in the prediction [74] and adjusts the weight between the relative variance and bias with the aid of a weight coefficient. The optimal regularization parameter is acquired through pursuing a balance between the weighted bias and variance. This strategy is conceptually general and independent of the adopted regularization approach.

5.2 Formulation of the New Nonlinear One-Probe Calibration

Consider a one-dimensional heat conduction problem in Cartesian coordinates having a front surface heat flux source at $x = 0$ while maintaining an adiabatic back surface at $x = L$. A schematic of the sample geometry is given in Fig. 5.2.1. If the temperature range of interest is large then the effect of temperature dependent thermophysical properties cannot be ignored. Under this assumption, the nonlinear heat equation becomes [33]

$$\rho c_p\big(T(x,t)\big)\frac{\partial T}{\partial t}(x,t) = \frac{\partial}{\partial x}\left[k\big(T(x,t)\big)\frac{\partial T}{\partial x}(x,t)\right], \quad x \in (0,L), \;\; t \geq 0, \qquad (5.2.1a)$$

subject to the boundary conditions

$$-k\big(T(0,t)\big)\frac{\partial T}{\partial x}(0,t) \triangleq q"(0,t) = q"_s(t),$$

$$\frac{\partial T}{\partial x}(L,t) = 0, \qquad t \geq 0, \tag{5.2.1b-c}$$

and the initial condition

$$T(x,0) = 0, \qquad x \in [0,L]. \tag{5.2.1d}$$

The initial condition is considered as zero since all the temperature data involved in Eqs. (5.2.1a-d) are actually the relative temperature defined from the initial uniform temperature condition. The boundary condition at $x = L$ is assumed unchanging for all tests. As such, only one in-depth probe is required. Recall that the primary focus of this chapter is to demonstrate a quantitative means for estimating the optimal regularization parameters.

Exact solutions available to practical heat conduction problems are available for only a limited number of cases. Moreover, most of the solutions can only be obtained under significant constraints. Hence, it is prudent to quasi-linearize the nonlinear system such that linear analysis tools become available. For this purpose, a piecewise time-step linearization assumption is proposed, implying that the thermophysical properties are fixed in any small time step and evaluated at the forward most probe position temperature $T(b,t)$ relative to the active heating surface.

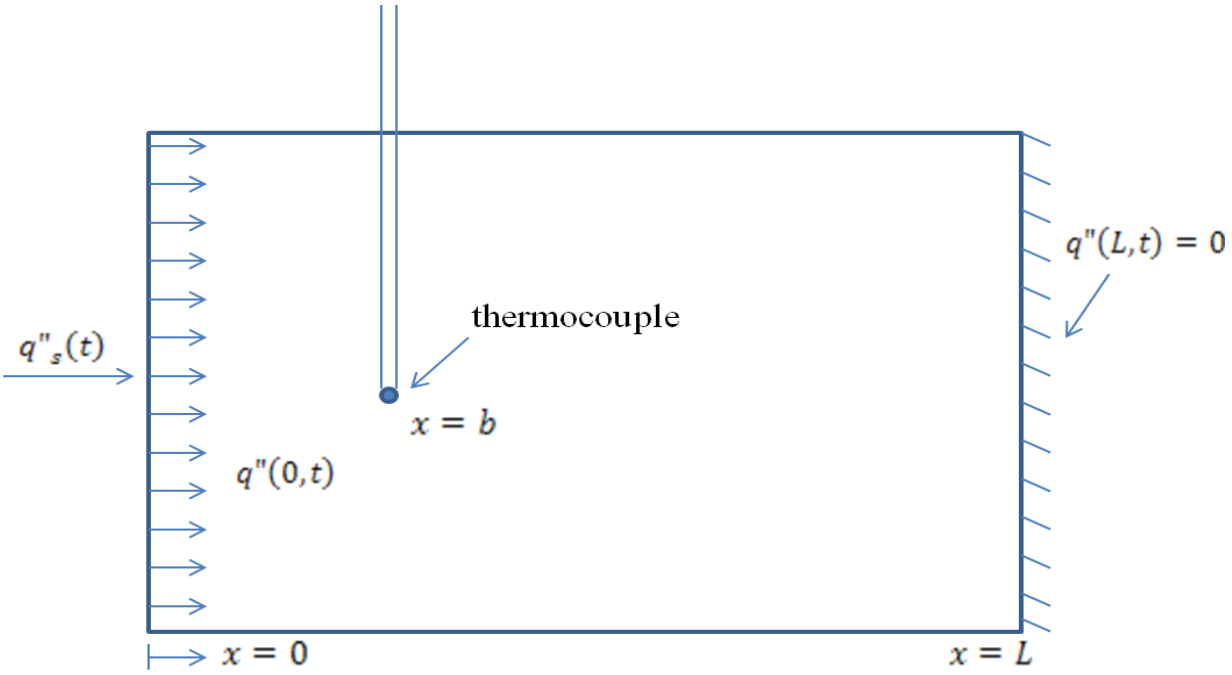

Figure 5.2.1: System setup for the one-dimensional heat conduction problem showing boundary conditions and the thermocouple position.

Explicitly, consider a heating process using $t_{max} = (N+1)\Delta t$, with any small interval $t \in [i\Delta t, (i+1)\Delta t]$ $(i = 0,1 \dots N)$. The governing heat equation, under this piecewise time-step linearization assumption, simplifies to

$$\frac{1}{\alpha\big(T(b, i\Delta t)\big)}\frac{\partial T_i}{\partial t}(x,t) = \frac{\partial^2 T_i}{\partial x^2}(x,t), \quad x \in (0,L), \quad t \in [i\Delta t, (i+1)\Delta t],$$

$$i = 0,1 \dots N, \qquad (5.2.2a)$$

where $T_i(x,t) = T(x,t), \ t \in [i\Delta t, (i+1)\Delta t]$ and subject to the boundary conditions

$$-k\big(T(b, i\Delta t)\big)\frac{\partial T_i}{\partial x}(0,t) = q"(0,t),$$

$$\frac{\partial T_i}{\partial x}(L,t) = 0, \quad t \in [i\Delta t, (i+1)\Delta t], \qquad (5.2.2b-c)$$

and the initial condition

$$T_i(x, i\Delta t) = T(x, i\Delta t), \quad x \in [0, L]. \qquad (5.2.2d)$$

Again, observe that all thermophysical properties are momentarily frozen in time and evaluated at the probe temperature $T(b, i\Delta t)$ in the time interval $[i\Delta t, (i+1)\Delta t], \ i = 0,1 \dots N$. However, the evaluated properties vary among different time steps. To achieve the quasi-linearization, two rescaling coefficients m_i and n_i are introduced to transform the local thermal diffusivity

$\alpha\big(T(b,i\Delta t)\big)$ and thermal conductivity $k\big(T(b,i\Delta t)\big)$ to system values evaluated at the initial temperature. These rescaling coefficients are defined as

$$m_i = \frac{k\big(T(b,0)\big)}{k\big(T(b,i\Delta t)\big)},$$

$$n_i = \frac{\alpha\big(T(b,0)\big)}{\alpha\big(T(b,i\Delta t)\big)}. \qquad (5.2.3a-b)$$

Based on Eqs. (5.2.3a-b), let us define

$$T_i^*(x,v) = T_i(x, n_i v + i\Delta t), \qquad v \in \left[0, \frac{\Delta t}{n_i}\right],$$

$$q''^*_i(0,v) = m_i q''(0, n_i v + i\Delta t). \qquad v \in \left[0, \frac{\Delta t}{n_i}\right], \qquad i = 0,1 \ldots N. \qquad (5.2.4a-b)$$

Upon substituting the above definitions given in Eqs. (5.2.4a-b) into Eqs. (5.2.2a-d), the heat equation can now be expressed as

$$\alpha\big(T(b,0)\big)\frac{\partial^2 T_i^*}{\partial x^2}(x,v) = \frac{\partial T_i^*}{\partial v}(x,v), \quad x \in (0,L), \quad v \in \left[0, \frac{\Delta t}{n_i}\right], \qquad (5.2.5a)$$

subject to the boundary conditions

$$-k\big(T(b,0)\big)\frac{\partial T_i^*}{\partial x}(0,v) = q''^*_i(0,v),$$

$$\frac{\partial T_i^*}{\partial x}(L,v) = 0, \qquad v \in \left[0, \frac{\Delta t}{n_i}\right], \tag{5.2.5b-c}$$

and the initial condition

$$T_i^*(x, v=0) = T(x, t=i\Delta t), \quad x \in [0,L], \quad i = 0,1 \dots N. \tag{5.2.5d}$$

Since all thermophysical properties are evaluated at the initial condition independent of selected time step, we can collect all rescaled temperatures $T_i^*(b,v)$ from time zero $(i=0)$ to the final time $(i=N)$ in sequence. This collection can be regarded as the linear thermal response induced by the rescaled surface heat flux which is formed through the reconstitution of $q''^*_i(0,v)$ from $i=0$ to $i=N$.

For notational compactness, define

$$n_{-1} = \infty, \tag{5.2.6a}$$

then the total sequential system for the surface heat flux and temperature can be expressed as

$$q''^*_{tN}(0,t) = m_j q''^*_j\left(0, t - \sum_{i=-1}^{j-1}\frac{\Delta t}{n_i}\right), \quad t \in \left[\sum_{i=-1}^{j-1}\frac{\Delta t}{n_i}, \sum_{i=-1}^{j}\frac{\Delta t}{n_i}\right), \; j = 0,1 \dots N, \tag{5.2.6b}$$

$$T_{tN}^{*}(x,t) = T_{j}^{*}\left(x, t - \sum_{i=-1}^{j-1}\frac{\Delta t}{n_i}\right), \qquad t \in \left[\sum_{i=-1}^{j-1}\frac{\Delta t}{n_i}, \sum_{i=-1}^{j}\frac{\Delta t}{n_i}\right), \quad j = 0, 1 \ldots N, \quad (5.2.6c)$$

respectively. Observe that the rescaling is based on the reference thermophysical properties $k\big(T(b,0)\big)$ and $\alpha\big(T(b,0)\big)$ which are evaluated at the initial temperature. The rescaling coefficients given by Eqs. (5.2.3a,b) can actually be based on any value. In fact, one can set the reference thermal diffusivity and thermal conductivity using L^2 and L, respectively such that $m_i = L^2 / k\big(T(b, i\Delta t)\big)$ and $n_i = L/\alpha\big(T(b, i\Delta t)\big)$. The corresponding heat equations given by Eqs. (5.2.5a,b) will possess a dimensionless form in terms of rescaling variables $x^* = x/L$ and $\theta^*(x^*, v) = T^*(x^*, v)/T^*(b^*, v_{max})$. However, this dimensionless form is not implemented since the calibration strategy does not require the specification of the probe position b or slab thickness L.

In the linear framework, Frankel et al [43-45] developed the calibration equation for the one-probe inverse problem as

$$\int_{u=0}^{t} q"_r(0,u)T_c\,(b, t-u)du = \int_{u=0}^{t} q"_c(0,u)T_r\,(b, t-u)du, \quad b \in [0, L], \quad t \geq 0, \qquad (5.2.7)$$

where $T_c(b,t)$ is the measured calibration temperature at some depth $x = b$; $q"_c(0,t)$ is the net surface heat flux imposed during the calibration test; $T_r(b,t)$ is the measured temperature of the same thermocouple in response to the unknown heat flux; and $q"_r(0,t)$ is the unknown surface

heat flux to be predicted. Again, note that these are reduced temperatures. This calibration integral equation has broad appeal since it does not require any knowledge of probe position or thermophysical properties.

Extending the linear calibration equation to a nonlinear framework requires the replacement of physical variables $q"(0,t)$ and $T(b,t)$ involved in Eq. (5.2.7) with the rescaling variables $q"^{*}_{tN}(0,t)$ and $T^{*}_{tN}(x,t)$ in Eqs. (5.2.6a-c). Performing this replacement produces

$$\int_{u=0}^{t} q"^{*}_{tN,r}(0,u)T^{*}_{tN,c}(b,t-u)du = \int_{u=0}^{t} q"^{*}_{tN,c}(0,u)T^{*}_{tN,r}(b,t-u)du, \quad t \in \left[0, \sum_{i=0}^{N} \frac{\Delta t}{n_i}\right),$$
$$i = 0,1 \ldots N. \qquad (5.2.8)$$

Two observations must be made: First, Eq. (5.2.8) requires knowledge of the explicit thermophysical property functions since the two rescaling coefficients m_i and n_i defined in Eqs. (5.2.3a,b) require the thermal conductivity and thermal diffusivity. The probe position can still be considered as unnecessary. Second, if all thermophysical properties are constant then Eq. (5.2.8) reduces to Eq. (5.2.7). This verifies that Eq. (5.2.8) is actually suitable for both linear and nonlinear situations.

To generalize this solution procedure, let $\Delta t = \lim_{N\to\infty} \frac{t_{max}}{N+1}$ such that for any time $t_M \in (0, t_{max}]$, it is possible to find an integer $M \in [0, N]$ to ensure $t_M \approx M\Delta t$. The sequential procedure produces the compact integral relation

$$\sum_{i=0}^{M} \frac{\Delta t}{n_i} \approx \int_{u=0}^{t_{M+1}} \frac{\alpha\big(T(b,u)\big)}{\alpha\big(T(b,0)\big)} du. \qquad (5.2.9a)$$

Therefore, the surface heat flux and temperature variables are expressed as

$$T(x, t_{M+1}) = T^*_{tM}\left(x, \int_{u=0}^{t_{M+1}} \frac{\alpha\big(T(b,u)\big)}{\alpha\big(T(b,0)\big)} du\right),$$

$$q"(0, t_{M+1}) = \frac{k\big(T(b,t_M)\big)}{k\big(T(b,0)\big)} q"^*_{tM}\left(0, \int_{u=0}^{t_{M+1}} \frac{\alpha\big(T(b,u)\big)}{\alpha\big(T(b,0)\big)} du\right), \qquad (5.2.9b-c)$$

respectively.

Next, we define the rescaled time variable t^* as

$$t^* = \int_{u=0}^{t} \frac{\alpha\big(T(b,u)\big)}{\alpha\big(T(b,0)\big)} du, \qquad (5.2.10a)$$

and we express the rescaled surface heat flux and temperature as

$$q"^*(0, t^*) = \frac{k\big(T(b,0)\big)}{k\big(T(b,t)\big)} q"(0,t),$$

and

$$T^*(x,t^*) = T(x,t), \qquad x \in [0,L], \;\; t \in [0,t_{max}], \qquad (5.2.10b-c)$$

respectively.

The final form of the calibration integral equation for the entire time domain that allows for variable thermophysical properties under the proposed assumption is

$$\int_{u=0}^{t^*} q''^*_r(0,u)T_c^*(b,t^*-u)du = \int_{u=0}^{t^*} q''^*_c(0,u)T_r^*(b,t^*-u)du, \qquad t^* \geq 0. \qquad (5.2.11)$$

After the prediction in the rescaled time domain is complete then it is necessary to transform the rescaled variables to the physical domain through

$$t = \int_{u=0}^{t^*} \frac{\alpha\left(T^*(b,0)\right)}{\alpha\left(T^*(b,u)\right)} du,$$

$$q''_r(0,t) = \frac{k\left(T^*(b,t^*)\right)}{k\left(T^*(b,0)\right)} q''^*_r(0,t^*), \qquad t^* \geq 0. \qquad (5.2.12a-b)$$

5.3 Regularization Parameter Search Strategy

The quasi-linearized calibration equation given by Eq. (5.2.11) is a Volterra integral equation of first kind for the unknown front surface heat flux. As remarked earlier, it is ill-posed. Its computation requires careful regularization to ensure a stable and an accurate prediction. The strategy adopted in this paper involves the classical Tikhonov regularization approach [82], singular-value decomposition (SVD) based regularization [80,81] and local future-time method [8]. Since the calibration equation given by Eq. (5.2.11) is resolved in rescaled time domain, it is necessary to transform the physical discrete experimental data to the rescaled variables according to Eqs. (5.2.10a-c) before any numerical operations are made. Afterwards, discretization is achieved in the rescaled time domain using $t^* \in [0, t^*_{max}]$ with $t^*_{max} = (N+1)\Delta t^*$. Let us define

$$G^*_q(t^*_i) = \int_{u=0}^{t^*_i} q''^*_r(0,u) T^*_c\,(b, t^*_i - u)du,$$

$$F^*_q(t^*_i) = \int_{u=0}^{t^*_i} q''^*_c(0,u) T^*_r\,(b, t^*_i - u)du, \qquad (5.3.1a-c)$$

$$t^*_i = i\Delta t^*,$$

which merely represent the left-hand and right-hand side of Eq. (5.2.11), respectively. These definitions are convenient in later analysis.

The local future-time method is a sequential regularization method [8]. Assuming that the rescaled heat fluxes from 0 to $(M-1)\Delta t^*$ are known then the unknown rescaled heat flux $q''^*_r(0, M\Delta t^*)$ can be obtained according to [45]

$$q''^*_r(0,t^*_M)=\frac{F^*_q(t^*_{M+S})-\int_{u=0}^{t^*_M} q''^*_r(0,u)T^*_c\,(b,t^*_{M+S}-u)du}{\int_{u=0}^{t^*_S} T^*_c\,(b,u)du},\quad M\in[0,N+1-S]. \quad (5.3.2)$$

Here, $\gamma = S\Delta t^*$ represents the future time increment and is considered as a regularization parameter. Small values of γ produce unstable predictions while large values of γ lead to the over-smoothed solutions associated with an excessive bias.

Both Tikhonov and singular-value decomposition (SVD) based regularization methods resolve the inverse problem using different means for defining regularization. In their conventional implementation, these methods are global while the local future time method preserves causality and locality. To apply these global methods for the present investigation, we first need to represent Eq. (5.2.11) in a compact matrix form based on a convenient left-hand rectangular discretization rule as

$$\boldsymbol{T_c q_r} = \boldsymbol{F_q}, \quad (5.3.3)$$

where $\boldsymbol{T_c}$ is a $(N+1)\times(N+1)$ matrix with $\boldsymbol{T_c}(i,j)=\Delta t^*\times T^*_c\left(b,t^*_{i-j+1}\right)$ for $i\geq j$ and $\boldsymbol{T_c}(i,j)=0$ for $i<j$, $\boldsymbol{F_q}$ is a $(N+1)\times 1$ vector with $\boldsymbol{F_q}(i)=F^*_q(t^*_i)$, and $\boldsymbol{q_r}$ is a $(N+1)\times 1$ vector to be determined with $\boldsymbol{q_r}(i)=q''^*_r(0,t^*_{i-1})$.

To better understand the principal of both Tikhonov and SVD based regularization methods, we impose singular-value decomposition on $\boldsymbol{T_c}$ as the first step. As a result, $\boldsymbol{T_c}$ can be written as the product of three matrices ($\boldsymbol{W}, \sum, \boldsymbol{V^T}$)

$$\boldsymbol{T_c} = \boldsymbol{W}\sum\boldsymbol{V^T} = \sum_{i=1}^{N+1} \boldsymbol{w}_i \sigma_i \boldsymbol{v}_i^T, \tag{5.3.4}$$

where $\boldsymbol{W} = (\boldsymbol{w}_1, \boldsymbol{w}_2, \boldsymbol{w}_3, \cdots, \boldsymbol{w}_{N+1})$ and $\boldsymbol{V} = (\boldsymbol{v}_1, \boldsymbol{v}_2, \boldsymbol{v}_3, \cdots, \boldsymbol{v}_{N+1})$ satisfying $\boldsymbol{W^T W} = \boldsymbol{V^T V} = \boldsymbol{I}$. The symbol $\sum$ is a $(N+1) \times (N+1)$ diagonal matrix whose diagonal value σ_i arranges in a descending order as

$$\sigma_1 \geq \sigma_2 \geq \cdots \geq \sigma_{N+1} \geq 0. \tag{5.3.5}$$

The direct inversion of Eq. (5.3.3) produces the forward formal prediction for $\boldsymbol{q_r}$ as

$$\boldsymbol{q_r} = \sum_{i=1}^{N+1} \frac{1}{\sigma_i} \boldsymbol{w_i^T F_q v}_i. \tag{5.3.6}$$

However, this result is unacceptable since small value of σ_i amplify the noise located in $\boldsymbol{F_q}$. We know that as the singular values σ_i become excessive small, instability grows and the system prediction is unreliable. To avoid this destabilization effect, we describe and implement two

techniques that regularize Eq. (5.3.3) in effective ways. First, the Tikhonov method is introduced. This method introduces the regularization parameter λ_0 through

$$\boldsymbol{q_r} = \sum_{i=1}^{N+1} \frac{\sigma_i}{\sigma_i^2 + \lambda_0^2} \boldsymbol{w_i^T F_q v}_i, \tag{5.3.7}$$

such that all $N + 1$ singular values are retained in the analysis. Here, we see that the denominator of Eq. (5.3.7) can never be driven to zero. Although the regularization parameter λ_0 is introduced to modify and control the behavior of the denominator shown in Eq. (5.3.7), this equation is actually a direct result of minimizing the objective function

$$J(q''^*_r(0, t_i^*)|_{i=0}^N) = \sum_{i=1}^{N+1} \left[G_q^*(t_i^*) - F_q^*(t_i^*)\right]^2 + \lambda_0^2 \sum_{i=0}^{N} [q''^*_r(0, t_i^*)]^2. \tag{5.3.8}$$

Second, we describe how to regularize Eq. (5.2.11) using SVD based regularization method with the aid of Eq. (5.3.3). In this case, any σ_i whose condition number (σ_i/σ_1) is smaller than a designed limitation (RN) is ignored. Then, if the index I can be found such that $\sigma_I > RN \times \sigma_1$ and $\sigma_i \leq RN \times \sigma_1$ for all $i \geq I$, regularized $\boldsymbol{q_r}$ can be represents as

$$\boldsymbol{q_r} = \sum_{i=1}^{I} \frac{1}{\sigma_i} \boldsymbol{w_i^T F_q v}_i. \tag{5.3.9}$$

Here, either the designed limitation RN or index I is considered as the regularization parameter. However, for both Tikhonov and SVD based regularization approaches, estimating the proper λ_0 and I are nontrivial tasks.

In this chapter, a new strategy is proposed for selecting an optimal regularization parameter independent of the applied regularized methodologies. Mathematically, we propose to investigate the two-component exponential function given as

$$P = e^{-(P1+mP2)}, \tag{5.3.10a}$$

where

$$P1 = \frac{\left\| q"^{*}_{r}(0,t_i^*) - q"^{*}_{r,f}(0,t_i^*) \right\|}{\left\| q"^{*}_{r,f}(0,t_i^*) \right\|},$$

$$P2 = \frac{\left\| G_q^*(t_i^*) - F_q^*(t_i^*) \right\|}{\left\| F_q^*(t_i^*) \right\|}, \tag{5.3.10b-c}$$

Here, $q"^{*}_{r,f}(0,t_i^*)$ represents the filtered form of $q"^{*}_{r}(0,t_i^*)$. For example, using a Gauss filter [74], we express $q"^{*}_{r,f}(0,t_i^*)$ as

$$q''^{*}_{r,f}(0,t_i^*)=\frac{\sum_{j=0}^{N} q''^{*}_{r}\left(0,t_j^*\right)e^{-\frac{\left(t_j^*-t_i^*\right)^2 w_c{}^2}{4}}}{\sum_{j=0}^{N} e^{-\frac{\left(t_j^*-t_i^*\right)^2 w_c{}^2}{4}}},\qquad i=0,1,\dots N,\qquad (5.3.11a)$$

where

$$w_c=2\pi f_c. \qquad (5.3.11b)$$

Here, f_c represents the cutoff frequency that must be defined based on $q''^{*}_{r,f}(0,t_i^*)$. It is well-known that a Gauss low pass filter is capable of effectively removing high frequency noise from the signal after introducing the proper f_c [74]. Hence, it can be applied to evaluate function smoothness. Here, we interpret smoothness as a representative measure of variance. Therefore, in Eq. (5.3.10a), $P1$ represents the magnitude of the prediction variance while $P2$ is used for the computation of the model bias which is represented as the normalized norm of the residual for the new calibration method given in Eq. (5.2.11). Since variance and bias are not equally important for the final prediction, a weight coefficient m is suggested to adjust their relative importance. The optimal regularization parameter is identified as the maximum value of P which indicates a balance between weighted bias and variance.

5.4 Results

In this section, the merit of the nonlinear calibration equation given by Eq. (5.2.11) is verified through numerically simulated temperature data generated at $x=b$. A schematic of the physical system is given in Fig. 5.2.1. For demonstration purpose, a slab of carbon material is

investigated with probe location $b = 2\text{mm}$ and depth $L = 1\text{cm}$. The front surface of this slab is exposed to distinct time-varying heat fluxes during testing while the back surface is modeled as adiabatic during all tests. This simplicity is introduced as it is the purpose of this investigation to study the optimal regularization search through Eq. (5.3.10a). Carbon composite is a common aerospace testing material. The assumed representative functions for bulk thermal conductivity and bulk heat capacity are expressed as

$$k(T) = (5.76 + 1.195 \times 10^{-3}T)\ (\text{Wm}^{-1}\text{K}^{-1}), \tag{5.4.1a}$$

$$\rho c_p(T) = (1.705 \times 10^{6} + 3629T - 3.075T^{2} + 9.334 \times 10^{-4}T^{3})\ (\text{Jm}^{-3}\text{K}^{-1}). \tag{5.4.1b}$$

Figures 5.4.1-5.4.3 display the thermal conductivity, heat capacity and thermal diffusivity $\alpha(T) = k(T)/(\rho c_p(T))$ functions, respectively. From these figures, we conclude that the temperature dependence of these properties should be accounted in the heat transfer analysis when a large temperature range is considered.

Noiseless temperature data $T(b,t)$ at the probe position require the temperature field $T(x,t), x \in [0,L], t \geq 0$ for a given set of boundary and initial conditions to be obtained by a forward solution. For this purpose, a finite difference method (FDM) [33] is applied on the domain $x \in [0,L],\ t \geq 0$ where fully temperature dependent thermophysical properties are assumed. For the FDM solution, the spatial grid, Δx and temporal grid, Δt are varied until the solution convergence is met to some predefined criteria. For this study, it was found that

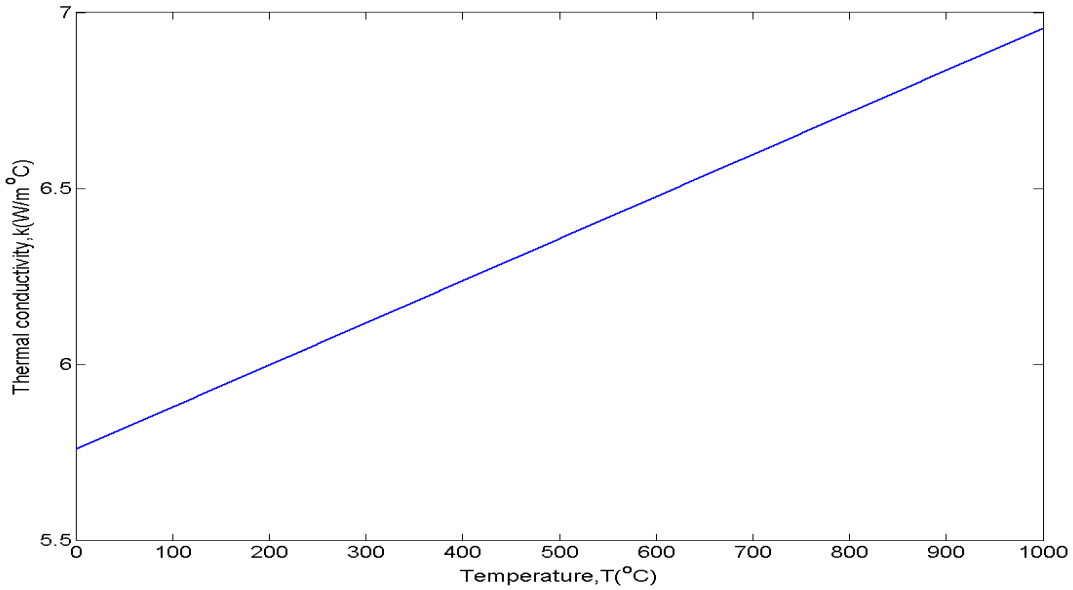

Figure 5.4.1: Approximate thermal conductivity for the carbon composite, Eq. (5.4.1a).

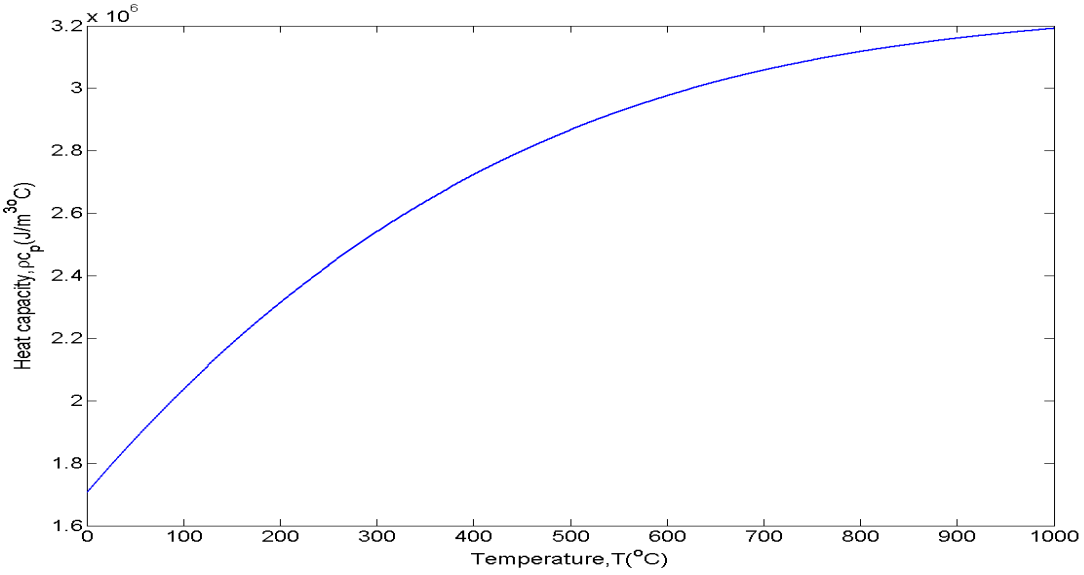

Figure 5.4.2: Approximate heat capacity for the carbon composite, Eq. (5.4.1b).

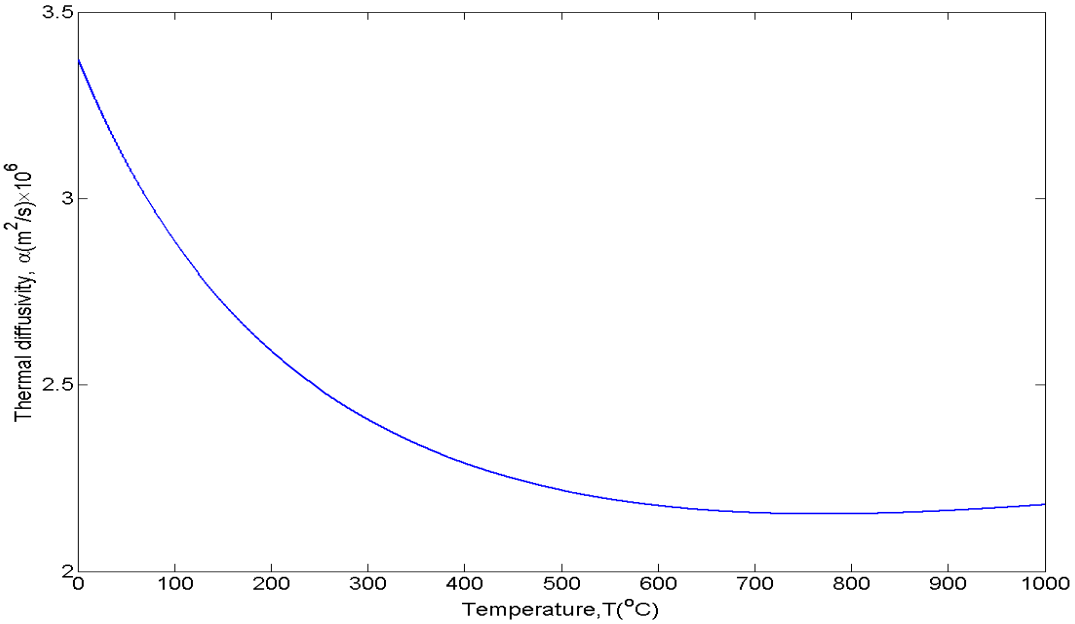

Figure 5.4.3: Approximate thermal diffusivity for the carbon composite, $\alpha(T) = k(T)/\rho c_p(T)$.

Δx=0.2mm and Δt =50μs work sufficiently well for all data collection reported based on an absolutely convergence of 0.01^{o}C.

The calibration heat flux is set to a constant $q"_c = 80\text{W/cm}^2$ lasting 30s, while the reconstruction test exploits an isosceles triangular heat flux starting at 2.5s and ending at 22.5s possessing a peak of 200W/cm^2. These heat fluxes and their corresponding probe temperature responses $T(b,t)$, as computed by the proposed forward model are presented in Fig. 5.4.4 and Fig. 5.4.5, respectively. Figure 5.4.5 indicates the large temperature variation at the probe position during both tests. Inclusions of nonlinear effects due to the thermophysical properties are required. In addition, Figure 5.4.6 presents the temperature histories at uniformly distributed spatial locations during the reconstruction test. For the reconstruction test, the surface temperature exceeds 1000 ^{o}C. The signal decay from surface to probe position at $x = b = 2\text{mm}$ is also pronounced.

Data without and with noise are investigated in this chapter. The first case establishes the new calibration approach in the presence of noiseless data. The purpose of applying the noiseless temperature data at $x = b$ are to (1) confirm the suitability of the nonlinear calibration model, and (2) verify the numerical method. Since all the computations are made in terms of rescaled variables, noiseless temperature data are immediately required to be rescaled in accordance to Eq. (5.2.10a-c). Before proceeding the reconstruction process based on $T_r(b,t)$, it is good to understand the intrinsic bias. To see this, the rescaled variables are then substituted into Eqs. (5.3.1a-c) for computing the normalized base residual ($\frac{G_q^*(t_i^*)}{F_q^*(t_i^*)} - 1,\ i = 0,1 \ldots N$) where the correct "unknown" surface heat flux is applied.

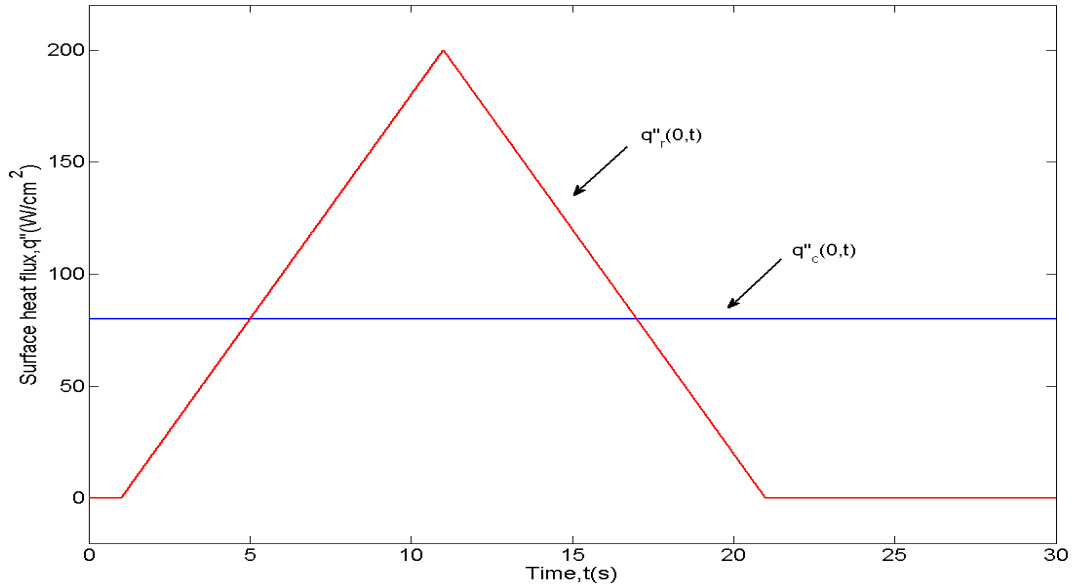

Figure 5.4.4: The known "calibration" surface heat flux $q"_c(0,t)$ and the "unknown" heat flux $q"_r(0,t)$ to be predicted.

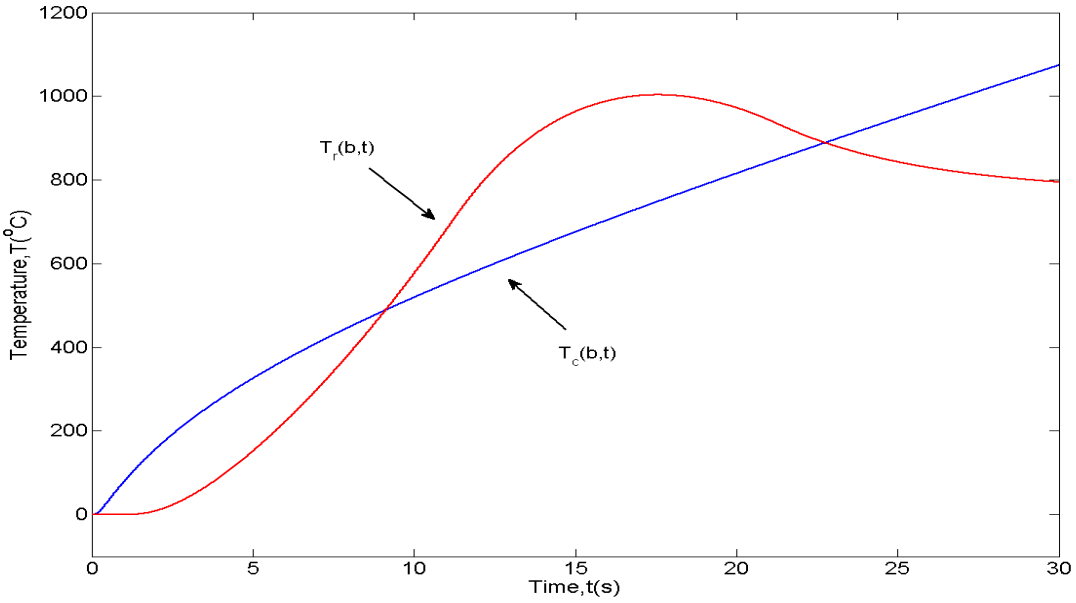

Figure 5.4.5: Noiseless temperature measurement $T_c(b,t)$ and $T_r(b,t)$ at the probe position for both the calibration and reconstruction tests, respectively.

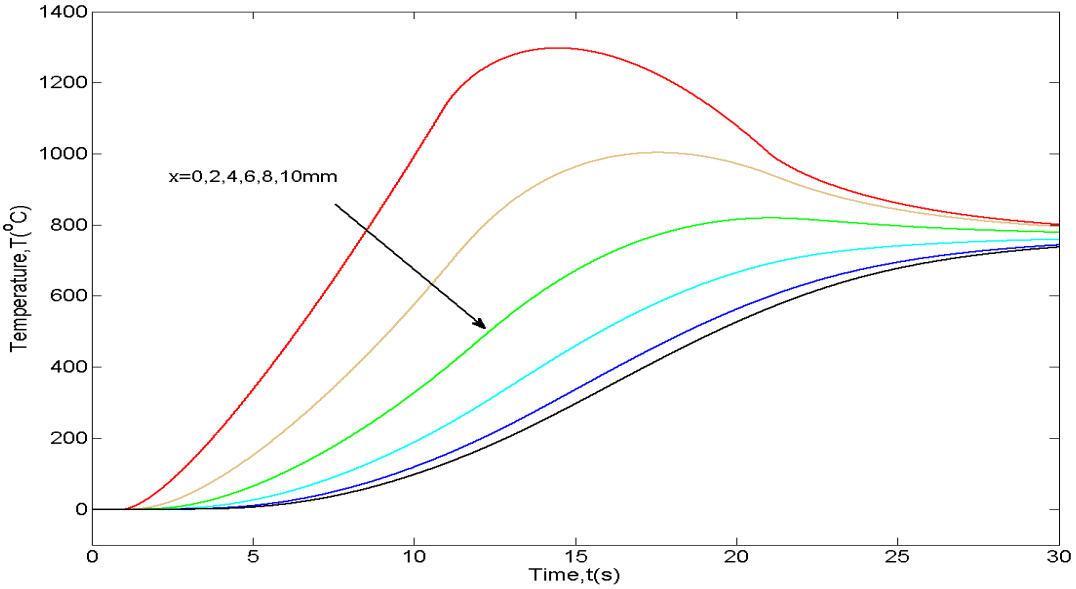

Figure 5.4.6: Temperature histories resulting from the reconstruction imposed heat flux $q"_r(0,t)$ at the indicated depths.

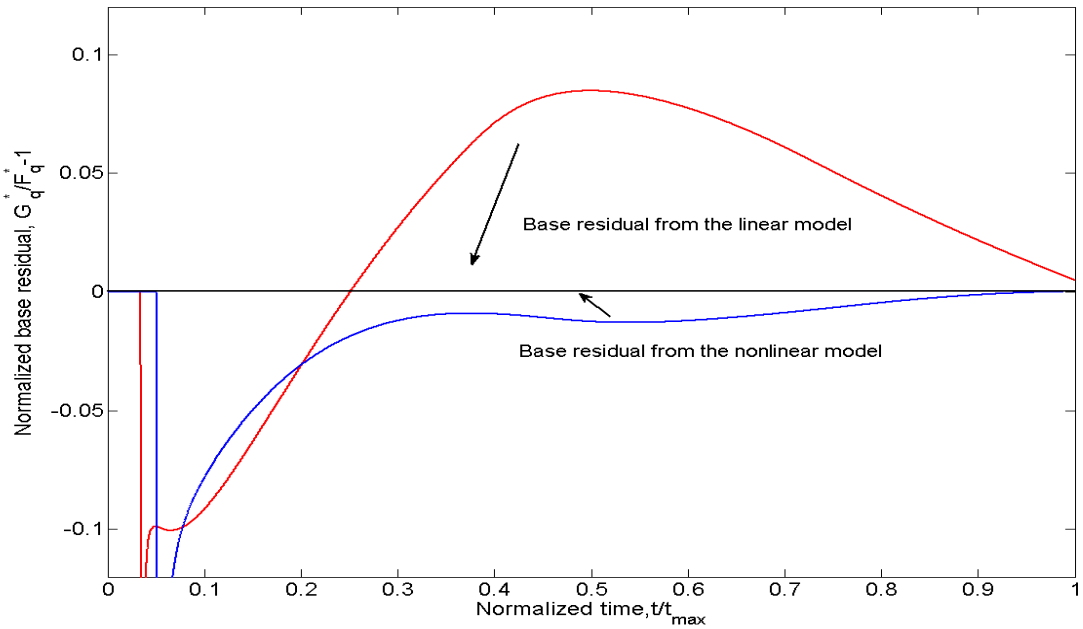

Figure 5.4.7: Normalized residual comparison between the linear model given by Eq. (5.2.7) and nonlinear model given by Eq. (5.2.11).

This base residual reflects the inherent bias in the proposed calibration model given by Eq. (5.2.11). Figure 5.3.7 presents a comparison of normalized base residuals between the linear model given by Eq. (5.2.7) and the nonlinear model given by Eq. (5.2.11). The linear model also used the temperature data collected by the nonlinear forward solution to emulate the corresponding physical process. For visualization, both rescaled time domain and physical time domain have been normalized by their maximum value in this figure. Results show that the nonlinear calibration model reduces the inherent model bias by properly accounting for the varying thermophysical properties. However, some bias remains due to the piecewise time-step linearization assumption.

In this chapter, the classical Tikhonov regularization given in Eq. (5.3.7), SVD based regularization given in Eq. (5.3.9) and local future-time method given in Eq. (5.3.2) are applied for regularization while their corresponding optimal regularization parameters are determined through observing the maximum value of P proposed in Eq. (5.3.10a) with $m = 100, 1000, 10000$. As an example, Figure 5.4.8 presents the optimal regularization parameter search process based on Tikhonov regularization with $m = 10000$ and $f_c = 1$Hz. It is clear that for a fixed m, the optimal regularization parameter corresponds to the peak of the function P. For all these cases, the cutoff frequency f_c is fixed at 1Hz while the weight coefficient m is adjusted (since the cutoff frequency f_c represents a standard for function smoothness). A high value of f_c accepts additional high frequencies in the filtering process and increases the variance involved in the final prediction. Therefore, the weight coefficient m and cutoff frequency f_c actually produce a similar effect in adjusting the weight between bias and variance. However, the weight coefficient m possesses more sensitivity than the cutoff

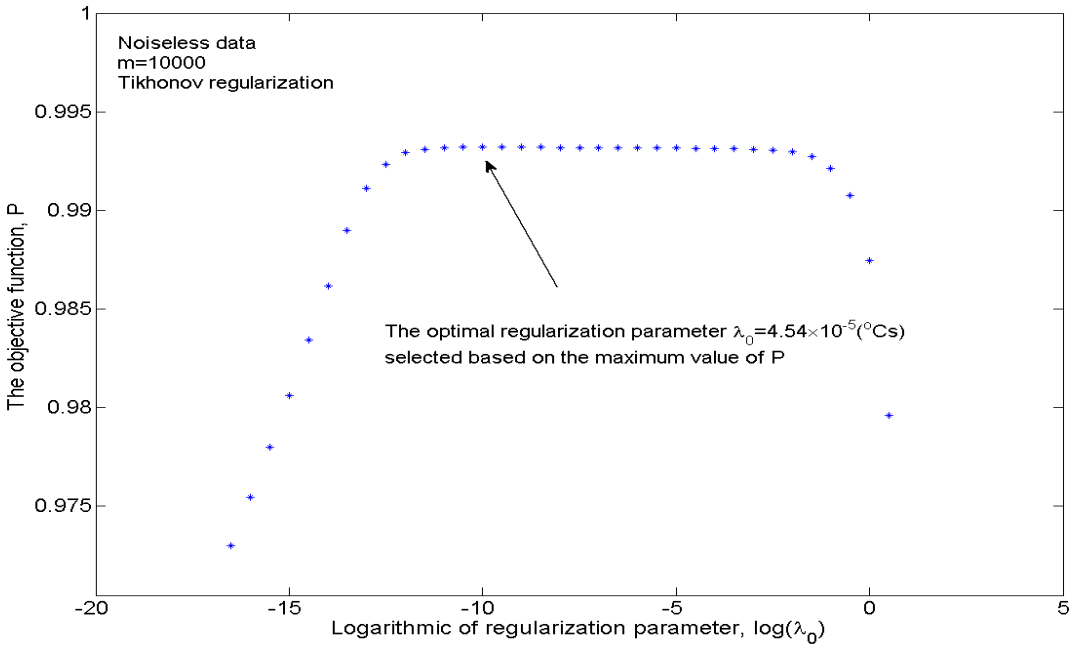

Figure 5.4.8: The selection of optimal regularization parameter based on the maximum value of function *P*.

frequency f_c, and hence is more useful. As an example, for all cases involved in this chapter, f_c =0.1-10Hz leads to almost the same optimal regularization parameter for fixed m. Conversely, for fixed f_c , the position of the maximum value of *P* strongly depends on *m*, especially when *m* is small (m =1-1000). A possible explanation for this observation lies in the fact that the weight coefficient *m* relates to relative weight between the bias and variance in a more direct way. As a result, the impact of m on the optimal regularization parameter becomes significant and must be carefully studied. In addition, bias is commonly a more important factor than variance when resolving inverse heat conduction problems. Therefore, the value of m must be set to a positive number greater than 1 to avoid the over-smoothness. To better understand variation of heat flux prediction with m , the optimal regularization parameters are determined based on $m = 100, 1000, 10000$. The front surface heat flux in the rescaled domain is resolved in accordance to Eq. (5.3.7), Eq. (5.3.9) and Eq. (5.3.2), corresponding to the classical Tikhonov regularization, SVD based regularization and local future-time method, respectively. As the last analysis step, all rescaled variables are transformed back to the physical ones in accordance to Eqs. (5.2.12a,b).

Figures 5.4.9-5.4.11, 5.4.12-5.4.14, and 5.4.15-5.4.17 present the final surface heat flux predictions in the physical time domain with $m = 100, 1000, 10000$ for all three regularization approaches. It is shown that all results are stable and possess comparable accuracy though some underestimation appears due to the linearization assumption. In addition, though different m values lead to different optimal regularization parameter, there are minor variations among the predictions. This verifies that there exists a significant flexibility in the choice of m. However, a proper domain of m is still required to avoid over-smoothness. For this purpose, the bias $P2$ is evaluated by substituting the rescaled prediction at the optimal regularization parameter into Eq.

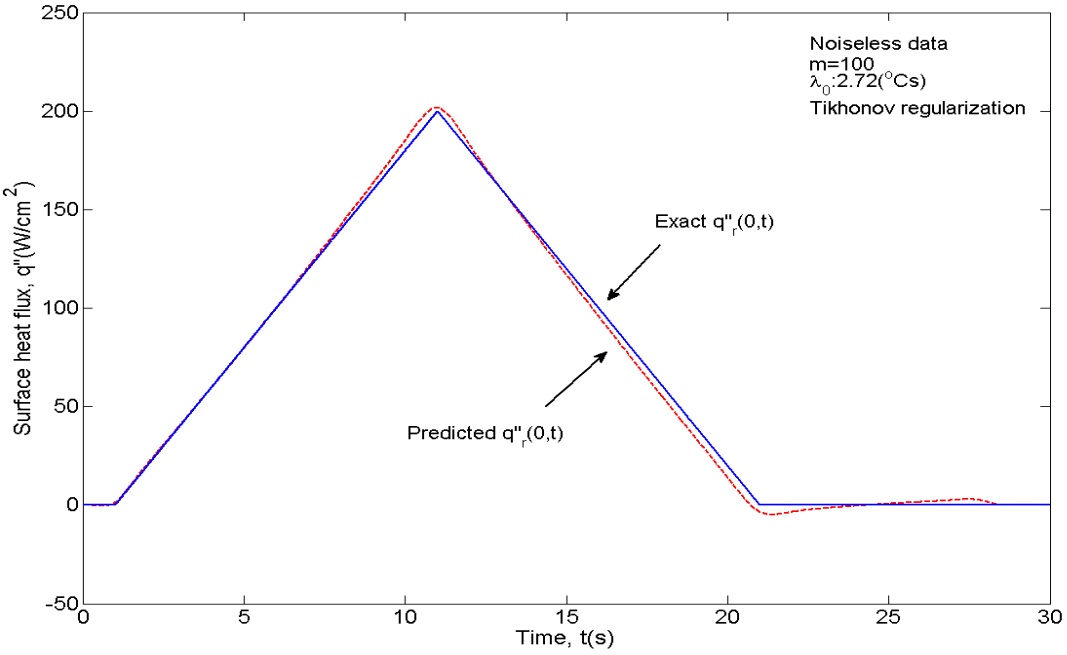

Figure 5.4.9: Predicted unknown surface heat flux $q_r"(0,t)$ with $m = 100$ by Tikhonov regularization.

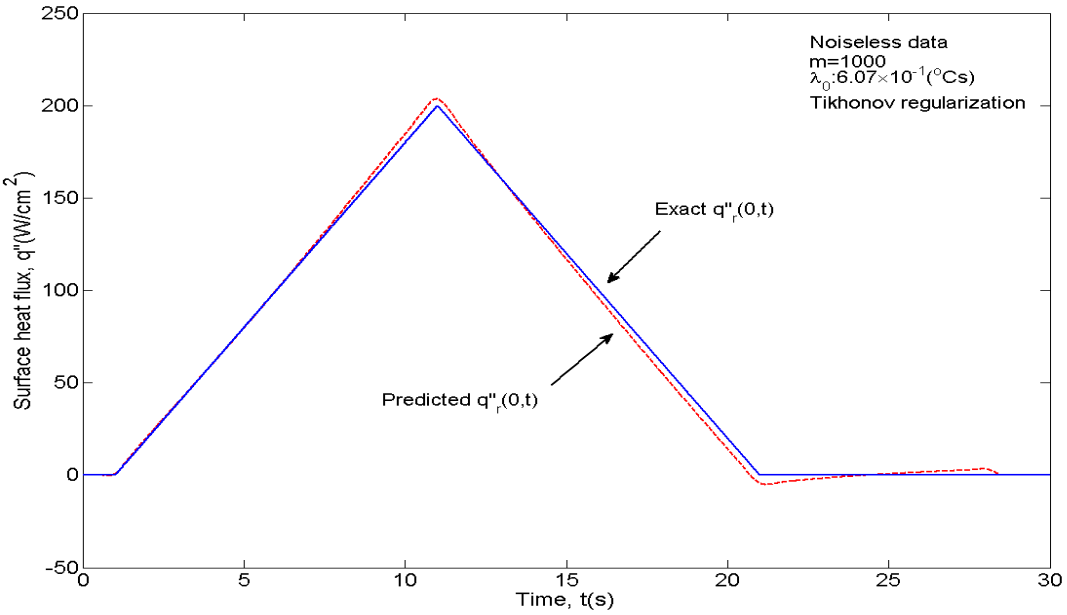

Figure 5.4.10: Predicted unknown surface heat flux $q_r"(0,t)$ with $m = 1000$ by Tikhonov regularization.

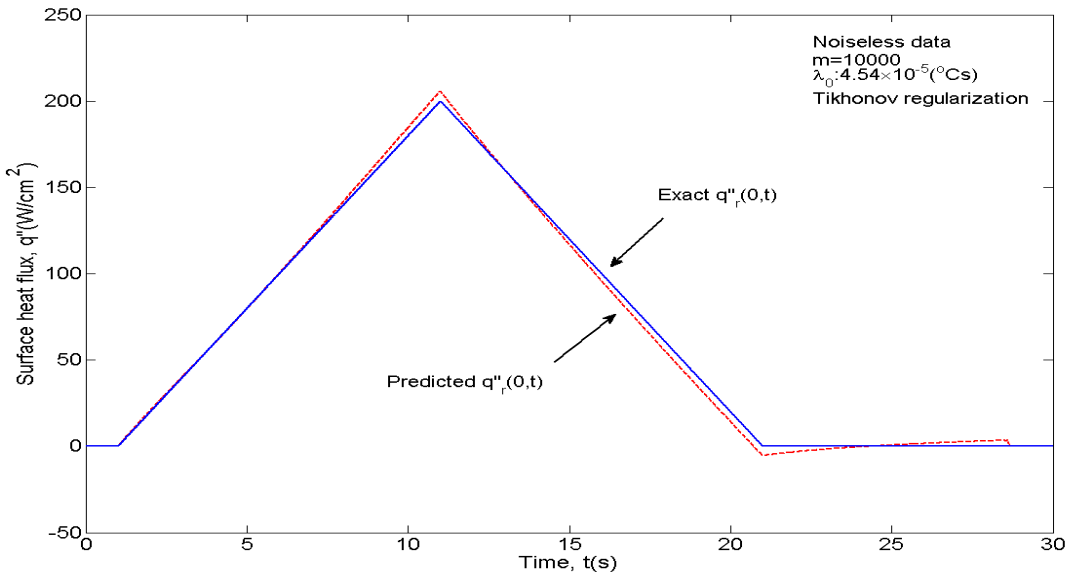

Figure 5.4.11: Predicted unknown surface heat flux $q_r"(0,t)$ with $m = 10000$ by Tikhonov regularization.

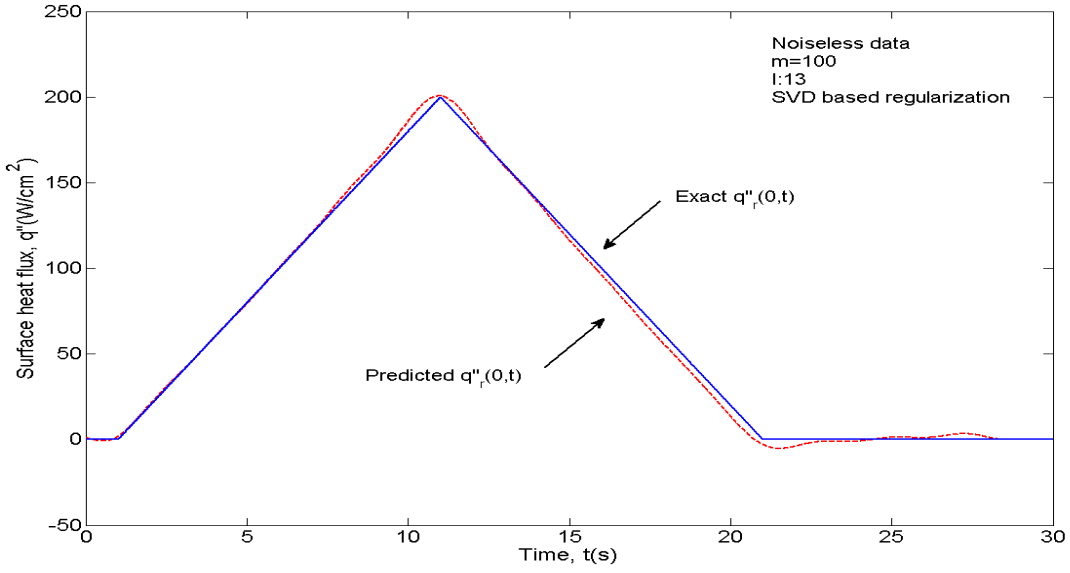

Figure 5.4.12: Predicted unknown surface heat flux $q_r"(0,t)$ with $m = 100$ by SVD based regularization.

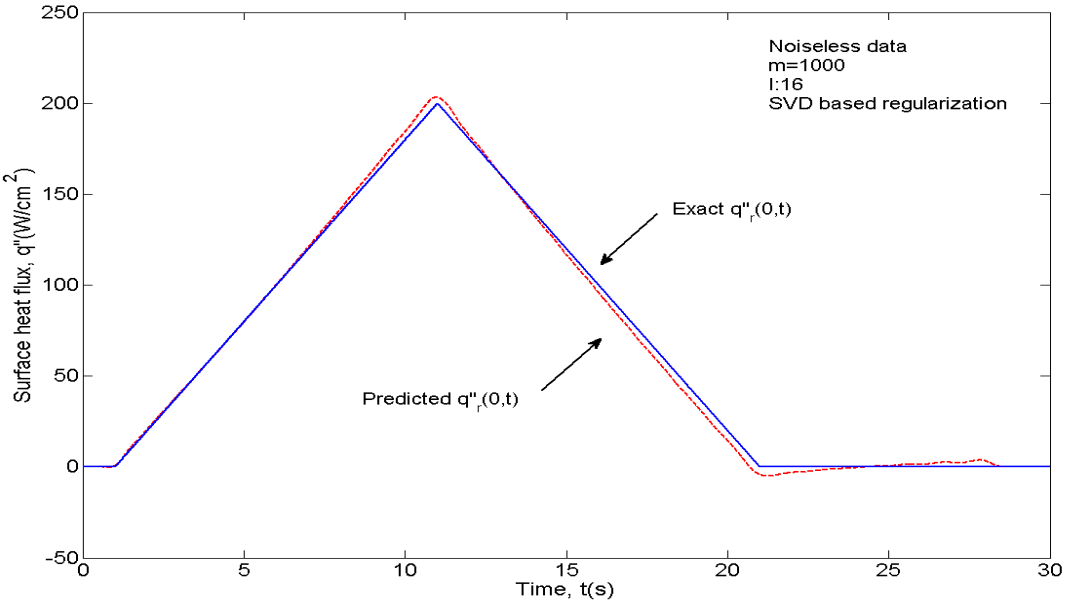

Figure 5.4.13: Predicted unknown surface heat flux $q_r"(0,t)$ with $m = 1000$ by SVD based regularization.

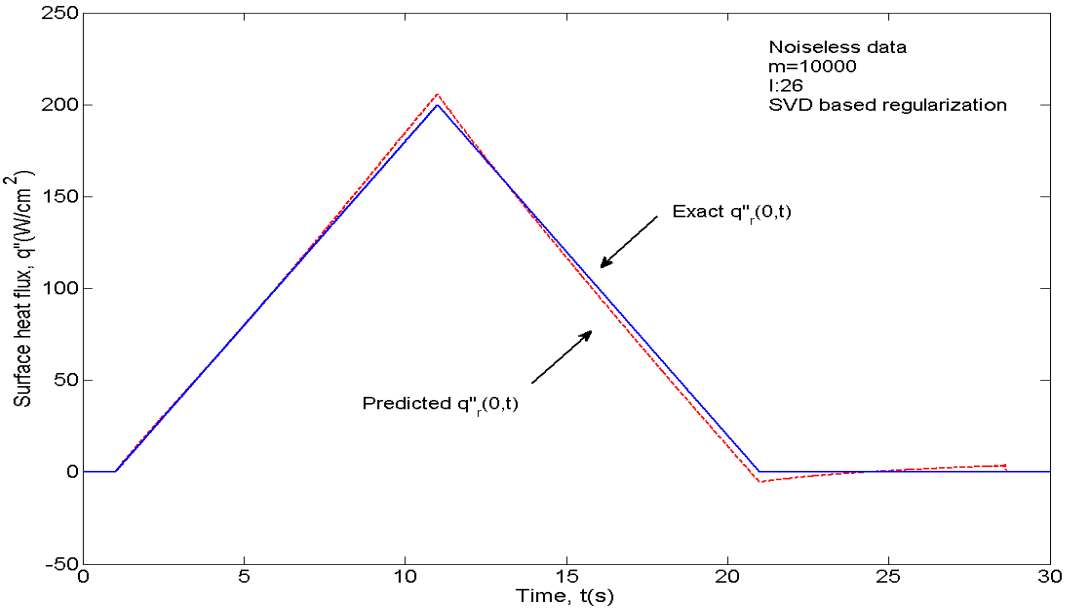

Figure 5.4.14: Predicted unknown surface heat flux $q_r"(0,t)$ with $m = 10000$ by SVD based regularization.

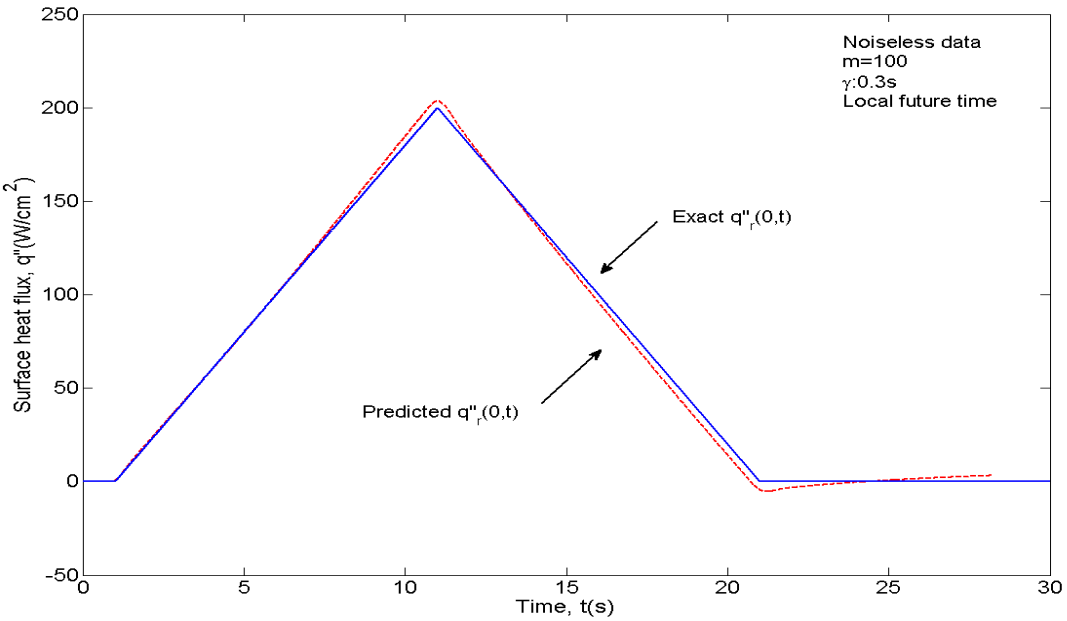

Figure 5.4.15: Predicted unknown surface heat flux $q_r"(0,t)$ with $m = 100$ by local future time.

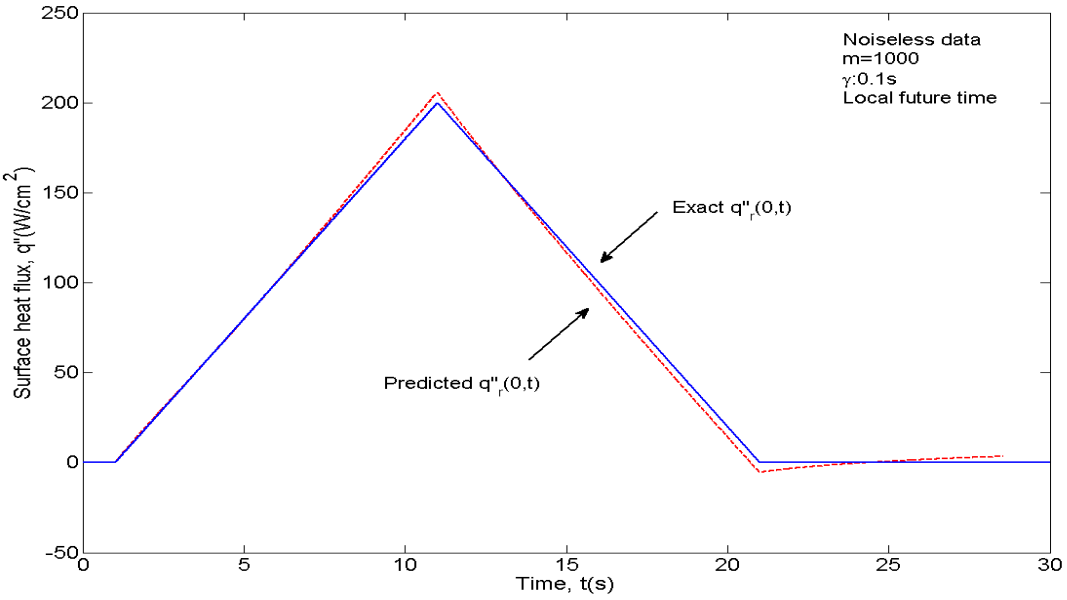

Figure 5.4.16: Predicted unknown surface heat flux $q_r"(0,t)$ with $m = 1000$ by local future time.

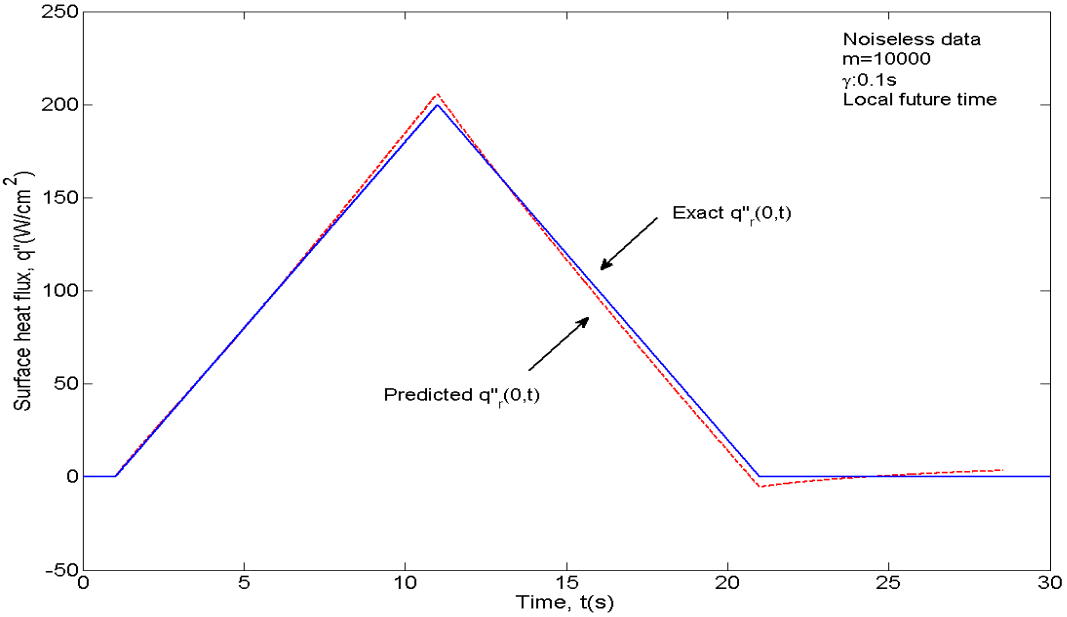

Figure 5.4.17: Predicted unknown surface heat flux $q_r"(0,t)$ with $m = 10000$ by local future time.

(5.3.10c) for fixed m. To reiterate, at a fixed m, all optimal regularization parameters are obtained by searching for the maximum value of the function P. Figures 5.4.18-5.4.20 display the development of the bias $P2$ as m varies, corresponding to the three regularization approaches applied in this chapter. The dash line is presented for mere visualization to indicate the L-shaped feature. The curves begin to converge near $m = 2000$ for all three approaches implying that for noiseless data an optimal prediction can be obtained if m is between $[2000,10000]$. The value of m for convergence can be defined on a range since the final prediction is insensitive to small changes in m. However, a larger or conservative value of m ensures that over-smoothness can be avoided. As a result (see Fig.5.4.20), the weight coefficient m can be considered as 2000 though convergence actually appears earlier. In this chapter, the estimated convergence point of this "L-shaped curve" is referred to as the elbow.

Figures 5.4.11, 5.4.14 and 5.4.17 can be considered as optimal predictions corresponding to Tikhonov regularization, SVD based regularization and local future-time method, respectively. The prediction accuracy is analyzed through unbiased standard deviation of the error σ, energy conservation ratio E_r and maximum value ratio M_r as defined by

$$\sigma\left(q"_{r,\mathrm{pred}}(0,t_i)\big|_{i=0}^{N}\right)=\left(\frac{1}{N}\sum_{i=0}^{N}\left(q"_{r,\mathrm{pred}}(0,t_i)-q"_{r,\mathrm{exact}}(0,t_i)\right)^2\right)^{1/2},$$

$$E_r\left(q"_{r,\mathrm{pred}}(0,t)\right)=\frac{\int_0^t q"_{r,\mathrm{pred}}(0,u)\,du}{\int_0^t q"_{r,\mathrm{exact}}(0,u)\,du}, \qquad (5.4.2a-b)$$

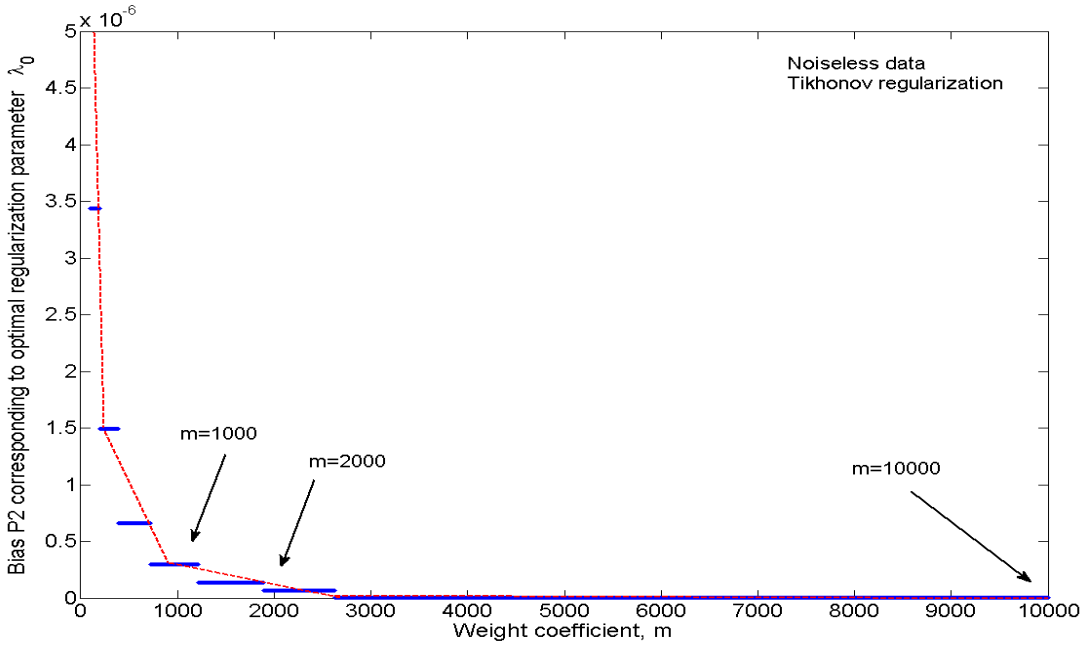

Figure 5.4.18: Bias $P2$ at optimal regularization parameter versus m (Tikhonov regularization).

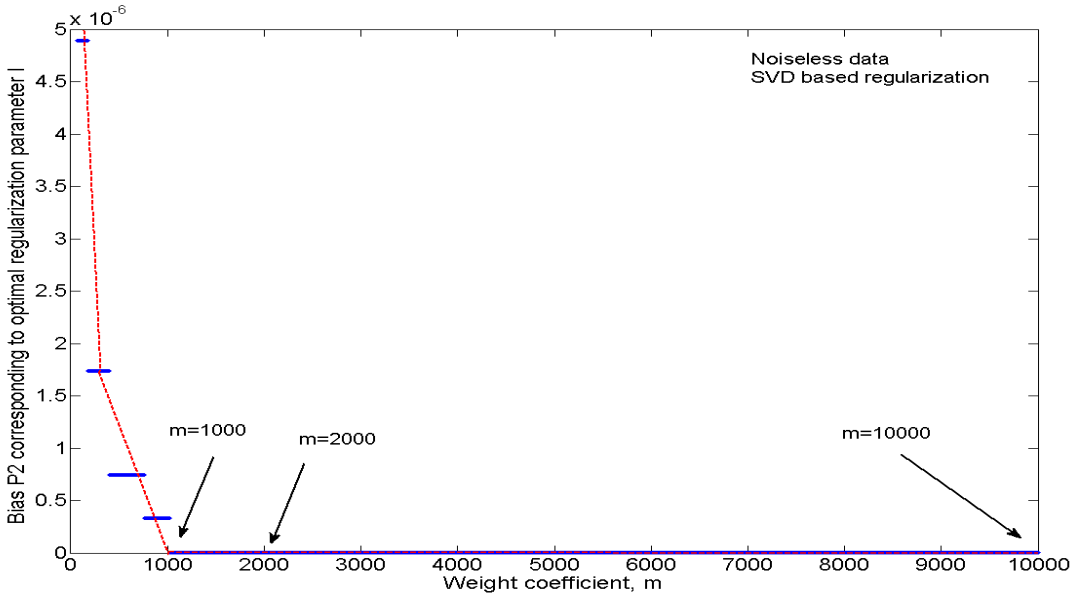

Figure 5.4.19: Bias $P2$ at optimal regularization parameter versus m (SVD based regularization).

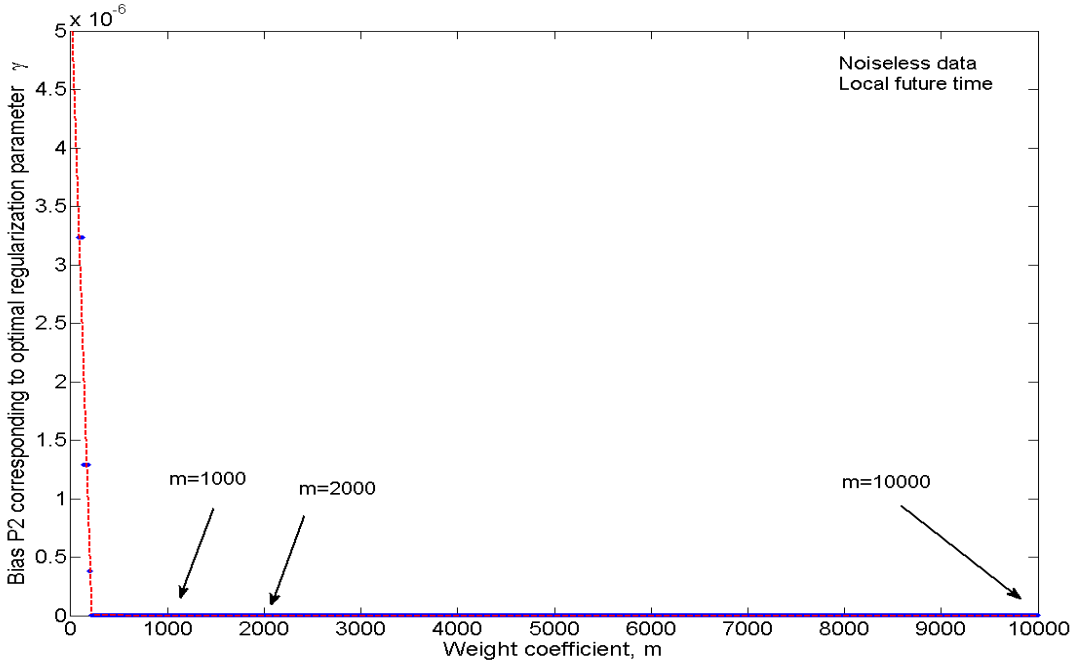

Figure 5.4.20: Bias $P2$ at optimal regularization parameter versus m (local future time).

$$M_r\left(q"_{r,\text{pred}}(0,t_i)\big|_{i=0}^{N}\right)=\frac{\max\left(q"_{r,\text{pred}}(0,t_i)\right)}{\max\left(q"_{r,\text{exact}}(0,t_i)\right)}, \qquad (5.4.2c)$$

respectively. Pertinent and statistical information, corresponding to $m = 100, 1000, 10000$, are included in Table 5.4.1 for reference.

Experimental data contains contamination (i.e, noise). To study the impact of this inclusion on the proposed method for acquiring the optimal regularization parameter, we add noise in accordance to [117]

$$T(b,t_i)|_{noise} = T(b,t_i) + \beta\varepsilon_i, \qquad i = 0,1,2,\cdots,N+1, \qquad (5.4.3)$$

where $T(b,t_i)$ represents the "noiseless temperature" at time $t_i = i\Delta t$ at position $x = b$. Here, ε_i is the discrete raw experimental noise ε at $t_i = i\Delta t$, which was generated from an inverse heat conduction experiment described in Ref. 117; β is a constant noise factor, whose value is set as 50 to ensure that the added noise has a standard deviation near 1^{o}C. The parameter N is set to $N = 6000$ since the experimental noise sampling rate was 200Hz and the maximum time for data collection is 30s. Figure 5.4.21 presents the added noise $\beta\varepsilon_i$ on $T(b,t_i)$ during both calibration and reconstruction tests. The noisy data are then rescaled and substituted into the proposed nonlinear calibration equation for resolving the unknown front surface heat flux according to Eq. (5.3.2), Eq. (5.3.7) and Eq. (5.3.9), respectively. The identical numerical procedure previously described in the context of noiseless data is repeated.

Table 5.4.1: Prediction accuracy analysis for noiseless data.

Tikhonov Regularization	$\boldsymbol{\lambda_0}$**(°Cs)**	**Standard Deviation of Prediction Error** $\boldsymbol{\sigma}$ **(W/cm^2)**	**Peak Ratio** $\boldsymbol{E_r}$	**Energy balance** $\boldsymbol{M_r}$
$\boldsymbol{m = 100}$	2.718	2.997	1.007	9.951×10^{-1}
$\boldsymbol{m = 1000}$	6.065×10^{-1}	3.008	1.018	9.954×10^{-1}
$\boldsymbol{m = 10000}$	4.540×10^{-5}	3.033	1.023	9.959×10^{-1}
SVD based Regularization	$\boldsymbol{I}$	**Standard Deviation of Prediction Error** $\boldsymbol{\sigma}$ **(W/cm^2)**	**Peak Ratio** $\boldsymbol{E_r}$	**Energy balance** $\boldsymbol{M_r}$
$\boldsymbol{m = 100}$	13	3.051	1.003	9.950×10^{-1}
$\boldsymbol{m = 1000}$	16	3.044	1.016	9.954×10^{-1}
$\boldsymbol{m = 10000}$	26	3.033	1.028	9.959×10^{-1}
Local Future Time	$\boldsymbol{\gamma}$**(s)**	**Standard Deviation of Prediction Error** $\boldsymbol{\sigma}$ **(W/cm^2)**	**Peak Ratio** $\boldsymbol{E_r}$	**Energy balance** $\boldsymbol{M_r}$
$\boldsymbol{m = 100}$	0.3	3.051	1.003	9.950×10^{-1}
$\boldsymbol{m = 1000}$	0.1	3.044	1.016	9.954×10^{-1}
$\boldsymbol{m = 10000}$	0.1	3.033	1.028	9.959×10^{-1}

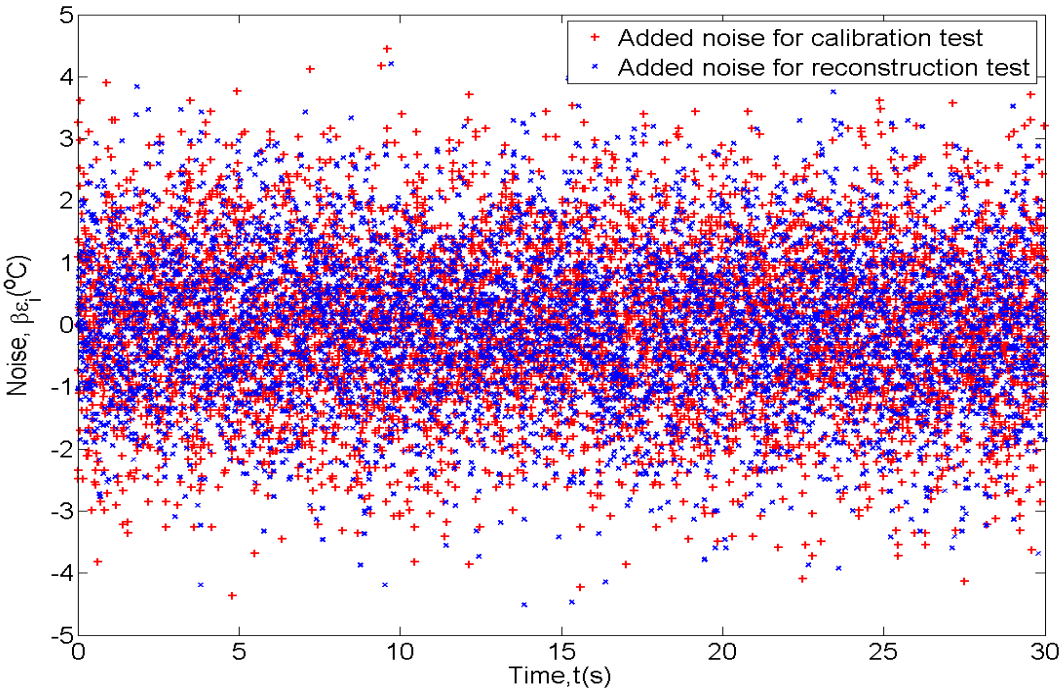

Figure 5.4.21: Added experimentally obtained noise per Eq. (5.4.3) using Ref.117 data.

After transforming all rescaled variables back to the physical ones according to Eqs.(5.2.12a,b), the surface heat flux predictions with $m = 100, 1000, 10000$ based on classical Tikhonov regularization, SVD based regularization and local future-time method are presented in Figs. 5.4.22-5.4.24, 5.4.25-5.4.27, 5.4.28-5.4.30, respectively. Results show that the predictions remain accurate even in presence of significant experimental noise and the differences among these predictions are not pronounced. All these results are deemed acceptable which verifies that the choice of m is not restrictive. To obtain a proper domain from where m can be chosen, we plot the bias $P2$ versus m, corresponding to the three regularization approaches. The logic is exactly the same as discussed when using the noiseless data. These results are presented in Figs. 5.4.31-5.4.33. Again, the L-shaped feature with a pronounced elbow near $m = 2000$ is observed. Given that the reduction in bias after $m = 2000$ is minimal, we can consider $m \in [2000,10000]$ as a proper domain for m. Another important observation is that the elbows of the L-shaped curves in Figs. 5.4.18-5.4.20 (noiseless data) and Figs. 5.4.31-5.4.33 (noisy data) all lie near $m = 2000$ independent of noise level and applied regularization methodology. This justifies the generality of the proposed regularization parameter strategy given in Eq. (5.3.10). It also indicates that in this example, the optimal weight ratio between bias and variance is approximated $2000:1$ for the selected cutoff frequency $f_c = 1\text{Hz}$. Table 5.4.2 summarizes pertinent prediction accuracy analysis for the noisy data study. In addition, though not explicitly contained in this chapter, stainless steel and copper were studied under similar heating scenarios. Combination of the nonlinear calibration model given in Eq. (5.2.11) and the proposed optimal regularization parameter strategy works equally well for these alternative materials. Finally, one can demonstrate the need for the fully nonlinear model by direct comparison with the linear model given by Eq. (5.2.7). Figure 5.4.34 uses the nonlinear temperature data sets described in

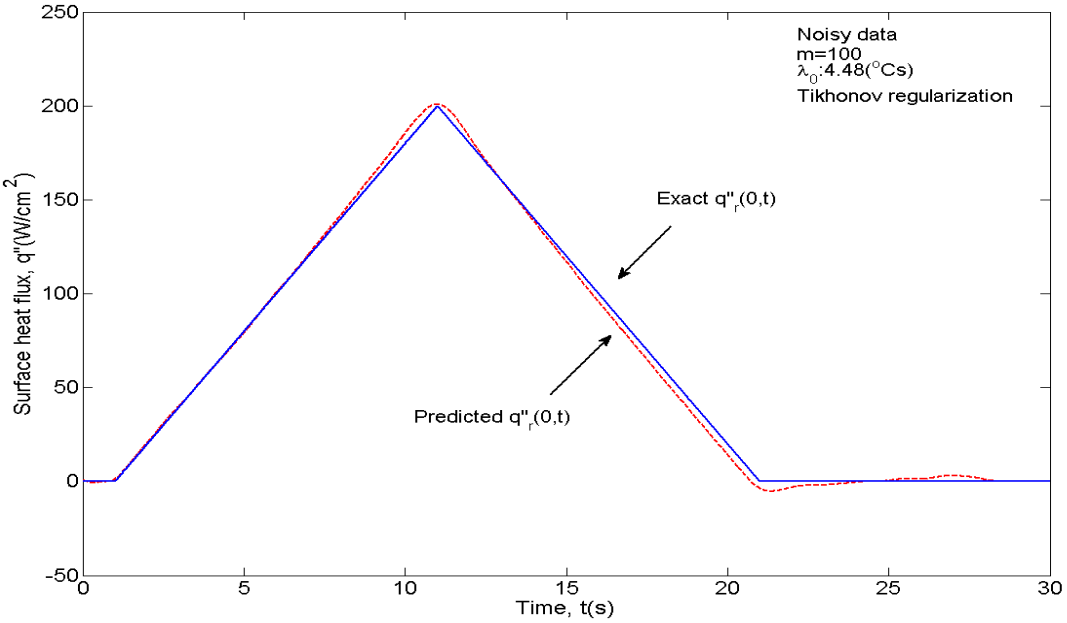

Figure 5.4.22: Predicted unknown surface heat flux $q_r"(0,t)$ with $m = 100$ by Tikhonov regularization (Noisy data).

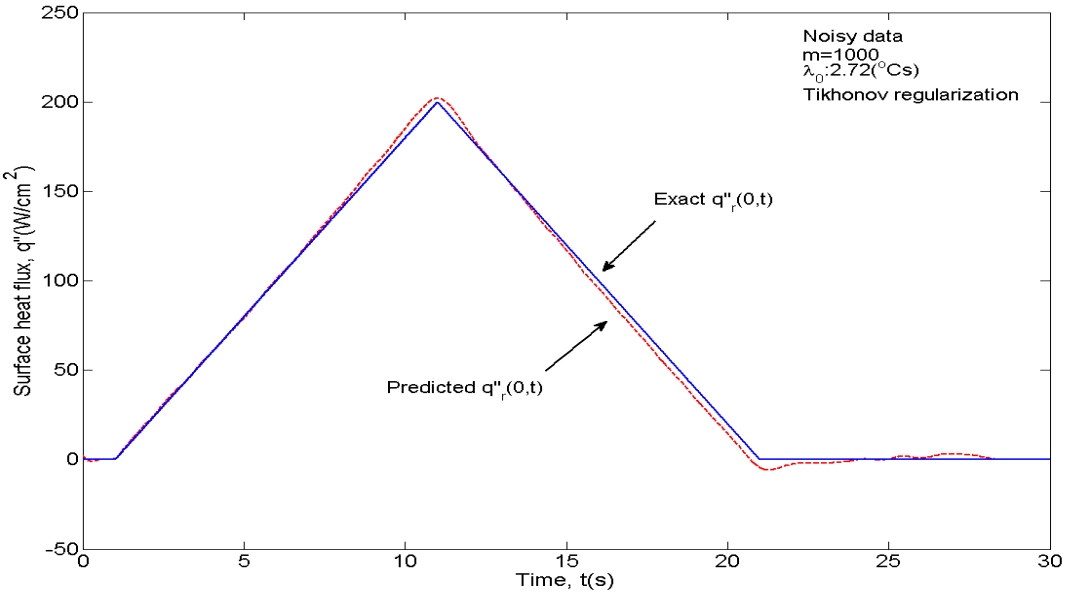

Figure 5.4.23: Predicted unknown surface heat flux $q_r"(0,t)$ with $m = 1000$ by Tikhonov regularization (Noisy data).

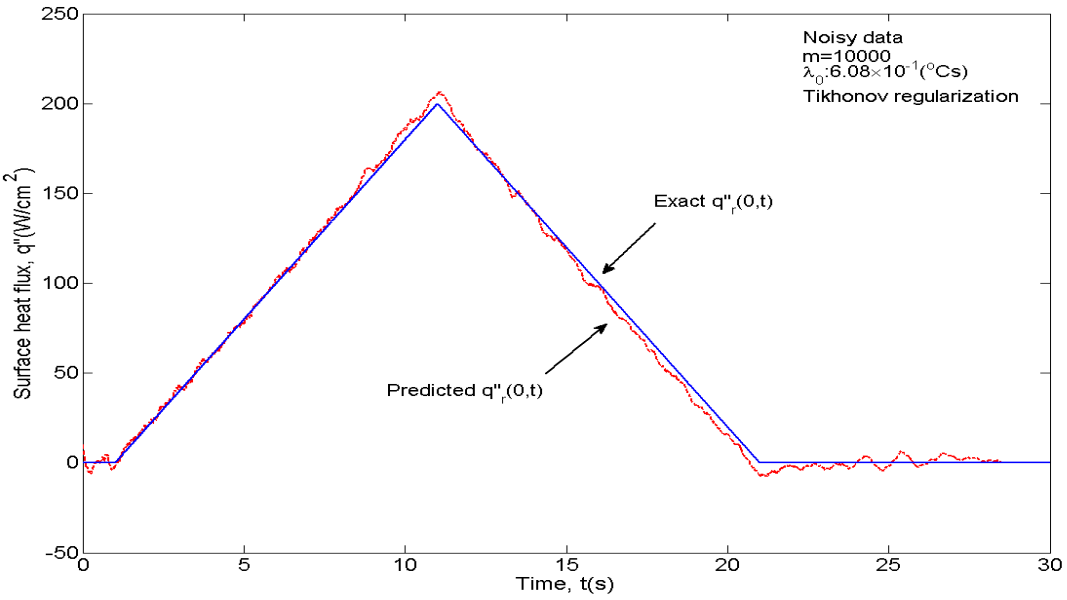

Figure 5.4.24: Predicted unknown surface heat flux $q_r"(0,t)$ with $m = 10000$ by Tikhonov regularization (Noisy data).

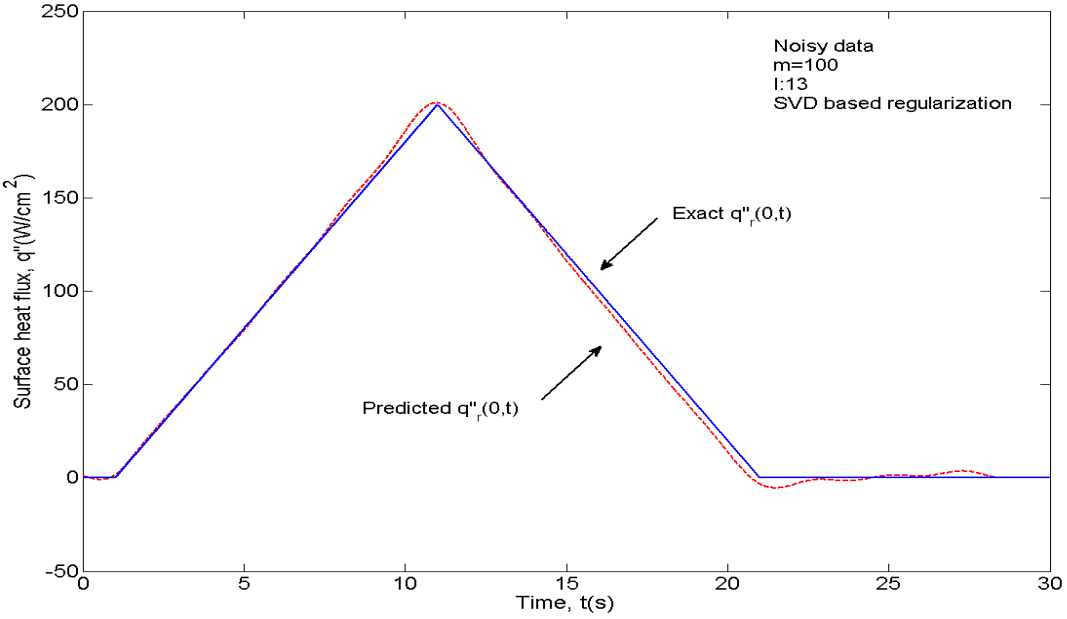

Figure 5.4.25: Predicted unknown surface heat flux $q_r"(0,t)$ with $m = 100$ by SVD based regularization (Noisy data).

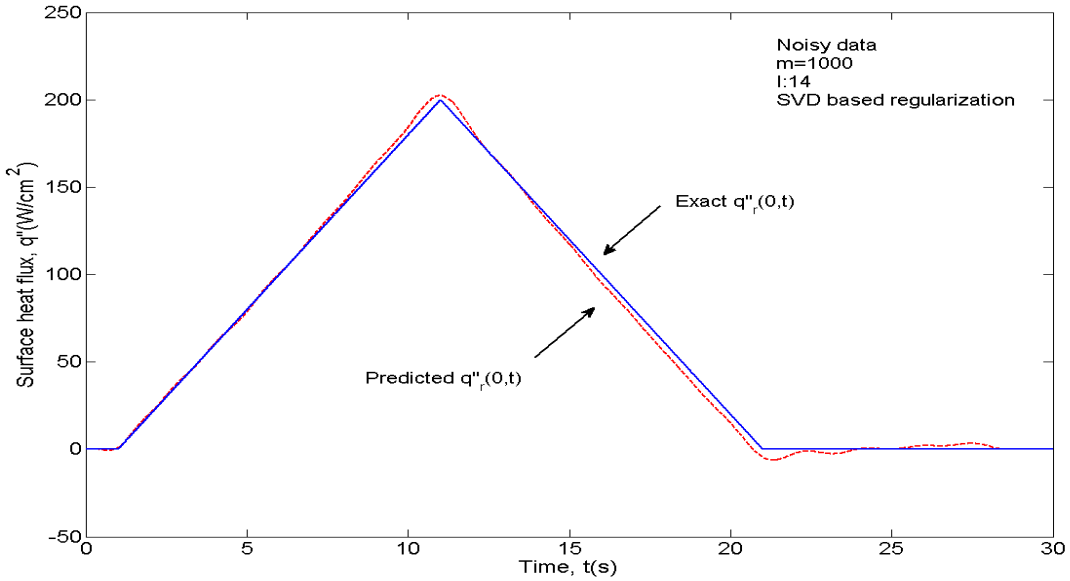

Figure 5.4.26: Predicted unknown surface heat flux $q_r"(0,t)$ with $m = 1000$ by SVD based regularization (Noisy data).

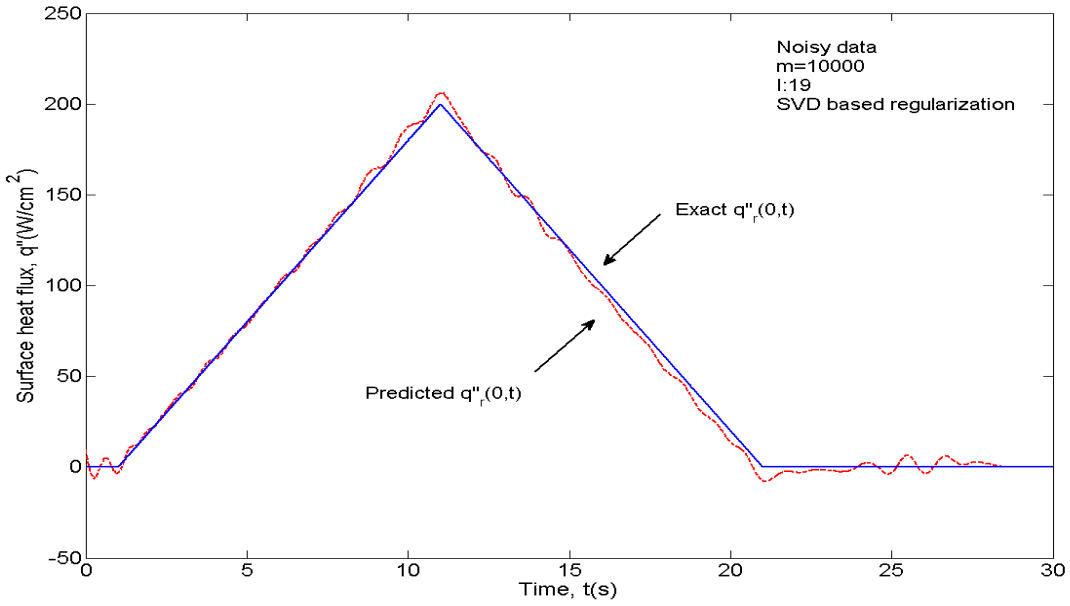

Figure 5.4.27: Predicted unknown surface heat flux $q_r"(0,t)$ with $m = 10000$ by SVD based regularization (Noisy data).

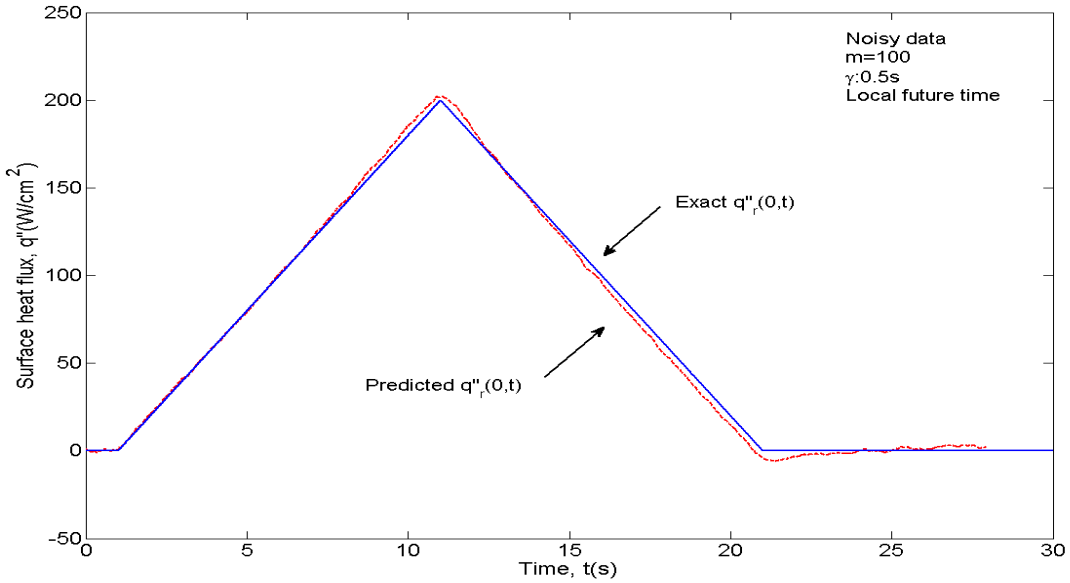

Figure 5.4.28: Predicted unknown surface heat flux $q_r"(0,t)$ with $m = 100$ by local future time (Noisy data).

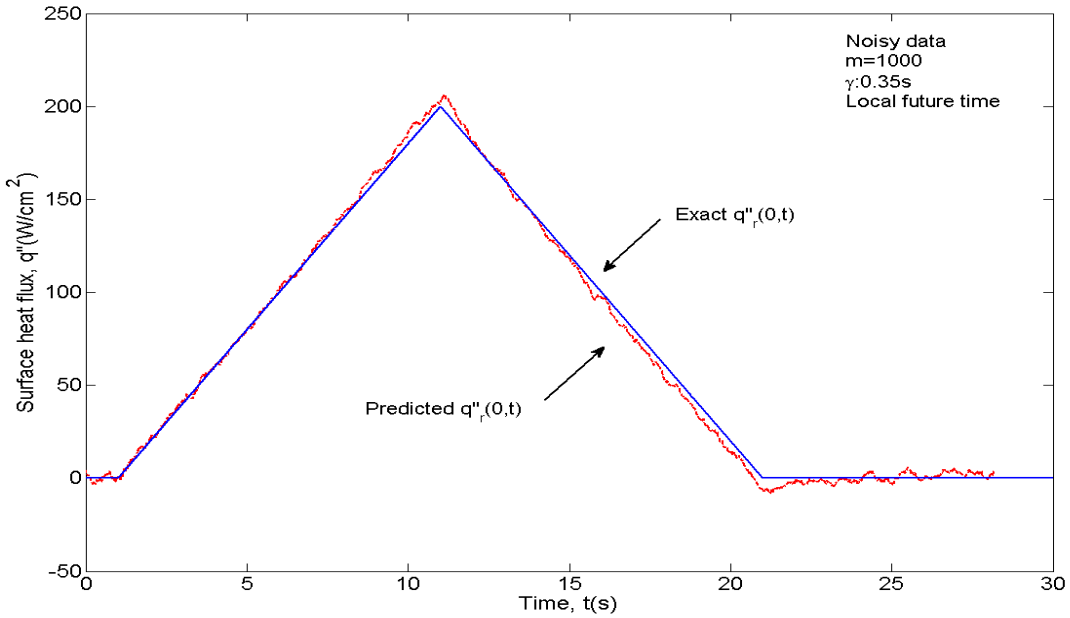

Figure 5.4.29: Predicted unknown surface heat flux $q_r"(0,t)$ with $m = 1000$ by local future time (Noisy data).

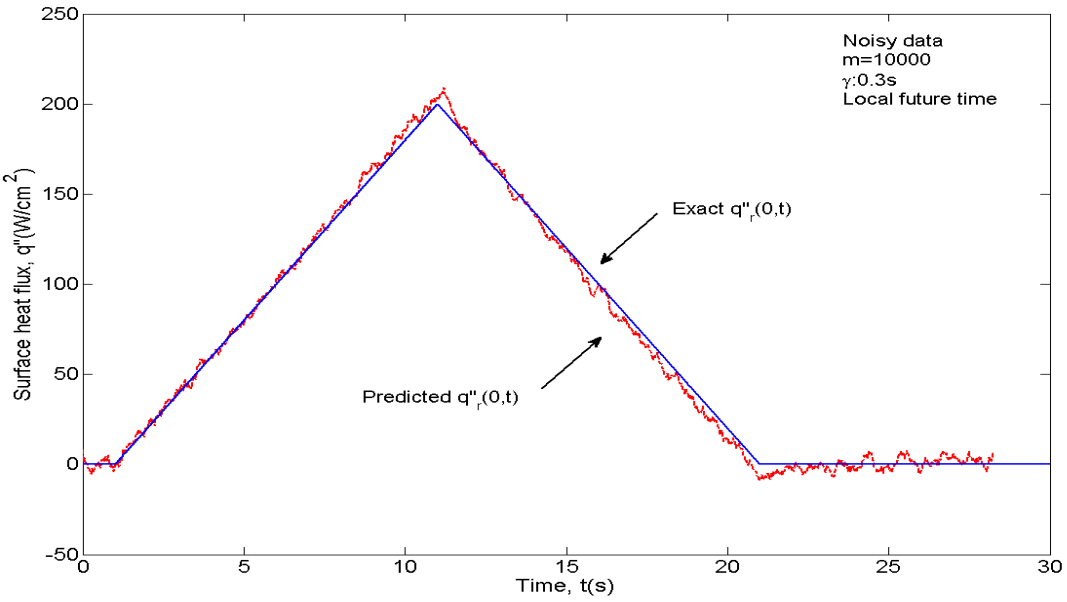

Figure 5.4.30: Predicted unknown surface heat flux $q_r"(0,t)$ with $m = 10000$ by local future time (Noisy data).

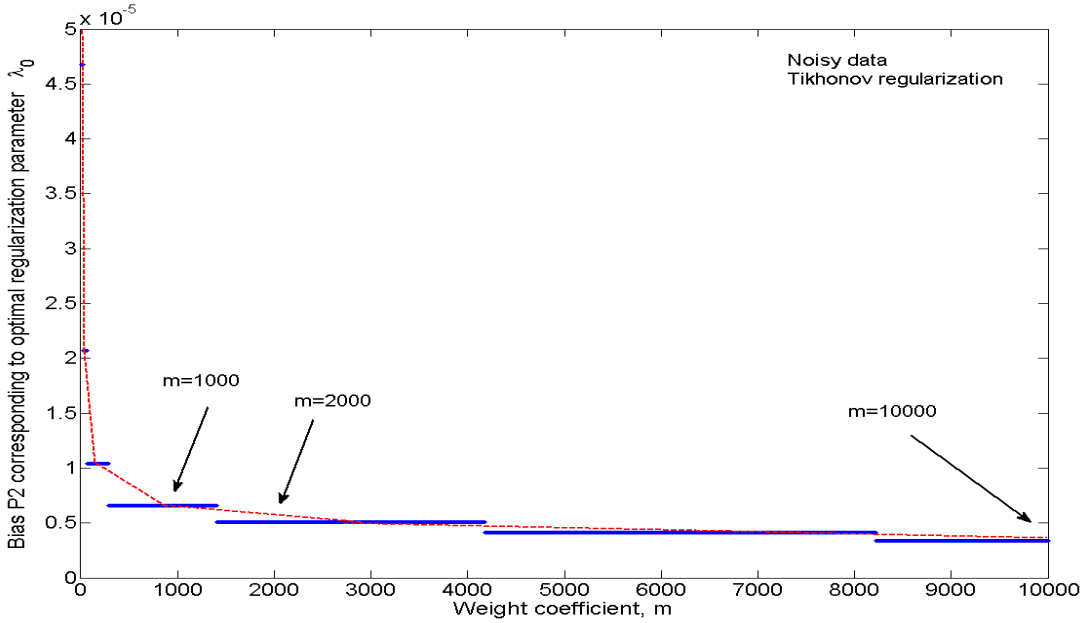

Figure 5.4.31: Bias $P2$ at optimal regularization parameter versus m (Tikhonov regularization, Noisy data).

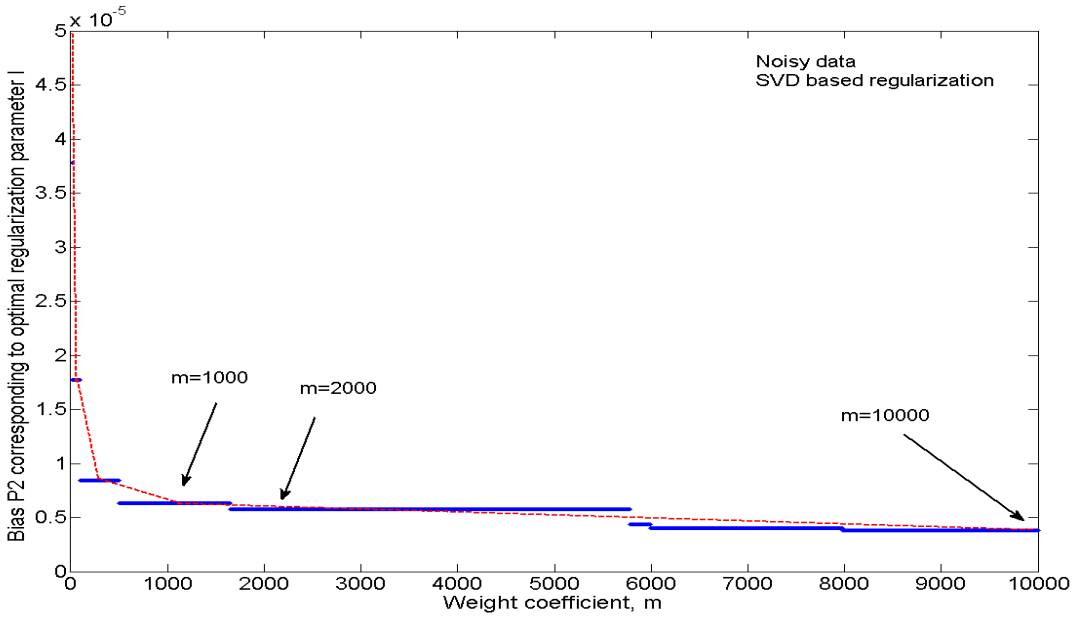

Figure 5.4.32: Bias $P2$ at optimal regularization parameter versus m (SVD based regularization, Noisy data).

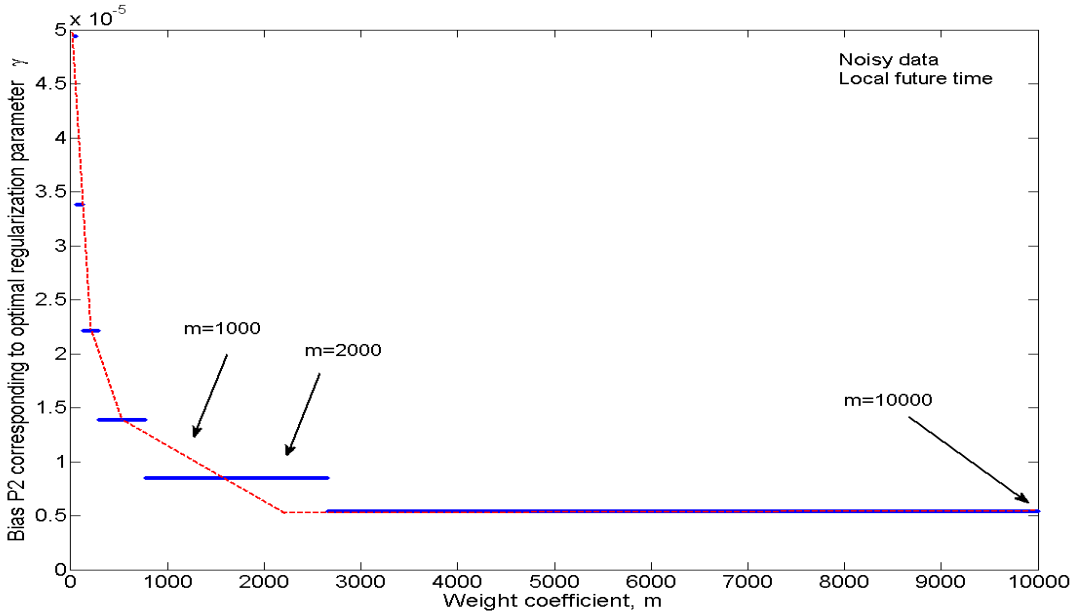

Figure 5.4.33: Bias $P2$ at optimal regularization parameter versus m (local future time, Noisy data).

Table 5.4.2: Prediction accuracy analysis for noisy data.

Tikhonov Regularization	λ_0(°Cs)	**Standard Deviation of Prediction Error σ (W/cm^2)**	**Peak Ratio E_r**	**Energy balance M_r**
$m = 100$	4.482	2.972	1.004	9.950×10^{-1}
$m = 1000$	2.718	2.991	1.010	9.951×10^{-1}
$m = 10000$	6.065×10^{-1}	3.453	1.033	9.953×10^{-1}
SVD based Regularization	I	**Standard Deviation of Prediction Error σ (W/cm^2)**	**Peak Ratio E_r**	**Energy balance M_r**
$m = 100$	13	3.041	1.005	9.953×10^{-1}
$m = 1000$	14	3.030	1.012	9.953×10^{-1}
$m = 10000$	19	3.538	1.032	9.952×10^{-1}
Local Future Time	γ(s)	**Standard Deviation of Prediction Error σ (W/cm^2)**	**Peak Ratio E_r**	**Energy balance M_r**
$m = 100$	0.5	3.018	1.011	9.950×10^{-1}
$m = 1000$	0.35	3.328	1.033	9.951×10^{-1}
$m = 10000$	0.3	3.766	1.045	9.952×10^{-1}

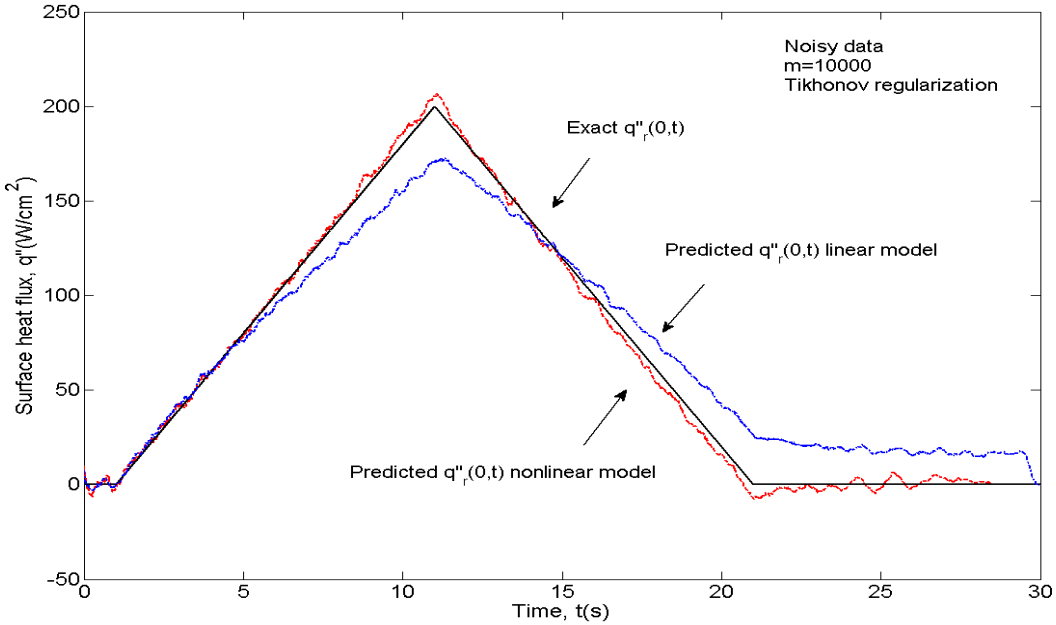

Figure 5.4.34: A comparison between linear and nonlinear models using noisy data based on Tikhonov regularization.

Fig. 5.4.5 contaminated with the experiment noise described in Ref. 115 and the calibration heat flux $q''_c(0,t)$ displayed in Fig. 5.4.4 to generate the reconstruction heat flux $q''_r(0,t)$ based on both linear (Eq. 5.2.7) and nonlinear (Eq. 5.2.11) models. As seen in this figure, the two models produce noticeably different predictions. It is evident that this test requires the proper accounting of the temperature dependent thermophysical properties.

5.5 Conclusions

This chapter proposes a nonlinear calibration formulation that incorporates rescaling principles for resolving the front surface heat flux in a one-dimensional nonlinear inverse heat conduction problem. Additionally, a new strategy is proposed for obtaining the optimal regularization parameter independent of the regularization technique. The nonlinear inverse heat conduction problem can be quasi-linearized by rescaling based on the piecewise time-step linearization assumption. For regularization, three different techniques were considered; namely, local future-time method, Tikhonov and SVD based regularization. The new strategy estimates the variance with the aid of a Gauss filter and determines the optimal regularization parameter based on a balance between the weighted bias and estimated variance. A weight coefficient is required since bias and variance are not equally important in reconstruction of the surface heat flux based on calibration approach. The proper weight coefficient domain is estimated by plotting the prediction bias $P2$ versus m. Here, the prediction bias $P2$ is obtained from the rescaled heat flux prediction at the optimal regularization parameter associated with the chosen regularization approach. The optimal regularization parameter is obtained corresponding to the

maximum value of P with respect to m. In this chapter, the proper weight coefficient domain is estimated in the range $m \in [2000,10000]$ based on a cutoff frequency $f_c = 1$Hz.

For physical reasons, the rescaled variables must be returned to the physical spaces for final prediction presentation. All obtained results in this chapter for the representative carbon composite are both stable and accurate in the presence of significant noise. This approach is also suitable for several other engineering materials such as the stainless steel and copper. One pronounced advantage of this proposed calibration method is that the precise sensor position does not need specification as it is implicitly included in the calibration test. The reliability of the new calibration method depends on accuracy of the piecewise time-step linearization assumption. Hence, if a high heat flux is applied over a short time span, then a substantive model bias results due to the failure of quasi-linearization. However, in an appropriate heat flux range, this new calibration method is suitable and is actually superior to the linear calibration model.

Chapter 6: A New Thermophysical Property Estimation Approach based on Calibration Equations and Rescaling Principle

This chapter is revised based on a paper to be submitted for publication by Yinyuan Chen, Majid Keyhani and Jay I. Frankel:

Chen, Y.Y., Keyhani, M., and Frankel, J.I., in preparation, "A New Thermophysical Property Estimation Approach based on Calibration Equations and Rescaling Principle".

My primary contributions to this paper include (1) conceptualization of the new model, (2) development of numerical and regularization methods (3) writing and implementing of the computer code (4) and served as lead writer of the manuscript.

6.1 Introduction

The need to accurately measure thermal conductivity and thermal diffusivity at high temperatures is significant to many engineering applications. Rapid advancement of new materials for high temperature applications necessitates this quantification and characterization for advanced engineering systems. For example, in thermal protection systems, low thermal diffusivity materials are required for protecting high-speed flight vehicles during glide and re-entry.

Presently, several methods exist for evaluating these important thermophysical properties [21,91-109,119]. The Flash method [98] is a classical and often called upon method for

estimating thermal diffusivity. This method is predicated on knowing the exact temperature solution of the linear heat equation for a thermally insulated solid exposed to a pulse of radiant energy impacting the front surface. Parker et al. [98] proposed this means of estimating thermal diffusivity based on a single graphical representation involving a dimensionless backside temperature versus dimensionless time plot. This method is appealing as the knowledge of the amount of energy absorbed at the front surface is not required for estimating the thermal diffusivity. However, the energy input must be specified when estimating the thermal conductivity. The Flash method is popular and has received significant attention over the past 50 years. Clark [99] investigated radiation heat losses associated with Flash method in a high temperature range and provided an experimental basis for evaluating radiative heat losses and forming a correction procedure. James [100] applied the Flash method to one-dimensional heat conduction through slabs of two materials in direct thermal contact. Baba and Ono [101] improved the Flash method by reducing uncertainties in thermal diffusivity measurements of solid materials above room temperature. The thermal property estimation is also achieved with the aid of the Laplace transform technique [119]. Based on a semi-infinite assumption in the transform variable, this transformation can be applied to solve the one-dimensional heat conduction problem when both the heat flux and temperature of the front surface are known. In this process, the thermal diffusivity can directly be expressed in terms of the temperature in the frequency domain while the thermal conductivity can be estimated with the aid of the estimated thermal diffusivity and known surface heat flux. Unlike the Flash method, this approach permits an arbitrary heating condition.

The least-square method is the most common approach for parameter estimation [105-109]. A significant amount of attention has been directed toward this technique as it is suitable to any experimental situation that can utilize either analytical or numerical solutions. After the initial guess is provided, optimization methods are introduced for updating the parameter space that minimizes the temperature difference between the experimental results and the model solution. The thermal diffusivity and thermal conductivity can simultaneously be determined by successive iteration. Sawaf and Ozisik [21] estimated the linearly temperature-dependent thermal conductivity components and heat capacity of an orthotropic medium through the combination of numerical solution and the Levenberg-Marquardt iterative procedure. Huang and Yan [105] utilized the conjugate gradient method of minimization and the adjoint equation in the optimization process such that the temperature-dependent thermal conductivity and heat capacity can be simultaneously measured. Battaglia et al. [106] indentified thermophysical properties from a metallic thin layer deposited on a silicon substrate through the combination of a Bayesian technique based on Monte Carlo Markov Chain and the Levenberg-Marquardt technique. Garcia and Scott [108, 109] applied genetic algorithms for simultaneously estimating thermophysical properties.

In contrast to the approaches previously noted, this chapter describes an alternative method for predicting the thermophysical properties based on system calibration principles. It is well known that several system parameters are required prior to extracting the thermophysical properties. That is, the probe positions and the sample configuration are necessary inputs. These system parameters introduce uncertainties into the analytical process. These uncertainties adversely affect the estimated thermal diffusivity and thermal conductivity. To avoid this

obstacle, the proposed method utilizes a calibration principle that intrinsically accounts for these parameters.

This calibration principle relies on analytical pre-processing for constructing a calibration or measurement equation that eliminates the unwanted system parameters. This concept has been demonstrated in the context of inverse heat conduction. Inverse heat conduction by a calibration approach was initially introduced as the Non-Integer System Identification (NISI) method [40-42]. This approach requires the estimation of a series of parameters and the identification of the optimal regularization parameter. In contrast, Frankel and Keyhani [43], Frankel et al. [44] and Elkins et al. [45] proposed a calibration methodology that also directly relates the net unknown surface heat flux to an in-depth temperature measurement but removes the need to resolve a set of intermediate coefficients. This calibration approach was derived in linear framework and has been experimentally verified [45] with excellent accuracy in an appropriate temperature range.

To extend the linear calibration equation to a nonlinear framework, Chen et al. [112] proposed a variation of the one-probe calibration method by achieving the quasi-linearization through the combination of Kirchhoff transformation and rescaling principles. In this process, the Kirchhoff transformation was exploited for the thermal conductivity linearization. In contrast, the time domain rescaling was incorporated to linearize the temperature-dependent thermal diffusivity. In the present chapter, the same rescaling principle is utilized for the thermophysical property estimation. First, a temperature calibration equation is proposed for estimating the thermal diffusivity. Second, the thermal conductivity is obtained based on using the estimated thermal diffusivity and a new heat flux calibration equation. Section 6.2 presents the detailed

derivations of the temperature and heat flux calibration equations based on rescaling principles. Section 6.3 presents the idealized experimental strategy and predicted results for two common engineering materials, namely, stainless steel 304 and a representative carbon composite using simulated data. Section 6.4 provides concluding remarks on the proposed calibration method for estimating both the thermal conductivity and thermal diffusivity over a large temperature range.

6.2 Formulation

Consider a one-dimensional heat conduction problem in Cartesian coordinates having a front surface heat flux source at $x = 0$ while maintaining an adiabatic back surface at $x = L$. A schematic of the sample geometry is given in Fig. 6.2.1. The heat equation is given as [33]

$$\rho c_p\big(T(x,t)\big)\frac{\partial T}{\partial t}(x,t) = \frac{\partial}{\partial x}\left[k\big(T(x,t)\big)\frac{\partial T}{\partial x}(x,t)\right], \qquad x \in (0,L),\ \ t \in [0,t_{max}], \qquad (6.2.1a)$$

where T is the temperature, k represents the thermal conductivity, and ρc_p represents the heat capacity. Since experimental data are involved, the time span is constrained up to $t = t_{max}$ where data collection ends. The boundary conditions are given as

$$-k\big(T(0,t)\big)\frac{\partial T}{\partial x}(0,t) \triangleq q"(0,t) = q"_s(t),$$

$$\frac{\partial T}{\partial x}(L,t) = 0, \qquad t \in [0,t_{max}]. \qquad (6.2.1b-c)$$

where $q"_s(t)$ describes the total surface energy externally contacting at $x = 0$ while $q"(0,t)$ is the net surface heat flux entering the body. If the surface temperature measurement $T(0,t)$ at $x = 0$ is included, the surface heat flux boundary condition imposed at $x = 0$ given by Eq. (1b) can be eliminated, thereby bypassing the need to specify the surface thermal conductivity $k\big(T(0,t)\big)$. The resulting thermal boundary condition at $x = 0$ is defined as

$$T(0,t) = T_s(t), \qquad t \in [0, t_{max}], \tag{6.2.1d}$$

where $T_s(t)$ represents the surface temperature measurement at $x = 0$. The initial condition is

$$T(x,0) = 0, \qquad x \in [0, L]. \tag{6.2.1e}$$

Here, the initial condition is considered as zero since all temperature data involved in Eqs. (6.2.1a-e) are defined in terms of the relative temperature, i.e., the deviation from the uniform initial temperature condition.

Suppose that the positional temperature at $x = b$ are measured and given as $T(b,t)$. For each heating time interval $[0, t_{max}]$, if the incurred temperature rise produces little change in the thermophysical properties then these properties are assumed to constant over this time interval of interest. Explicitly, we define the mean temperature in this time interval as

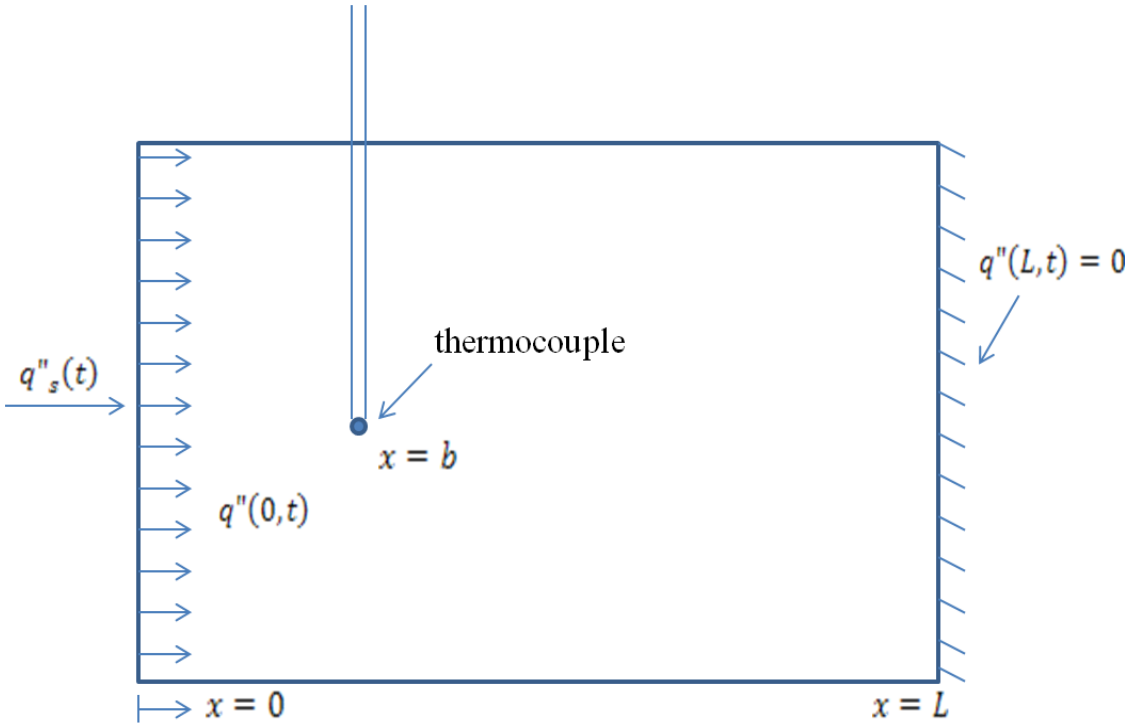

Figure 6.2.1: System setup for the one-dimensional heat conduction problem showing boundary conditions and the thermocouple position.

$$\bar{T}_M = \bar{T}_{initial} + \frac{T(b, t_{max})}{2}. \tag{6.2.2}$$

Here, $\bar{T}_{initial}$ represents the absolute initial temperature at $t = 0$. All constant thermophysical properties during time interval $[0, t_{max}]$ are evaluated at the mean temperature $\bar{T}_M$.

Based on this assumption, Eqs. (6.2.1a,c-e) simplify to

$$\frac{1}{\alpha(\bar{T}_M)} \frac{\partial T}{\partial t}(x,t) = \frac{\partial^2 T}{\partial x^2}(x,t), \qquad x \in (0, L), \;\; t \in [0, t_{max}], \tag{6.2.2a}$$

subject to the boundary conditions

$$T(0,t) = T_s(t),$$

$$\frac{\partial T}{\partial x}(L,t) = 0, \qquad t \in [0, t_{max}], \tag{6.2.2b-c}$$

with the initial condition

$$T(x,0) = 0, \qquad x \in [0, L]. \tag{6.2.2d}$$

After this quasi-linearization, it is found that the replacement of the heat flux boundary condition given by Eq. (6.2.1b) by the temperature boundary condition given by Eq. (6.2.1d) successively decreases the number of the unknown thermophysical properties from two $\left(\alpha(\bar{T}_M), k(\bar{T}_M)\right)$ to one $\left(\alpha(\bar{T}_M)\right)$.

The purpose of this chapter is to apply the calibration principle described in Refs. [43-45, 121] for estimating the unknown thermophysical properties evaluated at the mean temperature $\bar{T}_M$, when $\bar{T}_M$ is significantly greater than the room temperature. In this process, two tests are required in the experimental campaign. The first test is referred to as the calibration test (subscript *c*), which implicitly includes all physical information of the thermal system and requires the knowledge of both thermal conductivity and thermal diffusivity evaluated at $\bar{T}_{M,c}$. Many thermophysical properties near room temperature can be readily measured or found in the open literature. It is preferred that $\bar{T}_{M,c}$ is set near the room temperature. The second test is called the reconstruction test (subscript *r*) where the initial temperature can be set at a totally different value. The unknown thermophysical properties evaluated at $\bar{T}_{M,r}$ can then be estimated through the calibration from the known thermophysical properties evaluated at $\bar{T}_{M,c}$.

To successfully use the calibration principle, the rescaling concept needs to be applied to time domain [112]. Explicitly, let us define the rescaled temperature in the reconstruction test as

$$T_r^*(x,t) \triangleq T_r\left(x, \frac{\alpha\left(\bar{T}_{M,c}\right)}{\alpha\left(\bar{T}_{M,r}\right)} t\right), \qquad t \in \left[0, \frac{\alpha\left(\bar{T}_{M,r}\right)}{\alpha\left(\bar{T}_{M,c}\right)} t_{max}\right]. \tag{6.2.3}$$

To reiterate, the subscript "r" represents the reconstruction test in a defined temperature range that contrasts the temperature range from the calibration test. Upon implementing the above definitions into Eqs. (6.2.2a-d), we can describe the heating process for the reconstruction test based on the thermophysical properties evaluated at the calibration mean temperature $\bar{T}_{M,c}$, namely

$$\frac{1}{\alpha\left(\bar{T}_{M,c}\right)}\frac{\partial T_r^*}{\partial t}(x,t)=\frac{\partial^2 T_r^*}{\partial x^2}(x,t),\quad x\in(0,L),\ \ t\in\left[0,\frac{\alpha\left(\bar{T}_{M,r}\right)}{\alpha\left(\bar{T}_{M,c}\right)}t_{max}\right],\quad (6.2.4a)$$

subject to the boundary conditions

$$T_r^*(0,t)=T_{r,s}^*(t),$$

$$\frac{\partial T_r^*}{\partial x}(L,t)=0,\quad t\in\left[0,\frac{\alpha\left(\bar{T}_{M,r}\right)}{\alpha\left(\bar{T}_{M,c}\right)}t_{max}\right],\qquad (6.2.4b-c)$$

and initial condition

$$T_r^*(x,t=0)=0,\quad x\in[0,L].\qquad (6.2.4d)$$

In the linear framework, the temperature calibration equation [120] is given as

$$\int_{u=0}^{t} T_r(0,u)T_c\,(b,t-u)du = \int_{u=0}^{t} T_c(0,u)T_r\,(b,t-u)du,$$

$$b \in [0,L], t \in [0,t_{max}]. \quad (6.2.5)$$

The calibration equation displayed in Eq. (6.2.5) is suitable for an unchanging back boundary condition transpiring between the calibration and reconstruction tests. This formulation is applicable to the semi-infinite geometry or a slab with a fixed heat transfer coefficient at the back face, and uniform initial condition. The temperatures displayed Eq. (6.2.5) are the relative temperature. Since the thermal diffusivities of both T_c and T_r^* are evaluated at the same calibration mean temperature, it is only necessary to replace the physical temperature $T_r(x,t)$ involved in Eq. (6.2.5) with the rescaling temperature $T_r^*(x,t)$ defined in Eq. (6.2.3) such that Eq. (6.2.5) is available for thermophysical property estimation. Performing this replacement produces

$$\int_{u=0}^{t} T_r^*(0,u)T_c\,(b,t-u)du = \int_{u=0}^{t} T_c(0,u)T_r^*\,(b,t-u)du,$$

$$b \in [0,L], \quad t \in [0,t_{max}^*]. \quad (6.2.6a)$$

where

$$t_{max}^* = min\left[t_{max}, \frac{\alpha(\bar{T}_{M,r})}{\alpha(\bar{T}_{M,c})} t_{max}\right]. \quad (6.2.6b)$$

It is also necessary to return the rescaled temperature $T_r^*(x,t)$ back to the physical temperature $T_r(0,u)$ in accordance to Eq. (6.2.3), this implementation produces

$$\int_{u=0}^{t} T_r\left(0,\frac{\alpha(\bar{T}_{M,c})}{\alpha(\bar{T}_{M,r})}u\right)T_c\,(b,t-u)du = \int_{u=0}^{t} T_c(0,u)T_r\left(b,\frac{\alpha(\bar{T}_{M,c})}{\alpha(\bar{T}_{M,r})}(t-u)\right)du,$$

$$b \in [0,L],\ \ t \in [0,t_{max}^*]. \qquad (6.2.7)$$

Equation (6.2.7) is used to predict $\alpha(\bar{T}_{M,r})$ when an accurate value of $\alpha(\bar{T}_{M,c})$ is provided. The predicted result possesses uniqueness since the thermal conductivities for both tests are not included in this equation. Based on this consideration, the residual function utilizing the proposed temperature calibration equation is given as

$$R_{N,T}\left(\alpha(\bar{T}_{M,r})\right) = \frac{\sum_{i=1}^{N+1}[G_T^*(t_i)-F_T^*(t_i)]^2}{\sum_{i=1}^{N+1}F_T^*(t_i)^2}\,, \qquad (6.2.8a)$$

where

$$t_i = \frac{i}{N+1}t_{max}^*,\quad i = 0,1,2..N+1,$$

$$G_T^*(t_i) = \int_{u=0}^{t_i} T_r\left(0,\frac{\alpha(\bar{T}_{M,c})}{\alpha(\bar{T}_{M,r})}u\right)T_c\,(b,t_i-u)du, \qquad (6.2.8b-d)$$

$$F_T^*(t_i) = \int_{u=0}^{t_i} T_c(0,u)T_r\left(b,\frac{\alpha(\bar{T}_{M,c})}{\alpha(\bar{T}_{M,r})}(t_i-u)\right)du,\quad i = 0,1,2..N+1.$$

Here, the integer $N+1$ represents the number of time intervals uniformly distributed in $[0, t^*_{max}]$. The thermal diffusivity $\alpha(\bar{T}_{M,r})$ is obtained by minimizing this residual function given in Eq. (6.2.8a) with respect to the thermal diffusivity.

To estimate the unknown thermal conductivity $k(\bar{T}_{M,r})$, the heat flux boundary condition given in Eq. (6.2.1b) is required for both calibration and reconstruction tests. To ensure the thermal conductivity in the reconstruction test is transformed back to the value evaluated at the calibration mean temperature, we define the rescaled heat flux in the reconstruction test as

$$q''^*_r(0,t) \triangleq \frac{k(\bar{T}_{M,c})}{k(\bar{T}_{M,r})} q''_r\left(0, \frac{\alpha(\bar{T}_{M,c})}{\alpha(\bar{T}_{M,r})} t\right), \quad t \in \left[0, \frac{\alpha(\bar{T}_{M,r})}{\alpha(\bar{T}_{M,c})} t_{max}\right]. \tag{6.2.9}$$

Based on the constant thermophysical properties assumption referred to before, the substitution of Eq. (6.2.3) and Eq. (6.2.9) into Eqs. (6.2.1a-c,e) produces

$$\frac{1}{\alpha(\bar{T}_{M,c})} \frac{\partial T^*_r}{\partial t}(x,t) = \frac{\partial^2 T^*_r}{\partial x^2}(x,t), \quad x \in (0,L), \ \ t \in \left[0, \frac{\alpha(\bar{T}_{M,r})}{\alpha(\bar{T}_{M,c})} t_{max}\right], \tag{6.2.10a}$$

subject to the boundary conditions

$$-k(\bar{T}_{M,c}) \frac{\partial T^*_r}{\partial x}(0,t) = q''^*_r(0,t),$$

$$\frac{\partial T_r^*}{\partial x}(L,t)=0, \quad t\in\left[0,\frac{\alpha\left(\bar{T}_{M,r}\right)}{\alpha\left(\bar{T}_{M,c}\right)}t_{max}\right], \qquad (6.2.10b-c)$$

and initial condition

$$T_r^*(x,t=0)=0, \quad x\in[0,L]. \qquad (6.2.10d)$$

It is found that both thermophysical properties (α and k) given in Eqs. (6.2.10a-d) are evaluated at the calibration mean temperature after this transformation.

The linear heat flux calibration equation for a one-probe inverse heat conduction problem is also developed [43]

$$\int_{u=0}^{t} q"_r(0,u)T_c\,(b,t-u)du=\int_{u=0}^{t} q"_c(0,u)T_r\,(b,t-u)du,$$

$$b\in[0,L],\ \ t\in[0,t_{max}]. \qquad (6.2.11)$$

Similarly, to apply Eq. (6.2.11) for estimating the thermal diffusivity in the reconstruction test, the physical variables $q"_r(0,t)$ and $T_r(x,t)$ involved in Eq. (6.2.11) are replaced with the rescaling variables $q"_r^*(0,t)$ and $T_r^*(x,t)$ given by Eq. (6.2.3) and Eq. (6.2.9), respectively. Performing these replacements yields

$$\frac{k\left(\bar{T}_{M,c}\right)}{k\left(\bar{T}_{M,r}\right)}\int_{u=0}^{t} q"_r\left(0,\frac{\alpha\left(\bar{T}_{M,c}\right)}{\alpha\left(\bar{T}_{M,r}\right)}u\right)T_c\,(b,t-u)du=\int_{u=0}^{t} q"_c(0,u)T_r\left(b,\frac{\alpha\left(\bar{T}_{M,c}\right)}{\alpha\left(\bar{T}_{M,r}\right)}(t-u)\right)du,$$

$$b \in [0, L], \quad t \in [0, t^*_{max}]. \qquad (6.2.12)$$

Two variables $\left(\alpha\left(\bar{T}_{M,r}\right) \text{ and } k\left(\bar{T}_{M,r}\right)\right)$ are included in Eq. (6.2.12). However, the unknown thermal diffusivity $\alpha\left(\bar{T}_{M,r}\right)$ can be estimated with the aid of the residual function given by Eq. (6.2.8a). Based on the consideration, the residual function for the unknown thermal conductivity $k\left(\bar{T}_{M,r}\right)$ utilizing the proposed heat flux calibration equation is given as

$$R_{N,q}\left(k\left(\bar{T}_{M,r}\right)\right) = \frac{\sum_{i=1}^{N+1}\left[G_q^*(t_i) - F_q^*(t_i)\right]^2}{\sum_{i=1}^{N+1} F_q^*(t_i)^2}, \qquad (6.2.13a)$$

where

$$G_q^*(t_i) \triangleq \frac{k\left(\bar{T}_{M,c}\right)}{k\left(\bar{T}_{M,r}\right)} \int_{u=0}^{t} q"_r \left(0, \frac{\alpha\left(\bar{T}_{M,c}\right)}{\alpha\left(\bar{T}_{M,r}\right)} u\right) T_c\,(b, t-u)du, \qquad (6.2.13b-c)$$

$$F_q^*(t_i) \triangleq \int_{u=0}^{t} q"_c(0,u) T_r \left(b, \frac{\alpha\left(\bar{T}_{M,c}\right)}{\alpha\left(\bar{T}_{M,r}\right)}(t-u)\right) du.$$

To reiterate, the thermal diffusivity $\alpha\left(\bar{T}_{M,r}\right)$ during the reconstruction test is estimated by minimizing $R_{N,T}\left(\alpha\left(\bar{T}_{M,r}\right)\right)$ defined in Eq. (6.2.8a) with respect to α. After acquiring the estimated $\alpha\left(\bar{T}_{M,r}\right)$, the corresponding thermal conductivity $k\left(\bar{T}_{M,r}\right)$ is estimated through minimizing $R_{N,q}\left(k\left(\bar{T}_{M,r}\right)\right)$ given by Eq. (6.2.13a) with respect to k.

6.3 Results

In this section, results from implementing the calibration principles given by Eq. (6.2.7) and Eq. (6.2.12) for estimating the thermophysical properties during the reconstruction test are presented. A schematic of the physical system is given in Fig. 6.2.1. The front surface of the slab is exposed to a designed time-varying heat flux while the back surface is modeled as adiabatic. Two common engineering materials are considered in this chapter illustrating the generality of this new thermophysical property estimation approach. In-depth temperature data are collected at $x = b$. For the present study, the collected data are assumed to be representative of the positional temperature $T(b,t)$. In an appropriate temperature range $T \in [0, 1000]^{\circ}\mathrm{C}$, the representative functions for the bulk thermal conductivity and bulk heat capacity for stainless steel 304 are expressed as

$$k(T) = (14.4 + 0.0167T - 1.6 \times 10^{-6}T^2)\ (\mathrm{W/mK}), \qquad (6.3.1a)$$

$$\rho c_p(T) = (1.59 \times 10^5 + 388.87T + 6.395 \times 10^5 \ln(T + 273.15))\ (\mathrm{J/m^3K}), \quad (6.3.1b)$$

and for a representative carbon composite as

$$k(T) = (5.76 + 1.195 \times 10^{-3}T)\ (\mathrm{W/mK}), \qquad (6.3.2a)$$

$$\rho c_p(T) = (1.705 \times 10^6 + 3629T - 3.075T^2 + 9.334 \times 10^{-4}T^3)\ (\mathrm{J/m^3K}). \quad (6.3.2b)$$

Stainless steel is a standard testing material for verifying the effectiveness of the mathematical model and proposed methodology. Carbon composite materials have value at high temperature applications as associated with hypersonic flight.

For both stainless steel and the chosen carbon composite, four geometrical assignments are defined for verifying the estimation methodology. These four assignments are defined as (1) probe location $b = 2\text{mm}$ and depth $L = 5\text{mm}$; (2) probe location $b = 4\text{mm}$ and depth $L = 5\text{mm}$; (3) probe location $b = 2\text{mm}$ and depth $L = 1\text{cm}$; (4) probe location $b = 4\text{mm}$ and depth $L = 1\text{cm}$, respectively. Figure 6.3.1 presents the designed time-varying source heat flux applied to the front surface for both the stainless steel and the carbon composite. For stainless steel, the maximum experimental run time t_{max} is set as 15s using 10s of heating time and 5s cooling (source is off). During the heating period, the input source heat flux possesses an isosceles triangular shape in time with a peak of 18W/cm^2. For the representative carbon composite, the heating rate is fixed at 2.5W/cm^2 lasting the whole 15s. Utilizing different surface heat flux design is to verify the generality of the proposed calibration method. To obtain their thermophysical property functions $\alpha(T)$ and $k(T)$, eleven (11) simulated experiments are performed for each individual assignment where the input heat flux is spatially uniform. The initial temperature is varied from 25^{o}C (room temperature) to 825^{o}C using increments of 80^{o}C leading to the eleven (11) tests for the defined temperature range.

The calibration principle implies that if the thermophysical properties for one experiment are known in advance then Eq. (6.2.7) and Eq. (6.2.12) can be used to estimate the unknown

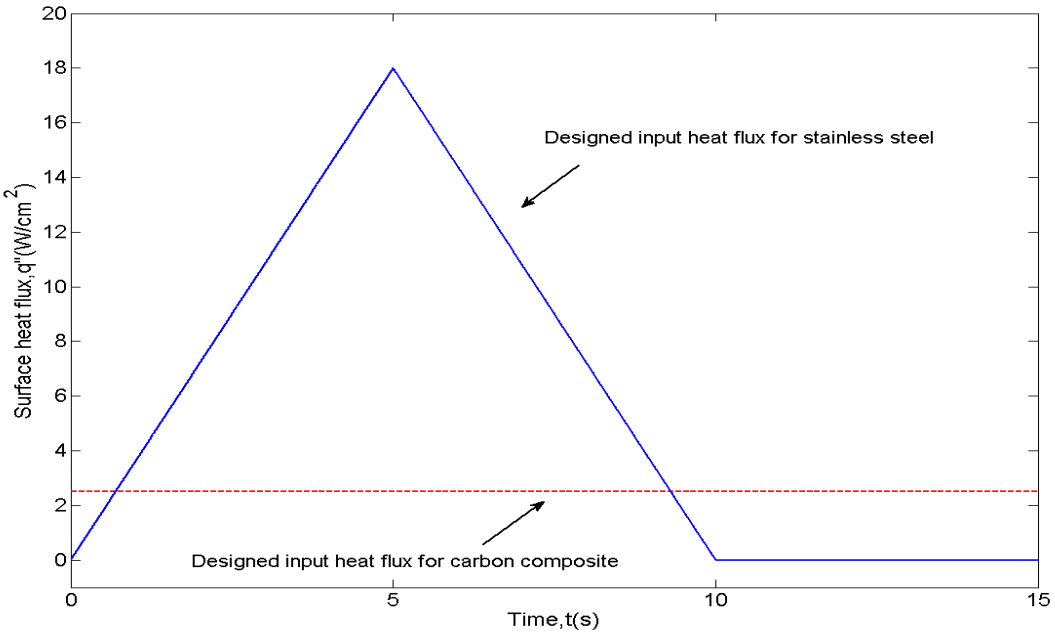

Figure 6.3.1: Time-varying input surface heat flux applied to the front surface of stainless steel and representative carbon composite.

thermophysical properties corresponding to other initial conditions. This process requires considering the known property experiment as the calibration test while further high temperature experiments are the reconstruction tests. In this chapter, we assume that the thermophysical properties for the first experiment corresponding to the room temperature 25^{o}C are known and use this information as the standard for predicting the bulk thermal diffusivity and thermal conductivity temperature-dependent functions for both stainless steel and the representative carbon composite.

The calibration equation given by Eq. (6.2.7) requires the temperature data $T(0,t)$ at the front surface and $T(b,t)$ at the probe position. The temperature field $T(x,t), x \in [0,L], t \geq 0$ for a given set of boundary and initial conditions is required for developing the appropriate simulated data. A finite difference method (FDM) [33] is applied on the domains $x \in [0,L],\ t \geq 0$ to form the forward solution where fully temperature dependent thermophysical properties are assumed (see Eqs. (6.3.1) and (6.3.2)). For the FDM solution, the spatial and temporal grids (Δx and Δt) are varied until solution convergence is met to a predefined criterion. Results shows that Δx=0.2mm and Δt =50μs work sufficiently well for all reported data based on an absolute convergence of 0.01^{o}C. Figures 6.3.2 and 6.3.3 present the temperature histories at the indicated uniformly distributed spatial locations for both materials based on $L = 5$mm and $\bar{T}_{initial} = 298.15$K ($25^{o}$C), i.e., the calibration test. The recovered (small) temperature rise in both the time and spatial domains verifies the reliability of the linearization assumption.

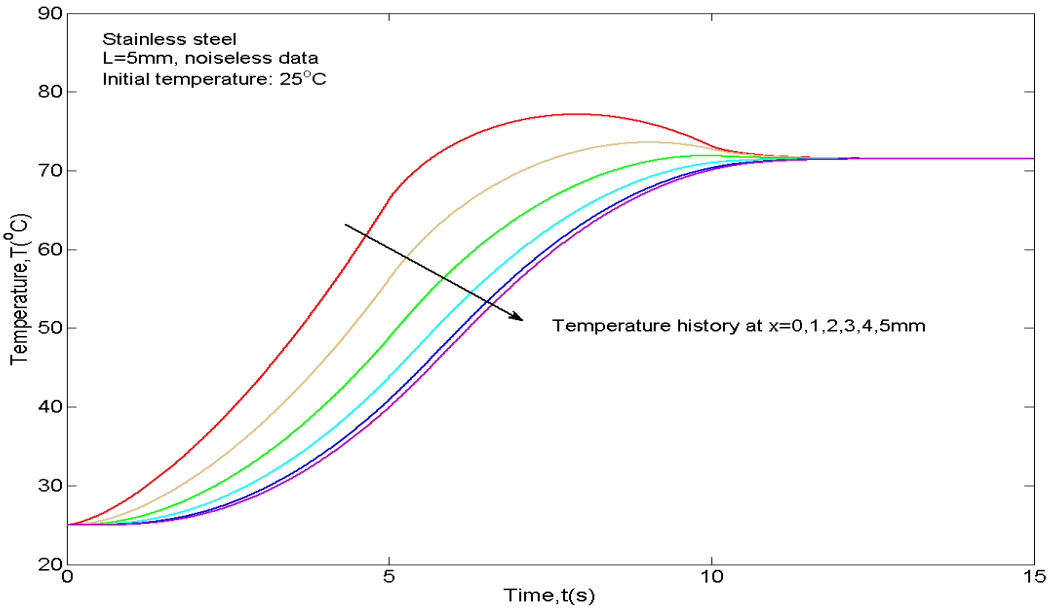

Figure 6.3.2: The temperature histories at uniformly distributed spatial locations for stainless steel with the slab thickness $L = 5\text{mm}$.

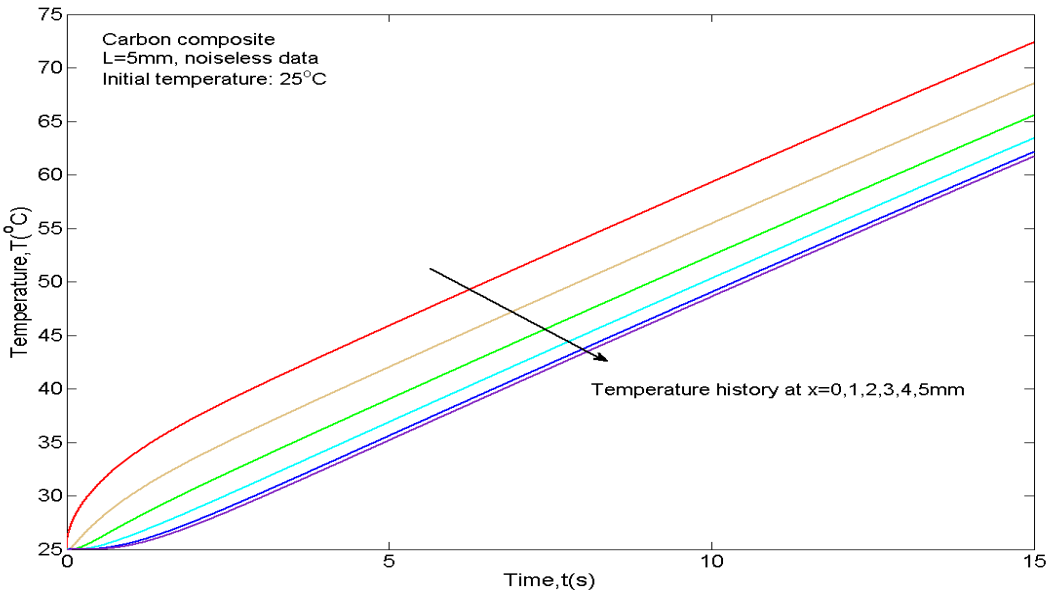

Figure 6.3.3: The temperature histories at uniformly distributed spatial locations for carbon composite with the slab thickness $L = 5\text{mm}$.

Thermophysical property prediction based on noiseless in-depth temperature data is first investigated. The purpose of using noiseless temperature data at $x = b$ allows for the evaluation of the implemented numerical method and model accuracy. For this purpose, $R_{N,T}\left(\alpha(\bar{T}_{M,r})\right)$ is formulated using noiseless temperature data $T(0,t)$ and $T(b,t)$, based on Eq. (6.2.8a). In this process, the simulated data using the initial temperature $\bar{T}_{initial} = 298.15\text{K}$ (25^{o}C) are considered as the calibration test while simulated data using higher initial temperatures are considered as the reconstruction tests whose thermophysical properties are estimated. Upon plotting the formulated $R_{N,T}$ against different α, the thermal diffusivity evaluated at the reconstruction mean temperature $\bar{T}_{M,r}$ is found corresponding to the minimum value of $R_{N,T}$. Figure 6.3.4 graphically describes how the thermal diffusivity is selected using the reconstruction test based on an initial temperature $\bar{T}_{initial} = 378.15\text{K}$ (105^{o}C) for the stainless steel sample with $b = 2\text{mm}$ and $L = 5\text{mm}$. The function $R_{N,T}$ plotted against α forms a V-shaped curve with a clear minimum. The same procedure is used for the other reconstruction tests based on the chosen family of initial conditions.

Figures 6.3.5 and 6.3.6 present the predicted thermal diffusivities for the stainless steel and representative carbon composite samples, respectively. All predictions produce excellent accuracy when compared to the exact properties used to generate the temperature data. The predicted results display more sensitivity to the slab thickness than the probe position. The reconstructed thermal diffusivity for the carbon composite possesses about a 2-3% bias based on the slab thickness $L = 5\text{mm}$. In contrast, the prediction based on the slab thickness $L = 10\text{mm}$ shows improved accuracy. For stainless steel, the situation is opposite. The thermal

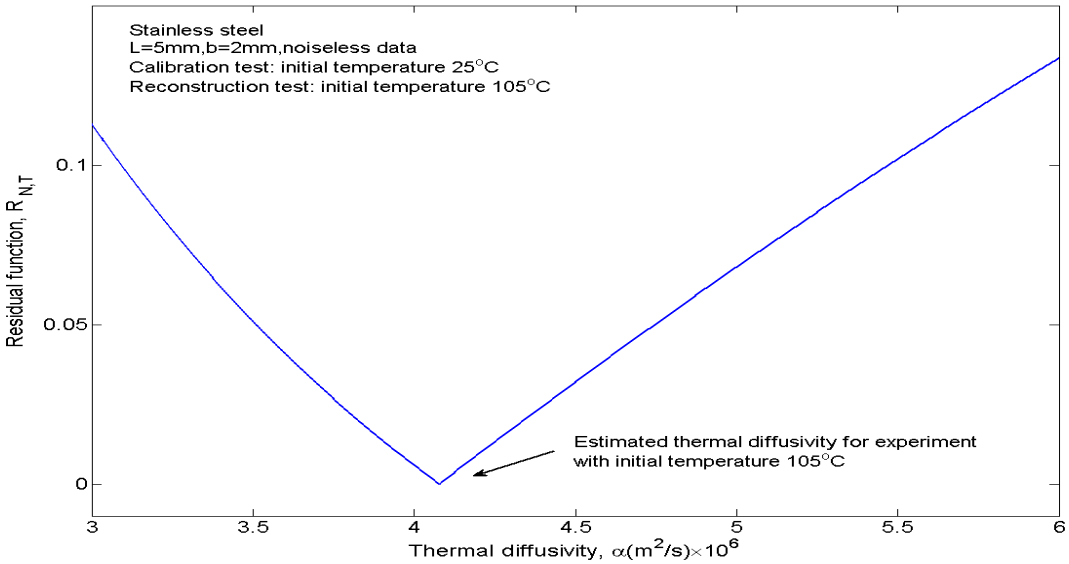

Figure 6.3.4: An example for the optimal thermal diffusivity selection: the optimal thermal diffusivity corresponds to the minimum value of residual function $R_{N,T}$.

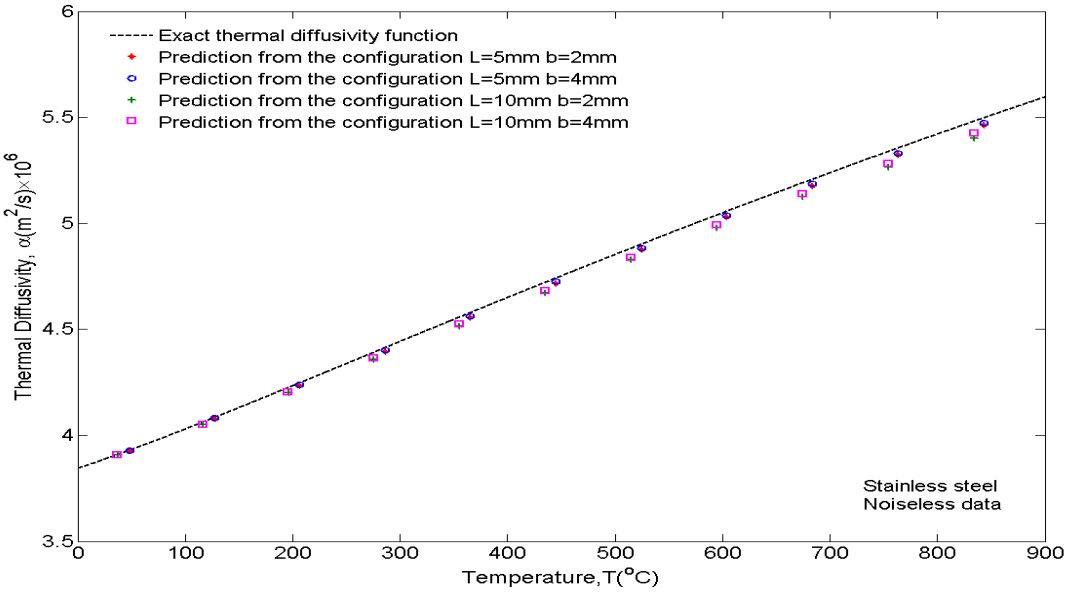

Figure 6.3.5: Predicted thermal diffusivity for stainless steel corresponding to different probe position and slab thickness.

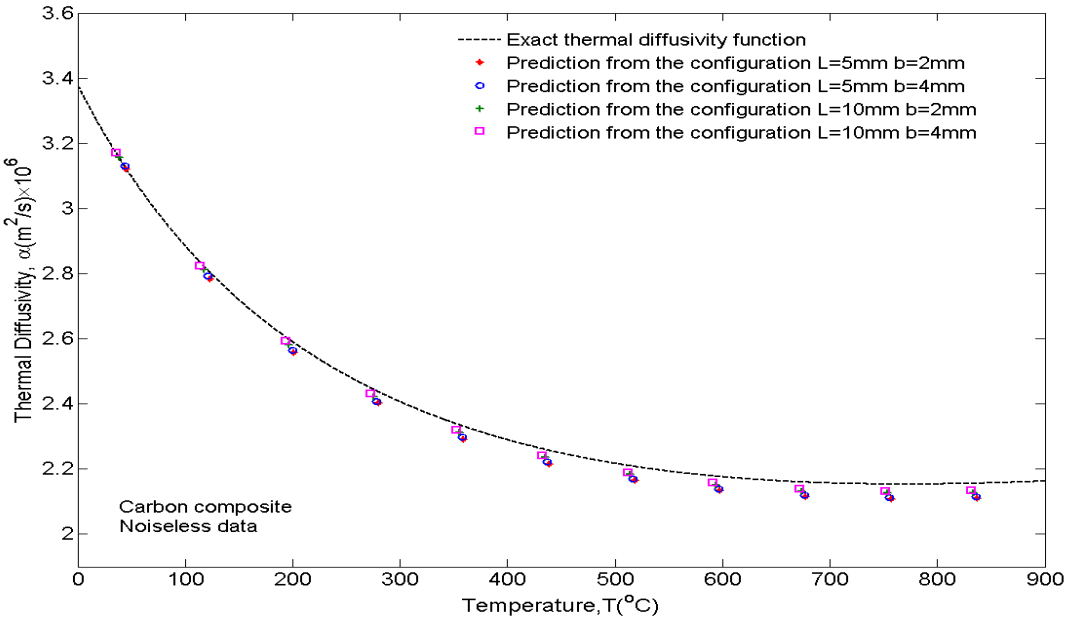

Figure 6.3.6: Predicted thermal diffusivity for carbon composite corresponding to different probe position and slab thickness

diffusivity of stainless steel is estimated better through the configuration $L = 5\text{mm}$ than $L = 10\text{mm}$. One possible explanation for this observation lies on the fact that the proposed parameter estimation algorithm is built upon a linearization assumption. This implies that for every individual experiment in the assignment set, both the thermal diffusivity and thermal conductivity in any of the eleven temperature ranges are considered constant. This linearization should exist in both the space and time domains to ensure model accuracy. However, if the slab thickness is excessive then a large temperature difference exists between the front and back surfaces such that the linearization in spatial domain is easily violated. In contrast, if the slab is too thin then the heating energy accumulates in the thin sample such that an excessive maximum temperature incurs and weakens the linearization assumption in the fixed time domain. This contradiction indicates that the slab thickness requires optimization based on different material properties and input heat fluxes. However, this further consideration is beyond the scope of the present chapter.

To estimate the unknown thermal conductivity, the residual function $R_{N,q}\left(k\left(\bar{T}_{M,r}\right)\right)$ is formulated using the same noiseless data defined by the test initial conditions. The estimated thermal diffusivities $\alpha\left(\bar{T}_{M,r}\right)$ previously acquired are assumed to be known. To estimate the thermal conductivity $k\left(\bar{T}_{M,r}\right)$, it is only necessary to plot $R_{N,q}$ against k and extract its minimum value. The identification process is similar to that described using Fig. 6.3.4 in the context of $\alpha\left(\bar{T}_{M,r}\right)$. Figures 6.3.7 and 6.3.8 present the predicted thermal conductivities for stainless steel and the carbon composite samples, respectively. Results indicate that the predicted thermal conductivities corresponding to the minimum value of $R_{N,q}$ produce favorable accuracy when compared to exact input thermal conductivity for generating the simulated temperature data.

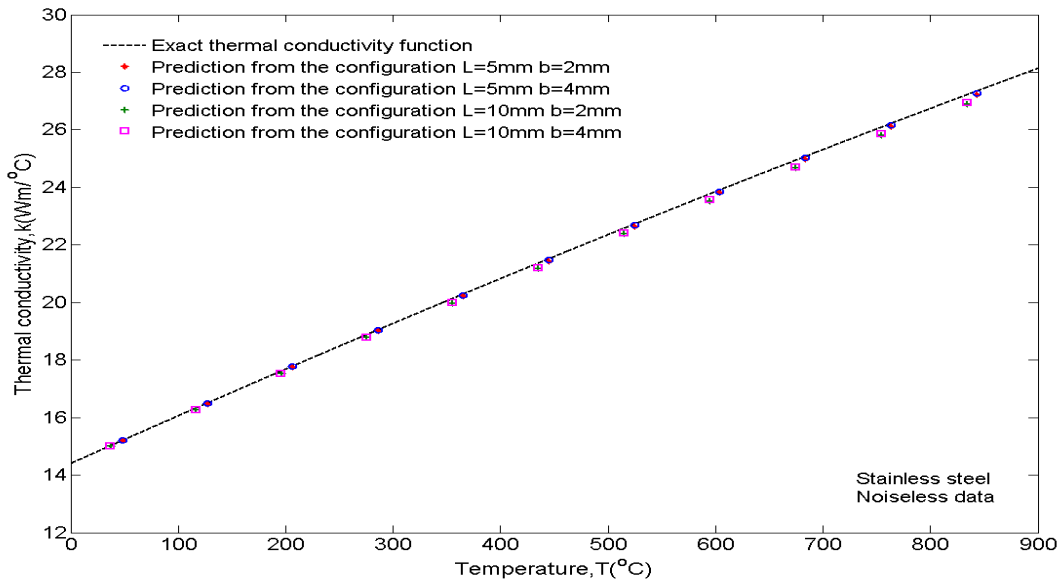

Figure 6.3.7: Predicted thermal conductivity for stainless steel corresponding to different probe position and slab thickness.

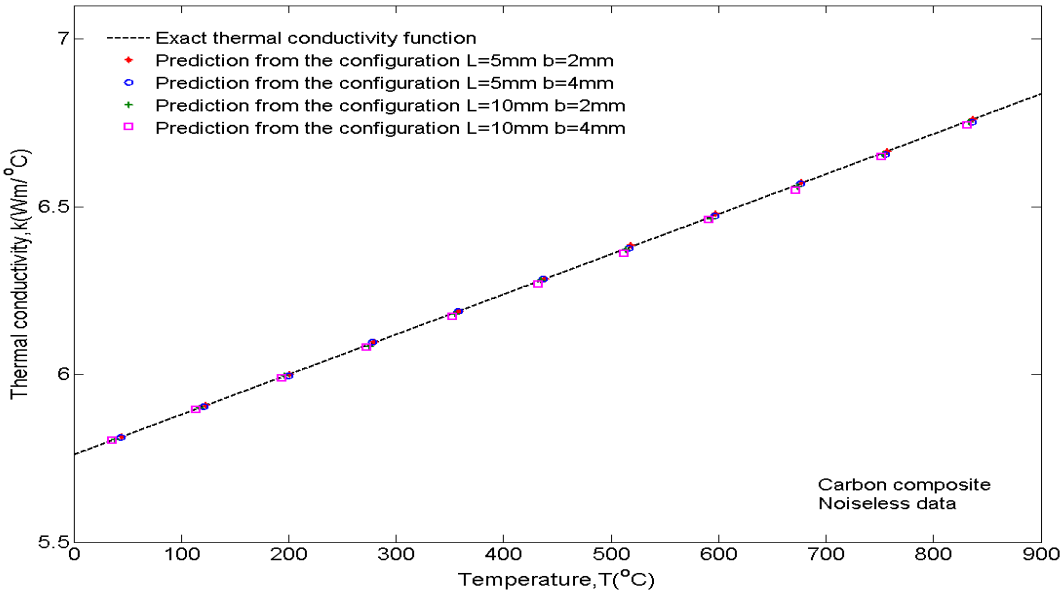

Figure 6.3.8: Predicted thermal conductivity for carbon composite corresponding to different probe position and slab thickness.

Tables 6.3.1-6.3.8 summarize the explicit comparison between the predicted thermophysical properties and their exact values. From these tables, it is found that the best geometric assignment for stainless steel 304 is probe location $b = 4\text{mm}$ and $L = 5\text{mm}$ while the best geometric assignment for the representative carbon composite is probe location $b = 4\text{mm}$ and $L = 10\text{mm}$. It should be noted that the thermal conductivity and thermal diffusivity of the carbon composite are lower that stainless steel 304. These differences can cause an excessive maximum temperature in the temporal domain of the carbon composite sample, weakening the linearization assumption. Therefore, the carbon composite requires a larger optimal slab thickness than the stainless steel 304 in order to decrease its maximum temporal temperature. In addition, the percent errors between the predicted and exact thermophysical properties are negative. This negative percent error is considered as model bias, and may come from the assigned mean temperature given by Eq. (6.2.2). It indicates that if there is a better way to calculate the mean temperature, the predicted result may have additional improvement.

The impact of noise is now considered on the proposed calibration method for acquiring the unknown thermophysical properties following the previously developed procedure. For this purpose, normally distributed noise ε_i with a standard deviation of 0.5^{o}C and mean of 0^{o}C are added to the "noiseless" probe temperature data $T(x, t_i)$ at $x = 0$ and $x = b$. All simulated random noise is obtained through the Matlab random number generator, "randn". Figure 6.3.9 presents an example of the generated temperature noise while Figure 6.3.10 presents the noisy temperature data $T(0, t)$ and $T(b, t)$ from the calibration test ($\bar{T}_{initial} = 298.15\text{K}\ (25^{\text{o}}\text{C})$) for the stainless steel sample with $b = 2\text{mm}$ and $L = 5\text{mm}$. The noisy temperature data are substituted into both $R_{N,T}$ and $R_{N,q}$ as given by Eq. (6.2.8a) and Eq. (6.2.13a), respectively. The identical

optimization procedure is applied as described by the noiseless data campaign. Figures 6.3.11 and 6.3.12 present the predicted thermal diffusivities based on noisy temperature data for stainless steel and the carbon composite samples, respectively when $b = 2\text{mm}$ and $L = 5\text{mm}$. Figures 6.3.13 and 6.3.14 present the corresponding predictions for the thermal conductivity. Accurate thermophysical properties are obtained in the presence of significant noise indicating that the calibration strategy is both stable and robust. Tables 6.3.9 and 6.3.10 compare the predicted thermophysical properties based on the noisy temperature data with exact thermophysical property function shown in Eq. (6.3.1) and Eq. (6.3.2).

The new thermophysical property estimation approach offers some additional advantages. First, two in-depth temperature measurements could be proposed instead of using a surface and single in-depth sensor arrangement as described and implemented in the present study. In this process, two in-depth sensors can be located at $x = b$ and $x = w$. If $b < w$ then the probe closer to the active side would be considered as new "surface" temperature $T(b, t)$ while the temperature data $T(w, t)$ would be considered as new sensor response. Second, the proposed calibration method is simple and straightforward. It is observed that the slab thickness and probe position are not required by the calibration equations given by Eq. (6.2.7) and Eq. (6.2.12). These parameters are inherently contained in the calibration data. The only parameters required in advance are the thermophysical properties used in the calibration test.

Table 6.3.1: Accuracy analysis for estimated thermophysical property of stainless steel (L=5mm, b=2mm, noiseless data)

Mean Temp $\overline{T}_{M,r}$ **(K)**	**Exact α** **(cm^2/s)**	**Predicted α** **(cm^2/s)**	**Exact k** **(W/mK)**	**Predicted k** **(W/mK)**
400.43	0.0408	0.0408	16.50	16.48
479.65	0.0425	0.0424	17.78	17.75
559.01	0.0441	0.0440	19.04	19.00
638.46	0.0458	0.0456	20.29	20.23
717.99	0.0474	0.0472	21.51	21.43
797.57	0.0490	0.0488	22.72	22.63
877.19	0.0506	0.0503	23.90	23.83
956.85	0.0521	0.0518	25.07	24.98
1036.53	0.0535	0.0532	26.22	26.10
1116.24	0.0550	0.0546	27.34	27.23

Table 6.3.2: Accuracy analysis for estimated thermophysical property of stainless steel (L=5mm, b=4mm, noiseless data).

Mean Temp $\overline{T}_{M,r}$ **(K)**	**Exact α** **(cm^2/s)**	**Predicted α** **(cm^2/s)**	**Exact k** **(W/mK)**	**Predicted k** **(W/mK)**
400.43	0.0408	0.0408	16.50	16.50
479.65	0.0425	0.0424	17.78	17.78
559.01	0.0441	0.0440	19.04	19.03
638.46	0.0458	0.0456	20.29	20.25
717.99	0.0474	0.0473	21.51	21.48
797.57	0.0490	0.0488	22.72	22.68
877.19	0.0506	0.0504	23.90	23.85
956.85	0.0521	0.0519	25.07	25.03
1036.53	0.0535	0.0533	26.22	26.15
1116.24	0.0550	0.0547	27.34	27.28

Table 6.3.3: Accuracy analysis for estimated thermophysical property of stainless steel (L=10mm, b=2mm, noiseless data).

Mean Temp $\overline{T}_{M,r}$ **(K)**	**Exact α** **(cm^2/s)**	**Predicted α** **(cm^2/s)**	**Exact k** **(W/mK)**	**Predicted k** **(W/mK)**
389.79	0.0406	0.0405	16.33	16.28
469.32	0.0423	0.0420	17.61	17.53
548.93	0.0439	0.0436	18.88	18.78
628.61	0.0456	0.0452	20.13	19.98
708.33	0.0472	0.0467	21.36	21.18
788.08	0.0488	0.0483	22.58	22.38
867.86	0.0504	0.0498	23.77	23.53
947.67	0.0519	0.0512	24.94	24.68
1027.49	0.0534	0.0527	26.09	25.80
1107.33	0.0548	0.0540	27.22	26.90

Table 6.3.4: Accuracy analysis for estimated thermophysical property of stainless steel (L=10mm, b=4mm, noiseless data).

Mean Temp $\overline{T}_{M,r}$ **(K)**	**Exact α** **(cm^2/s)**	**Predicted α** **(cm^2/s)**	**Exact k** **(W/mK)**	**Predicted k** **(W/mK)**
389.52	0.0406	0.0405	16.32	16.28
469.09	0.0422	0.0421	17.61	17.53
548.74	0.0439	0.0437	18.88	18.78
628.44	0.0456	0.0452	20.13	20.00
708.18	0.0472	0.0468	21.36	21.20
787.96	0.0488	0.0484	22.57	22.40
867.76	0.0504	0.0499	23.76	23.58
947.57	0.0519	0.0514	24.94	24.70
1027.41	0.0534	0.0528	26.09	25.85
1107.26	0.0548	0.0542	27.22	26.95

Table 6.3.5: Accuracy analysis for estimated thermophysical property of carbon composite (L=5mm, b=2mm, noiseless data).

Mean Temp $\overline{T}_{M,r}$ **(K)**	**Exact α** **(cm^2/s)**	**Predicted α** **(cm^2/s)**	**Exact k** **(W/mK)**	**Predicted k** **(W/mK)**
396.10	0.0280	0.0278	5.91	5.91
474.47	0.0259	0.0256	6.00	6.00
553.28	0.0244	0.0240	6.09	6.10
632.41	0.0233	0.0229	6.19	6.19
711.75	0.0226	0.0222	6.28	6.28
791.26	0.0221	0.0217	6.38	6.38
870.89	0.0218	0.0213	6.47	6.48
950.60	0.0216	0.0212	6.57	6.57
1030.39	0.0215	0.0211	6.66	6.66
1110.23	0.0216	0.0211	6.76	6.76

Table 6.3.6: Accuracy analysis for estimated thermophysical property of carbon composite (L=5mm, b=4mm, noiseless data).

Mean Temp $\overline{T}_{M,r}$ (K)	**Exact α (cm^2/s)**	**Predicted α (cm^2/s)**	**Exact k (W/mK)**	**Predicted k (W/mK)**
394.42	0.0281	0.0279	5.90	5.90
472.81	0.0259	0.0256	6.00	6.00
551.65	0.0244	0.0241	6.09	6.10
630.80	0.0233	0.0230	6.19	6.19
710.17	0.0226	0.0222	6.28	6.28
789.70	0.0221	0.0217	6.38	6.38
869.35	0.0218	0.0214	6.47	6.47
949.09	0.0216	0.0212	6.57	6.57
1028.90	0.0215	0.0211	6.66	6.66
1108.76	0.0216	0.0211	6.76	6.75

Table 6.3.7: Accuracy analysis for estimated thermophysical property of carbon composite (L=10mm, b=2mm, noiseless data).

Mean Temp $\overline{T}_{M,r}$ **(K)**	**Exact α** **(cm^2/s)**	**Predicted α** **(cm^2/s)**	**Exact k** **(W/mK)**	**Predicted k** **(W/mK)**
390.33	0.0282	0.0281	5.90	5.90
469.41	0.0260	0.0258	5.99	6.00
548.74	0.0244	0.0242	6.09	6.08
628.23	0.0234	0.0231	6.18	6.18
707.84	0.0226	0.0224	6.28	6.28
787.53	0.0221	0.0218	6.37	6.37
867.30	0.0218	0.0215	6.47	6.46
947.11	0.0216	0.0213	6.57	6.56
1026.96	0.0215	0.0213	6.66	6.66
1106.85	0.0216	0.0213	6.76	6.75

Table 6.3.8: Accuracy analysis for estimated thermophysical property of carbon composite (L=10mm, b=4mm, noiseless data).

Mean Temp $\overline{T}_{M,r}$ (K)	**Exact α (cm^2/s)**	**Predicted α (cm^2/s)**	**Exact k (W/mK)**	**Predicted k (W/mK)**
387.41	0.0283	0.0282	5.90	5.90
466.55	0.0261	0.0259	5.99	5.99
545.93	0.0245	0.0243	6.09	6.08
625.47	0.0234	0.0232	6.18	6.17
705.13	0.0226	0.0224	6.28	6.27
784.87	0.0221	0.0219	6.37	6.36
864.67	0.0218	0.0216	6.47	6.46
944.53	0.0216	0.0214	6.56	6.55
1024.42	0.0215	0.0213	6.66	6.65
1104.33	0.0216	0.0213	6.75	6.74

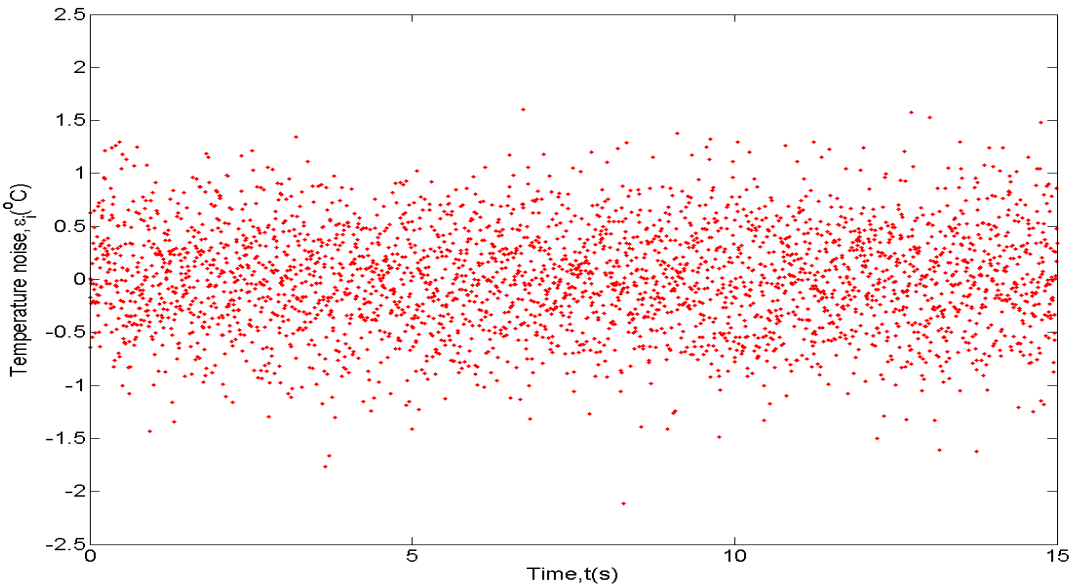

Figure 6.3.9: An example of the simulated noise added to the noiseless temperature with mean of 0°C and standard deviation of 0.5°C.

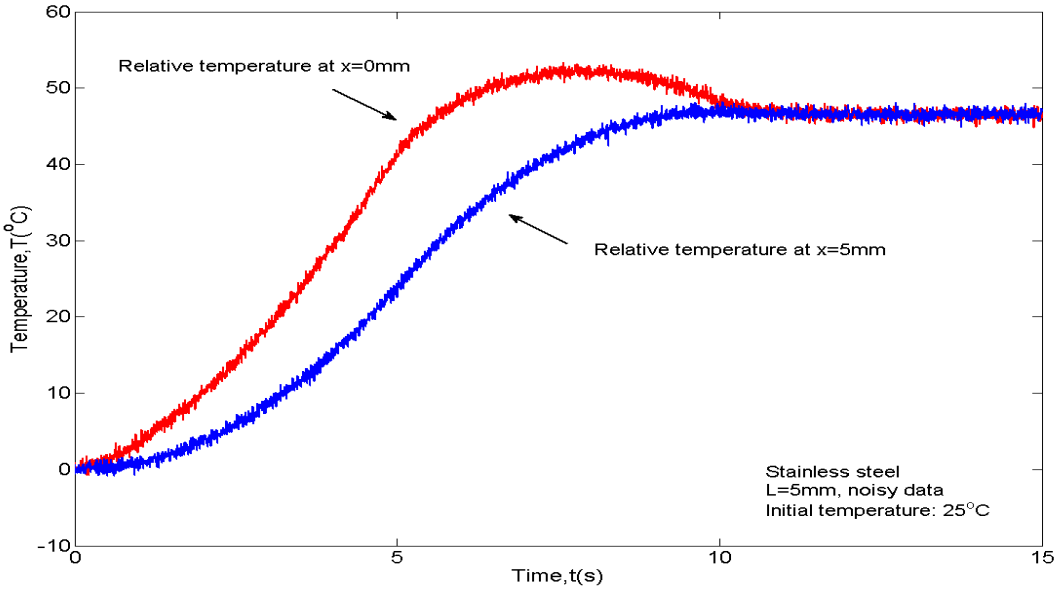

Figure 6.3.10: The noisy temperature data $T(0,t)$ and $T(b,t)$ of stainless steel for the experiment with initial temperature 25°C.

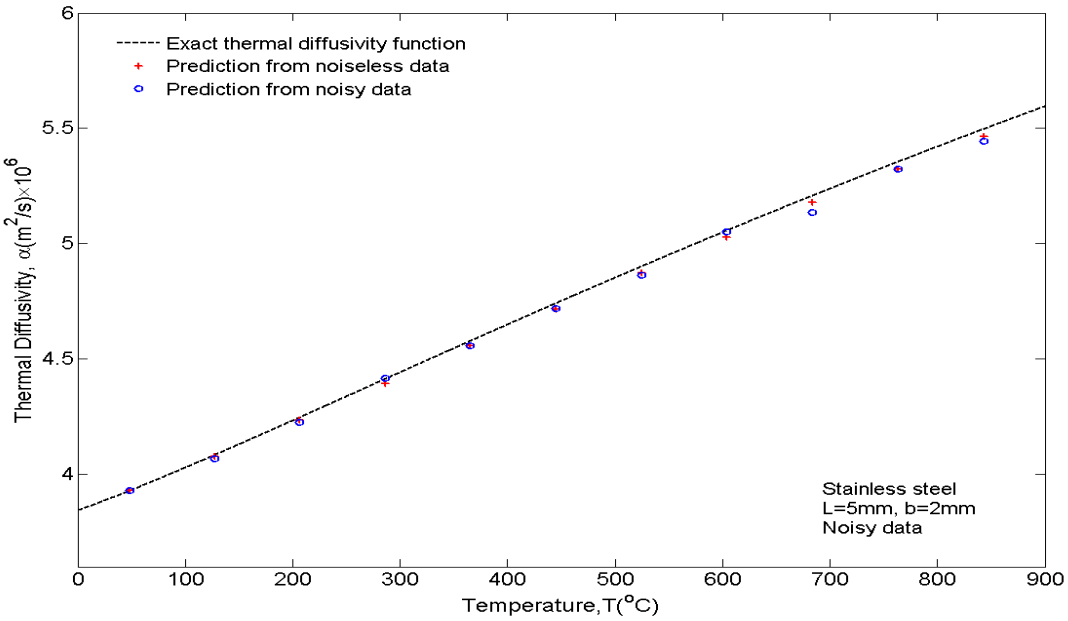

Figure 6.3.11: Predicted thermal diffusivity for stainless steel based on noisy data.

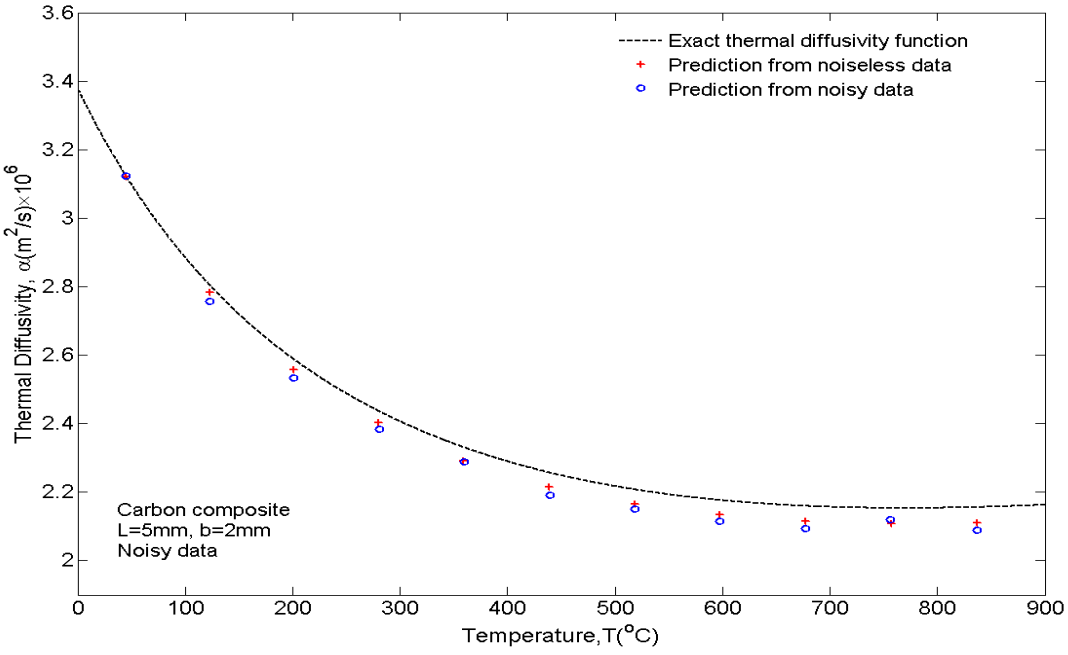

Figure 6.3.12: Predicted thermal diffusivity for carbon composite based on noisy data.

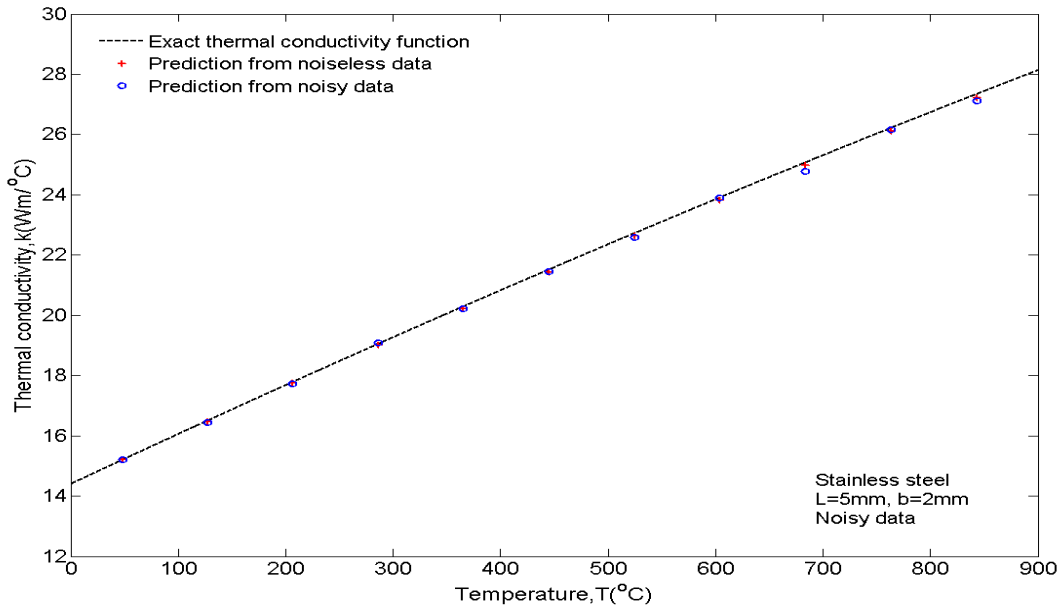

Figure 6.3.13: Predicted thermal conductivity for stainless steel based on noisy data.

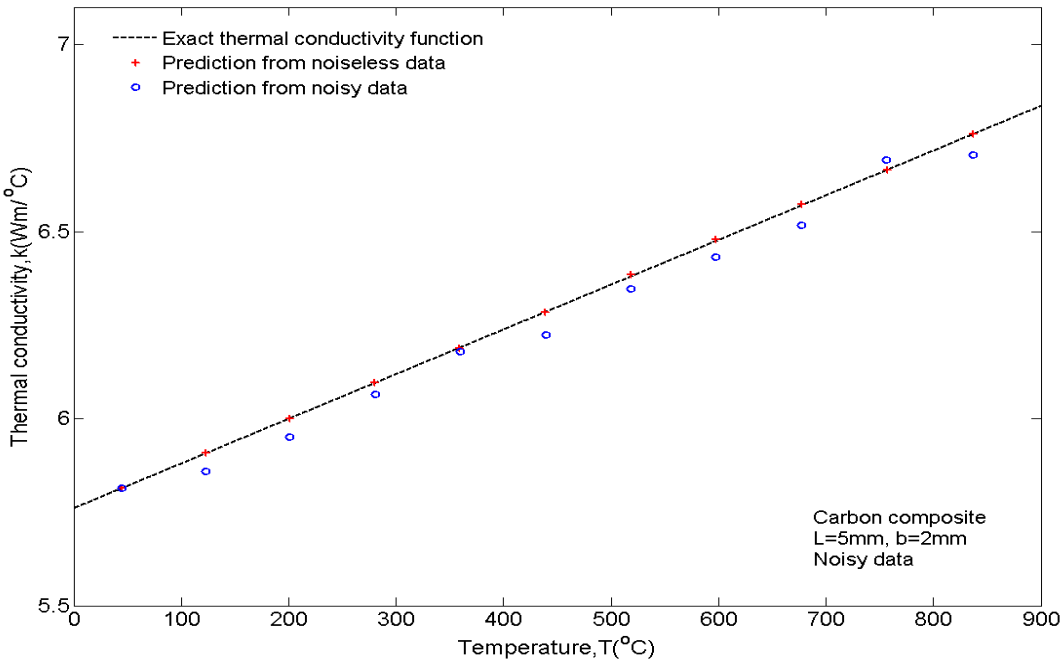

Figure 6.3.14: Predicted thermal conductivity for carbon composite based on noisy data.

Table 6.3.9: Accuracy analysis for estimated thermophysical property of stainless steel (L=5mm, b=2mm, noisy data).

Mean Temp $\overline{T}_{M,r}$ (K)	**Exact α (cm^2/s)**	**Predicted α (cm^2/s)**	**Exact k (W/mK)**	**Predicted k (W/mK)**
400.43	0.0408	0.0407	16.50	16.45
479.65	0.0425	0.0423	17.78	17.73
559.01	0.0441	0.0442	19.04	19.08
638.46	0.0458	0.0456	20.29	20.23
717.99	0.0474	0.0472	21.51	21.45
797.57	0.0490	0.0486	22.72	22.58
877.19	0.0506	0.0505	23.90	23.90
956.85	0.0521	0.0514	25.07	24.78
1036.53	0.0535	0.0533	26.22	26.15
1116.24	0.0550	0.0545	27.34	27.13

Table 6.3.10: Accuracy analysis for estimated thermophysical property of carbon composite (L=5mm, b=2mm, noisy data).

Mean Temp $\overline{T}_{M,r}$ (K)	**Exact α (cm^2/s)**	**Predicted α (cm^2/s)**	**Exact k (W/mK)**	**Predicted k (W/mK)**
395.67	0.0281	0.0276	5.91	5.86
474.20	0.0259	0.0253	6.00	5.95
553.69	0.0244	0.0238	6.10	6.06
633.14	0.0233	0.0229	6.19	6.18
712.48	0.0226	0.0219	6.28	6.22
791.31	0.0221	0.0215	6.38	6.35
870.70	0.0218	0.0212	6.47	6.43
950.56	0.0216	0.0209	6.57	6.52
1029.80	0.0215	0.0212	6.66	6.69
1109.85	0.0216	0.0209	6.76	6.70

6.4 Conclusions

This chapter proposes a novel calibration approach that incorporates rescaling principles for estimating the temperature-dependent thermophysical properties of materials. The proposed calibration approach relies on the assumption that all thermophysical properties in both the calibration and reconstruction test can be considered as constants over a fixed and incremental temperature range. A proper temperature range that permits this assumption is required for all tests. The rescaling temperature calibration equation is used for estimating the thermal diffusivity. The estimated thermal diffusivity is combined with the rescaling net heat flux calibration equation to predict the thermal conductivity. Results verify that the new property estimation approach works well for both a representative carbon composite and stainless steel sample. Due to the limitation of the linearization assumption, an optimal slab thickness may exist corresponding to the choice of material and input heat flux. Some additional predicative improvement could result if implemented. Finally, this approach does not require the explicit knowledge of the slab thickness or probe position.

This new thermophysical property estimation method has additional advantage for resolving the unknown surface thermal condition in a nonlinear one-dimensional thermal system. The nonlinear calibration equation [112] requires the Kirchhoff transformation and time domain rescaling to make the quasi-linearization. Also, the implementation of both the Kirchhoff transformation and the time domain rescaling rely on the knowledge of the thermal conductivity and diffusivity ratio. These ratios could be obtained through the temperature and heat flux calibration methods (Eq. (6.2.7) and Eq. (6.2.12)) proposed in this dissertation since both of

these equations are represented in terms of ratios. Therefore, it is possible to acquire the thermophysical property ratio function without the specification of the thermophysical properties during the calibration temperature range (near room temperature) and then use the calculated property ratio functions to resolve the unknown surface thermal condition based on the nonlinear calibration equation.

Chapter 7: Conclusion and Recommendation for Future Research

This dissertation provides a novel approach for resolving the nonlinear one-dimensional inverse heat conduction problems with temperature-dependent thermophysical properties. A new rescaling principle is introduced and combined with a calibration concept [43-45] to derive a series of calibration equations that are available for both linear and nonlinear inverse heat conduction problems. To regularize the ill-posed system associated with the proposed calibration equations, a new regularization parameter search strategy is proposed independent of the applied regularization approach. To illustrate the versatility of the methodology, the calibration and rescaling principles are also applied for estimating thermophysical properties.

7.1 Conclusions

In Chapter 2, the linear one-probe calibration method [43-45] relating the unknown surface (net) heat flux or temperature to a single in-depth temperature measurement are reviewed for the one-dimensional linear heat equation. The Laplace transform technique [33] is used to obtain the exact solution. The surface heat flux and temperature calibration equations given by Eq. (2.2.10) and Eq. (2.3.8) are constructed based on equating the impulsive thermal responses given by Eq. (2.2.7a) and Eq. (2.3.6) in the frequency domain. Both equations are applicable to constant thermophysical properties with a passive side boundary condition that maintains a constant heat transfer coefficient on the backside boundary between the calibration and reconstruction tests.

Chapter 3 generalizes the one-probe linear calibration method to a nonlinear framework. Quasi-linearization is achieved by combining the principle of time domain rescaling as given by Eq. (3.2.15a) and the Kirchhoff transform given by Eq. (3.2.2). In this process, the Kirchhoff transformation is exploited for linearizing the temperature-dependent thermal conductivity. Time domain rescaling is incorporated for linearizing the temperature-dependent thermal diffusivity. The reliability of this quasi-linearization relies on the piecewise time-step linearization assumption. That is, at each time step, the thermophysical properties are held constant throughout the spatial domain though they are allowed to vary with advancing time. Results displayed in Figure 3.4.26 justify the accuracy of this new calibration equation given by Eq. (3.2.15d) for resolving the unknown surface heat flux in stainless steel 304. In this test, significant temperature-dependent effects and noise are present.

The nonlinear calibration equation presented in Chapter 3 is limited to an adiabatic back boundary condition. Chapter 4 introduces a new calibration method that permits both a varying back boundary condition and temperature-dependent thermophysical properties. This method combines the attributes of the linear two-probe calibration formulation [43-45] with the nonlinear one-probe calibration equation [112]. Unlike the one-probe calibration method, the second temperature measurement at $x = w,\ T(w,t)$ is required to eliminate the Robin's condition imposed at $x = L$ given by Eq. (4.2.1c). Correspondingly, two distinct calibration tests are required in the test campaign rather than one. Figures 4.4.19-4.4.26 verify that this new two-probe calibration method given by Eq. (4.2.24) is applicable to both stainless steel 304 and a representative carbon composite. Comparisons between Fig. 4.4.27a and Fig. 4.4.27b; and, Fig.

4.4.28a and Fig. 4.4.28b show that the ill-conditioning effects imposed by the kernel can significantly be reduced when cooling (first calibration test) and heating (second calibration test) back boundary condition combinations are applied. Figures 4.4.32a and 4.4.32b indicate that the prediction for unknown surface heat flux is both stable and accurate in the presence of a significant noise.

Chapter 5 introduces a new strategy for estimating the optimal regularization parameter that is independent of applied regularization technique. Each previously described calibration equation in Chapters 2-4 is expressed in term of a Volterra integral equation of the first kind. This form of functional equation is ill-posed and hence requires regularization. For this purpose, the L-curve strategy [83] is applied for estimating the optimal regularization parameter. However, the L-curve strategy strongly depends on the visualization of the elbow (Fig. 3.4.23). A poor visualization of the elbow leads to either an over-smoothed or oscillatory prediction. The new parameter search strategy given by Eq. (5.3.10a) is based on Gaussian filtering the surface heat flux prediction sets given by Eq. (5.3.10b) and Eq. (5.3.11a) for estimating the variance. The normalized residual given by Eq. (5.3.10c) is applied for evaluating the model bias. The best regularization parameters are obtained by balancing the weighted bias and variance. The effectiveness of this method is examined through three common regularization approaches; namely, the classical Tikhonov regularization approach [82], the singular-value decomposition (SVD) based method [80,81] and the local future-time method [8]. Figures 5.4.22-5.4.4.30 present encouraging results in the presence of significant noise for a representative carbon composite. Over-smoothness in the final prediction is avoided while the stability is maintained.

Chapter 6 presents an extension of the calibration method for estimating unknown thermophysical properties. This approach utilizes a single in-depth temperature measurement and a set of known boundary conditions throughout the test campaign. To acquire both thermal diffusivity and thermal conductivity, two distinct test stages are proposed for extracting these properties. The first stage relies on the temperature calibration equation given by Eq. (6.2.7) for estimating the unknown thermal diffusivity. This stage determines the thermal diffusivity by minimizing the residual of the temperature calibration equation with respect to the thermal diffusivity. Figure 6.3.4 graphically describes how the thermal diffusivity is selected. The second stage uses the estimated thermal diffusivity and the heat flux calibration equation given by Eq. (6.2.12) for estimating the unknown thermal conductivity. This stage produces the desired thermal conductivity by minimizing the residual of the heat flux calibration equation with respect to the thermal conductivity. Figures 6.3.5-6.3.8 illustrate that the proposed calibration equation accurately estimate both the thermal conductivity and thermal diffusivity in the context of stainless steel 304 and a representative carbon composite. Significant flexibility exists in the selection of the slab thickness and probe position. Figures 6.3.11-6.3.14 indicate that the proposed parameter estimation remained stable and accurate even in the presence of significant noise.

7.2 Recommendations for Future Research

Chapters 3-6 provide details of a new methodology for resolving inverse heat conduction problems based on numerically simulated data. However, experimental verification is still required since additional nuances exist in experimental systems beyond what is normally

imposed in a computational study. To verify the nonlinear calibration equations (Chapter 3 and 4) for resolving unknown surface heat flux, one could use a high-powered laser that would impinge energy on the front surface of the carefully designed and instrumental specimen. The spectral absorptivity and total hemisphere emissivity of this surface must be known in advance to determine the net surface heat flux required by the calibration tests. In addition, prior to resolving the net unknown surface heat flux for the reconstruction test, one would need the surface temperature during the calibration tests such that the radiation losses at the heated surface could be properly accounted. However, direct measurement of the surface temperature is difficult even in the laboratory. A method for avoiding this obstacle would require the addition of another layer (calibration plate) perfected attached onto the front heating surface of the specimen. The calibration plate needs to be thin and possess a high thermal conductivity such that the temperature distribution in this plate could be considered as spatially uniform. A probe would be inserted into this layer to measure its temperature history. Though this temperature measurement does not equal to the temperature at the front surface of the sample due to contact resistance, the net heat flux entering the front surface of the sample could be determined through an energy balance. A filter might be necessary for calculating the time derivative of temperature associated with energy in the calibration plate. Natural convection effects can be shown to be minimum at elevated temperatures and hence neglected.

To experimentally verify the unknown thermophysical property estimation method, an electrically heated sandwich facility [117] is recommended. The proposed parameter estimation method includes two stages. The first stage involves applying the temperature calibration equation given by Eq. (6.2.7) to estimate the unknown thermal diffusivity. However, the surface

temperature in Eq. (6.2.7) is difficult to directly measure. To handle this issue, two in-depth temperature measurements could be implemented instead of using a surface and single in-depth sensor arrangement. In this process, two in-depth sensors can be located at $x = b$ and $x = w$. If $b < w$ then the probe closer to the active side would be considered as new "surface" temperature $T(b, t)$ while the temperature data $T(w, t)$ would be considered as new sensor response. When the thermal diffusivity function is determined, the second stage would utilize the estimated thermal diffusivity and heat flux calibration equation given by Eq. (6.2.12) to predict the unknown thermal conductivity. In this process, the symmetric heating provided by the electrically heated sandwich facility is able to remove the constraint of accounting for radiation effects in the front surface.

This dissertation combines the calibration equation with a rescaling principle to account for temperature-dependent thermophysical properties in a one-dimensional setting. However, multi-dimensional and multi-layer equations have not been considered in the context of this proposed framework. Careful analysis is required to consider the possibility of forming the multi-dimensional and multi-layer calibration equations in the nonlinear framework using rescaling or other principles.

List of References

[1] Tarantola, A., *Inverse Problem Theory and Methods for Model Parameter Estimation*, SIAM, Paris, France, 2005.

[2] Nguyen, K.M., Truong, T.T., Bui, H.D., and Delabre, J.L., "A Novel Inverse Problem in γ-Rays Emission Imaging", *Inverse Problems in Science and Engineering*, Vol.12, No.2, 2004, pp. 225-246.

[3] Hirst, B., Gillespie, S., and Podlaha, O., "Oil and Gas Prospecting by Ultra-Sensitive Optical Gas Detection with Inverse Gas Dispersion Modeling", *Geophysical Research Letters*, Vol.31, No.12, 2004, L12115.

[4] Volegova, A.A., and Stepanov, R.A., "Helicity Detection Astrophysical Magnetic Fields from Radio Emission Statistics", *JETP Letters*, Vol.90, No.10, 2010, pp. 637-641.

[5] Bui, H.D., Chaillat, S., Constantinescu, A., and Grasso. E., "Identification of a Planar Crack in Zener Type Viscoelasticity", *Annals of Solid and Structure Mechanics*, Vol.1, No.1, 2010, pp. 3-8.

[6] Benedetti, M., Lesselier, D., Lambert, M., and Massa, A., "A Multi-Resolution Technique based on Shape Optimization for the Reconstruction of Homogeneous Dielectric Objects", *Inverse Problems*, Vol.25, No.1, 2009, 015009.

[7] Gatenby, R.A., Maini, P.K., and Gawlinski, E. T., "Analysis of Tumor as an Inverse Problem Provides a Novel Theoretical Framework for Understanding Tumor Biology and Therapy", *Applied Mathematics Letters*, Vol.15, No.3, 2002, pp. 339-345.

[8] Beck, J.V., Blackwell, B., and St. Chair, C.R., *Inverse Heat Conduction Ill-Posed Problems*, Wiley, New York, 1985.

[9] Shumakov, N.V., "A Method for the Experiment Study of the Process of Heating a Solid Body", *Soviet Physics-Technical Physics*, Vol.2, 1957, pp. 771-781.

[10] Stolz, G., Jr., "Numerical Solution to an Inverse Problem of Heat Conduction for Simple Shapes", *Journal of Heat Transfer,* Vol.82, 1960, pp.20-26.

[11] France, D.M., and Chiang T., "Analytical Solution to Inverse Heat Conduction Problems with Periodicity", *Journal of Heat Transfer,* Vol.102, 1980, pp. 579-581.

[12] Howse, T.K.J., Kent, R., and Rawson, H., "The Determination of Glass-Mould Heat Fluxes from Mould Temperature Measurements", *Glass Technology*, Vol.12, 1971, pp.91-93.

[13] Alkidas, A.L., "Heat Transfer Characteristics of Spark-Ignition Engine", *Journal of Heat Transfer,* Vol.102, 1980, pp.189-193.

[14] Vyacheslav, S.V., *Heat Conduction-Basic Research*, InTech, Croatia, 2011.

[15] Beck, J.V., Litkouhi, B., and St. Chair, C.R., "Efficient Sequential Solution of the Nonlinear Inverse Heat Conduction Problem", *Numerical Heat Transfer*, Vol.5, No.3, 1982, pp.275-286.

[16] Alifanov, O.M., "Solution of an Inverse Problem of Heat Conduction by Iteration Methods", *Journal of Engineering Physics*, Vol.26, No.4, 1974, pp.471-476.

[17] Cialkowski, M.J., and Grysa, K., "A Sequential and Global Method of Solving an Inverse Problem of Heat Conduction", *Journal of Theoretical and Applied Mechanics,* Vol.48, No.1, 2010, pp.111-134.

[18] Reinhardt, H.J., Hao, D.N., Frohne, J., and Suttmeier, F.T., "Numerical Solution of Inverse Heat Conduction Problems in Two Spatial Dimensions", *Journal of Inverse and Ill-Posed Problems*, Vol.15, No.5, 2007, pp.181-198.

[19] Shiguemori, H.E., Da Silva, J.D., and De Campos Velho, H.F., "Estimation of Initial Conduction in Heat Conduction by Neural Network", *Inverse Problems in Science and Engineering*, Vol.12, No.3, 2004, pp.317-328.

[20] Pereverzyev, S.S., "Initial Temperature Reconstruction for Nonlinear Heat Equation: Application to a Coupled Radiative-Conductive Heat Transfer Problem", *Inverse Problems in Science and Engineering*, Vol.16, No.1, 2005, pp. 55-67.

[21] Sawaf, B., and Ozisik, M.N., "An Inverse Analysis to Estimate Linearly Temperature Dependent Thermal Conductivity Components and Heat Capacity of an Orthotropic Medium", *International Journal of Heat and Mass Transfer*, Vol.38, No.16, 1995, pp. 3005-3010.

[22] Onyango, T.T.M., Ingham, D.B., and Lesnic, D., "Reconstruction of Heat Transfer Coefficients Using the Boundary Element Method", *Computers and Mathematics with Application*, Vol.56, No.1, 2008, pp.114-126.

[23] Yi, Z., and Murio, D.A., "Source Term Identification in 1-D IHCP", *Computers and Mathematics with Applications*, Vol.47, 2004, pp.1921-1933.

[24] Ikehata, M., "An Inverse Source Problem for the Heat Equation and the Enclosure Method", *Inverse Problems*, Vol.23, No.1, 2007, pp.183-202.

[25] Fan, Y., and Li, D.G., "Identifying the Heat Source for the Heat Equation with Convection Term", *International Journal of Mathematical Analysis*, Vol.3, No.27, 2009, pp.1317-1323.

[26] Cheng, C.H., and Chang, M.H., "Shape Design for Cylinder with Uniform Temperature Distribution on the Outer Surface by Inverse Heat Transfer Model", *International Journal of Heat and Mass Transfer*, Vol.46, No.1, 2003, pp. 101-111.

[27] Ren, H.S., "Application of the Heat-Balance Integral to an Inverse Stefan Problem", *International Journal of Thermal Science*, Vol.15, No.5, 2007, pp.118-127.

[28] Orlande, R.B., "Inverse Problems in Heat Transfer: New Trends on Solution Methodologies and Applications", *Journal of Heat Transfer*, Vol. 134, 2012, 031011, pp.1-13.

[29] Myers, G.E., *Analytical Methods in Conduction Heat Transfer*, AMCHT Publications, Madison, WI, 1998.

[30] Feng, Z.C., Chen, J.K., and Zhang, Y.W., "Real-Time Solution of Heat Conduction in a Finite Slab for Inverse Analysis", *International Journal of Thermal Science*, Vol.49, 2012, pp.762-768.

[31] Monde, M., and Misutake, Y., "Analytical Method in Inverse Heat Transfer Problem Using Laplace Transform Technique", *International Journal of Heat and Mass Transfer*, Vol.43, No.21, 2000, pp.3965-3975.

[32] Monde, M., Arima, H., Liu, W., Mitutake, Y., and Hammad, J.A., "An Analytical Solution for Two-Dimension Inverse Heat Conduction Problems Using Laplace Transform", *International Journal of Heat and Mass Transfer*, Vol.46, 2003, pp.2135-2148.

[33] Ozisik, M.N., *Heat Conduction*, John Wiley and Sons, New York, 1980.

[34] Beck, J.V., "Calculation of Surface Heat Flux from an Internal Temperature History", *ASME Paper*, No.62-HT-46, 1962.

[35] Beck, J.V., Blackwell, B., and Haji-Sheikh, "A Comparison of Some Inverse Heat Conduction Methods Using Experiment Data", *International Journal of Heat and Mass Transfer*, Vol.39, No.17, 1996, pp.3649-3657.

[36] Beck, J.V., "Filter Solutions for the Nonlinear Inverse Heat Conduction Problem", *Inverse Problems in Science and Engineering*, Vol.16, No.1, 2008, pp.3-20.

[37] Burggraf, O.R., "An Exact Solution of the Inverse Problem in Heat Conduction Theory and Application", *Journal of Heat Transfer*, Vol. 86, 1964, pp.373-382.

[38] Trefftz, E., "Ein Gegenstuck zum Ritzschen Vefahren", *Proceedings of the 2nd International Congress of Applied Mechanics*, Orell Fussli Verlag, Zurich, Switzerland, 1926.

[39] Osborne, G.E., Frankel, J.I., and Keyhani, M., "The Function Decomposition Method and its Application in Thermal Inverse Analysis", *Proceedings of the ASME Heat Transfer Division*, Vol.5, 1998, pp.117-129.

[40] Loehle, S., Battaglia, J.L., and Batsale, J.C., "Estimation of High Heat Flux in Supersonic Plasma Flows", *Proceedings of IEEE Industry Electronics*, Vol.4, 2006, pp.5336-5373.

[41] Loehle, S., Battaglia, J.L., and Jullien, P., "Improvement of High Heat Flux Measurement Using a Null Point Calorimeter", *AIAA Journal of Spacecraft and Rocket*, Vol.23, 2008, pp.76-81.

[42] Gardarein, J.L., Battaglia, J.L., Loehle, S., "Heat Flux Sensor Calibration Using Non-integral System Identification: Theory, Experiment and Error Analysis", *Review of Scientific Instruments*, Vol.80, 2009, 205102.

[43] Frankel, J.I., and Keyhani, M., "A New Surface Heat Flux Calibration Method for Thin-Film Resistive Temperature Gauges and Co-Axial Thermocouples", *Shock Waves*, Vol.23, 2013, pp. 177-188.

[44] Frankel, J.I., Keyhani, and M., Elkins, B.S. "Surface Heat Flux Prediction through Physics-based Calibration- Part 1: Theory", *AIAA Journal of Thermophysics and Heat Transfer*, Vol.27, 2013, pp.189-205.

[45] Elkins, B.S., Keyhani, M., and Frankel, J.I. "Surface Heat Flux Prediction through Physics-based Calibration- Part 2: Experimental Verification", *AIAA Journal of Thermophysics and Heat Transfer*, Vol.27, 2013, pp.206-216.

[46] Incropera, F.P., Dewitt, D.P, Bergman, T.L., and Lavine, A.S., *Fundamentals of Heat and Mass Transfer, 6th Edition*, Wiley, New York, 2006.

[47] Pourgholi, R., Esfahani, A., and Abtahi, M., "A Numerical Solution of a Two-Dimensional IHCP", *Journal of Applied Mathematics and Computing*, Vol.41, 2013, pp.61-79.

[48] Carasso, A.S., "Space Marching Difference Schemes in the Nonlinear Inverse Heat Conduction Problem", *Inverse Problems*, Vol.8, No.1, 1992, pp. 25-43.

[49] Carasso, A.S., "Slowly Divergent Space Marching Schemes in the Inverse Heat Conduction Problems", *Numerical Heat Transfer, Part.B*, Vol.23, No.1, 1992, pp. 111-126.

[50] Murio, D.A., and Hinestroza, D., "The Space Marching Solution of the Inverse Heat Conduction Problem and the Identification of the Initial Temperature Distribution", *Computer and Mathematics with Applications*, Vol.25, No.4, 1993, pp.55-63.

[51] Al-Khalidy, N., "Analysis of Boundary Inverse Heat Conduction Problems Using Space Marching with Sacitzky-Gollay Digital Filter", *International Communications in Heat and Mass Transfer*, Vol.26, No.2, 1999, pp.199-208.

[52] Elkins, B.S., Keyhani, M., and Frankel, J.I, "Global Time Method for Inverse Heat Conduction Problem", *Inverse Problems in Science and Engineering*, Vol.20, No.5, 2012, pp.651-664.

[53] Ling, X., Cherukuri, H.P., and Cherukuri, H.P., "A Modified Sequential Function Specification Finite Element Based Method for Parabolic Inverse Heat Conduction Problems", *Computational Mechanics*, Vol.36, 2005, pp. 117-128.

[54] Lu, T., Liu, B., and Jiang, P.X., "Inverse Estimation of the Inner Wall Temperature Fluctuations in a Pipe Elbow", *Appl. Therm. Eng.*, Vol.31, No.11-12, 2011, pp. 1976-1982.

[55] Pasquetti, R., and Niliot, C.L., "Boundary Element Approach for Inverse Heat Conduction Problems: Application to a Bidimensional Transient Numerical Experiment", *Numerical Heat Transfer, Part B*, Vol.20, No.20, 1991, pp.169-181.

[56] Onyango, T.T.M., Ingham, D.B., and Lesnic, D., "Restoring Boundary Conditions in Heat Conduction", *Journal of Engineering Mathematics,* Vol.62, 2008, pp.85-101.

[57] Beck, J.V., and Arnold, K.J., *Parameter Estimation in Engineering and Science*, Wiley, New York, 1977.

[58] Khajehpour, S., Hematiyan, M.R., and Marin, L., "A Domain Decomposition Method for the Stable Analysis of Inverse Nonlinear Transient Heat Conduction Problems", *International Journal of Heat and Mass Transfer*, Vol. 58, No.1-2, 2013, pp.125-132.

[59] Ozisik, M.N., and Orlande, H.R.B., *Inverse Heat Transfer: Fundamental and Applications*, Taylor & Francis, New York, 2000.

[60] Zhou, J.H., Zhang, Y.W., Chen, J.K., and Feng, Z.C., "Inverse Estimation of Surface Heating Condition in a Three-Dimensional Object Using Conjugate Gradient Method", *International Journal of Heat and Mass Transfer,* Vol. 53, 2010, pp.2643-2654.

[61] Huang, C.H., and Chen, W.C., "A Three-Dimensional Inverse Forced Convection Problem in Estimating Surface Heat Flux by Conjugate Gradient Method", *International Journal of Heat and Mass Transfer,* Vol. 43, 2000, pp.3171-3181.

[62] Hasanov, A., and Pektas, B., "Identification of an Unknown Time-Dependent Heat Source Term from Overspecified Dirichlet Boundary Data by Conjugate Gradient Method", *Computers and Mathematics with Application,* Vol. 65, 2013, pp.42-57.

[63] Levenberg, K., "A Method for the Solution of Certain Non-Linear Problems in Least Squares", *Quarterly of Applied Mathematics,* Vol.2, 1944, pp.164-168.

[64] Marquardt, D.W., "An Algorithm for Least Squares Estimation of Nonlinear Parameters", *Journal of the Society for Industrial and Applied Mathematics,* Vol.11, 1963, pp.431-441.

[65] Rouquette, S., Guo, J., and Masson, P.L., "Estimation of the Parameter of a Gaussian Heat Source by the Levenberg-Marquardt Method: Application to the Electron Beam Welding", *International Journal of Thermal Sciences,* Vol.46, No.2, 2007, pp. 128-138.

[66] Colaco, M.J., Orlande, H.R.B., and Dulikravich, G.S., "Inverse and Optimization Problems in Heat Transfer", *Journal of the Brazilian Society of Mechanical Sciences and Engineering*, Vol.28, 2006, pp.1-24.

[67] Gosselin, L., Tye-Gringras, M., and Mathieu-Potvin, F., "Review of Utilization of Genetic Algorithms in Heat Transfer Problems", *International Journal of Heat and Mass Transfer,* Vol. 52, 2009, pp.2169-2188.

[68] Jones, M.R., Tezukaa, A., and Yamada, Y., "Thermal Tomographic Detection of Inhomogeneities", *Journal of Heat Transfer-Transactions of the ASME 117*, Vol.4, 1995, pp.969-975.

[69] Verma, S., and Balaji, C., "Multi-Parameter Estimation in Combined Conduction Radiation form a Plane Parallel to Participating Medium Using Genetic Algorithms", *International Journal of Heat and Mass Transfer,* Vol. 50, No.9-19, 2007, pp.1706-1714.

[70] Raudensky, M., Woodbury, K.A., Kral, J., and Brezina, T., "Genetic Algorithm in Solution of Inverse Conduction Problems", *Numerical Heat Transfer*, *Part B*, Vol.28, No.3, 1995, pp.293-306.

[71] Raudensky, M., Horsky, J., and Krejsa, J., "Usage of Neural Network for Coupled Parameter and Function Specification for Inverse Heat Conduction Problem", *International Communications in Heat and Mass Transfer,* Vol.22, No.5, 1995, pp.661-670.

[72] Deng, S., and Hwang, Y., "Applying Neural Networks to the Solution of Forward and Inverse Heat Conduction Problems", *International Journal of Heat and Mass Transfer*, Vol.49, 2006, pp.4732-4750.

[73] Deng, S., and Hwang, Y., "Solution of Inverse Heat Conduction Problems using Kalman Filter Enhanced Bayesian Back Propagation Neural Network Data Fusion", *International Journal of Heat and Mass Transfer*, Vol.50, No.11-12, 2007, pp.2089-2100.

[74] Frankel, J.I., "Regularization of Inverse Heat Conduction by Combination of Rate Sensor Analysis and Analytical Continuation", *Journal of Engineering Mathematics*, Vol.57, 2007, pp.181-198.

[75] Deng, Z.L., Fu, C.L., Feng, X.L., Zhang, Y.X., "A Mollification Regularization Method for Stable Analytical Continuation", *Mathematics and Computers in Simulation*, Vol.81, 2011, pp.1593-1608.

[76] Welch, G., and Bishop, G., *An Introduction to the Kalman Filter*, UNC-Chapel Hill, North Carolina, 2006.

[77] Ijaz, U.Z., Khambampati, A., Kim, M.C., and Kim, K.Y., "Estimation of Time-Dependent Heat Flux and Measurement Bias in Two Dimensional Inverse Heat Conduction Problems", *International Journal of Heat and Mass Transfer*, Vol.49, 2006, pp. 4117-4130.

[78] LeBreux, M., Desilets, M., and Lacroix, M., "Fast Inverse Prediction of Phase Change Banks in High Temperature Furnaces with a Kalman Filter Coupled with a Recursive Least-Square Estimator", *International Journal of Heat and Mass Transfer*, Vol.53, 2010, pp.5250-5260.

[79] Linz, P., *Analytical and Numerical Methods for Volterra equations*, SIAM, Philadelphia, 1985.

[80] Shenefelt, J.R., Luck, R., Taylor, R.P., and Berry, J.T., "Solution to Inverse Heat Conduction Problems Employing Singular Value Decomposition and Model-Reduction", *International Journal of Heat and Mass Transfer*, Vol.45, No.1, 2002, pp.67-74.

[81] Garcia, J.A.M., Cabeza, J.M.G., and Rodriguez, A.C., "Two-Dimensional Non-Linear Inverse Heat Conduction Problem Based on Singular Value Decomposition", *International Journal of Thermal Sciences*, Vol.43, No.2, 2004, pp. 145-155.

[82] Tikhonov, A.N., and Arsenin, V.Y., *On the Solution of Ill-Posed Problems*, John Wiley and Sons, New York, 1977.

[83] Hanson, P.C., and O'Leary, D.P., "Analysis of Discrete Ill-Posed Problems by Means of the L-Curve", *SIAM Review*, Vol.34, 1992, pp.561-580.

[84] Morozov, V.A., *Method for Solving Incorrectly Posed Problems*, Springer, New York, 1984.

[85] Engl, H.W., Hanke, M., and Neubauer, A., *Regularization of Inverse Problems*, Kluwer Academic Publishers, the Netherlands, 1996.

[86] Lamm, P.K., "Full Convergence of Sequential Local Regularization Methods for Volterra Inverse Problems", *Inverse Problems*, Vol.21, 2005, pp.785-803.

[87] Berntsson, F., "An Inverse Heat Conduction Problem and Improving Shielded Thermocouple Accuracy", *Numerical Heat Transfer, Part A*, Vol.61, No.10, 2012, pp.754-763.

[88] Jarny, Y., Ozisik, M.N., and Bardon, J.P., "A General Optimization Method Using Adjoint Equation for Solving Multidimensional Inverse Heat Conduction", *International Journal of Heat and Mass Transfer*, Vol.34, 1991, pp.2911-2919.

[89] Alifanov, O., "Mathematical and Experiment Simulation in Designing and Testing Heat-Loaded Engineering Objects", *Inverse Problems in Engineering: Theory and Practice*, Vol.1, 2002, pp.12-21.

[90] Calvetti, D., and Somersalo, E., *Introduction to Bayesian Scientific Computing*, Springer, New York, 2007.

[91] American National Standard, "Stand Method of Test for Thermal Conductivity of Materials by Means of Guarded Hot Plate", *ASTM Comm.* C-16, designation C177-71, 1971, pp. 15-28.

[92] Beck, A., Sc., B., and Inst, P.A., "A Steady State Method for the Rapid Measurement of the Thermal Conductivity of Rocks", *Journal of Scientific Instruments*, Vol.34, No.5, 1957, pp. 186-189.

[93] Blackwell, J.H., "A Transient-Flow Method for Determination of Thermal Constants of Insulating Materials in Bulk Part 1-Theory", *Journal of Applied Physics*, Vol.25, No.2, 1954, pp.137-145.

[94] Herzen, R.V., "The Measurement of Thermal Conductivity of Deep-Sea Sediments by a Needle-Probe Method", Journal of Geophysical Research, Vol.64, No.10, 1959, pp. 1557-1563.

[95] Lobo, H., and Cohen, C., "Measurement of Thermal Conductivity of Polymer Melts by the Line-Source Method", *Polymer Engineering and Science*, Vol.30, 1990, pp.65-70.

[96] Coufal, H., and Hefferle, P., "Thermal Diffusivity Measurements of Thin Films with a Pyroelectric Calorimeter", *Applied Physics A*, Vol.38, 1985, pp. 213-219.

[97] Kato, R., Maesono, A., and Hatta, I., "Thermal Diffusivity Measurements of a Thin Film in the Direction across the Film by AC Calorimetric method", *Journal of Applied Physics*, Vol.32, 1993, pp. 6353-6355.

[98] Parker, W.J., Jenkins, R.J., Butler, C.P., and Abbott, G.L., "Flash Method of Determining Thermal Diffusivity, Heat Capacity and Thermal Conductivity", *Journal of Applied Physics*, Vol.32, 1961, pp. 1679-1684.

[99] Clark III, L.M., and Taylor, R.E., "Radiation Loss in the Flash Method for Thermal Diffusivity", *Journal of Applied Physics*, Vol.46, 1975, pp. 714-719.

[100] James, H.M., "Some Extension of the Flash Method of Measuring Thermal Diffusivity", *Journal of Applied Physics*, Vol.51, 1980, pp. 4666-4672.

[101] Baba, T., and Ono, A., "Improvement of the Laser Flash Method to Reduce Uncertainty in Thermal Diffusivity Measurements", *Measurement Science and Technology*, Vol.12, 2001, pp. 2046-2057.

[102] Gaal, P.S., Thermitus, M.A., and Stroe, D.E., "Thermal Conductivity Measurements Using Flash Method", *Journal of Thermal Analysis and Calorimetry*, Vol. 78, 2004, pp. 185-189.

[103] Sato, Y., and Taira, T., "The Studies of Thermal Conductivity in $GdVO_4$, YVO_4, and Y_3AlO_{12} Measured by Quasi-One-Dimensional Flash Method", *Optics Express*, Vol.14. No.22, 2006, pp. 10528-10536.

[104] Monde, M., and Mitsutake, Y., "A New Estimation Method of Thermal Diffusivity Using Analytical Inverse Solution for One-Dimensional Heat Conduction", *International Journal of Heat and Mass Transfer*, Vol.44, 2001, pp.3169-3177.

[105] Huang, C.H., and Yan, J.Y., "An Inverse Problem in Simultaneously Measuring Temperature-Dependent Thermal Conductivity and Heat Capacity", *International Journal of Heat and Mass Transfer*, Vol.38, 1995, pp.3433-3441.

[106] Battaglia, J.L., Schick,V., and Rossignol, C., "Global Estimation of Thermal Parameters from a Picoseconds Thermoreflectometry Experiment", *International Journal of Thermal Sciences*, Vol.57, 2012, pp. 17-24.

[107] Chen, H.T., and Lin, J.Y., "Simultaneous Estimation of Temperature-Dependent Thermal Conductivity and Heat Capacity", *International Journal of Heat and Mass Transfer*, Vol.41, No.14, 1998, pp.2237-2244.

[108] Garcia, S., and Scott, E.P., "Use of Genetic Algorithms in Thermal Property Estimation: Part 1-Experimental Design Optimization", *Numerical Heat Transfer, Part A*, Vol.33, 2007, pp.135-147.

[109] Garcia, S., and Scott, E.P., "Use of Genetic Algorithms in Thermal Property Estimation: Part 2-Simultaneous Estimation of Thermal Properties", *Numerical Heat Transfer, Part A*, Vol.33, 2007, pp.149-168.

[110] D'Souza, N., "Numerical Solution of One-Dimensional Inverse Transient Heat Conduction by Finite Difference Method", *ASME Paper*, No. 75-WA/HT-81, Winter Annual Meeting, Houston, TX, 1974.

[111] Frankel, J.I., Keyhani, M., "Calibration Integral Equation Method for Two-Probe Inverse Heat Conduction Analysis", *Journal of Thermophysics and Heat Transfer*, Vol.28, 2014, pp.548-553.

[112] Chen, Y.Y., Frankel, J.I., and Keyhani, M., "A New Nonlinear Surface Heat Flux Calibration Method based on Kirchhoff Transformation and Rescaling Principles", *Inverse Problems in Science and Engineering*, Vol.22, No.8, 2014, pp. 1394-1421.

[113] McCarthy, P.J., "Direct Analytical Model of the L-curve for Tikhonov Regularization Parameter Selection", *Inverse Problems*, Vol.19, 2009, pp.643-663.

[114] Taler, J.,"A New Space Marching Method for Solving Inverse Heat Conduction Problems", *Forschungim Ingenieurwesen*, Vol.66, 1999, pp.296-306.

[115] Kimmel, R.L., and Adamczak, D., "HIFIRE-1 Preliminary Aerothermodynamic Measurement", *AIAA paper*, 2011-3413, 41st AIAA Fluid Dynamics Conference and Exhibit, Honolulu, Hawaii, 2011.

[116] Vadasz, P., "Analytical Solution to Nonlinear Thermal Diffusion: Kirchhoff versus Cole-Hopf Transformations", *Journal of Heat Transfer*, Vol.132, 2010, 121302-(1-6).

[117] Jake, J., Elkins, B.S., Keyhani, M., and Frankel, J.I., "Heat Transfer Analysis via Rate based Sensors", *AIAA paper*, 2012-0810, 50th AIAA Aerospace Sciences Meeting and Exhibit, Nashville, TN, 2012.

[118] Elkins, B.S., Keyhani, M, Frankel, J.I., "A New Fully Implicit Inverse Heat Conduction Method", *AIAA* paper, 2008-1189, 46th AIAA Aerospace Sciences Meeting and Exhibit, Reno, NV, 2008.

[119] Kavianipour, A., Beck, J.V., "Thermal Property Estimation Utilizing the Laplace Transformation with Application to Asphaltic Pavement", *International Journal of Heat and Mass Transfer*, Vol.20, 1977, pp. 259-267.

[120] Frankel, J.I., Allison, S., and Beshears, D.L., "Design of Phosphor Thermometry System for Transient High Heat Flux Surface Thermometry", 58th International Instrumentation Symposium, June 4-8, 2012, San Diego, CA.

Vita

Yinyuan Chen studied Bioengineering in East China University of Science and Technology, China and obtained his bachelor degree in 2008. After that, he studied Biomedical Engineering in University of Tennessee, Knoxville (UTK) and obtained his master degree in 2012. Right now he is a doctoral student in Mechanical Engineering of UTK. His research interests include model design and numerical methods in thermal fluid sciences with a focus on the inverse heat conduction problems, thermophysical property estimation for aerospace materials, and the nonlinear analysis.